Politecnico di Torino

Master's degree in Automotive engineering

Propulsion System Development

A.Y. 2021/2022

Multi-Body modelling and mechanical analysis of a steering system adopted on a light-duty commercial vehicle

Supervisor:

Enrico Galvagno

Candidate:

Felice Romano

Company Tutor:

Luigi Bianco (Iveco Group)

Raffaele Garofalo (Iveco Group)

Angelo Casolo (MSC Software)

Daniele Catelani (MSC Software)

Abstract

A work like this wants to define a procedure that can be taken as standard when developing a model that wants to simulate how a vehicle works in terms of driving dynamics. The first focus is on the modelling side of the work, modelling took the majority of time in this work, this is mainly due to the fact that a new software had to be learned to fully develop a reliable model.
Every steering system is different, from this premise it is almost impossible to create a standard guide and procedure valid for every study case. Some components are common among Adams Car models, this made possible to define at least how some components are commonly created. Additionally, two appendices were added to this work, these two brief documents define the procedure to get two of the most important model elements that were needed by this thesis.
Concerning the work done on simulations, the main objective was to check that each model used in the software gave reliable results. The modelling work was focused on the steering part of the vehicle, for this reason the first simulation study was only on the steering system, the steering assembly was evaluated when steering motions were performed.
From this it was possible to pass the study to the front suspension, when doing a steering test, the suspension will be involved in some way. To check that the steering system did not cause a conflict with the way the suspension worked, parallel and opposite wheel travel tests were performed, giving a good idea on the suspension travel, tests were made to understand the behaviour of the system under these conditions and to check that the behaviour of the system was realistic.
The tests that gave the best review in terms of vehicle performance are the ones made on the complete vehicle, each test has a different objective, the ramp steering test has the role of defining the limit of grip of the vehicle and the forces and acceleration that are subjected to the vehicle components.
The step steer has the objective to understand how well the vehicle reacts to a sudden manoeuvre and its ability to stabilize itself. At last, the sweep steer test evaluates the frequency response of the system, these three tests were carried out to validate the models created when applied to the full vehicle model.
This work wants to underline the procedure followed to fully define and compare dynamic behaviour, from the basis of this thesis more accurate models could be used to deliver even more accurate results. A study like this is also capable of being versatile to different configurations, this is especially useful when talking about commercial vehicles, which are often created in a myriad of different configurations, the results presented in this thesis are introduced to define which are the most important parameters that can be used in evaluating the vehicle dynamic performance, by following the steps of this work it is possible to have a procedure to define and compare different vehicles.

Table of contents

1 Introduction

1.1 Case of study analysed

The vehicle studied in this analysis is an Iveco Daily 35S, as shown in Figure 1.1. This vehicle belongs to the light commercial vehicles category, in the Italian market it means that the vehicle must have a maximum gross weight not above 3500 kg.

For what concerns the mechanical layout, the front suspension is of the double wishbone type, while the rear suspension is a solid axle with leaf springs. The vehicle is rear wheel driven with the engine in the front, in a longitudinal layout.

The model used in this study is split in different assemblies, one for each suspension and one for the full vehicle.

Figure 1.1: Side view of an Iveco Daily like the one analysed in the study

Copyright: Iveco Group

Usually, light duty commercial vehicles (LCVs) have many different configurations, due to the different mission profiles that these vehicles have to be designed for.

This variability leads to different parameters such as wheelbase and height depending on the configuration. Sometimes, different layouts have different suspension systems. For example, in the case of the Iveco Daily it is possible to find pneumatic or leaf spring rear suspensions. This means that the study performed in this thesis is not valid for all the possible configurations of the vehicle, but just for the ones considered. It was decided to focus the analysis on two different body styles, one in short wheelbase form in fully loaded configuration and another in a longer wheelbase form but with no cargo, in unladen condition.

The main objective of the study is to find the behaviour of the elements related to the steering system, and the relationship that the steering model has in the full vehicle analysis.

The study is split in different parts: at the beginning there is a brief theoretical background required for the study, then an overview on how the system is modelled and finally the results on different tests and simulations are presented.

2 Theoretical background

2.1 Steering mechanics

2.1.1 Ackermann steering and steering ratio

The steering is one of the main components in the study of a vehicle's behaviour, both at low and high speeds.

Low speed manoeuvres are characterized by a negligible tire side-slip angle, defined as the angle between the traces on the X-Y plane (plane where the vehicle is seen from the top) of the vehicle X-axis and the projection of the instantaneous vehicle velocity [1]. These manoeuvres may have high steering angles, especially when parking.

In these conditions no cornering forces are coming from the wheels to balance the centrifugal force coming from the trajectory: this type of steering is commonly referred as Kinematic Steering .

The relationship that must exist to allow kinematic steering is easily found, by imposing the condition that the perpendiculars to the mid-planes of the front wheels must meet those of the rear wheels at the same point [2].

This can be seen in Figure 2.1, where the point O represents the meeting point of the front and rear axle.

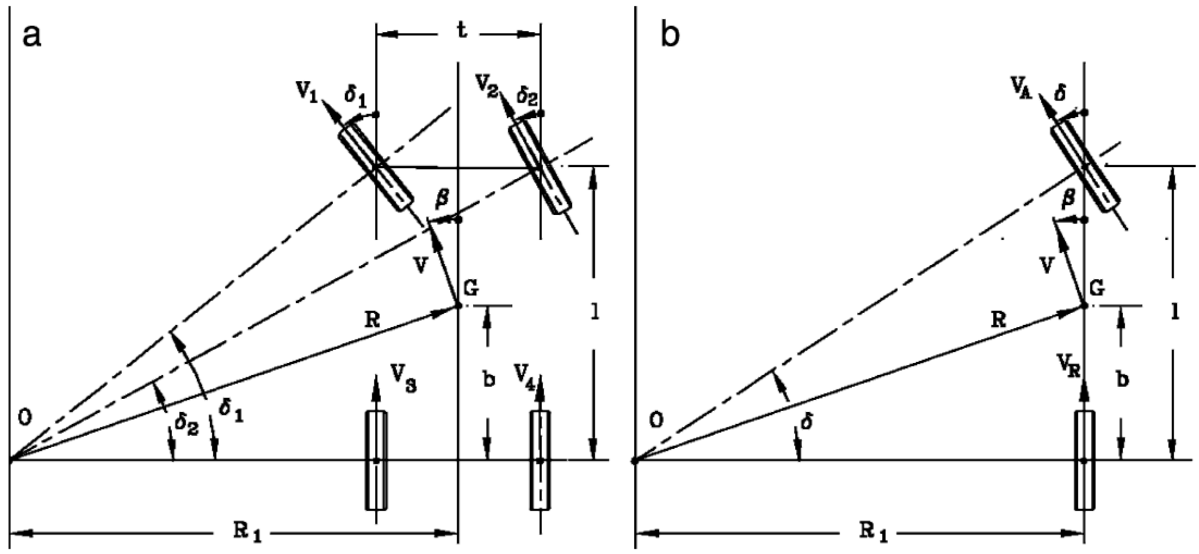

Figure 2.1: Kinematic steering condition, bicycle model shown in figure b

Copyright: Genta, G., Morello, L.: The Automotive Chassis Volume 1: Components Design, Second Edition, Springer, Heidelberg, 2009

In Figure 2.1 it is possible to see the vehicle from the top, *'δ'* represents the steer angle of each wheel, *'β'* represents the vehicle side-slip angle, *'G'* is the centre of mass of the vehicle, *'t'* the track and *'l'* is the wheelbase of the vehicle, defined as the distance between the front and rear axle.

This condition is ideal, and it is not always possible to have a system that follows exactly the idea behind kinematic steering. A system following the kinematic steering condition, or more precisely the Equation 2.1, is called Ackermann steering.

$$(2.1)\ \cot\delta_1 - \cot\delta_2 = \frac{t}{l}$$

In Equation 2.1 the track *'t'* is defined as the distance between the two steering axes: it means that it is equal to the wheel track minus two times the scrub radius, defined as the distance between the king pin axis and the centre of the wheel contact patch. The Ackermann angle is specified as the difference between the inside and outside steering wheel angle [3], as it is seen in Figure 2.2. Ackermann steering, like kinematic steering, is a condition that is ideal. At low speed it is possible to have steering systems that respect it. This is reflected by the fact that it is possible to have the inner steered wheel with a steer angle higher than the one of the outer one.

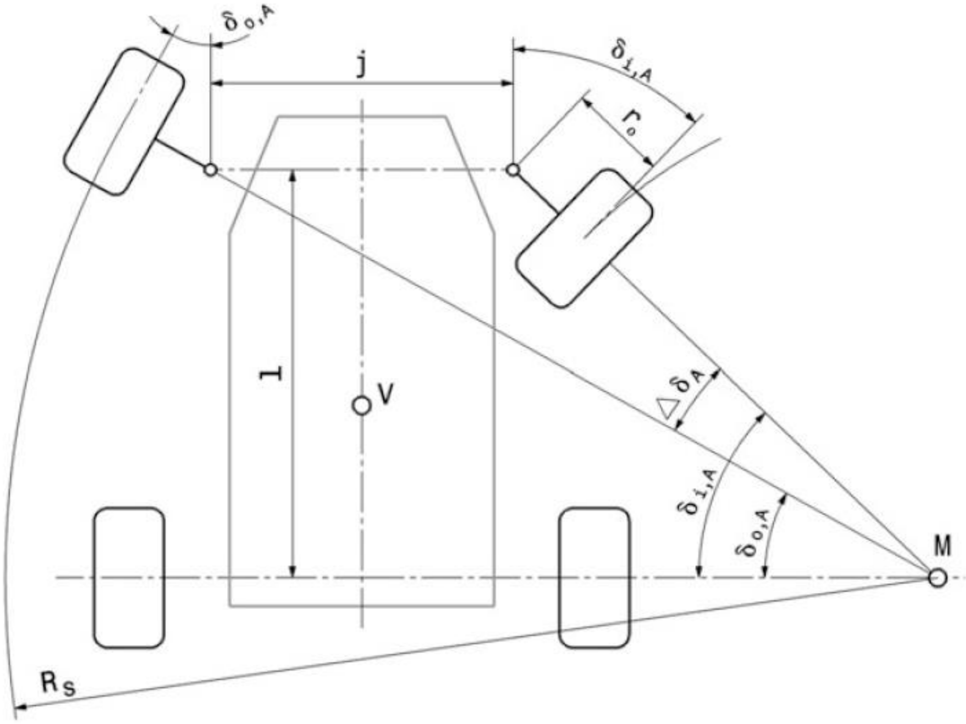

Figure 2.2: Ackermann steering condition, $\Delta\delta_A$ Ackermann angle, R_S track arc radius
Copyright: Harrer, M., Pfeffer, P.: Steering Handbook; First Edition, Springer, London, 2017

To express how far the system is from the ideal condition a parameter called steering error, or Ackermann error, is introduced, as it is possible to see in Equation 2.2, where $\Delta\delta_F$ expresses the steering error, $\Delta\delta_A$ the toe-out on turns according to Ackermann and $\Delta\delta$ the artificial toe-out on turns.

$$(2.2)\ \Delta\delta_F = \delta_o - \delta_{o,A} = \Delta\delta_A - \Delta\delta$$

$$(2.3)\ \Delta\delta_A = \delta_{i,A} - \delta_{o,A}$$

$$(2.4)\ \Delta\delta = \delta_i - \delta_o$$

Another useful parameter in the definition of the steering system is the steering ratio, this value considers how the angle changes from the one in input: In the case of a vehicle the steering wheel angle applied by the driver, and the steer angle seen at the wheels.

This change in angle is due to all the different elements that connect the steering wheel to the front wheels of the vehicle. The main element that has an effect on it is the steering rack, but also the different shafts, and their joints, that connect the steering wheel to the rack have an effect on it.

By analysing how the steering ratio changes, it is possible to have an idea on how the connecting elements of the steering system act on the steering motion.

The kinematic steering ratio i_s is defined in Equation 2.5, where δ_H is the steering wheel angle and δ_m is the mean steer angle of the tires, defined as the average between the inner and the outer steer angle. Steer angle is evaluated at the wheels, steering angle is instead the angle of the steering wheel.

$$(2.5)\ i_s = {}^{\delta_H}\!/_{\delta_m}$$

This ratio will not be the same all over the steering range. Equation 2.5 therefore applies only to individual ranges of wheel angle and steering wheel angle. Usually, the lower limit of the steering ratio is set by the fact that at high speed the steering response should be indirect, while the upper limit is related to the steering force while parking [3].

The kinematic steering ratio does not consider the fact that all the transmission elements will not behave in an ideal way. Connecting elements will affect how the input given by the steering wheel translates into an actual steer angle at the wheels. This leads to higher steering angles to achieve the same steer angle compared to the kinematic condition; besides this, servo-assistance has an effect on the system and usually moves the real steering condition away from the ideal kinematic condition. Every element that is added to the steering system will affect in some way the steering motion, due to the fact that some variation from the ideal motion will be induced by each element.

Real steering systems do not have to work always under kinematic conditions, this means that the fact that a system is kinematic or not, is not an indication of a system that works in a proper way: It may work flawlessly and be very far from the kinematic condition.

2.1.2 Steering axis definition and parameters related to it

To fully understand the results of the simulations is necessary to know how the steering axis is defined and what are the parameters that help define it.

Starting from Figure 2.3, it is possible to see a front view showing how the camber angle is defined.

The white line defines the vertical axis of the system, the orange line follows the inclination of the wheel, the angle between these lines defines the camber angle, which in this case shows a positive value. A negative angle will see the lower part of the wheel in an outer position compared to the upper part and vice versa for a positive angle.

In all the calculations performed, camber angle is defined as the angle the wheel plane makes with respect to the vehicle's vertical axis [4]. It is not calculated with respect to the road surface, that angle in Adams Car it is called inclination angle.

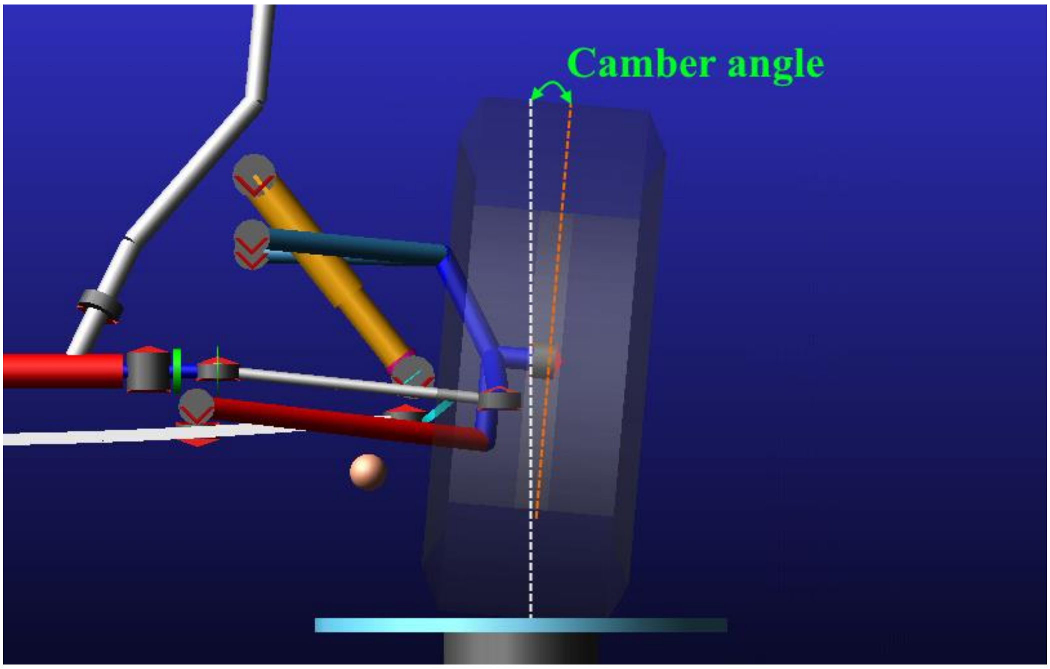

Figure 2.3: Front view of the suspension with a positive camber angle

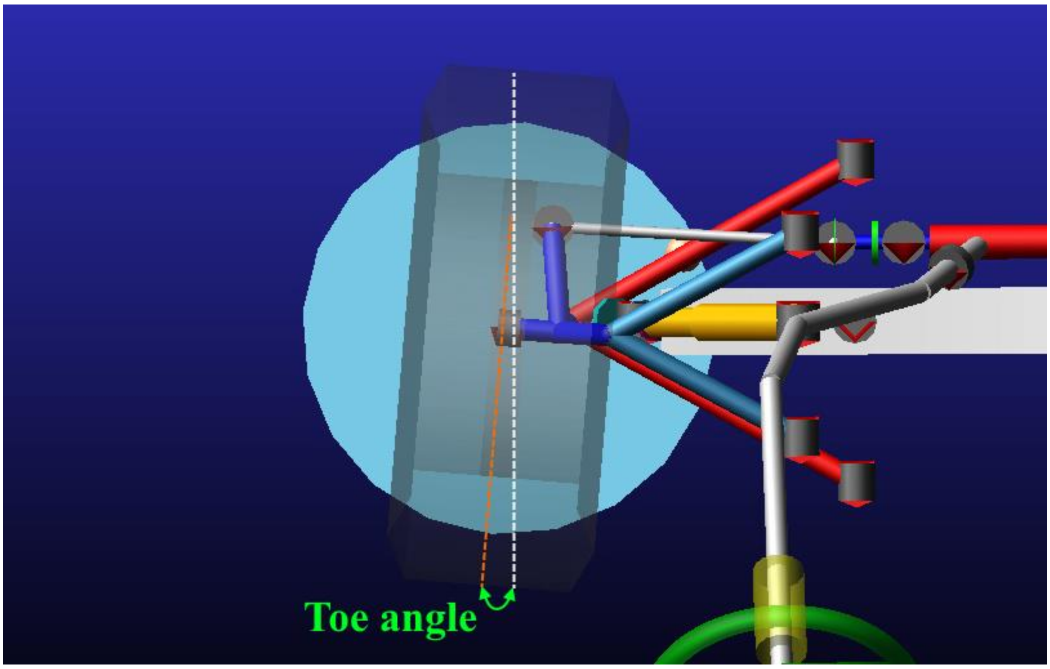

Figure 2.4: Top view of the suspension with a positive toe angle

Toe angle is explained in Figure 2.4, where the view is from the top of the vehicle, the white line represents the longitudinal axis, while the orange one follows the wheel position: the angle between these lines is the toe angle.
This figure shows a positive toe angle, this condition will also be called toe-in. In this condition, the other wheel has to be tilted in the opposite direction, specular to the one in figure. The opposite condition where the two wheels will point towards the outer part of the vehicle will be representative of negative toe angles and will be called toe-out.

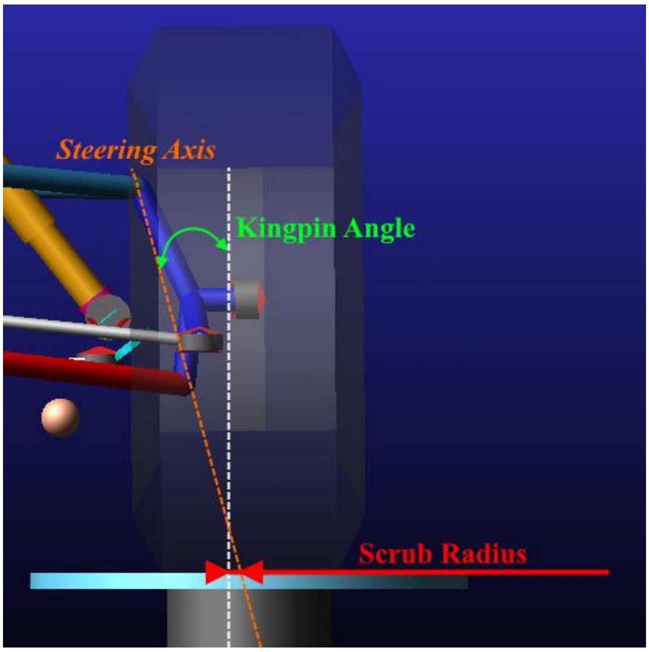

Figure 2.5: Front view of the suspension in design condition

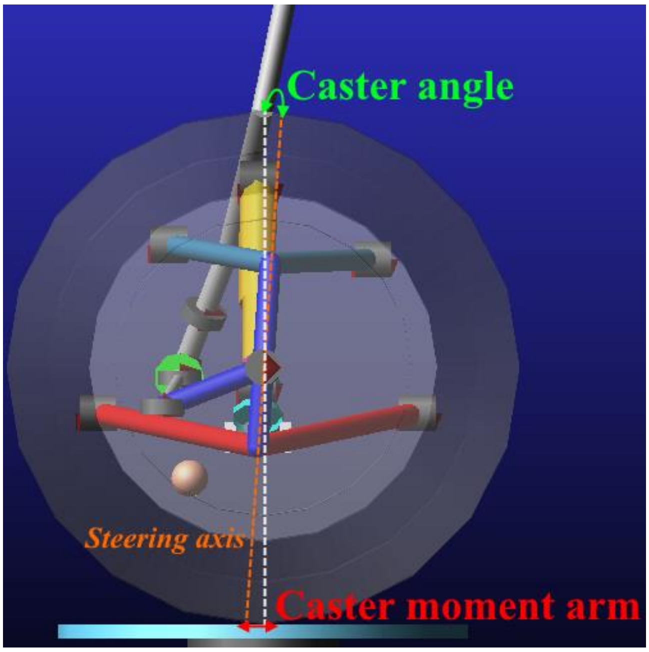

Figure 2.6: Side view of the suspension in design condition

Kingpin angle and scrub radius are strictly related as it is possible to see in Figure 2.5. The kingpin angle is the angle between the steering axis of the system, defined by the line connecting the two outer ball joints of the double wishbone, and the vertical axis that defines the wheel. The projection that this angle creates on the ground is called scrub radius.

A radius like the one in figure will be defined as negative. If the intersection between the two axes is below the ground, the scrub radius will be positive. These two parameters will define the steering axis in frontal view.

In Figure 2.6, caster angle is defined in lateral view as the angle between the vertical line of the wheel and the steering axis, obtained connecting the two ball joint of the arms that make the double wishbone suspension. The projection of this angle on the ground is called caster moment arm.

In Figure 2.7 it is possible to see how these parameters are defined when the wheel is steered.

The offsets are defined by the distance between the centre of the tire contact patch and the point of intersection between the steering axis and the ground, that is marked with the yellow dot in figure. The black reference system considers the wheels as straight, while the white system is the system related to the steered condition.

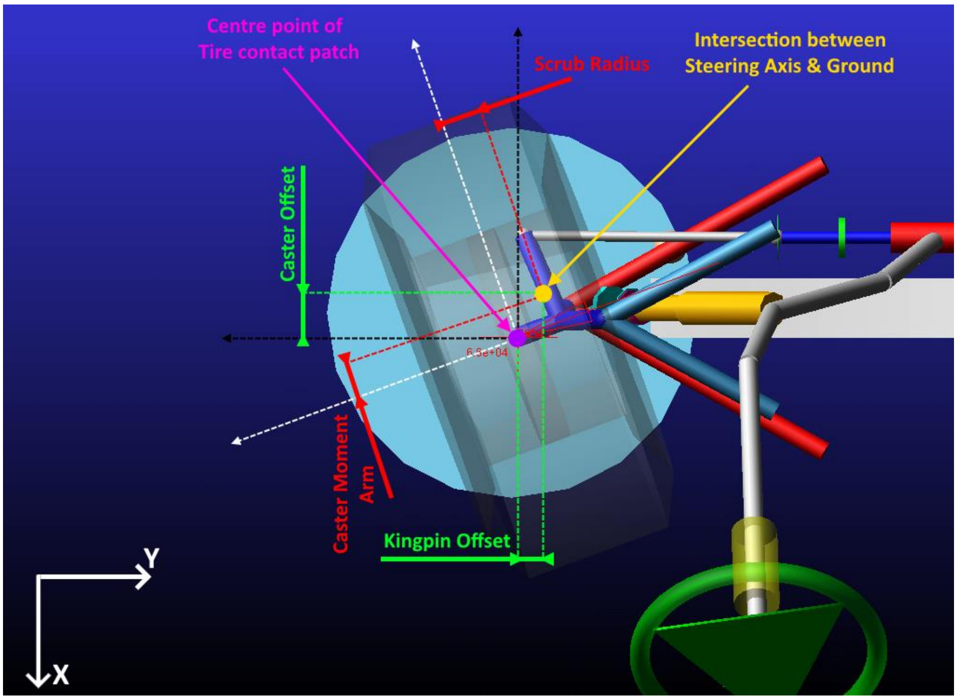

Figure 2.7: Top View of the wheel when is steered, showing the characteristic quotes of scrub radius and caster moment arm

2.2 Different elements used by the model

2.2.1 Rack and pinion steering system

The vehicle in analysis uses a rack and pinion steering system. This device is shown in Figure 2.8: It transforms, through the geared couple of the pinion 3 and the rack 1, the rotary motion of the steering

wheel into a linear motion of the spheric heads 2, which operate the steering mechanism.
This system has the advantage of a very good mechanical efficiency, due to the reduced friction between teeth flanks and the simplicity of the mechanism. As a drawback a system like this has the steering ratio value limited by the tooth size, due to fatigue resistance and minimum number of teeth that can be cut without interference [2]. This system makes the steering wheel immediately responsive, this is good for cars and light duty commercial vehicles, but precludes the application to heavy duty vehicles, due to limitations in strength.

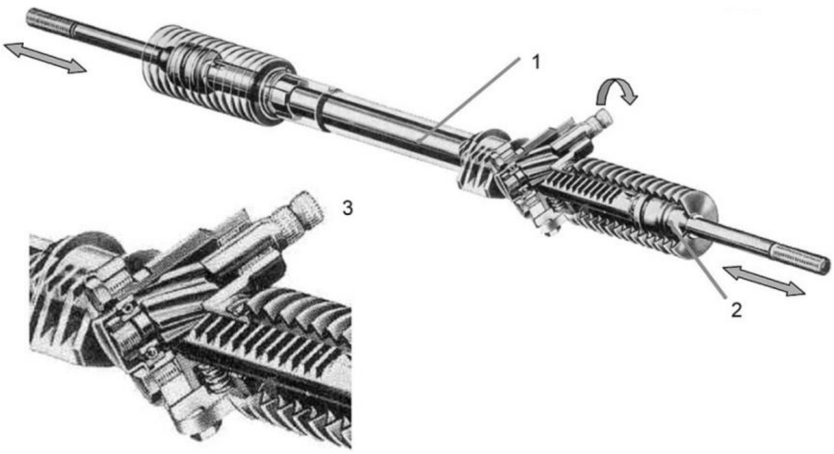

Figure 2.8: Rack and pinion steering box, in the enlarged part the gearing point between the two elements is seen, 1=Rack, 2=Spheric heads, 3=Pinion

Copyright: Genta, G., Morello, L.: The Automotive Chassis Volume 1: Components Design, Second Edition, Springer, Heidelberg, 2009

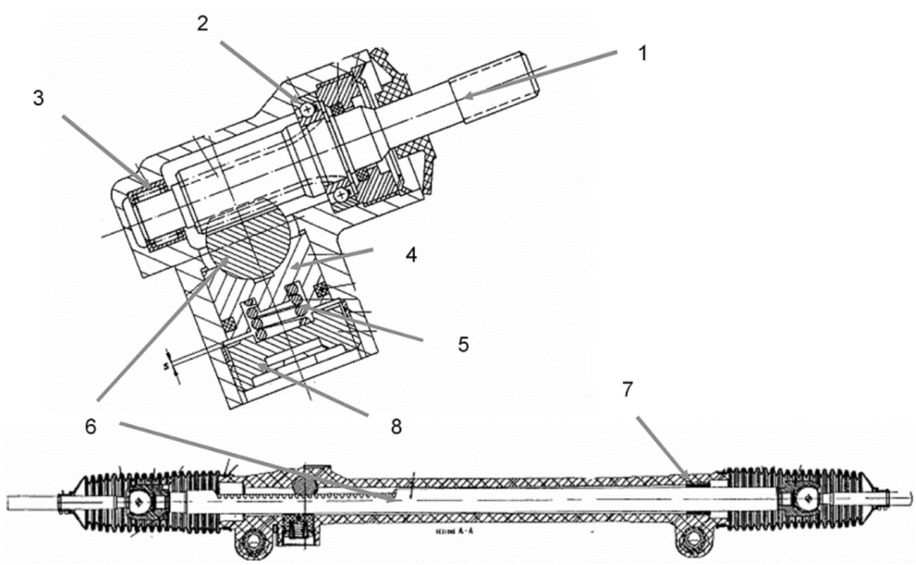

Figure 2.9: Elements that constitute the rack and pinion steering rack

Copyright: Genta, G., Morello, L.: The Automotive Chassis Volume 1: Components Design, Second Edition, Springer, Heidelberg, 2009

Figure 2.9 shows all the different elements that compose the system: The pinion is the element marked with the number 1, supported by the ball bearing 2 (reacting to radial and axial loads) and by the needle bearing 3 (reacting only to radial loads). The sliding block 4 supports the rack, being pushed by the spring 5 that controls pressure between rack 6 and pinion 1, sliding bush 7 offers a second bearing point, threaded ring 8 determines the mounting clearance of the sliding block 4.

2.2.2 Steering column and intermediate shafts

The steering column and the intermediate shafts were the main elements to be created in the modelling phase in Adams Car. These components have the role to connect the steering wheel to the steering rack, this makes these elements very relevant in how torque and forces sustained by the steering gear is transmitted to the steering wheel, and so, to the driver [3].

The steering column must support the upper steering shaft primarily, but it also needs to meet the ergonomics requirements for the driver, in terms of position but also adjustability, this two needs will usually bring the design to a compromised solution.

The intermediate steering shafts are usually made of a cardan shaft with two universal joints at the end, length compensation systems are often used to compensate for tolerances, to adjust the length of the steering column or for safety reasons.

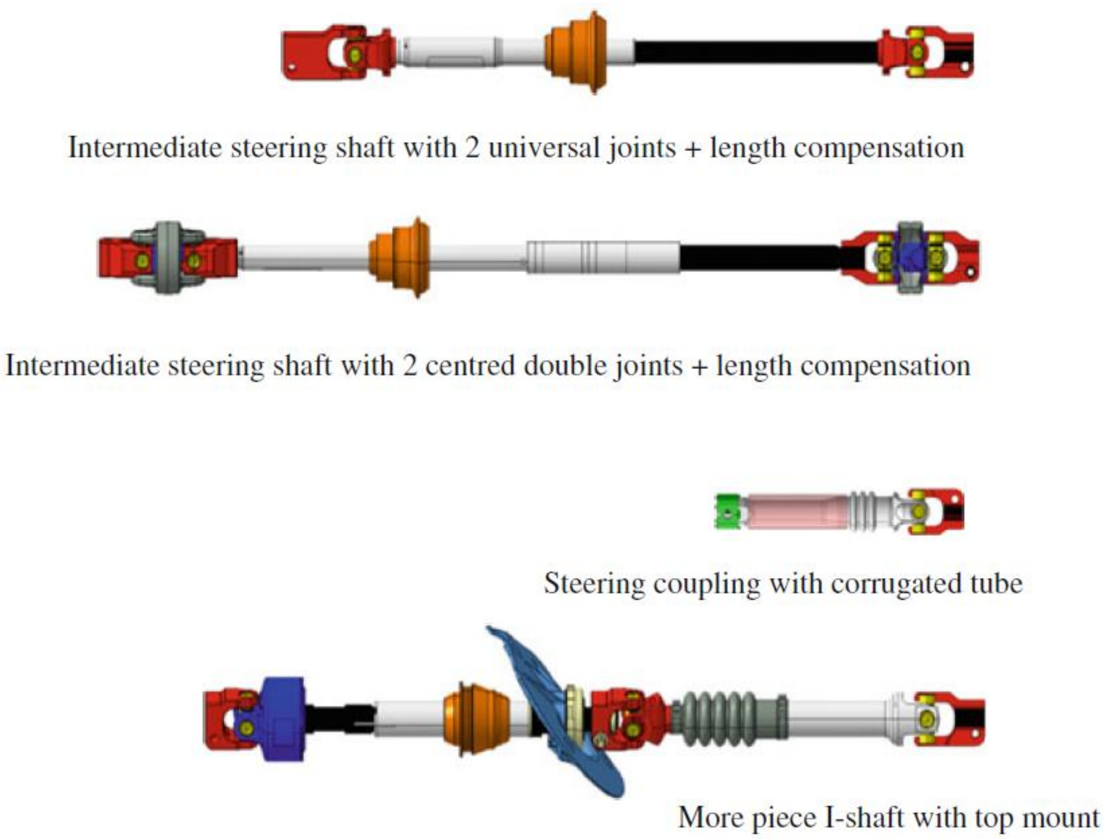

Figure 2.10: Different types of intermediate shafts

Copyright: Harrer, M., Pfeffer, P.: Steering Handbook; First Edition, Springer, London, 2017

In Figure 2.10 it is possible to see different possibilities for the intermediate shaft: The shaft pictured in the bottom could represent the assembly of the upper and second shaft assembly, the steering coupling could define the pinion that connects the steering rack to the shafts of the steering column. No length compensation elements are defined in the model, an element like this compensates for extensions that shafts may be subjected to, shafts are mostly rigid in the model used.
Characteristic angles of a universal joint are found in Figure 2.11: The output angle ϕ_2 follows the input angle ϕ_1 in an asynchronous way due to kinematics, the deviation is expressed by a sinusoid curve that jitters around the gimbal error [3]. The power balance has to be fulfilled at the input and output side, this leads to the possibility of computing the ratio of angular speed and torque from the rotary angle of the universal joint, like what is represented in Equation 2.6: Leading to a sinusoidal conversion of angular speed and torque with twice the frequency of the joint.

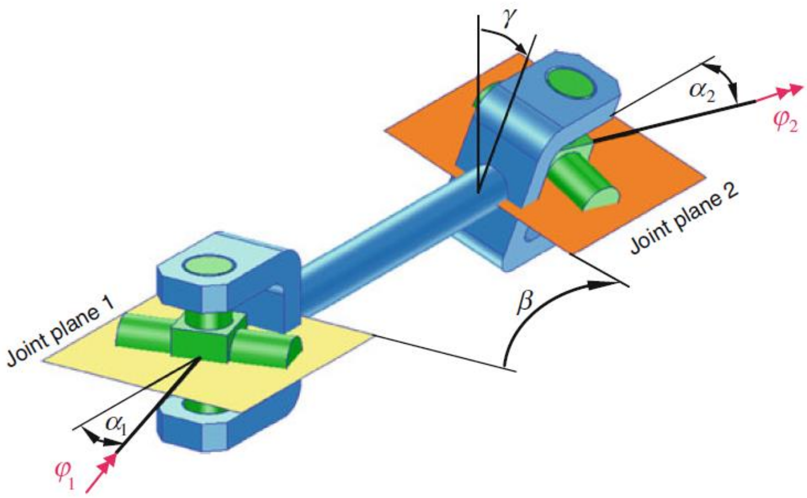

Figure 2.11: Characteristic angles of a universal joint
α = working angle, β = angle between joint planes γ = fork angle
Copyright: Harrer, M., Pfeffer, P.: Steering Handbook; First Edition, Springer, London, 2017

$$(2.6)\ i = \frac{\omega_{output}}{\omega_{input}} = \frac{M_{input}}{M_{output}} = \frac{2 \cdot \cos(\alpha)}{2 - \sin(\alpha)^2[1 + \cos(2 \cdot \phi_{input})]}$$

It is possible to define a relation between the two rotational angles φ in Equation 2.7, defined by F. Duditza:

$$(2.7)\ \tan(\varphi_2) = \frac{\cos\alpha_2(1 + \tan^2(\gamma - \beta))\tan(\varphi_1)}{\cos\alpha_1\,(1 + \cos^2\alpha_2 \cdot \tan^2(\gamma - \beta)) - \sin^2\alpha_2 \cdot \tan(\gamma - \beta) \cdot \tan(\varphi_1)}$$

The lowest transmission ratio is obtained when the offset angle is equal to the angle between the joint planes, in this case Equation 2.7 will become equal to Equation 2.8: From this Equation it is still possible to see the familiarity with the previous one, but in this case the formulation is simpler.

$$(2.8)\ \tan(\varphi_2) = \frac{\cos\alpha_2 \cdot \tan(\varphi_1)}{\cos\alpha_1}$$

Two joints with equal working angles allow to fully compensate the gimbal error, this condition is not always possible due to space constraints. The transmission ratio ‘i’ expressed in Equation 2.6 is function of the working angles. When looking at Equation 2.8 it is possible to see how Duditza’s model changes when $\gamma = \beta$: When the two working angles are the same, the two rotational angles φ will be equal, leading to synchronous movements between the shafts that will lead to a null gimbal error given that the two shafts will move in the same way.
Movements are synchronous when the two working angles are equal, a higher level of asymmetry will lead to a less stable condition, this behaviour is relevant even for straight driving: It is preferred to make sure that asymmetry is low but also that the behaviour for left and right steering is similar, to do so avoid that the steering centre is placed in the point where the sinusoidal function changes sign because it would lead to two different behaviours.
An example of gimbal error computations is seen in Figure 2.12, gimbal error represents the non-uniformity of the transmission of torque and speed by universal joint, this parameter was considered in the study to evaluate the irregularity of the steering system and how it was affected by phase angles, as it is possible to see in paragraphs 4.4 and 4.5.

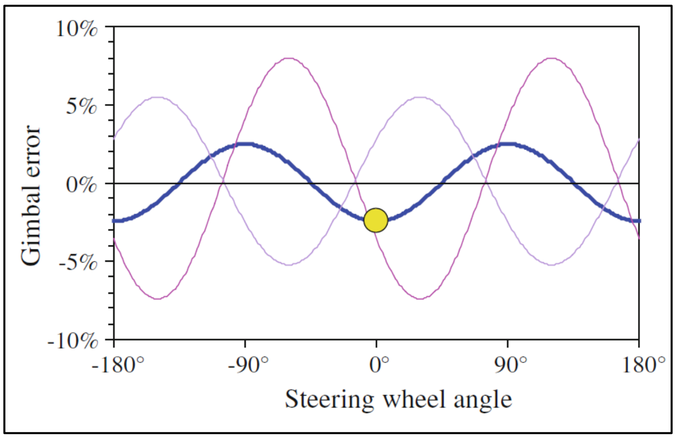

Figure 2.12: Gimbal error around the steering centre
Copyright: Harrer, M., Pfeffer, P.: Steering Handbook; First Edition, Springer, London, 2017

3 Modelling in Adams Car

3.1 Steering system modelling

The focus of the study is on the steering system, a rack and pinion system in this case: It is made of four different shafts as it is possible to see in Figure 3.1, the system is complemented by a steering rack assembly and a steering wheel.

The shafts are connected by three different universal joints, the system has been defined starting from different hardpoints, that define the geometries of the system:

- Two symmetrical hardpoints defining the inner mounting points of the tie rods.
- An hardpoint defining the pivot point of the pinion.
- Two symmetrical hardpoints defining the mounting points of the rack housing.
- Four hardpoints defining the three points of connection of the shafts plus the point where the steering wheel is mounted, the points of connection will be referred as Hardpoint #1, #2 and #3, while the steering wheel mounting point will be called SWH centre.

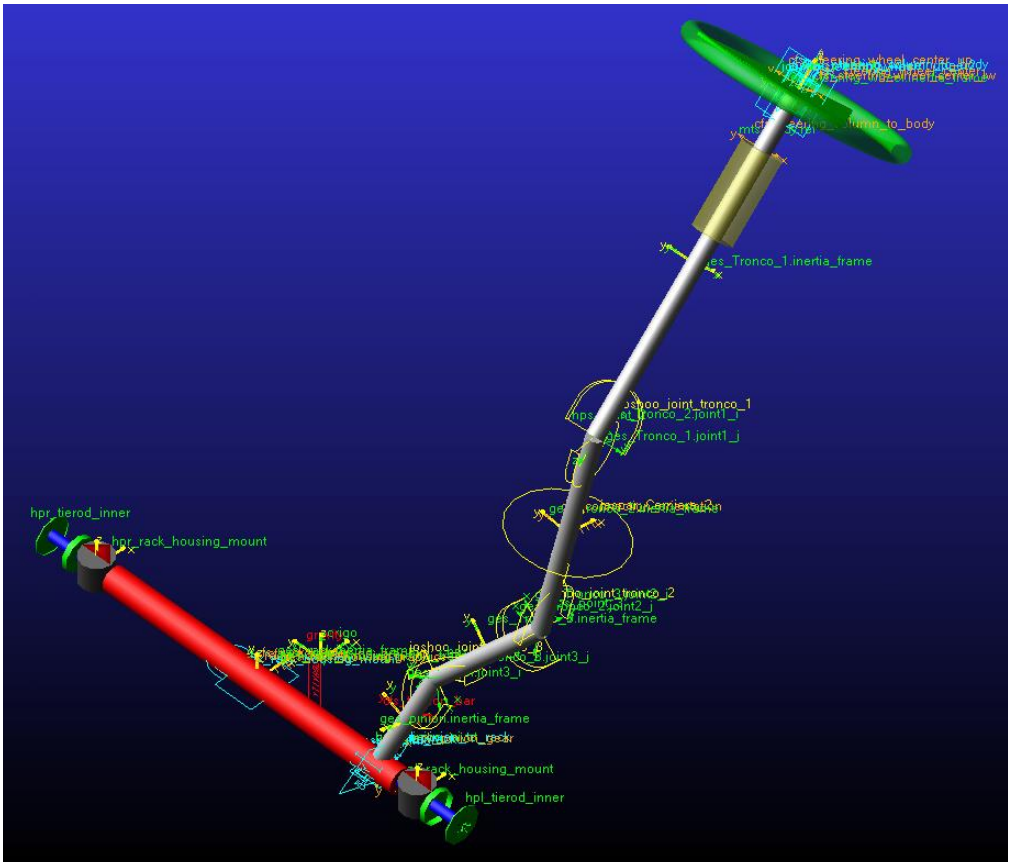

Figure 3.1: ISO Three quarter view of the steering system model, showed in the rigid steering version

The system has been designed in two different versions: One where the steering is completely rigid, and one where some compliance is introduced.

This compliance is set through a torsion bar, made of two shafts with a bushing placed in the middle, this system substitutes the single shaft that represented the pinion in the rigid configuration. The bushing is defined through a property file: To correctly define the bushing only the elastic characteristic in term of torque and the torsion angle/torque characteristic around the Z-axis are defined, leaving force and torque components around the other axes null.
Figure 3.2 shows the configuration of the torsion bar, the bushing is placed exactly in the middle, this means that the two shafts that make the connection are of equal length, the rotational stiffness characteristic is linear.

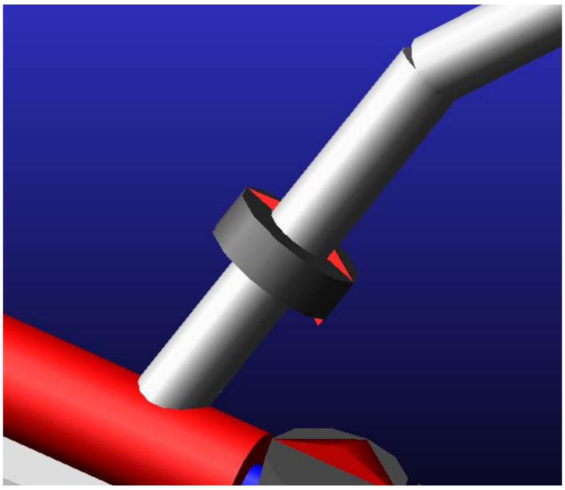

Figure 3.2: Torsion Bar connection to steering rack

In each shaft it was implemented a function to evaluate its angular speed, this not only allows an evaluation about the speed of each shaft. It also enables the possibility to impose an angular speed to the first shaft, this makes possible to work in terms of speeds and not only of steering angles as input. These functions were implemented using the 'Measures' function present in the Adams View interface.

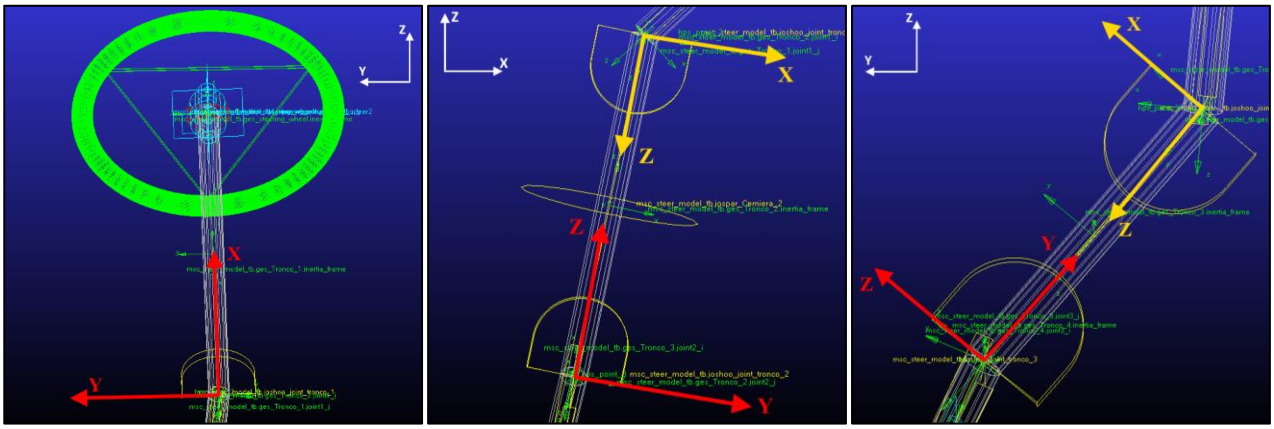

Figure 3.3: Aligned reference system from which phase angles are defined. The left and right pictures are shown in front view, while the picture in the middle represents a side view of the steering system

One of the most important parameters of an universal joint is the phase angle, in order to better study its relevance with respect to the results, these angles where implemented in a parametrical way: For each angle the reference system has been defined, each system has been obtained from Adams Car keeping the orientation equal to the one of the system that defines the line from the previous hardpoint to the one where the joint is defined, in Figure 3.3 it is possible to see the reference systems used by the different joints.

The definition of phase angles started from the condition where all the joints are aligned: This case has all the universal joints placed like in Figure 3.3, first of all the first hooke joint had to be placed in space. It was decided to have the first fork aligned on the same reference system that defines the upper shaft orientation, this was done by aligning the cross shaft of the first hinge to the Y-axis of the upper shaft frame, the position of the first hinge automatically defines how the second hinge is placed, fully defining the first cardan joint.

The second cardan joint definition follows the same basic idea of the first one, the picture in the middle of Figure 3.3, taken from the side of the shaft, has the upper hooke hinge placed in the same orientation of the second shaft, the second hooke is defined by sharing the same Z-axis with the upper hooke lower hinge. The cross shaft that connects the hinges of the second joint is aligned with the Y-axis shown in red, that is on the same orientation of the shaft reference frame, this will mean that the X-axis of the upper hooke and the Y-axis of the second hooke are aligned.

The same basic idea is followed for the definition of the third hooke, this time the Y-axis of the third hooke will be aligned to the Z-axis of the second one and the Z-axis with the X-axis. Due to the fact that the system is in the global space defined in Adams Car, that not always shares the same reference systems, the phase angles in aligned condition are not defined as zero in the parameter variable function, but as the difference in angle between the standard reference systems that Adams Car selects in defining the variables and the systems defined in Figure 3.3.

3.2 Overview on the different type of joints present

Further attention has been applied to the type of joints present in the system. The joints typology affects the degrees of freedom of the system and so its ability to correctly work in analysis.

The system in study has the set of joints shown in Table 3.1, some acronyms are found in this table: ‘SWH’ stands for ‘Steering Wheel’ and ‘TB’ stands for ‘Torsion Bar’, all these joints create some constraint inside the system, some joints represent true connections, while others are used by the system to create an environment that would work during simulations.

To fulfil the evaluation on the degrees of freedom removed by these connections it’s important to include the reduction gears present in the system, as shown in Table 3.2.

Only one gear is modelled inside the steering system, this gear is the one present inside the steering rack. This gear is, obviously, different from the joints that were listed in Table 3.1, but it still removes one degree of freedom from the system.

In Adams Car, gears are created with all the parameters needed for a correct definition of their geometry, additionally, gears are defined in terms of how the gear constrains the system in study: By choosing the joints among which the element works, in this case the revolute joint around the pivot point and the translational joint inside the steering rack. It is important for the software to fully define the role of the gear in the system in study.

Joint	Location	Parts constrained	DOF Removed
Perpendicular	SWH centre	Steering wheel & steering column	1
Cylindrical	SWH centre	Steering column & body (dash)	4
SWH Revolute	SWH centre	Steering wheel & body (dash)	5
Upper Hooke	Hardpoint #1	Steering column & first intermediate shaft	4
Intermediate Hooke	Hardpoint #2	First & second intermediate shafts	4
Lower Hooke	Hardpoint #3	Second intermediate shaft & torsion bar	4
Parallel Axes	Half point of first intermediate shaft	First intermediate shaft & body (firewall)	2
TB Revolute	Bushing of torsion bar	Upper & lower shafts of torsion bar	5
Translational	Pivot point	Steering rack housing & steering rack	5
Pivot Revolute	Pivot point	Torsion bar & steering rack housing	5
Fixed	Rack centre	Steering rack & body (chassis)	6

Table 3.1: List of joints present in the system

Gear	Joints interested	DOF Removed
Rack reduction gear	Pivot revolute & Translational	1

Table 3.2: List of geared elements present in the system

In Adams Car there are two types of joints, the first type represent joints that have a real counterpart, while the second is made of ideal joints called 'Joint primitives'.

These joints do not usually have a physical analogue and are predominately useful in enforcing standard geometric constraints [4].

In Figure 3.4 it is possible to see all the different joints available from the software: Of all of these joints only the 'Inline', 'Inplane', 'Orientation, Parallel_axes' and 'Perpendicular' are Joint primitives, while all the other joints have a respective in the real world. These type of joints were used in this case when a connection or a constraint, that was not defined by a common joint, was needed.

Joint name:	Number of DOF:	Type of motion DOFs allow:
Translational	1	Translation of one part with respect to another while all axes are co-directed.
Revolute	1	Rotation of one part with respect to another along a common axis.
Cylindrical	2	Translation and rotation of one part with respect to another.
Spherical	3	Three rotations of one part with respect to the other while keeping two points, one on each part, coincident.
Planar	3	The x-y plane of one part slides with respect to another.
Fixed	0	No motion of any part with respect to another.
Inline	4	One translational and three rotational motions of one part with respect to another.
Inplane	5	Two translational and three rotational motions of one part with respect to another.
Orientation	3	Constrains the orientation of one part with respect to the orientation of another one, leaving the translational degrees of freedom free.
Parallel_axes	4	Three translational and one rotational motions of one part with respect to another.
Perpendicular	5	Three translational and two rotational motions of one part with respect to another.
Convel	2	Two rotations of one part with respect to the other while remaining coincident and maintaining a constant velocity through the spin axes.
Hooke	2	Two rotations of one part with respect to the other while remaining coincident.

Figure 3.4: Type of different joints available in Adams

Copyright: https://www.me.ua.edu/me364/Student_Version/Connections.pdf, University of Alabama, 2008

After the full definition of the joints present it was possible to define the degrees of freedom of the system.

Two different results are expected, in case of the system with the torsion bar two degrees of freedom are expected to be left, while only one is expected for the rigid steering, a result that is not coherent with this will mean that the system is not correctly placed. Numerical computations are shown in Equations 3.2 and 3.3, the sum of degrees of freedom removed by each joint is done following the same order of Table 3.1, in the case of the system with torsion bar there are five additional DOF constrained by the revolute joint placed between the torsion bar shafts.

$$(3.2)\ DOF(Rigid\ Steering) = 6 \times 6 - (1 + 4 + 5 + 4 + 4 + 4 + 2 + 5 + 5) = 36 - 35 = 1$$

$$(3.3)\ DOF(Torsion\ Bar) = 6 \times 7 - (1 + 4 + 5 + 4 + 4 + 4 + 2 + 5 + 5 + 5) = 42 - 40 = 2$$

The evaluation on the degrees of freedom of the system is crucial in the evaluation of the geometry of the steering assembly model, but it is also needed to discuss the design choices behind this particular system, this steering assembly starts from a previous model where only two universal joints were present, at a first glance that system could seem better, it in fact has less complexity that in production and mechanics is crucial to have a cheap and reliable working system.
Adding a third joint, and so an additional shaft between two joints, increases the complexity of the system, but increases the flexibility in terms of packaging, the mounting points of the steering wheel and of the steering rack are, more or less, fixed by other constraints when a steering system is designed, being obliged to connect the steering column to the steering rack by a single shaft with two joints at its end may be limiting in terms of packaging constraints.
Another effect coming from the addition of another joint comes from what will be studied in paragraph 4.4: An universal joint will, for a given input angular speed, return a fluctuation on its output angular speed, adding another shaft may add a way to reduce irregularities without changing too much phase angles of the joints. The last effect to consider is the fact that splitting the system in more joints enables to use smaller shafts, these shafts could be safer in the case of a crash avoiding intrusion inside the cabin, even if today collapsible shafts are widely used, a smaller shaft will, more than likely, reduce the probability of injuries for the cabin occupants.
In these calculations, fixed joints and the body of the vehicle were not considered: These joints constrain all the six degrees of freedom possible and so they nullify themselves with the contribution from the body in the first member, to sum up the results from the two computations it is possible to say that:

- For the rigid steering system, there are six different rigid bodies and a total of 35 DOF constrained by the joints, this leads to a total of one free degree of freedom that is coherent with what was expected.
- For the steering with torsion bar, there are now seven different rigid bodies because the pinion is now split in two parts, this system now constrains 40 DOF leading to two remaining degrees of freedom, again coherent with what was expected.

3.3 Front & rear suspension modelling

For what concerns the front and rear suspension, the model was mostly provided by IVECO Group, just some small modifications were performed, mostly on the front axle.

The front suspension of the Iveco Daily is particular, this type of suspension has no anti-roll bar in the front, the anti-roll function is done by a transversal leaf spring that is shared between the two front wheels. In Adams this leaf spring is modelled by connecting many elements one after the other, these elements will sustain the forces applied to them, leading to a deflection like the one of a leaf spring, bushings are placed at the ends of the spring leaving some compliance in the mounting points.

The suspension geometry is of the double wishbone type, the suspension is connected to the steering rack through the tie rod, in Adams it is important to check that the hardpoint that defines the end of the rack and the hardpoint that defines the inner mounting point of the tie rod have the same coordinates, in order to avoid misplacements.

The suspension is simply made of four main parts: Two wishbones, one on top of the other, connected together by a wheel hub, at last a shock absorber is introduced to provide damping to the suspension.

In Figure 3.5, besides the front suspension, there is another element shown: the test rig.

This element has the role to evaluate all the results in term of displacements and forces of the wheels, this is needed to evaluate the steer angle for example.

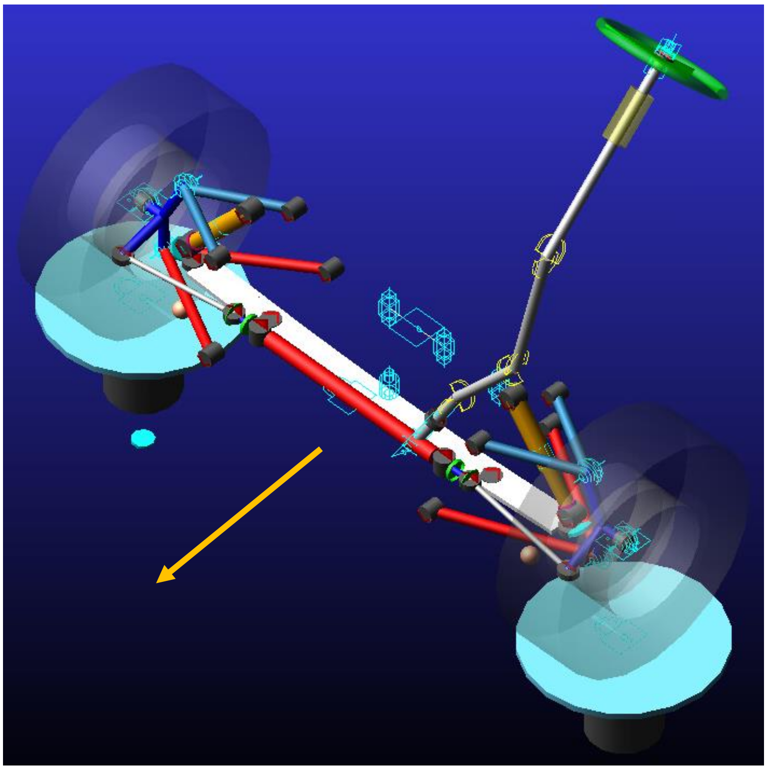

Figure 3.5: Front suspension assembly with test rig, yellow line showing direction of the vehicle frontal part

For this analysis the steering system has no power steering implemented, it was decided to work only on the dynamics of the system and how the steering components affected the behaviour of the vehicle. To have an idea on how the power steering implementation may affect the results it is useful to mention the work from which this thesis started, a previous thesis named ‘Analisi numerica e sperimentale delle caratteristiche elastocinematiche delle sospensioni di un veicolo commerciale leggero' from Mr. Andrea Candela, this work preceded this thesis and used a two-shaft steering system mounted on the same vehicle of this study, on that thesis the power steering characteristics were fully analysed, results from that thesis also apply to this work.

In Figure 3.6 it is possible to see how the front suspension looks when it is seen from the rear, in this picture it is possible to see how the roll centre is defined. The roll centre definition starts from the definition of the two instantaneous centres, these are defined by the intersection of the lines that passes through the two ball joints of each arm of the front double wishbone suspension: By connecting these two points with the centre of the contact patch of each wheel it is possible to get two lines that will intersect in a point, this intersection point will be the roll centre, this point is instantaneous, it means that changes as ride height changes during motion, in this case it has been defined for the stationary vehicle condition.

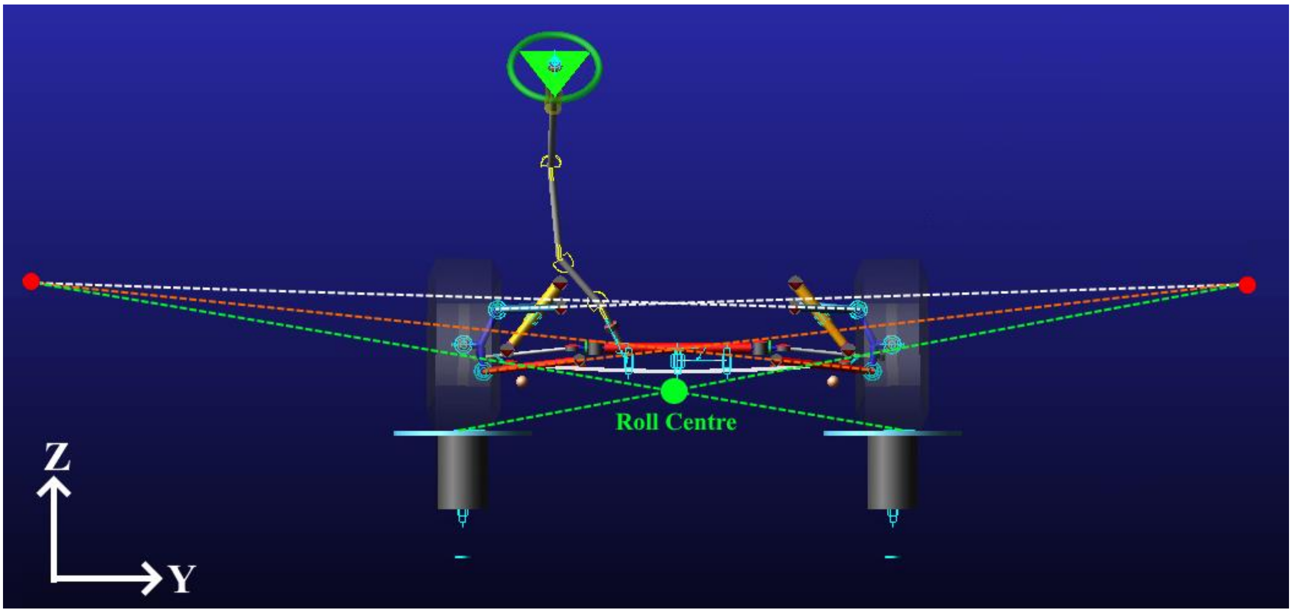

Figure 3.6: Front suspension seen from the rear, showing the definition of the roll centre

The rear suspension is, instead, more traditional: It is a rigid axle suspension with longitudinal leaf springs, modelled like that in the front, through connected elements one after the other. At the two ends of the spring there are the mounting points to the body, the point towards the front of the vehicle has a single bushing, while the other mounting point has two bushings one on top of the other, it also has a traditional anti-roll bar, again mounted to the body with bushings.

The main part of the system is the solid axle itself: In the software it is modelled through the differential that is showed as the blue sphere in Figure 3.7, two hollow beams that create the housing to the drive axles that connect each wheel to the differential, two tripots connects the axles to the differential, one on each side, the system is completed by two shock absorbers.

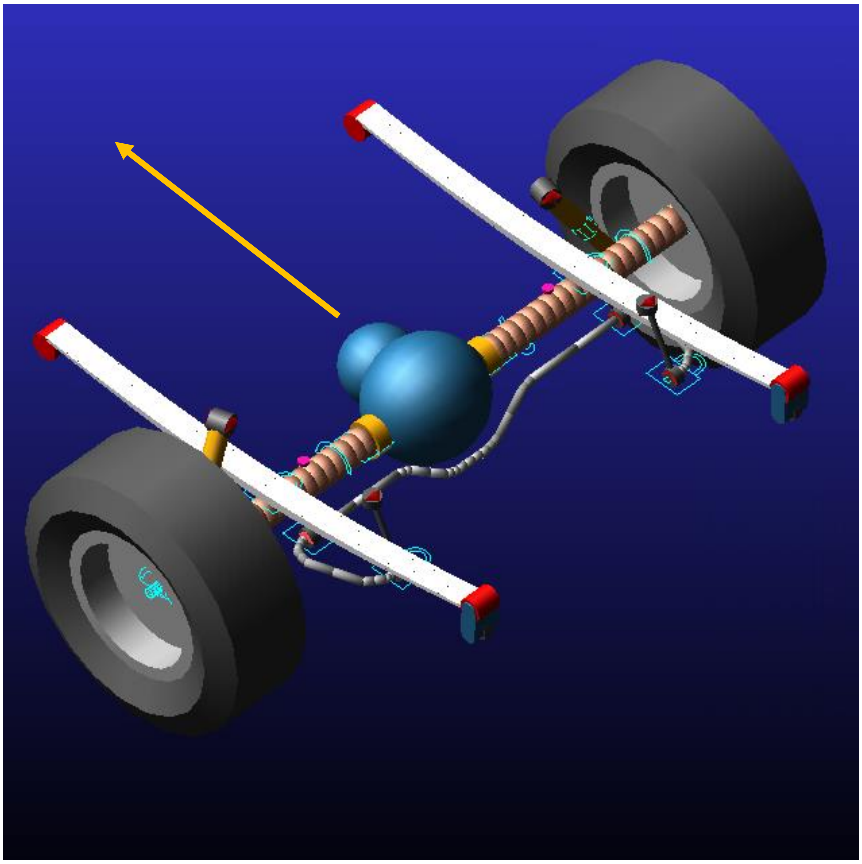

Figure 3.7: Rear Suspension Assembly, yellow line showing direction of vehicle front side of the vehicle

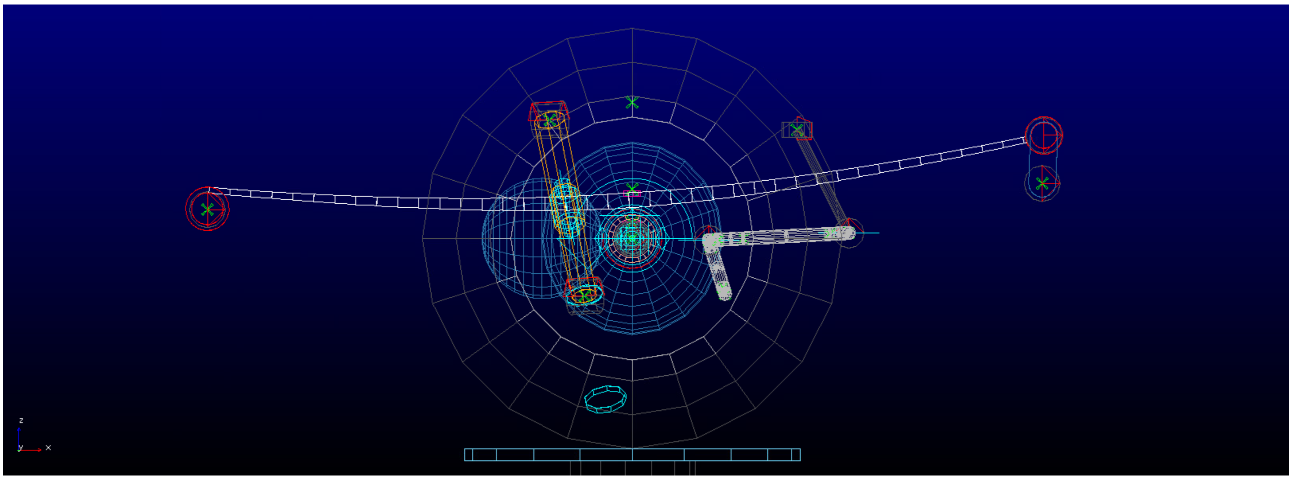

Figure 3.8: Figure that shows the joints that connects the rear suspension to the body, represented as the red bushings

This type of vehicle has different rear suspension assemblies depending on the configuration, some vehicles have a dually suspension with double tires on each side, for this study it was decided to work on a configuration with single rear wheels, this configuration is used by the configurations that are designed towards light-duty applications such as deliveries or passengers transportation, the majority of heavy-duty application employs double rear wheels. In Figure 3.8 it is possible to see how the suspension is seen from the side, the red bushings represent the points where the leaf spring connects to the body.

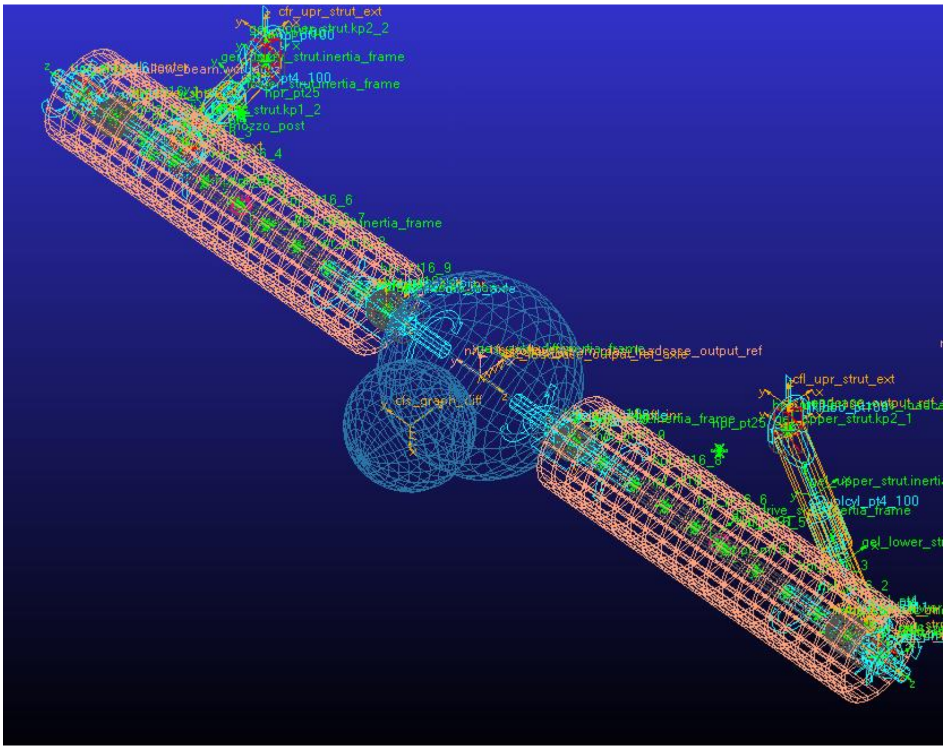

Figure 3.9: Rigid axle model, as seen in the Adams Car interface

The rigid rear axle is not modelled as a rigid element: in Figure 3.9 it is possible to see different hollow cylinders that form the axle itself, two constant velocity joints, one at the wheel and one at the differential side, have the role to simulate the axle shaft that trasmit the torque from the differential to the wheels, translational joints are placed between the shafts and the differential, while spherical joints are placed between the shafts and the wheels, both of these two last joints examined are placed in the same place of the constant velocity joints.
The last element present is the damper, this element is divided in two parts, an upper and a lower strut, these two parts are connected by a cylindrical joint.
At last, two hooke joints connect the damper to its mounting points, the same criteria, both for the dampers and the axle shafts is followed by the front suspension elements.

3.4 Full vehicle model

The full vehicle model, if it is seen from Figure 3.10 and 3.11, may seem just like a composition of the two suspension assemblies, in reality each element present in the vehicle has been modelled.
Mainly three parts are present further from front and rear suspension and wheels:

- Vehicle powertrain, as the name suggests, it presents all the information about the powertrain components, mainly engine and transmission, this includes upshift and downshift points, engine torque, gear ratios, operating engine speeds and other parameters.

- Vehicle body, it has all the information about wheelbase, weight, and centre of gravity position as well as all the information about the aerodynamics of the vehicle.
- Vehicle driveline, it has all the parameters needed to simulate the differential and the driveline, such as torque preload and locking coefficient of the differential.

The most important setting required for the full model is the definition of the centre of gravity and, as a result, the weight distribution of the vehicle.
The suspension geometry has a large effect on how the vehicle reacts to different motions that happens during different manoeuvres.

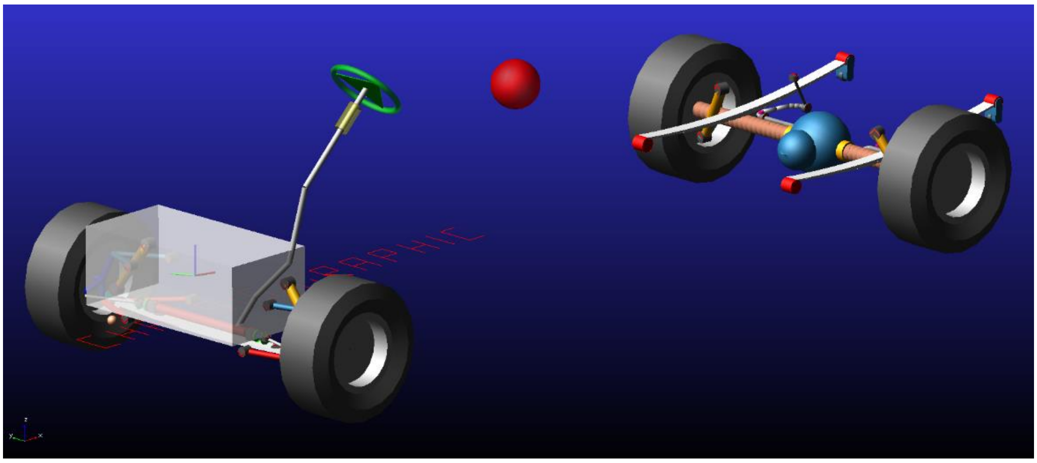

Figure 3.10: Three-Quarter view of the full vehicle model

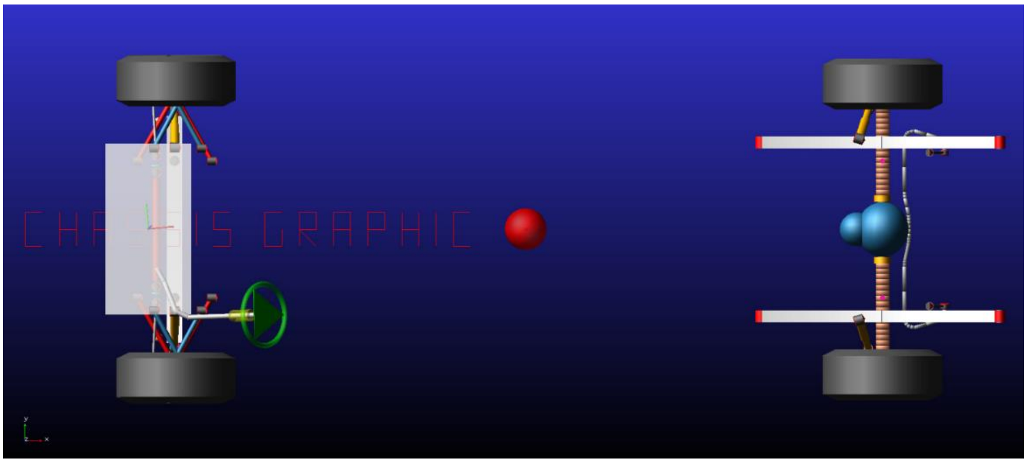

Figure 3.11: Top view of the full vehicle model

For what concerns straight line performance the main parameters that are considered are anti-dive during braking and anti-squat during acceleration, anti-dive is present on the front axle, while anti-squat is present on the rear axle, anti-dive and anti-squat have their correspondent on the other axle, mainly anti-lift on the rear during braking and anti-lift on the front during acceleration, at least for a rear wheel drive vehicle like the one in analysis.

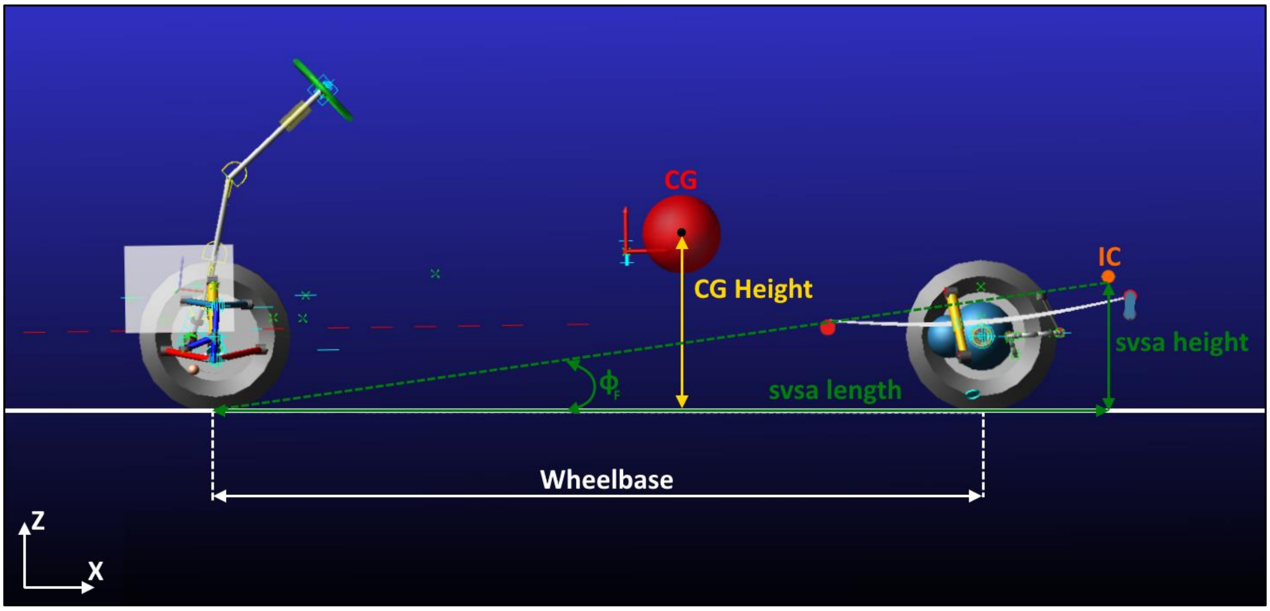

Figure 3.12: Side view of the model in SWB form, showing the measures needed to evaluate anti-dive

In this study the focus is mainly in anti-dive during braking, being that the study is focused on the front suspension in terms of modelling, anti-lift during braking will also be briefly analysed.

Figure 3.12 shows the main parameters that are needed to define the percentage of anti-dive in the front, as it is shown in Equation 3.4 [1]:

$$(3.4)\ \%\ anti - dive\ front = \frac{tan\vartheta}{tan\bar{\vartheta}_F} \cdot 100$$

$$(3.5)\ tan\bar{\vartheta}_F = \frac{\Delta F_Z}{F_{xF}} = \frac{m\ddot{x}\frac{h_G}{L}}{m\ddot{x}p} = \frac{h_G}{Lp}$$

$$(3.6)\ tan\vartheta = \frac{svsa\ height}{svsa\ length}$$

In this Equation ‘m’ represents the vehicle weight, multiplied for the acceleration, ‘p’ represents the force percentage that is acting on the front axle, ‘L’ represents the vehicle wheelbase.

‘svsa’ represents the side view swing arm and is expressed in terms of height and length calculated from the contact point of the tire up to the instantaneous centre in side view, that is obtained from the intersection of the lines that define the two front arms of the suspension.

The analysis included in this work are done using two vehicle models, the first is a representation of the van in short wheelbase form with a wheelbase length of 3520mm, while the second represents a longer configuration where the vehicle has a wheelbase longer of 600mm, totalling at 4120mm.

The two systems share the same suspension geometries front and rear and the same powertrain, unfortunately they are in two different conditions, the shorter vehicle is configured to be at the maximum payload level, meaning that the vehicle carries its maximum allowable weight, the longer wheelbase vehicle is instead in its minimum weight configuration, meaning that the cargo area is completely empty, this is mainly related to the fact that reliable data where found in case of the empty vehicle, for this vehicle it is possible to say that the model represents with good approximation the real van.

This condition is not ideal because the two configurations are not directly comparable, but it gives the possibility to evaluate how the vehicle behaves when it is loaded and unloaded, even if between the two vehicles there will be some differences due to the different body style.

The short vehicle model was provided by the manufacturer, the long wheelbase model was obtained starting from the short one and changing the position of the rear axle with respect to the front one, and the weights of the vehicle and their distribution front to rear, due to the variation in space position of the centre of gravity.

Parameter	SWB Full Load	LWB Unladen
Total weight	Reference	-24,93%
F/R weight distribution	Reference	+52,80%
C.G. height	Reference	+24,77%
Bounce natural freq.	Reference	+5,04%
Pitch natural freq.	Reference	+31,10%
Ride frequency ratio	Reference	+24,58%
SVSA Height	Reference	+5.18%
SVSA Length	Reference	-0,52%

Table 3.3: Difference of the long wheelbase vehicle model from the short wheelbase one

In Table 3.3 it is possible to have an idea on how much the long wheelbase vehicle changes its parameters compared to the short one that was provided by the manufacturer: As expected the longer vehicle will have lower weight and higher centre of gravity due to the fact that it is in unloaded conditions, the highest difference comes from the weight distribution: A commercial van is designed to work at full weight, by considering it in fully unloaded configuration the weight distribution will largely change, natural frequencies and ride frequency ratio are included for completeness.

The bounce natural frequency defines how the suspension reacts to bounces, while pitch frequency is experienced over a braking manoeuvre when the nose of the vehicle pitches forward.

Ride frequency ratio is related to the ride rate, these three frequencies will define how stiff the suspension is and define its reaction to uneven surfaces and corners. A higher frequency will result in a stiffer suspension, mind that ride rate is computed at the wheel, not at suspension level.

4 Steering system test & validation

4.1 Steer angle & steering ratio in function of steering wheel angle

The first part of the study focuses on the comparison between different versions of the steering system model used in analysis.

The simulations were carried out in the order shown in Table 4.1: This follows the idea of starting from the most ideal condition, the one made with constant velocity joints and rigid steering, up to the most realistic model that best represents the design condition, this allowed to check the differences between the different cases and how they affected the steering behaviour of the vehicle.

Configuration	Type of Joint	Type of steering
1	Convel joint	Rigid steering
2	Convel joint	Torsion bar
3	Universal joint	Rigid steering
4	Universal joint	Torsion bar

Table 4.1: Type of configurations used in simulations; design configuration highlighted in yellow

The first parameter analyzed is the steer angle, before showing the results it is useful to understand the meaning of this parameter.

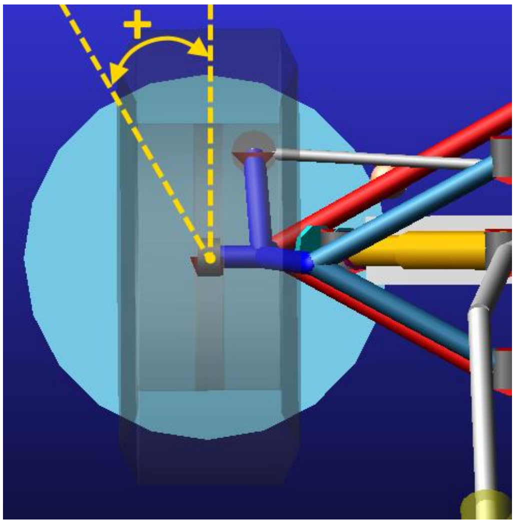

Figure 4.1: Sign convention applied for rotation

The steer angle is defined as the angle that the wheel mid-plane makes with respect to the straight wheel condition. Since the wheel can steer in two directions a sign convention is needed, in this simulation it was chosen to refer as positive the rotation towards the left, as it is highlighted in Figure 4.1. This is valid for both the steering angle and the steer angle: These two angles are not equal, due to the fact that there is a steering ratio different than one between the steering wheel and the actual tires, if the steering ratio would be exactly unitary the two angles will be the same.

The difference in angles exists because of all the elements that connect the steering wheel to the two front wheels, the most influent is the steering rack and its reduction ratio, but also all the shafts and joints between the rack and the steering wheel have an effect.

The steering test was carried out considering a full turn of the steering wheel in both directions, meaning an angle of -360° when steered towards the right, and an angle of +360° when steered in the other direction, the simulations consisted of 720 steps, this led to a simulation where a single step corresponded exactly to a steering wheel angle variation of one degree.

The objective of these simulations is to find differences among the values and the characteristics of the steer angles: This is needed not only to evaluate the differences between the various configurations, but also to have a first glance at what will result from steering ratio evaluations that will better define how each system behaves.

The steering ratio difference among variations depends only on the steer angle results, given that reduction ratio and steering wheel angle are fixed among tests, this explains why results found from steer angles draw similar conclusions to tests on steering ratio.

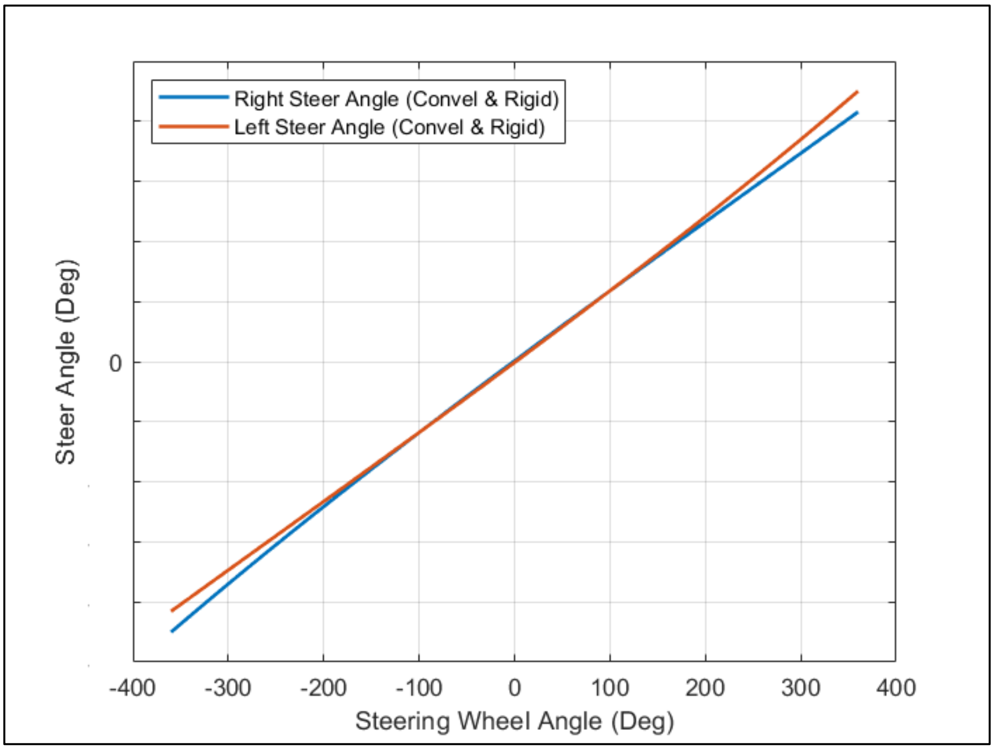

Figure 4.2: Comparison between front and right steer angle in configuration one

In Figure 4.2 it is possible to see the results from the simulation performed on right and left steer angles of the first configuration, the most ideal one with convel joints and rigid steering.

Even at first glance, it is possible to see that steering is not symmetric in the two directions, both for the right and the left wheel, towards the full rotation of the steering wheel the difference between the two angles on each side becomes clearer, by looking at the shape of the curve it is possible to see a slightly parabolic characteristic.

Near the centre of the steering wheel the differences between the two wheels are almost negligible, each wheel will steer more when it is placed on the inner side of the corner.

Configuration two, consisting of convel joints and a steering system with torsion bar, shows a similar characteristic, albeit with slightly lower steer angles.

The only difference between the two systems is the torsion bar implementation, the fact that the angles are lower when the steering is not rigid anymore is coherent with what is expected. Results from the analysis on configuration two are presented in Figure 4.3.

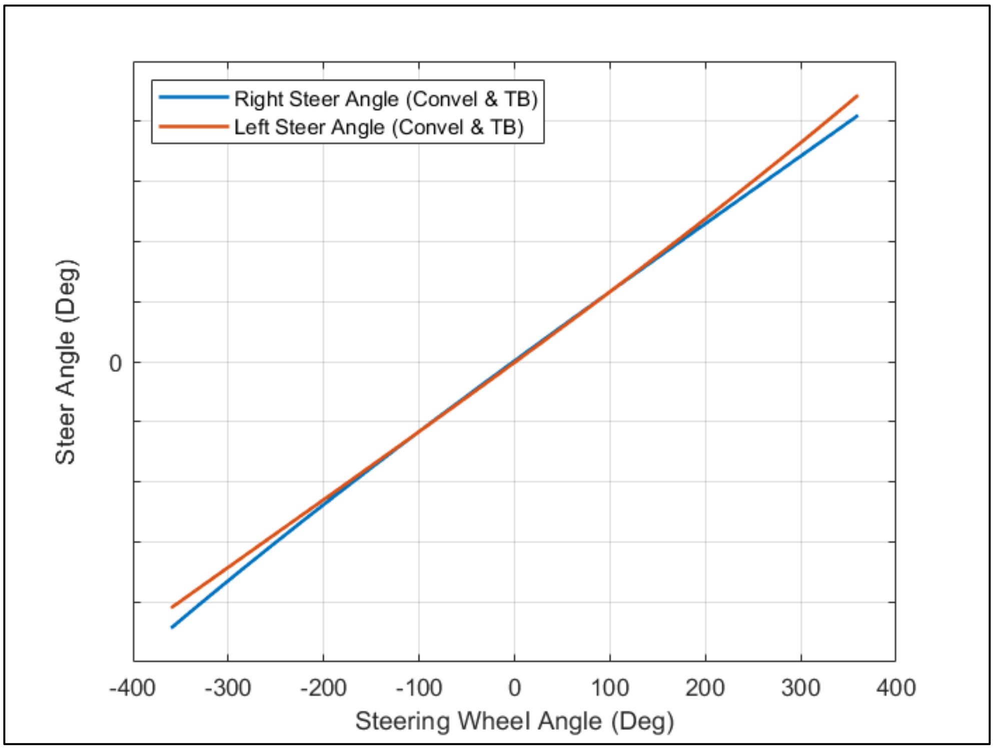

Figure 4.3: Comparison between front and right steer angle in configuration two

Configuration three is the first with cardan joints, moving away from the constant velocity joints used in the first two, this configuration uses a rigid steering system.

Towards high steering wheel angles, the system complies with the Ackermann condition, this means that the inner wheel steers more than the outer one.

The wheel’s trends of configuration three are visible in the graphs in Figure 4.4. The trend is linear throughout the steering test, instead of the slight parabolic shape of the constant velocity joint configurations, here a sightly sinusoidal characteristic is present.

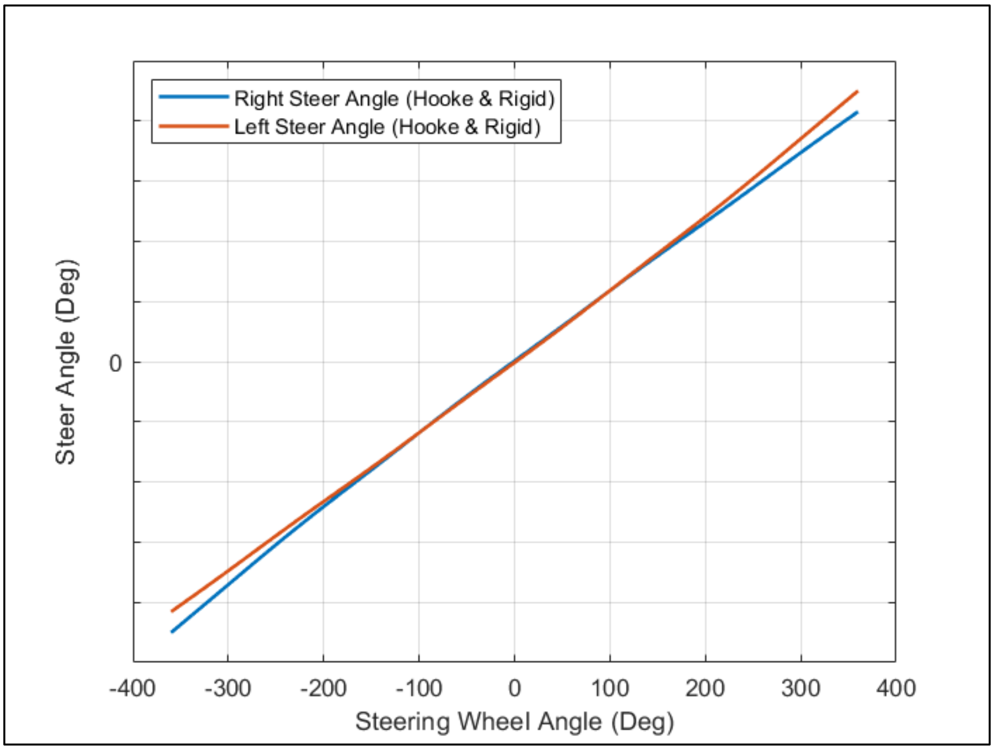

Figure 4.4: Comparison between front and right steer angle in configuration three

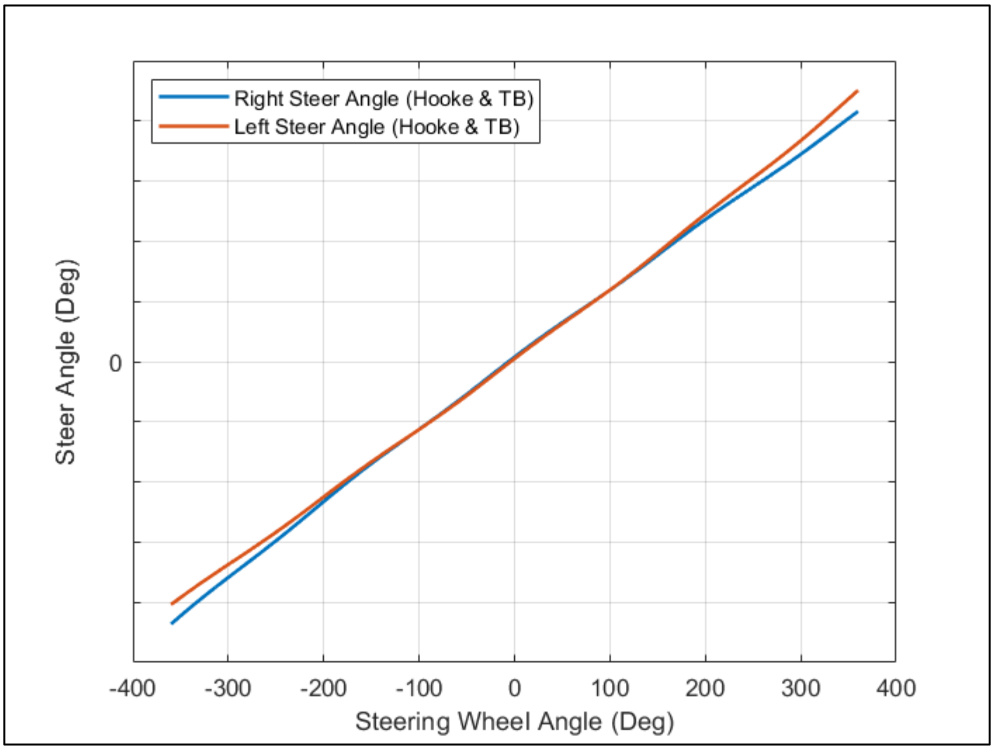

Figure 4.5: Comparison between front and right steer angle in configuration four

The last test has the system with cardan joints and torsion bar, referred as configuration four. In this simulation the trend remained like in configuration three, the values have, however, changed. The steering angles are smaller compared to those seen in the configuration without the torsion bar.

The results of configuration four are in Figure 4.5, the maximum and minimum values obtained in this simulation are like those of the first two configurations.
What was seen in the study of steering angles is confirmed by the study on the steering ratio seen from Figure 4.6 to 4.9, defined as the ratio between the steering wheel angle and the average steering angle, to have an alternative representation, and avoid the error in calculation that happens at low steering angles, the MATLAB 'diff' function was used, evaluating the ratio of the delta between steering wheel angles and the delta between steer angles, as shown in Equation 4.1. Minding that steering angle represents the angle of the steering wheel, while steer angle the one at the wheels.

$$(4.1)\ Diff = (Steering\ Angle_X - Steering\ Angle_{X-1})/(Steer\ Angle_X - Steer\ Angle_{X-1})$$

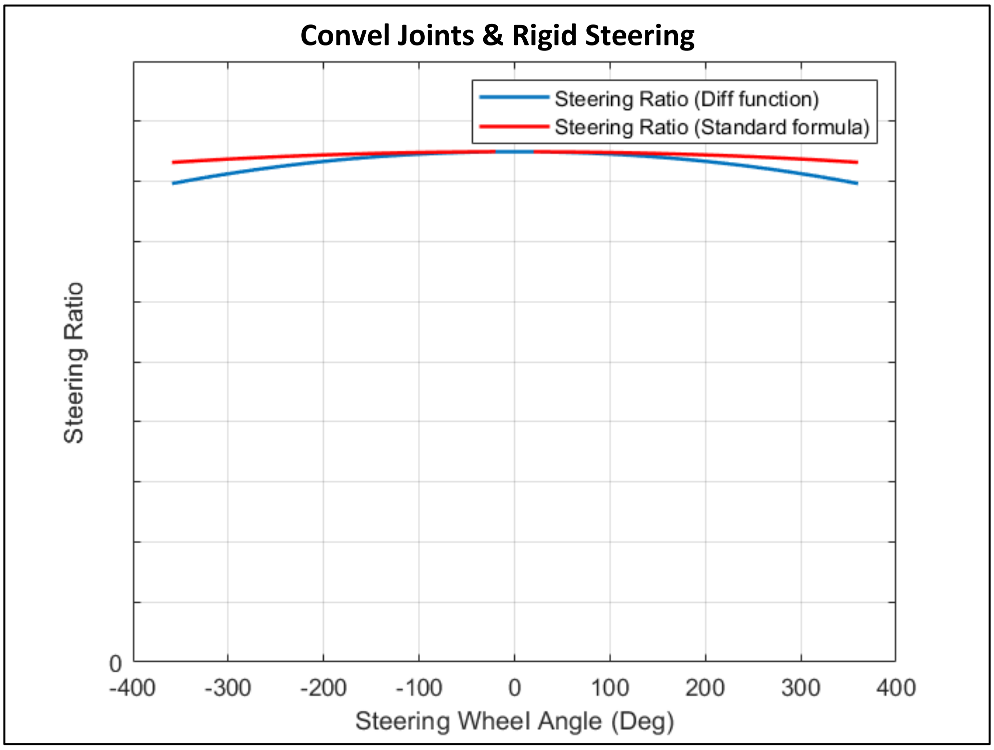

Figure 4.6: Steering ratio of configuration one, using convel joints and a rigid steering system

In the graphs shown from Figure 4.6 to 4.9 it is possible to see the comparison between the two formulations, for the overall formulation, obtained with formula 4.3, the values between -20° and 20° of steering wheel angle have been removed, to eliminate the outliers that result for small angles: In this range the steering ratio is affected by the steering wheel angle, being at the numerator when it goes near zero, it will make the steering ratio function converge to zero, as shown in Equation 4.3. This mainly explains why the 'diff' function is used.

$$(4.2)\ Mean\ steer\ angle = \frac{Right\ steer\ angle + Left\ steer\ angle}{2}$$

$$(4.3)\ Steering\ ratio = \frac{Steering\ wheel\ angle}{Mean\ steer\ angle}$$

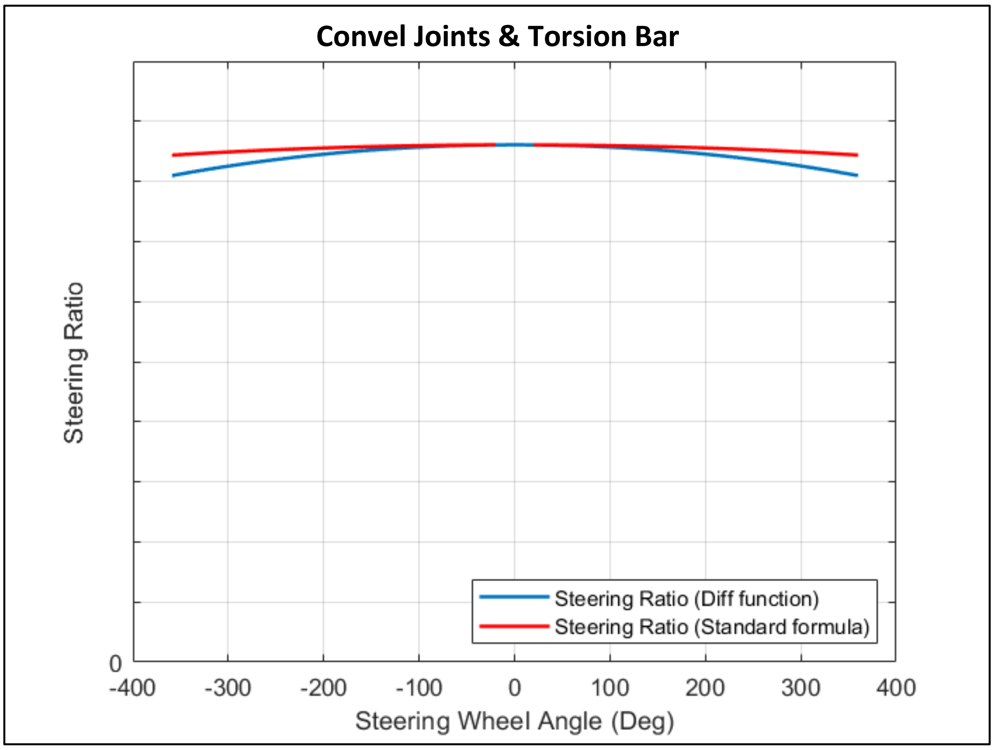

Figure 4.7: Steering ratio of configuration two, using convel joints and a torsion bar

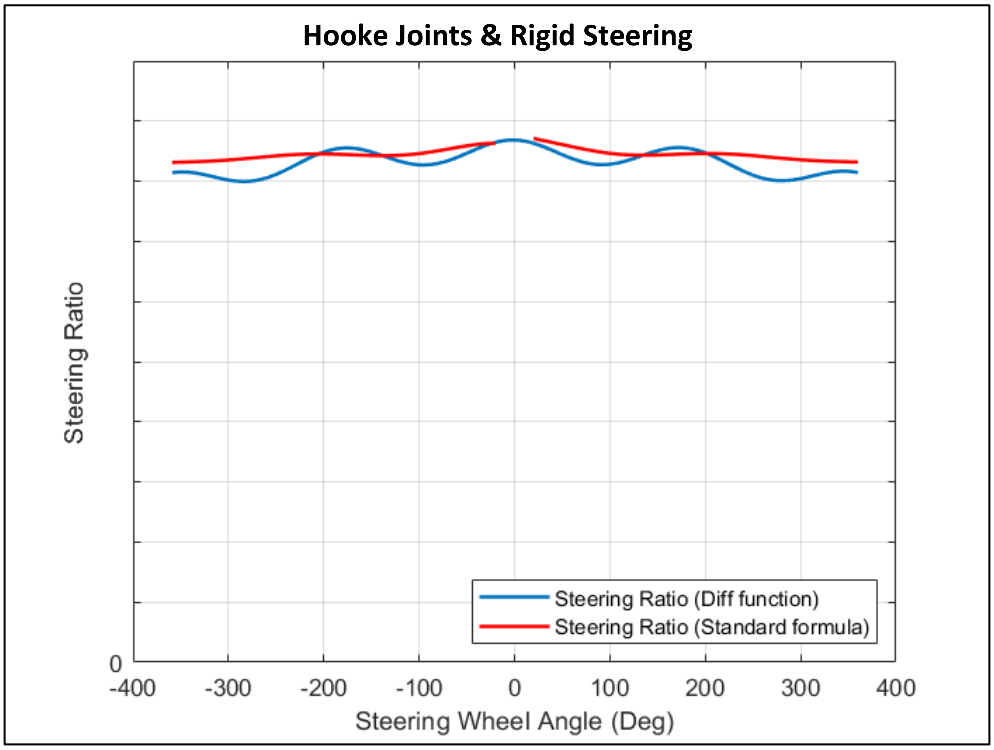

Figure 4.8: Steering ratio of configuration three, that uses Hooke joints and a rigid system

The confirmation of the trends seen in the study on the steer angle is visible from the trends of the steering ratios, it is possible to see two widely different curves between the configurations with universal joints and the configurations with constant velocity joints.
The difference in shape between different formulations is marginal, the ‘diff’ formulation allows for a better evaluation near the centre, the standard formulation may be more accurate as the steering angles increases.
The difference in shape is due to the motion irregularity that will be induced by Cardan joints. For what concerns the comparison between the two methods it is possible to understand that the ‘diff’ function help defining the steering ratio at low angles but may amplify the fluctuations due to irregularity, the standard formulation is reliable as the steering angle gets higher.
The configurations with constant velocity joints will show small differences between the two formulations, the utilization of the ‘diff’ function is not required by these systems, because results are reliable after just a small range of small steering angles.
The systems with Hooke joints show higher differences between the two methods, especially when the torsion bar is implemented, for that case the removal of angles from -20° to 20° is not enough. Results like these beneficiates from the MATLAB function, because data starts to be reliable only after 100° circa of steering angle, leaving an important portion of the analysis behind, this shows that the function may help in some cases, while in others is not important to obtain reliable results.

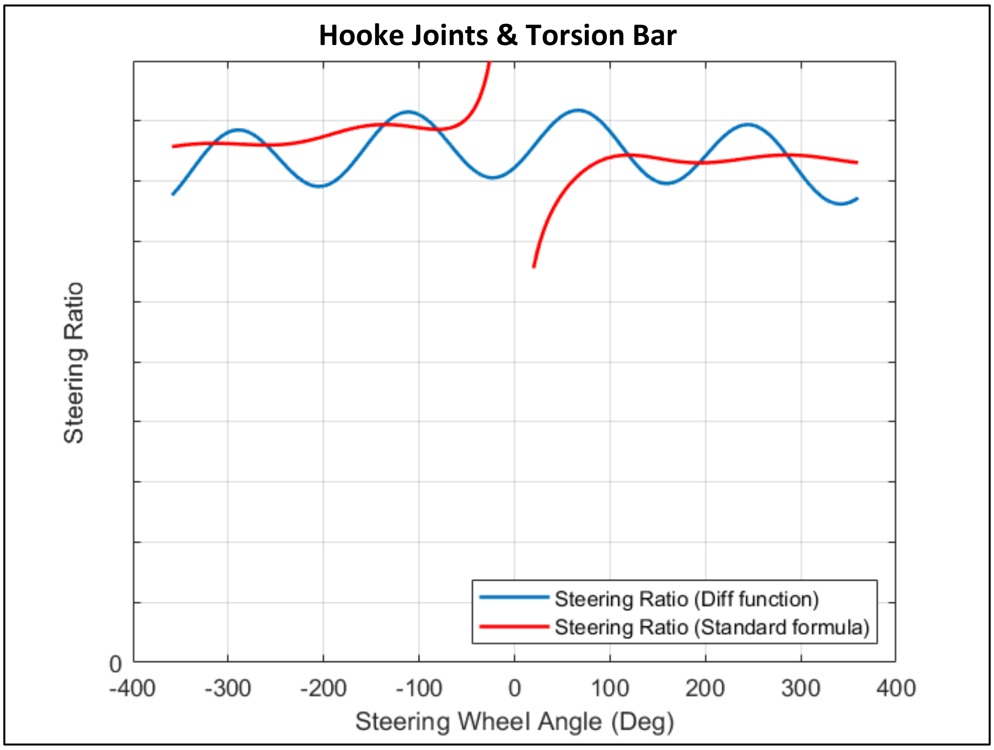

Figure 4.9: Steering ratio of configuration four, using Hooke joints and a torsion bar

4.2 Comparison between the different configurations

To have a further comparison between the different configurations, the Ackermann error is calculated, the results are visible in Figure 4.10 and 4.11, respectively for each of the two wheels.

By looking at the graphs it is possible to see that the Ackermann error is null when the wheel considered in the graph is on the inner side of the corner. For the right wheel the error will be null for negative steering angles and vice versa, this is not an error in calculation but it is something that is characteristic of Adams Car, the software uses the inside wheel to compute the turn center, this leads to a null error when the analyzed wheel is on the inside [4].

It is possible to see that, on the left side, the configuration with Hooke joints and torsion bar shows the lowest error, while the configuration that uses Hooke joints and rigid steering shows the highest error. The right wheel shows closer results between the configurations, the highest error will be reached by the configuration that presents Hooke joints and a torsion bar.

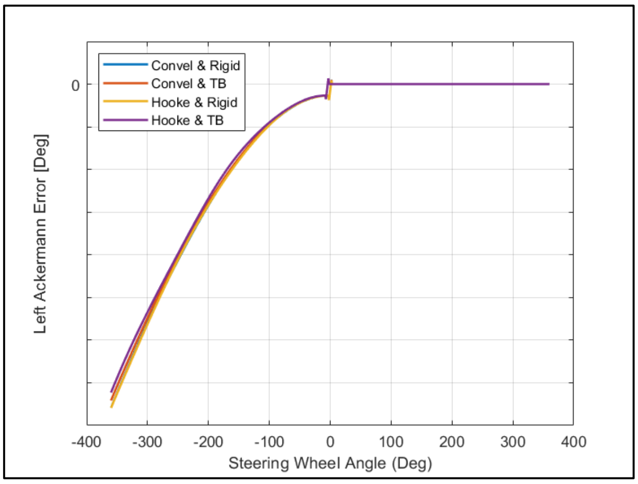

Figure 4.10: Left wheel Ackermann error

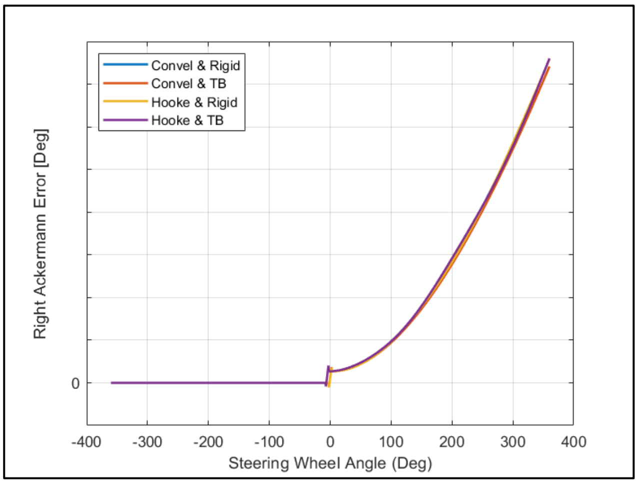

Figure 4.11: Right wheel Ackermann error

By looking at Figure 4.12 and 4.13 the differences between the configurations are very small, this is interesting being that configurations employ different elements and the steering system is also different in terms of rigidity between configurations.

Differences in steer angles are only noticeable towards high steering angles, making the difference relevant mainly in parking manoeuvers, for low steering angles the configurations in study will behave almost in the same way.

Highest differences between simulations are experienced for negative steering angles, for both wheels, for the left and right wheel the system that uses Hooke joints and a rigid steering shows the highest steer angle when the steering wheel is rotated towards negative angles, for positive angles differences between configurations are smaller.

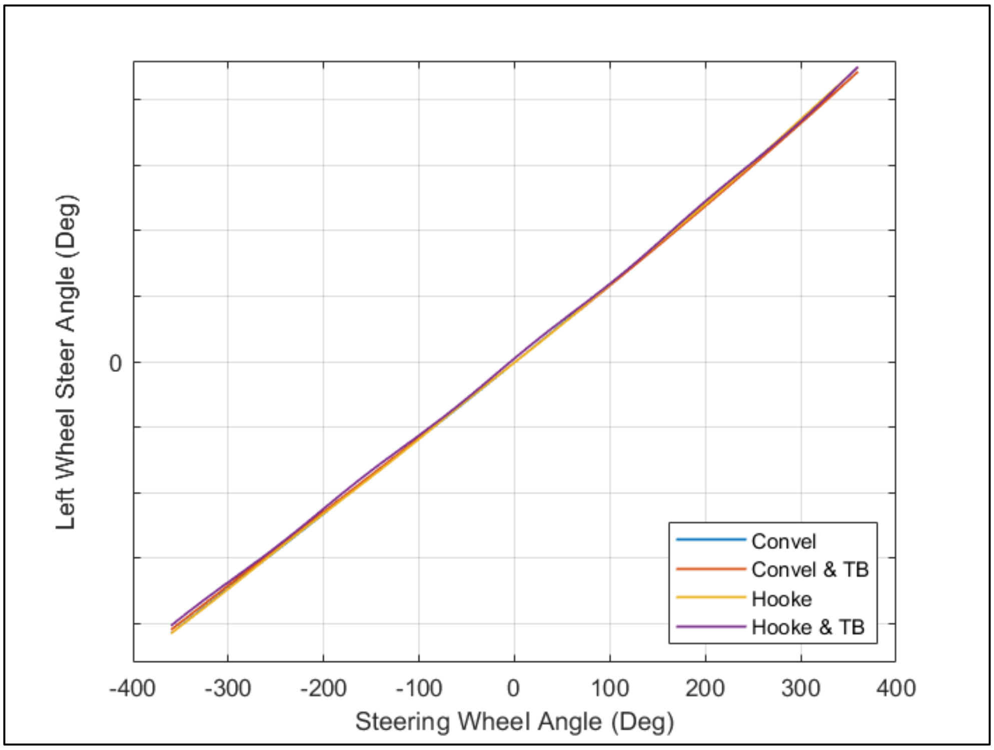

Figure 4.12: Comparison between right steer angle of all four configurations

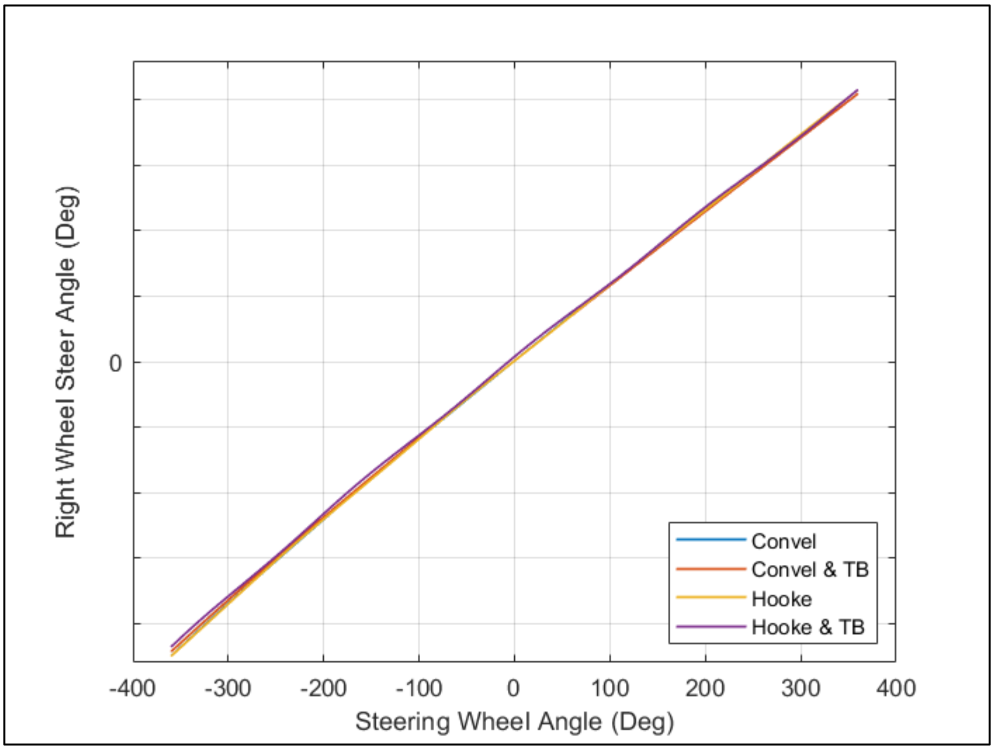

Figure 4.13:: Comparison between left steer angle of all four configurations

In Figure 4.14 and 4.15 it is possible to see a comparison in steering ratio between configurations with the same joint, leading to a comparison where the only difference comes from the selection of a rigid system or not, the steering ratio is higher for the compliant system for both types of joint.

The differences in value reflect what resulted from the simulations performed on paragraph 4.1 for the steer angles, a result like this is coherent with what is expected, since the employment of a torsion bar reduced the steer angles obtained.

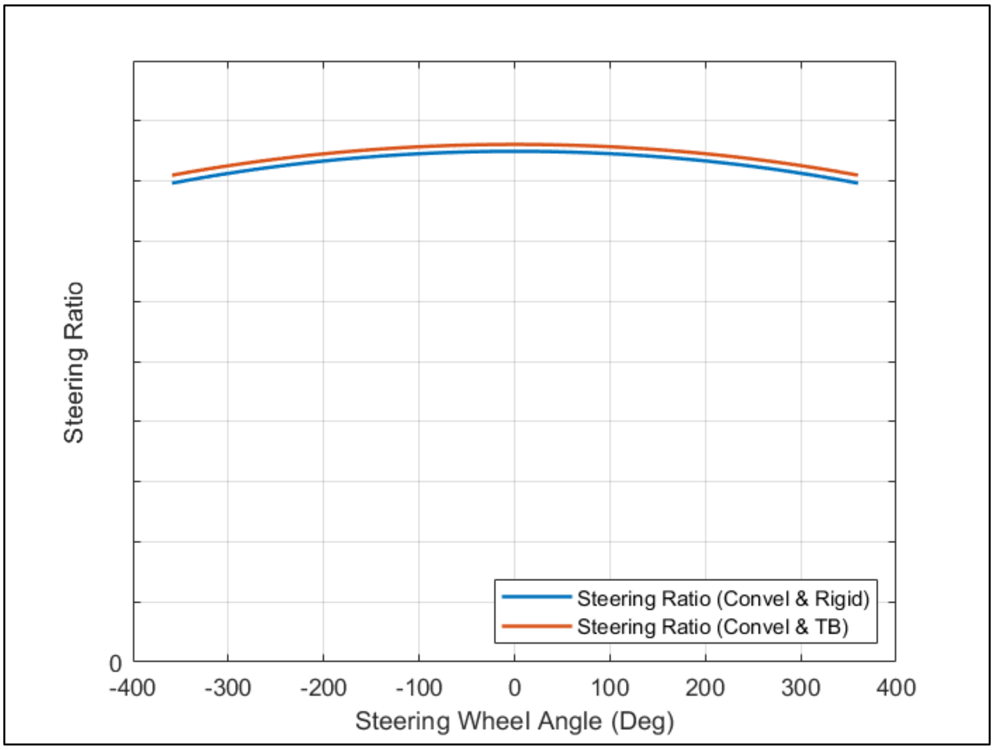

Figure 4.14: Comparison between steering ratios of the configurations with constant velocity joints

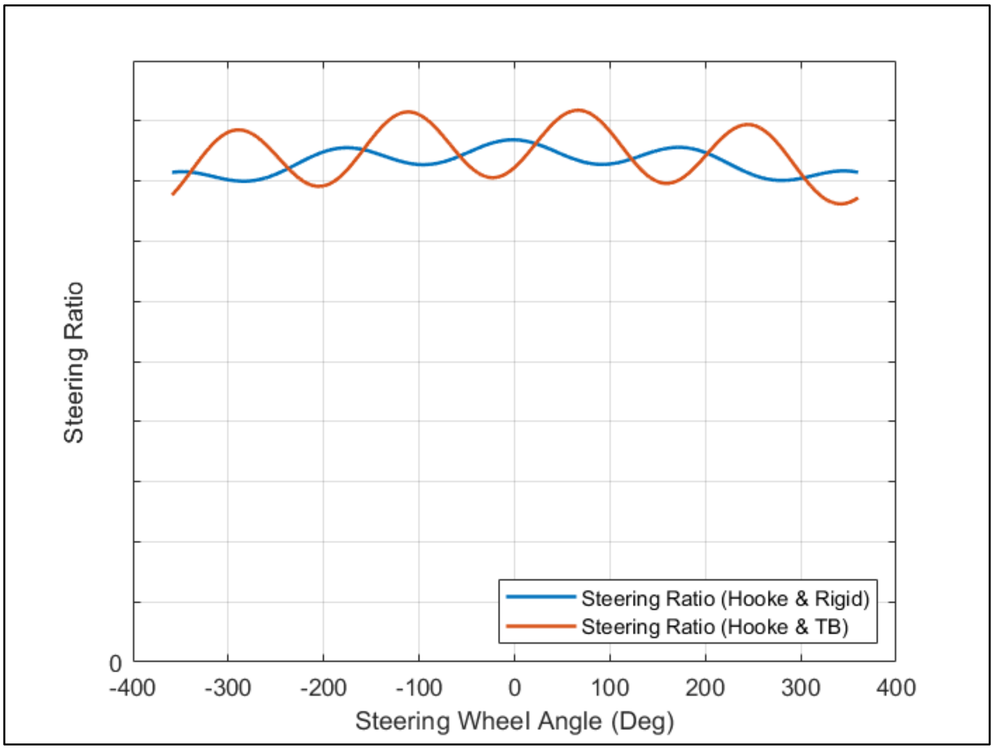

Figure 4.15: Comparison between steering ratio of the configurations with universal joints

The fact that a torsion bar is implemented will introduce another element between the steering wheel and the wheels, as it was found before, each element that is not rigid will create some variability in the relationship between angles at input and output, like what happens when adding up efficiencies in a mechanical system made of many components. Largest difference is seen in term of behaviour between the two joints used.

In the case of universal joints there is a clear sinusoidal behaviour in the steering ratio: This mainly comes from the fact that the system is made up of concurrent Hooke joints. As it was explained in paragraph 2.2.2: The angular speed that is imposed at input will not be exactly the same at output but will have some degree of irregularity, represented by the amplitude of a sinusoid around the input value. The constant velocity joint will, by definition, have the same speed between the two elements that are connected and so no fluctuations are shown.

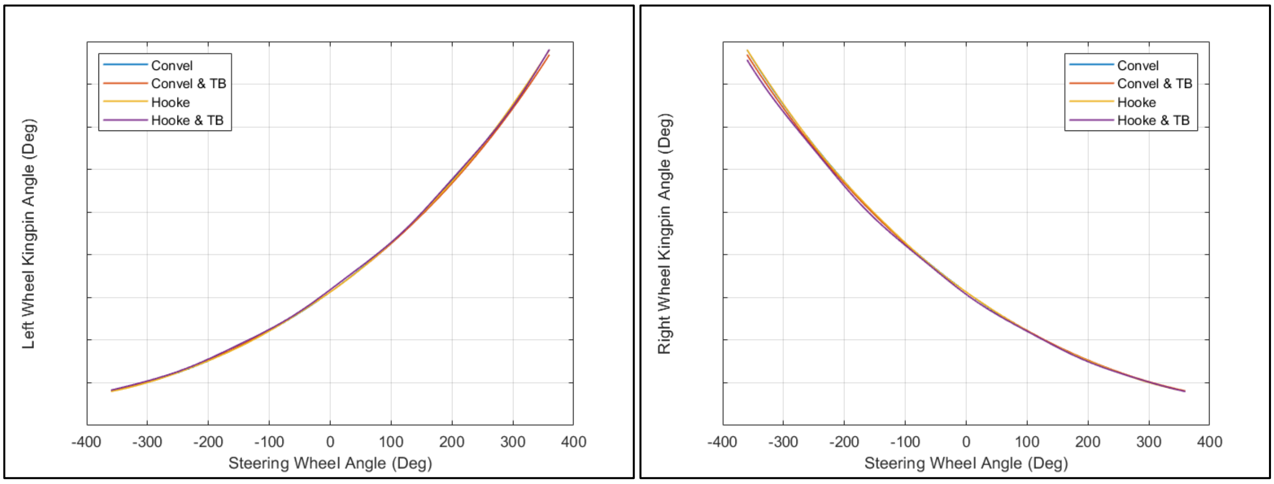

Figure 4.16: Kingpin angle evolution between the different configurations

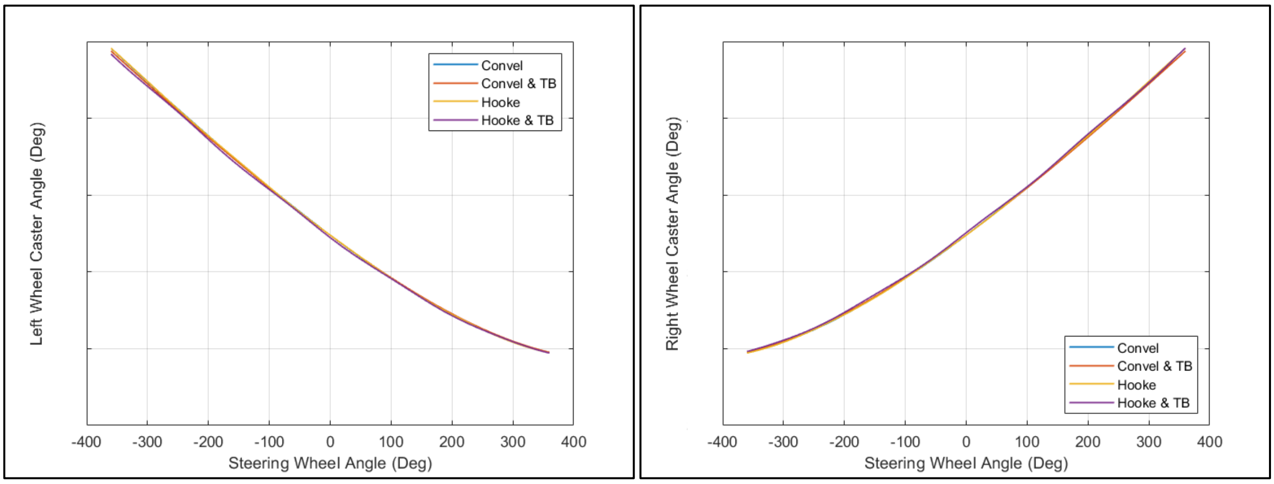

Figure 4.17: Caster angle evolution between the different configurations

After having analysed the change in steer angle and steering ratio, it was deemed useful to evaluate how other angles that define the steering axis change during this test, an evaluation was carried out on Kingpin and Caster angle as well as on the arms related to them: Scrub radius & Caster moment arm.

Concerning angles, as it is possible to see in Figure 4.16 and 4.17, the right and left wheel have similar characteristics, albeit specular, like what was seen in previous comparisons.

Each characteristic shows a plateau, caster angle will plateau towards positive steering angles for the left and vice versa for the right, kingpin angle will react in the opposite way. This means that these parameters will change almost linearly up to a certain point where they will be more constant. This condition is met at high steering angles that will largely change the suspension geometry. Differences between configurations are appreciable only at high values of caster or kingpin angle, the rigid steering with universal joints will show the highest caster angle on the left wheel and the highest kingpin angle on the right wheel, among all the different configurations created.

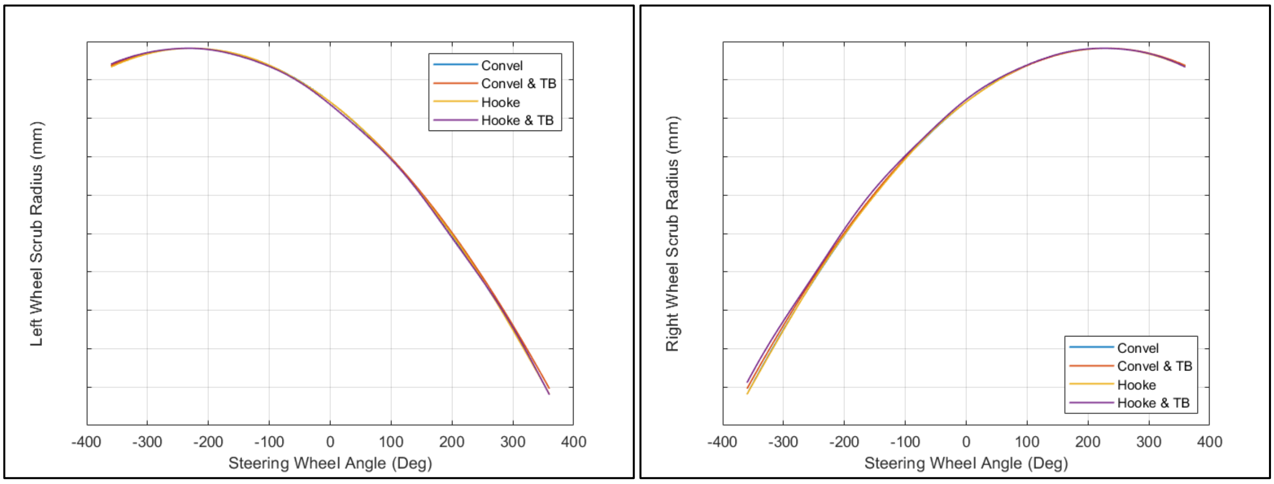

Figure 4.18:Scrub radius evolution between the different configurations

Scrub radius will instead grow up to a maximum at 200° of steering wheel angle circa and then start to fall back to lower values, this point is equivalent to the point at which the plateau starts to form in the graphs related to the two angles, the characteristic is shown in Figure 4.18.

Caster moment arm is showed for both wheels in Figure 4.19, this parameter will be almost symmetrical between the two wheels, this parameter evolves symmetrically. If its average is plotted like in Figure 4.20 for the configuration with convel joints and rigid steering, it is possible to see that the average value is constant, one wheel compensates the other keeping the average equal to the value that was found when wheels were not turned, no appreciable variation is shown in caster moment arm, the configuration are very similar, especially in the middle range of steering angles.

From this analysis it was found that different combinations of joints and steering systems delivered similar results, this is not something that is unrealistic, the steering systems and suspension are equal in terms of geometry, and most importantly, the reduction ratio of the steering rack reduction ratio is the same between all the configurations, what is found is how the shape of the curve changes when joints that will show a degree of irregularity such as Hooke joints are used.

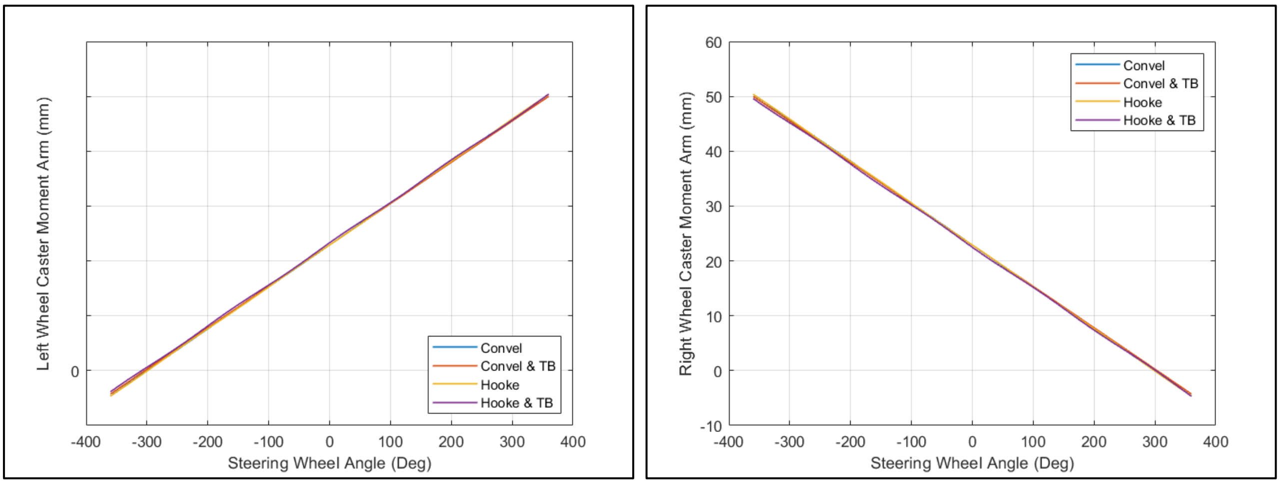

Figure 4.19: Caster moment arm on the left and right wheel

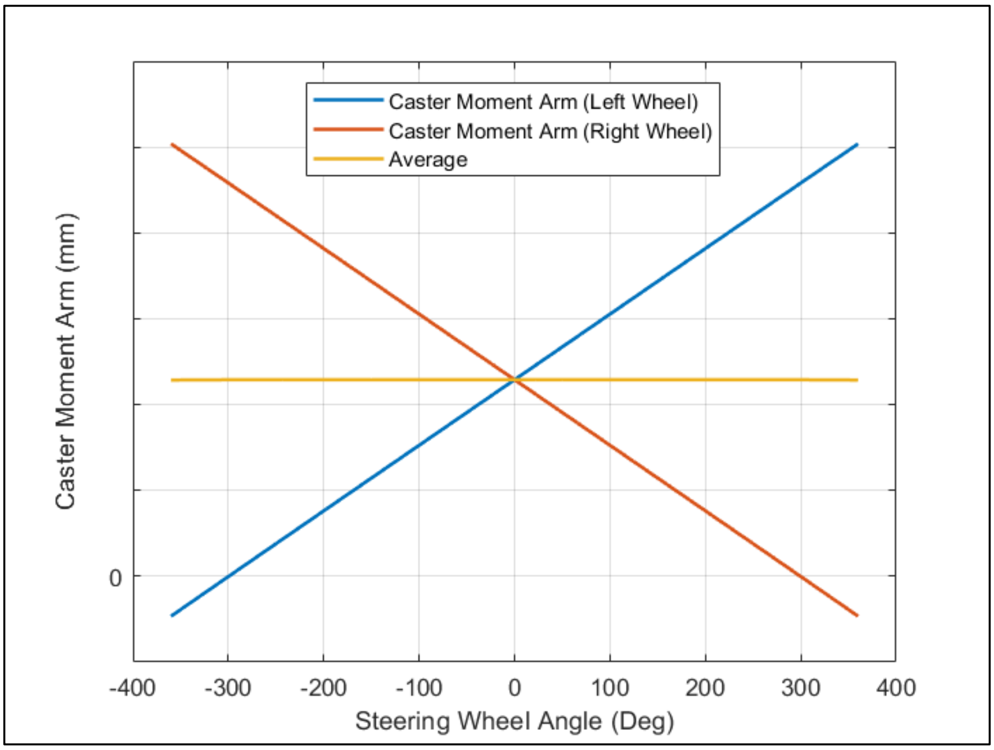

Figure 4.20: Figure showing the almost perfect symmetry between the two wheels for the caster moment arm

Figure 4.21 shows the variation in toe angle as the steering wheel angle changes, this parameter is strongly related to the steer angle and follows a similar pattern, in this case the convention of sign is different than that of steer angle, in static toe definition the wheels will point towards the inner part of the vehicle when the toe angle is positive (toe-in) or towards the outer part of the vehicle when the angle is negative (toe-out). When wheels are steered one will point towards the outer part of the vehicle while the other will point towards the inner part of it, hence the difference in sign is explained.

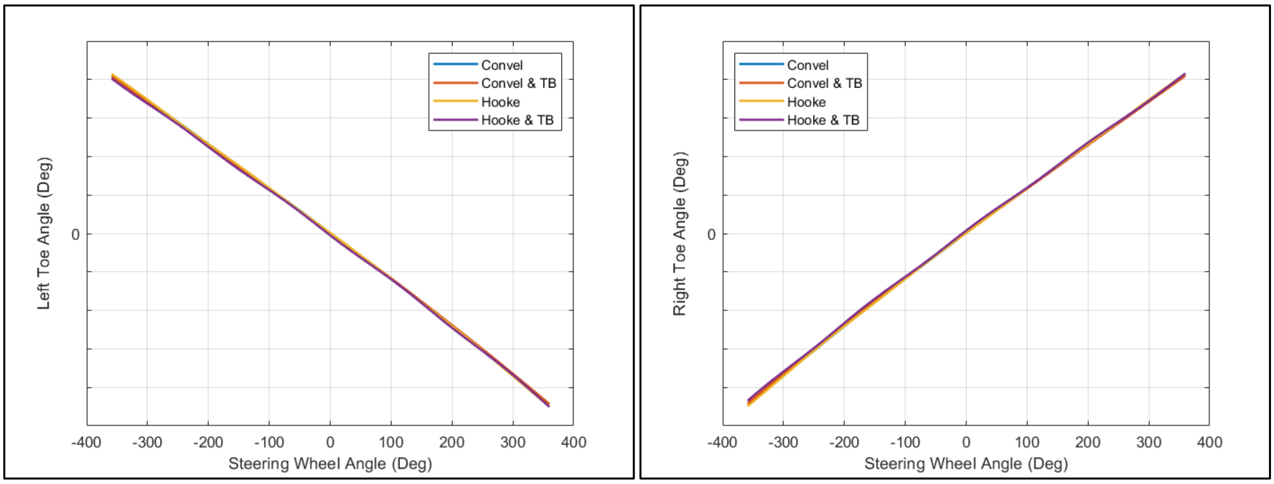

Figure 4.21: Toe Angle variation with steering wheel angle

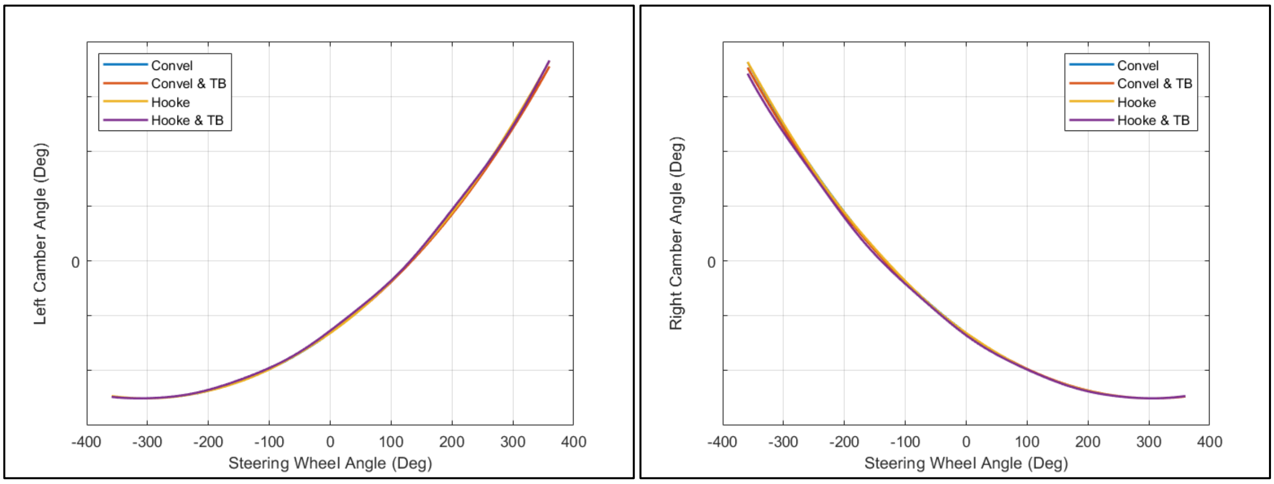

Figure 4.22: Camber Angle variation with steering wheel angle

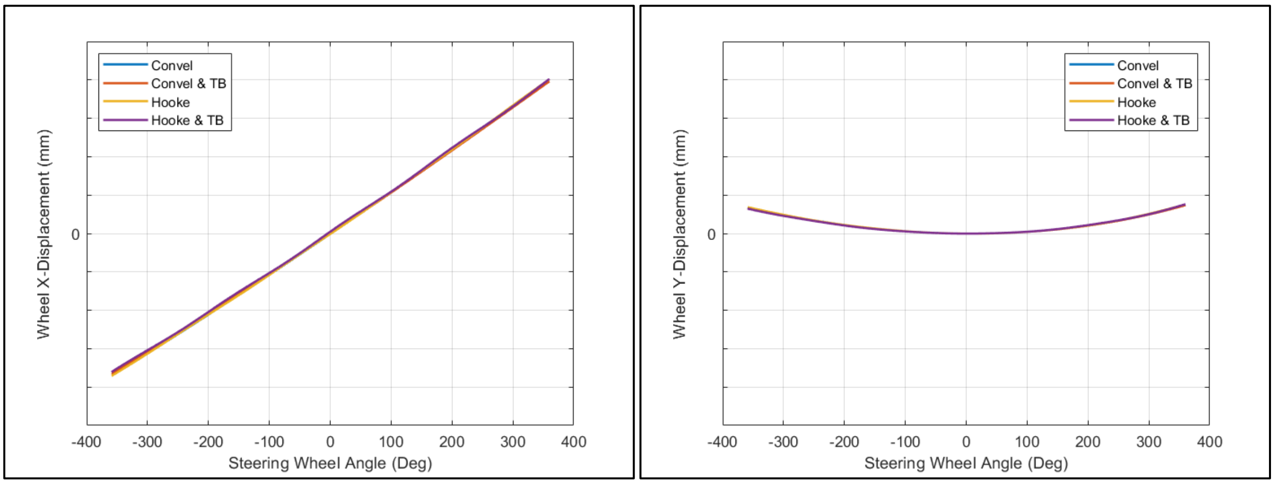

Figure 4.23: Wheel displacements as steering angle varies

Camber angle variations are found in Figure 4.22, for the inner wheel camber will move towards more positive angles, meaning that the upper part of the wheel is in an outer position compared to the lower part of it, the opposite effect will happen when the interested wheel is on the outer side.

In Figure 4.23 it is possible to appreciate variation in displacement for the two wheels of the front axle.

Displacement along the normal direction Z is not showed because variation is negligible.

The variation along the X-axis represents the variation along the axis that defines the length of the vehicle and is the most relevant. Variation along the Y-axis represents variation in track and are less noticeable.

4.3 Torque and torsion angle through the torsion bar

In Figures 4.24 and 4.25, it is possible to see the characteristic of torsion and torque seen from the torsion bar in the configurations where it is present. Values found in configuration four are almost identical between the two configurations, which is expected from the fact that both torsion bars were created using the same characteristic and the only difference between the two systems comes from the different joints used.

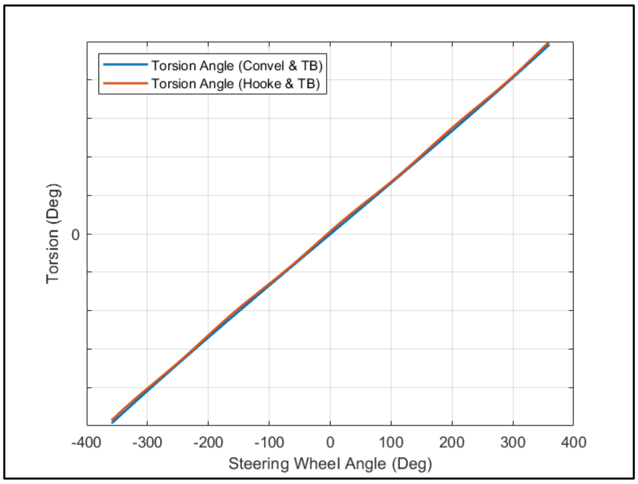

Figure 4.24: Torsion angle characteristic

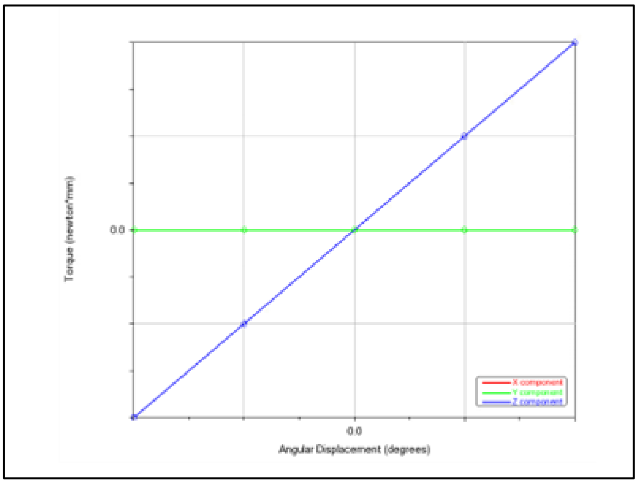

Figure 4.25: Torque through the torsion bar

Besides values it is relevant to understand how torque and torsion vary with steering angles, torsion will have a linear relationship with steering wheel angle, stiffness is defined in Deg/mm and follows a linear characteristic, the value of stiffness is set as constant and defines the linear characteristic with a curve that shows the same sign between torque and torsion angular displacement, due to the fact that stiffness is defined as a positive parameter.

Torque is defined only on the Z-component, this is expected by the fact that only torsion has to be defined, leaving the other rotations null, the axis around which torsion is created is the Z-axis, this explains the torque characteristic.

4.4 Evaluation of motion irregularity

In the second part of the analysis, through the variation of the phase angles of the joints, the study, through phase angle variation, evaluates the possibility of reducing the motion irregularity of the steering system.

All the simulations were performed on the steering system with hooke joints and rigid steering, this was done because in Adams Car it is easier to create the element that computes the angular velocity on a simple shaft with no torsion bar included, given the fact that all the joints are placed upstream of the pinion a condition like this can be considered reliable enough.

The analysis started from the design condition of the system and the aligned condition, the design condition shows the phase angle set in the same values used by design, while the aligned condition has all the joints aligned one after the other, like it was explained in paragraph 3.1.

Equal variations were analyzed on each joint starting from the aligned condition to evaluate which of the three joints was most relevant for a study on uniformity, the configurations are shown in Table 4.2, a variation of 90° with respect to the aligned condition was chosen to evaluate how each cardan joint reacted.

#	Test	Description
D	**Design**	Configuration that uses phase angles in design configuration
A	**Aligned**	All the cardan joints are aligned one after the other
1	**90° Rotation #1**	Upper cardan joint shifted of 90° from aligned condition
2	**90° Rotation #2**	Middle cardan joint shifted of 90° from aligned condition
3	**90° Rotation #3**	Lower cardan joint shifted of 90° from aligned condition
4	**90° Rotation #4**	Second and third cardan joint shifted of 90° from aligned condition
5	**Design Improvement**	Lower cardan joint shifted like in case three, the other two like design

Table 4.2: Study cases considered, each defining a modification of the phase angles

The irregularity of motion can be evaluated as the amplitude of the sinusoid of the angular velocity at the system output, in this case the output is the pinion that connects the third shaft to the rack.

In Figure 4.26 it is possible to see, graphically, how the irregularity is defined, when doing an analysis like this an acceptable value of irregularity is set as an objective, each steering system will usually show a degree of fluctuation. It is important to minimize it as much as possible, considering mechanical and geometric constraints of the system, the irregularity was analyzed between the first shaft and the pinion that connects the column to the rack.

An angular velocity of 100 deg/s was imposed to the system through an input function placed by

Adams Car in the first shaft through a 'Joint Motion' element, the angular velocity at the output was then evaluated.

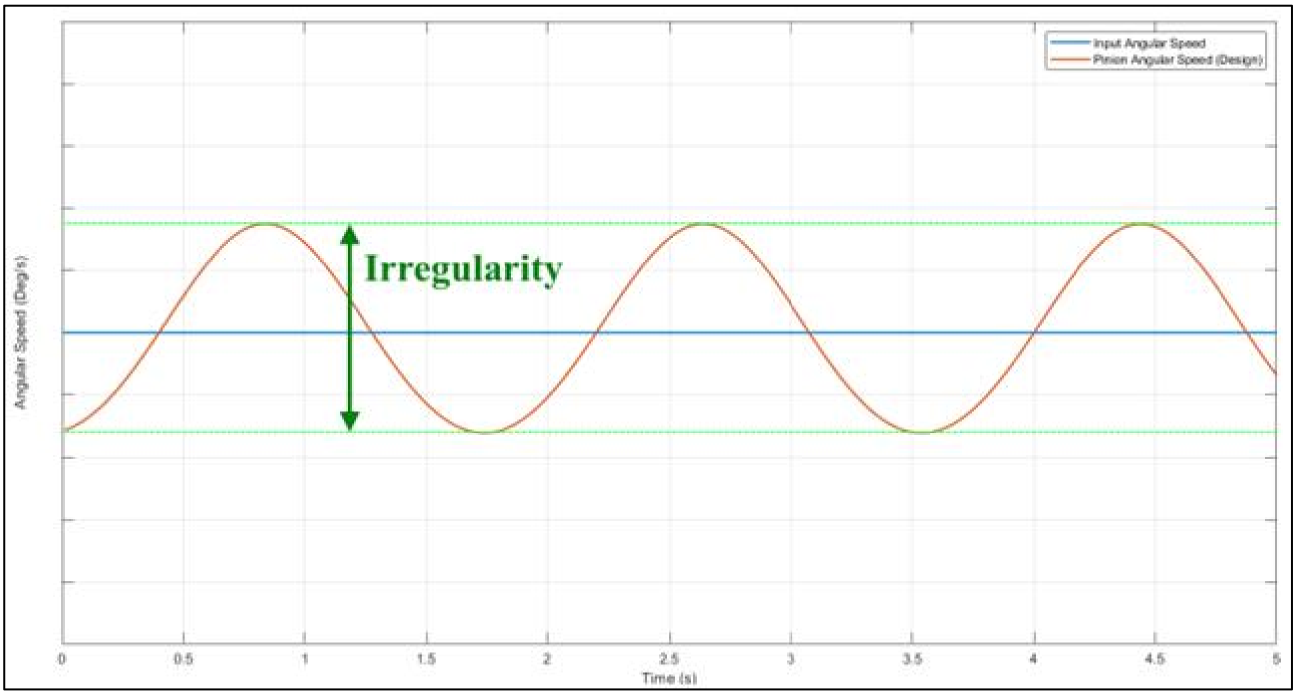

Figure 4.26: Comparison between the input speed and the design condition

The cases analyzed are those shown in Table 4.2, in this case the design condition was already good in terms of irregularity, being already in the ballpark of the limits set by the manufacturer.

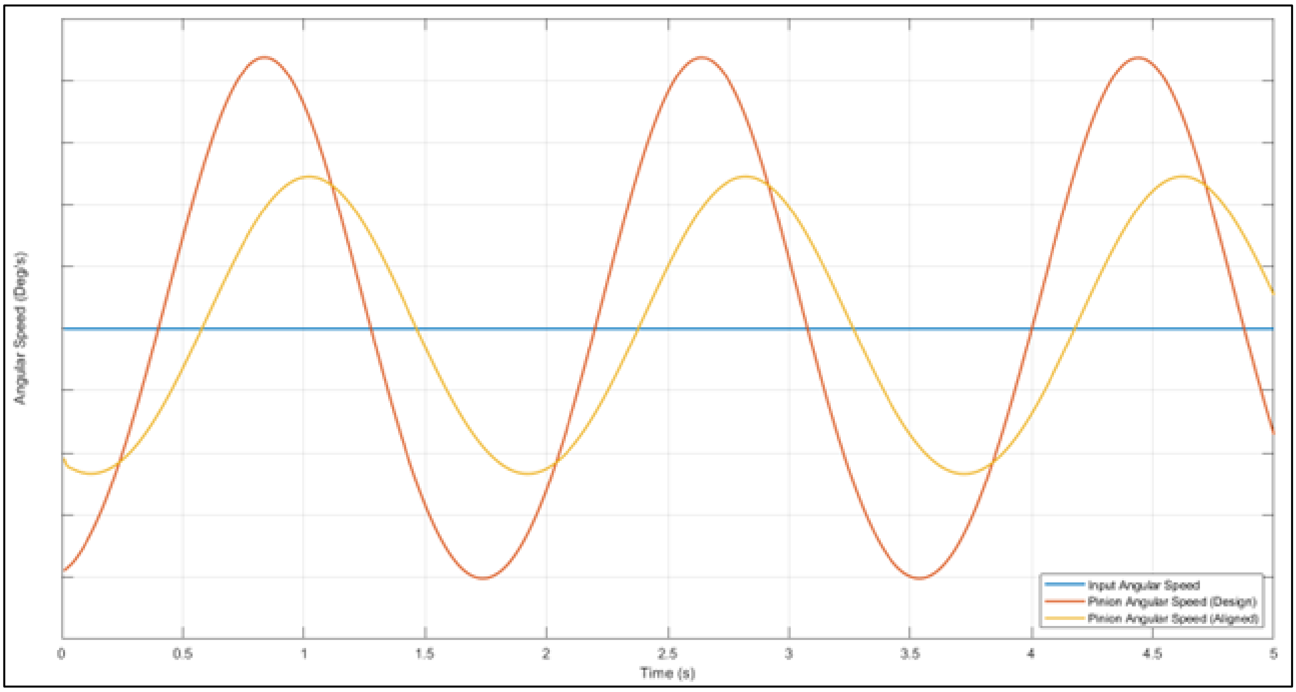

Figure 4.27: Comparison between design case and aligned case

At this point the configuration with all the joints aligned was analyzed, as it is possible to see in Figure 4.27, this configuration showed good improvements compared to the design condition. The total irregularity is well below the objective set by the manufacturer, a slight phase shift is also present compared to the design condition, the peaks of the sinusoid are moved slightly forward.
To assess which of the three joints has the greatest effect on the irregularity a rotation of 90° was imposed on each of the joints keeping the other two in the aligned condition.
In Figure 4.28 it is possible to see all the three shifts on the same graph, all the shifts resulted in a worsening of the irregularity compared to the aligned condition, but the amplitudes of each sinusoid were different, the irregularity increased as the joint shifted was placed further from the pinion pivot point, this meant that the first test where the upper joint was shifted of 90° gave the worst results in term of irregularity, while the rotation of the lower joint brought less irregularity to the system, a condition that is still worse than the design one but not so far from it.
From this analysis it was clear that acting on the lower joint is easier, because shifts in phase angle will bring moderate changes in irregularity compared to the other two joints, this preliminary study aimed at finding the relevance to irregularity for each joint and it is clear that the further the joint is from the pivot, the more irregularity will be affected.

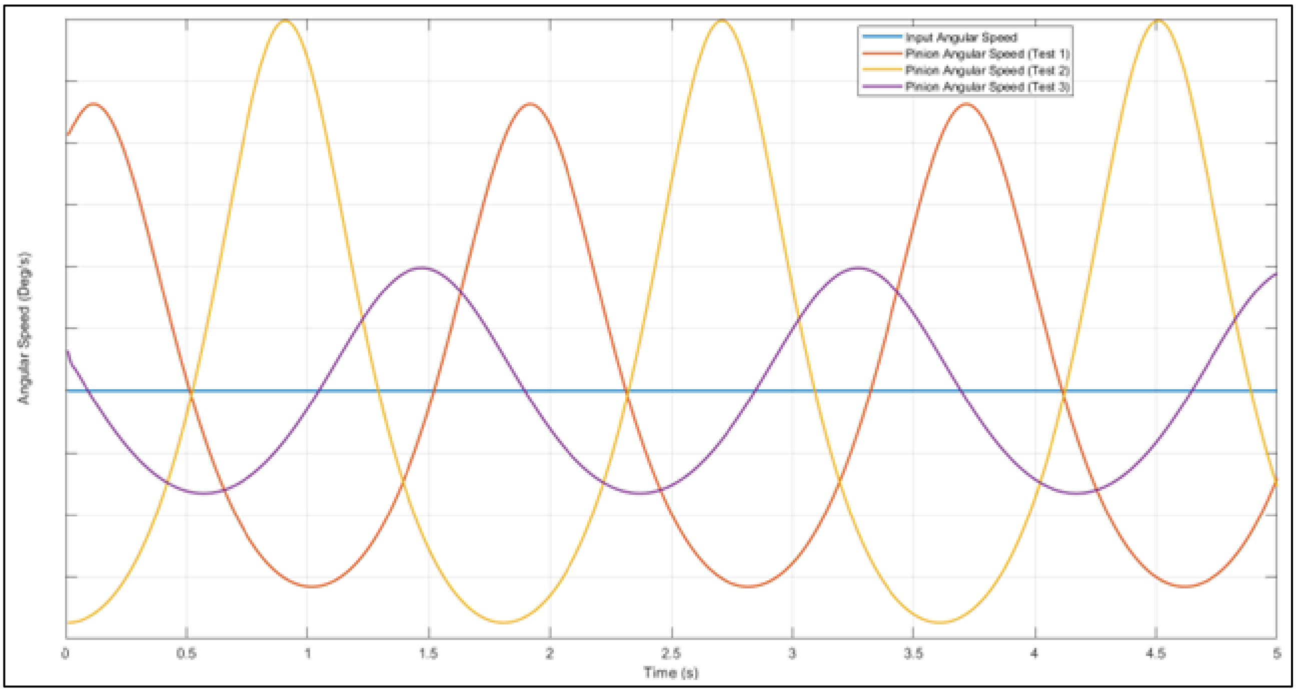

Figure 4.28: Comparison between the three shifts of 90 degrees performed on the aligned case

After the results from the first three tests, it was decided to perform a fourth test, this test consisted of a shift of the second and third joints, while the upper joint is kept in the aligned position.
In term of irregularity this test did not give any good results, as it is possible to see in Figure 4.29,

but a confirmation of what was found in the former tests was found, the shape of the curve is very similar in terms of amplitude to the one of the second test, with a phase shift of circa 90° compared to that curve, this result basically tells that in this case the position of the lower joint is not influent enough on irregularity, it just acts on the phase shift of the sinusoid.

From these results it is possible to understand that a proper optimization is required to find the best values in term of phase angles for what concerns the system irregularity.

If possible, from geometric and functional constraints of the system, adopting the aligned condition would improve the system by a good margin, to evaluate if what was found in these tests could bring a first improvement to the behavior, a last test was performed as can be seen in Figure 4.30.

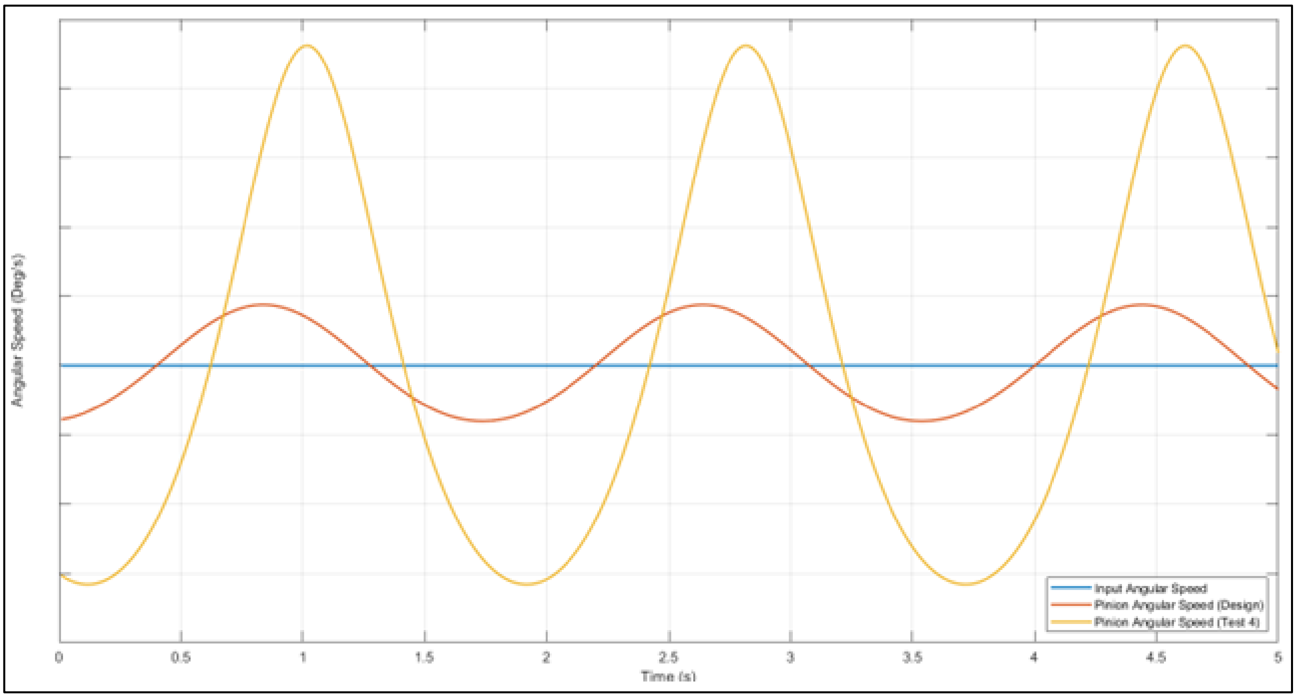

Figure 4.29: Evaluation of test four

This test is referred as improvement condition, a simple modification was performed to the steering system, the upper and middle joint were kept equal to the design condition, while the lower joint was set to have the same angle that it would have in the aligned condition: The difference in value between these two angles is small, but an improvement was found.

This test was performed in this way because this modification is the easiest to make, the angles between the two conditions are very close, and the angles of the first two joints were left at the design values, avoiding worsening of the system characteristics due to the high sensitivity to irregularity of those joints, this analysis cannot be referred as an optimization, but it confirms what was found in previous tests.

After all these evaluations on motion irregularity it is important to contextualize these results, irregularity is relevant in having a good relationship between the steering wheel angle and the steer angle, expressed in this case by the steering ratios, but it is not the only objective in a steering system, it is also important to have a symmetric ratio in some cases, this enables the steering motion to be equal between left and right, which in many cases is a feature wanted by users and manufacturers.

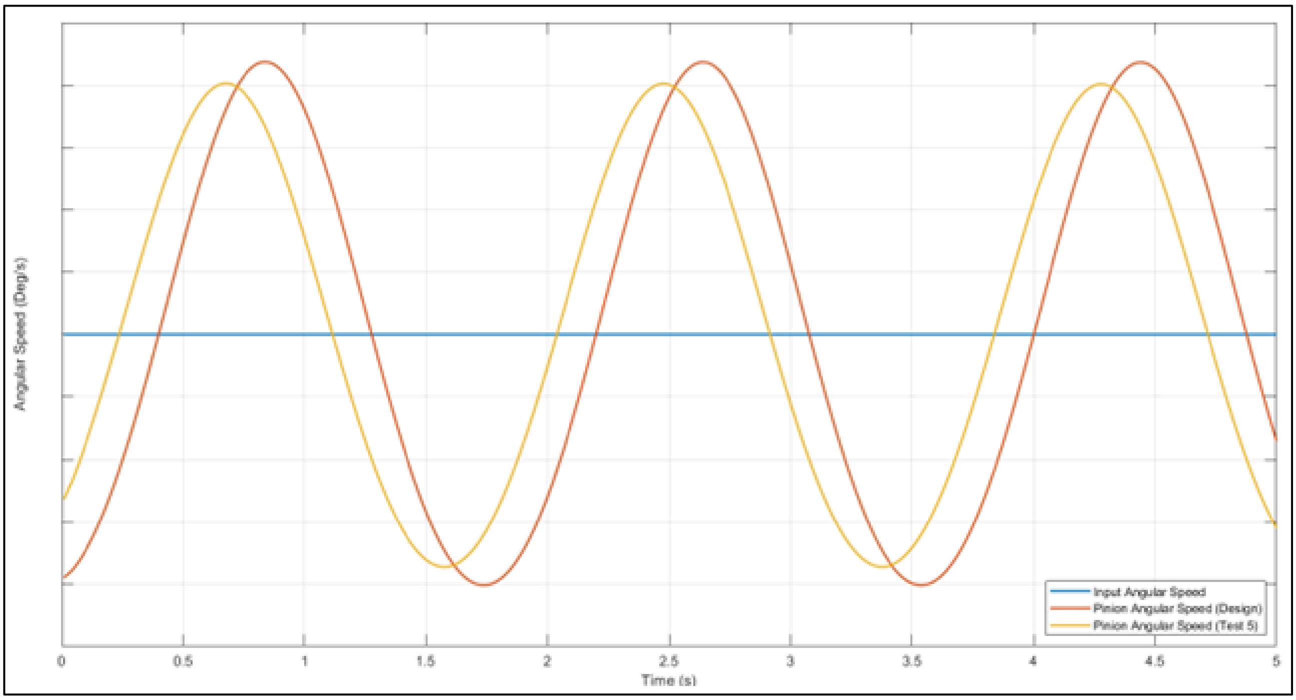

Figure 4.30: Comparison between the design condition and the improved condition

4.5 Optimization of phase angles in relation to motion irregularity

The study performed in paragraph 4.4 can be seen as a preliminary analysis on how the phase angles affect the movement of the steering assembly and its irregularity.

An approach of optimization can improve the system through a thoughtful analysis on the system behaviour, thankfully the software used is connected to a design of experiment software called Adams Insight, this additional software can evaluate how the modification of given parameters from a simulation can affect the parameter result set as objective.

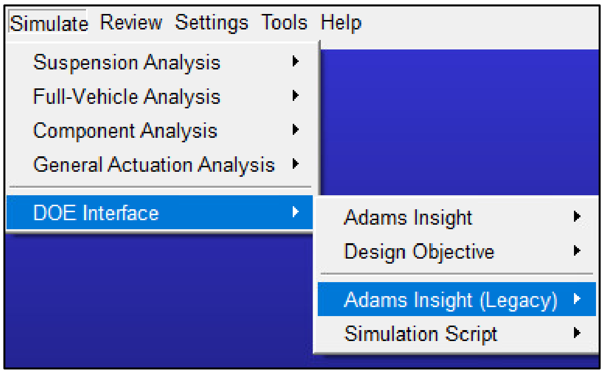

Figure 4.31: DOE Interface different windows to be selected

The Adams Insight tool from MSC Software is an external application from the Adams Car tool, in order to let the software free to perform its optimization, it is first needed to run a simulation in Adams Car, in this case the simulation that was ran is the same used to compute irregularities in paragraph 4.4, the simulation was set to run with phase angles in the design condition.
After the simulation, the objective of the experiment is decided under the DOE Interface, opened as shown in Figure 4.31, it is possible to set the design objective, the objective has to be set among all the different outputs of the system, in this case the objective was set as the RMS value of the pinion angular speed.
At this point, the work on Adams Car is complete, from the software it is possible to move to Adams Insight directly, after having decided an experiment file name, in Adams Insight the software imports all the outputs of the simulation and the particular objective that was set in Adams Car.
From this point it is possible to set not only the desired parameters that the simulation aims to optimize but also their settings.
In this specific study the parameters that are to be optimized are the three phase angles of the cardan joints, these parameters were set in parametric way in the Adams Car model, this enables them to be set as factors to be modified since they are included as parameter variables in the model, these variables will set the 'Factors' that the software uses to optimize the system.
The objective is mostly set, as said before, from the Adams Car interface, the only important thing to be set in Insight is the desired action to do on the objective, in this case the minimization of the amplitude of the angular speed, under the different options available in Adams Insight it is possible to set the desired action, in this case it was chosen to minimize the objective.
After having set all the different parameters needed for the optimization it is possible to decide the type of experiment to be performed and then run the experiment itself.
Adams Insight will run all the different trials of the simulation changing the phase angles run by run, after all the simulations are completed it is possible to move back to the Insight interface, from here it is possible to let the system evaluate the optimal values of the decided factors under the optimize window, the optimize option will simply tell to the user which are the optimal values to reach the objective, among all the factors that were set to be modified during the experiment, in this case the phase angles themselves.
In the case of study the objective is the angular speed calculated at the pinion shaft, not as absolute value but as amplitude of its sinusoid. The program could not directly put the amplitude as the objective: It was chosen to set the objective as the minimum RMS value of the output angular velocity, being that the root mean square value is directly related to the amplitude and it is available among the selections to make in Adams Car.

In order to perform an investigation the software asks for two things, on one side it is needed to specify the ‘Candidates’, these values are the parameters that the study wants to optimize, in this case the output angular velocity of the system, in this category also the type of optimization is specified, in the study a minimization of the RMS value is needed.

The other set is represented by the ‘Factors’, these parameters are the ones which are modified in order to obtain the desired objective, in this case the three values of phase angles of each universal joint.

For each factor the typology of variation is defined, each case is specified by a normal distribution with a standard deviation defined by a coefficient of variation of 5%, cut-off limits are set in a way to obtain three standard deviations, after all the parameters are set, it is needed to set the design specification, as shown in Figure 4.32.

Investigation Strategy	Regression Model	Runs
Full factorial DOE Response Surface	Cubic	64
Monte Carlo	Linear	80
Latin Hypercube	Linear	80

Table 4.3: Different investigation strategies in analysis

Different investigation strategies are available to be used, in order to understand which investigation strategy worked best, three different methods were tested, a full factorial design of experiment approach, with a cubic model, a Monte Carlo method and a Latin Hypercube approach, these strategies are summarized in Table 4.3.

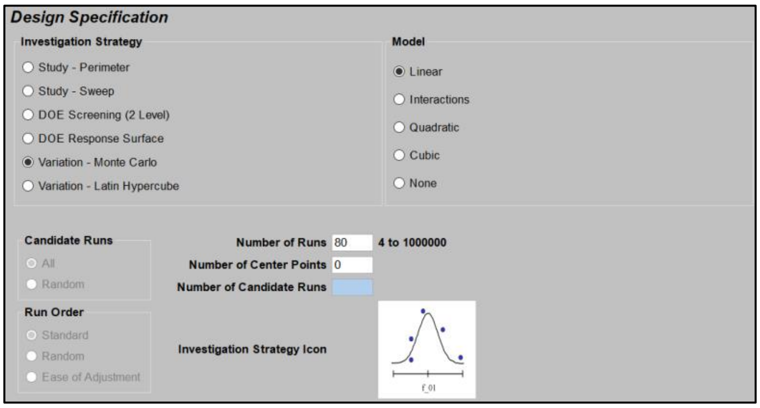

Figure 4.32: Design specification window in case of the design using a Monte Carlo method

The first part of the optimization is aimed at finding which of these approaches is the most robust in terms of results, again the software come in help, through the fit results tab it is possible to see how good each experiment is, the software evaluates the experiment through three different parameters, the Goodness-of-fit, the Term significances and the Residuals.

In Figure 4.33 and 4.34 it is possible to compare how the different strategies work to find the optimal RMS value, in the full factorial design of experiment approach the analysis follows a specific staircase like pattern, gradually reducing the objective value as the runs go on.

The Monte Carlo approach instead shows a random approach in how the runs are performed, it modifies the factors and evaluates the results without showing a particular pattern, this approach may require more runs to be effective but it can have higher possibilities of finding better results.

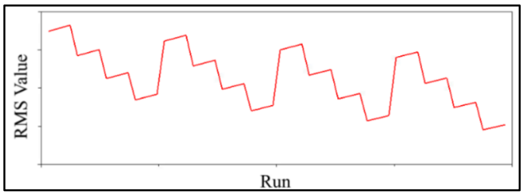

Figure 4.33: RMS Value evolution as runs proceed for a full factorial DOE approach

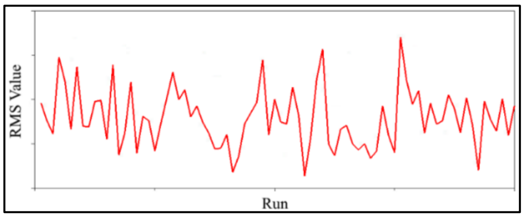

Figure 4.34: RMS value evolution with runs in a Monte Carlo approach

The first method analysed is the full factorial DOE approach with a cubic regression model, this method delivered average fit and residuals but some warnings about some term significances, mainly related to the first joint phase angle and the quadratic and cubic terms of the third joint phase angle. Given that there are only three warnings and no errors this method can be considered good enough for this type of analysis, regression results are shown in Figure 4.35.

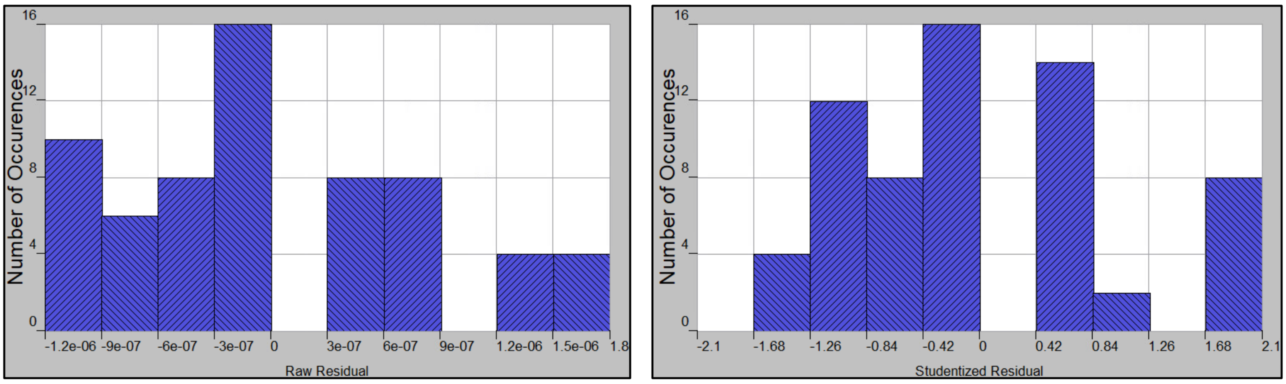

Figure 4.35: Results of the raw and studentized residuals in case of the full factorial approach

Following up, the Monte Carlo approach was tested, this method gave a satisfactory goodness-of fit and term significances, with just two out of the eighty runs with residuals out of scale, this method behaved even better than the previous one in terms of robustness of the analysis.

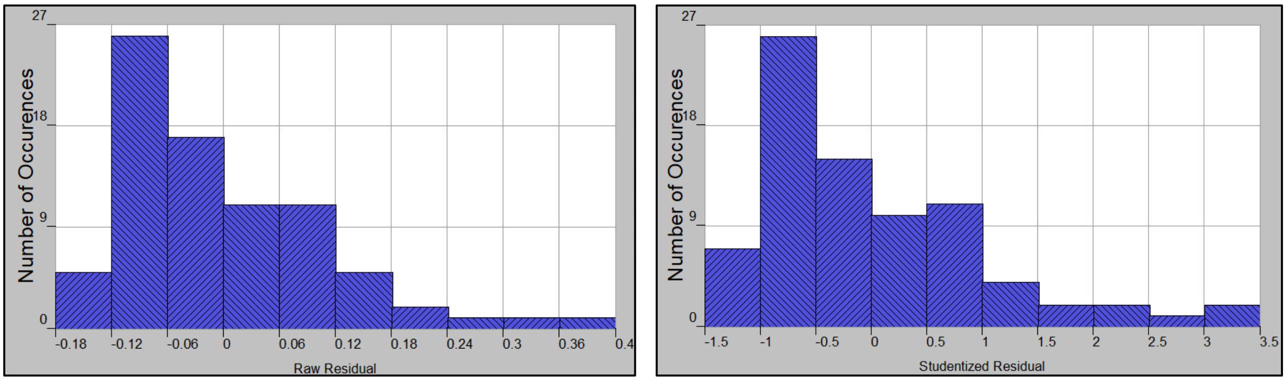

Figure 4.36: Results of the raw and studentized residuals for the Monte Carlo approach

The last analysis performed was based on the Latin Hypercube method, this method resulted in some discrepancies in term of residuals and term significances: Mainly a discrepancy in the value of the third cardan joint and two residuals which seemed out of scale, but still a very good goodness of fit, comparable to the one found for the Monte Carlo method.

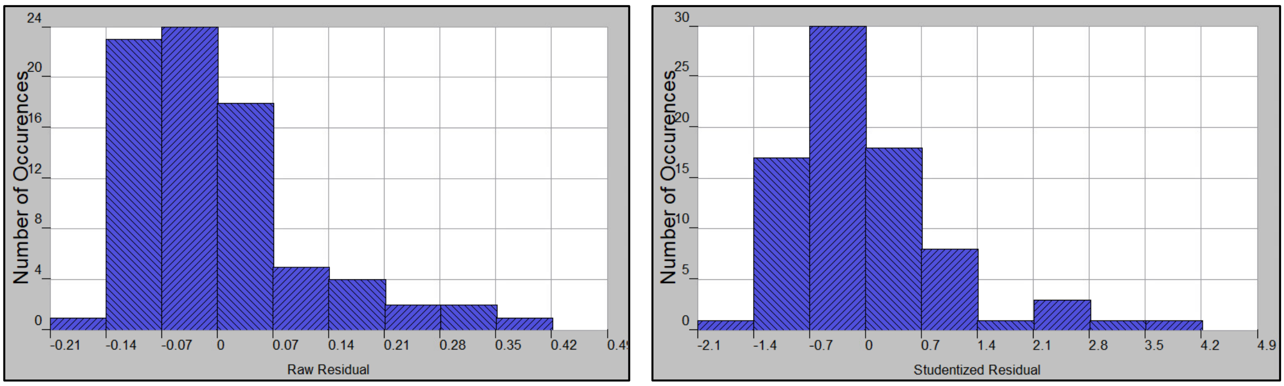

Figure 4.37: Results of the raw and studentized residuals for the Latin Hypercube approach

Of the three strategies analysed, all gave acceptable results, the one that seems most reliable in terms of results is the Latin Hypercube method, by looking at Figure 4.36 and 4.37 it is possible to see how residuals are smaller and more uniform than what is found in the cubic DOE approach.

After this, the optimization could be performed, Adams Insight offers a function that directly finds the optimal values to get the desired objective. Starting from the design condition it was possible to find the set of phase angles that mostly reduces the irregularity, the optimization was performed without constrains, this means that each angle is free to be modified between the range that the software finds, among this range the analysis gives as a result the optimal triad of values to reduce the irregularity. It is interesting to see that each method delivered a different set of values, obviously depending on the results coming from the investigation.

For each experiment, a different set of phase angles were obtained from the optimization, to find which of the strategies delivered the best improvement the plot in Figure 4.38 was created.

All the strategies resulted in an improvement with respect to the design condition, the full factorial approach showed the least improvement compared to the design condition, but nevertheless a noticeable one. The Monte Carlo and the Latin Hypercube approach delivered the best improvement, with the latter method in slight advantage, both analyses resulted in a degree of irregularity close to the desired objective, the choice of one method with respect to the other mostly relies on its reliability, the Monte Carlo approach showed a good response in term of significance with the Latin Hypercube method just behind. Both methods could be considered good enough for a first optimization analysis, they in fact delivered a good improvement compared to what was present in the design condition, all three tests were better than what was experimented in test five of paragraph 4.4, which represented a trial at improving the design condition. A statistical method like the ones used in this analysis will have better result compared to a pure trial and error approach.

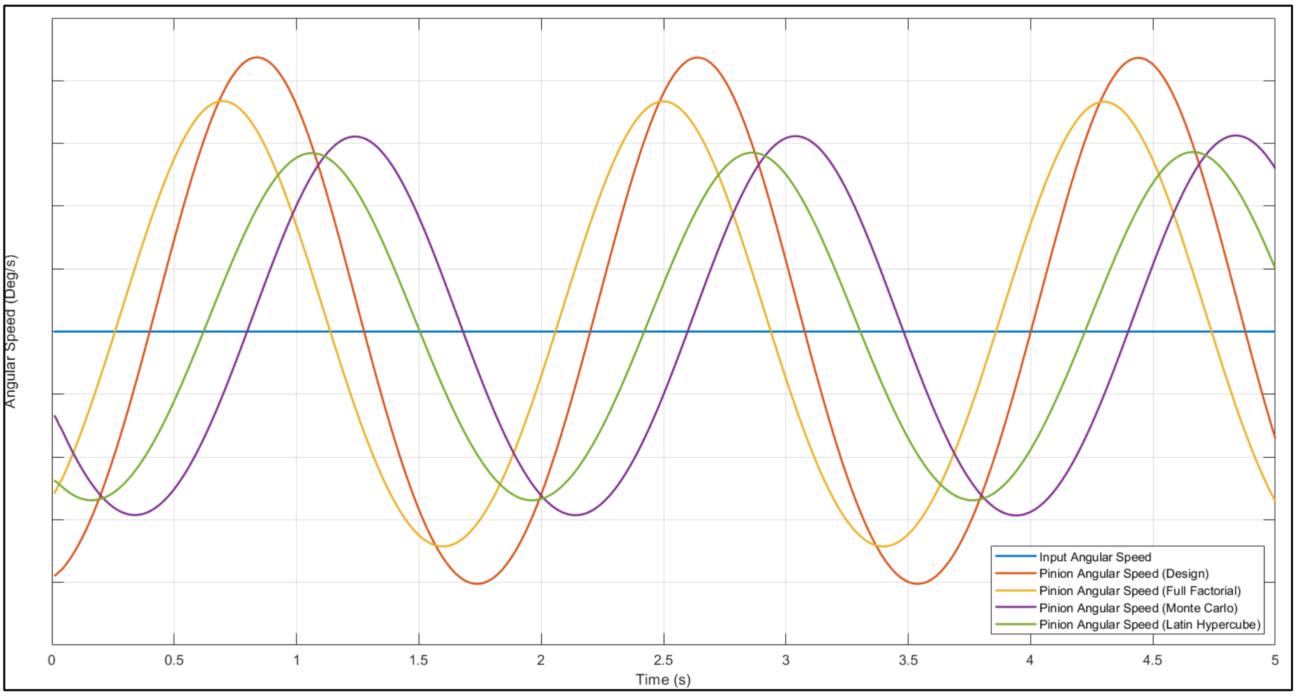

Figure 4.38: Comparison of the output angular velocities between the different investigations

Figure 4.39 shows the comparison between steering ratios of the analysis performed with the different optimization methods, plus the design condition: This result was obtained through a steering simulation like that performed in the first part of this chapter.

The steering ratio is expressed in the standard formulation, not the one that uses the 'diff' function in MATLAB, it is important to notice that the steering ratio results were removed for small steering angles and results were plotted just for positive steering angles. As the steering angle is reduced the ratio will be less reliable in terms of calculations, to avoid confusing data these values were removed. The full factorial approach shows a condition that is very close to the design condition, the other two methods are closer together with the Latin Hypercube method showing a lower steering ratio compared to the results of the Monte Carlo method.

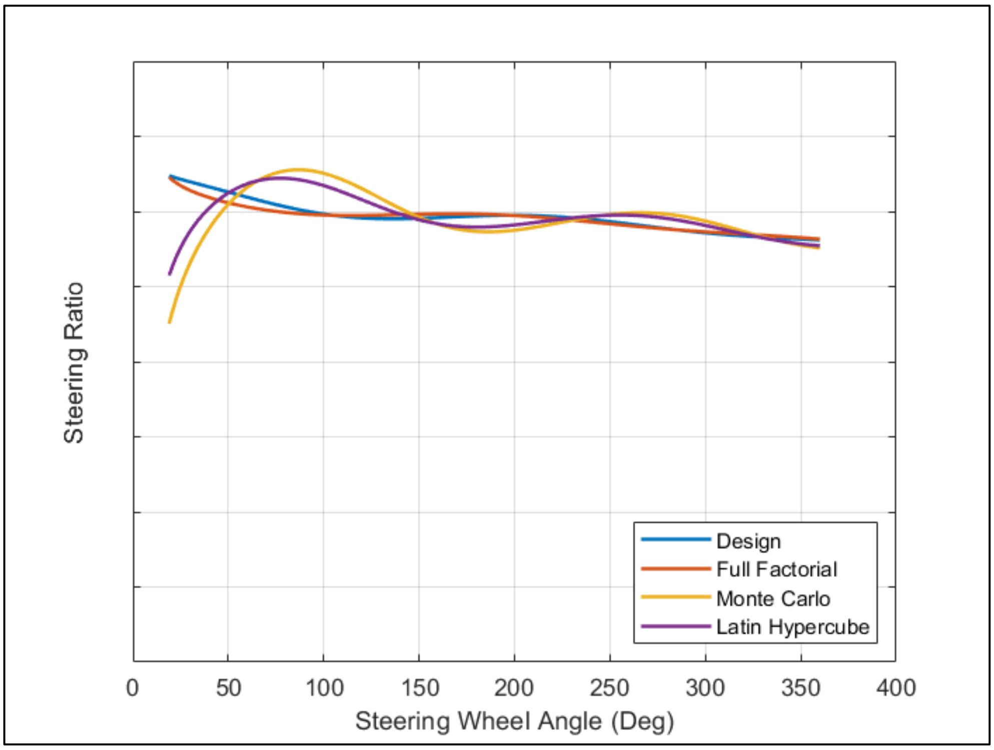

Figure 4.39: Steering ratio comparison between the most relevant test cases

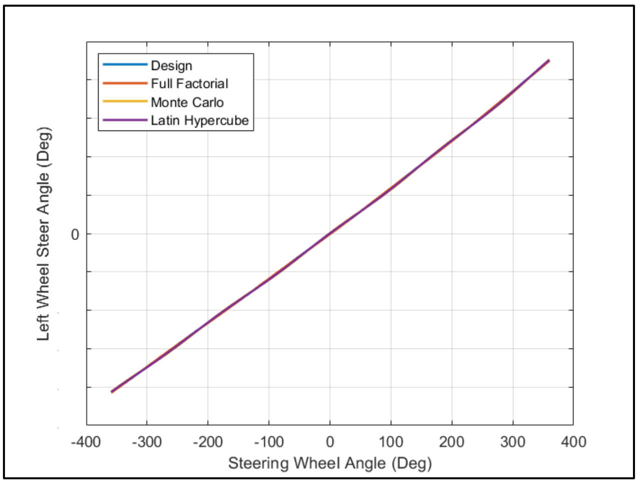

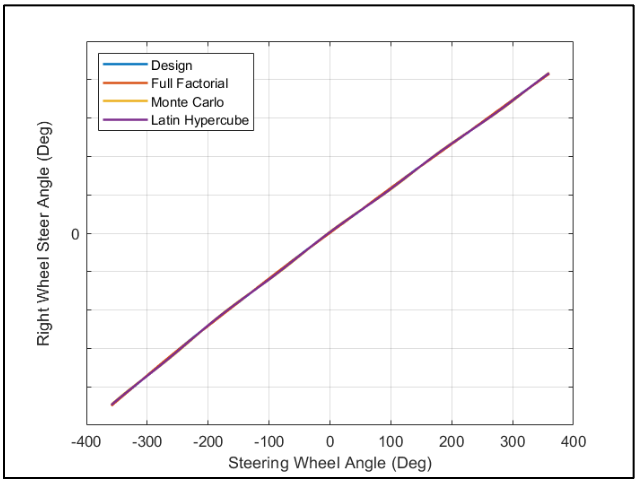

Figure 4.40: Left steer angle comparison

Figure 4.41: Right steer angle comparison

In Figure 4.40 and 4.41 it is possible to see a comparison between right and left steer angles between the different tests performed, in both figures it is difficult to catch differences between the design and the optimized conditions.

The steer angle will vary sinusoidally like the steering ratio does, this will overlap the lines in different points, differences in values are very small but there is still an effect on the steering ratio.

In this comparison it is also possible to see the fact that the two wheels will not steer of the same value, the inner wheel shows a higher steer angle compared to the outer one. Differences in results among different methods are not noticeable.

To end the discussion on motion irregularity it is important to state that an alternative method could be used to find the optimal configuration in irregularity reduction, using the difference between the two ϕ angles that are characteristic of the hooke joint: These angles are plotted in Adams Car by calculating the angle between the inertia frame of the shaft as the shaft rotates and a fixed reference set at the starting position of the inertia frame. The difference between this angle computed at the first shaft and the angle computed at the pinion will give another hint on how regular the system moves. The graph obtained in Figure 4.42 is similar to those found when using angular speed as it was done in the previous computations, in this case the sinusoid will be around zero because that condition happens when the two angles are the same, the less is this difference the less will be the system irregularity.

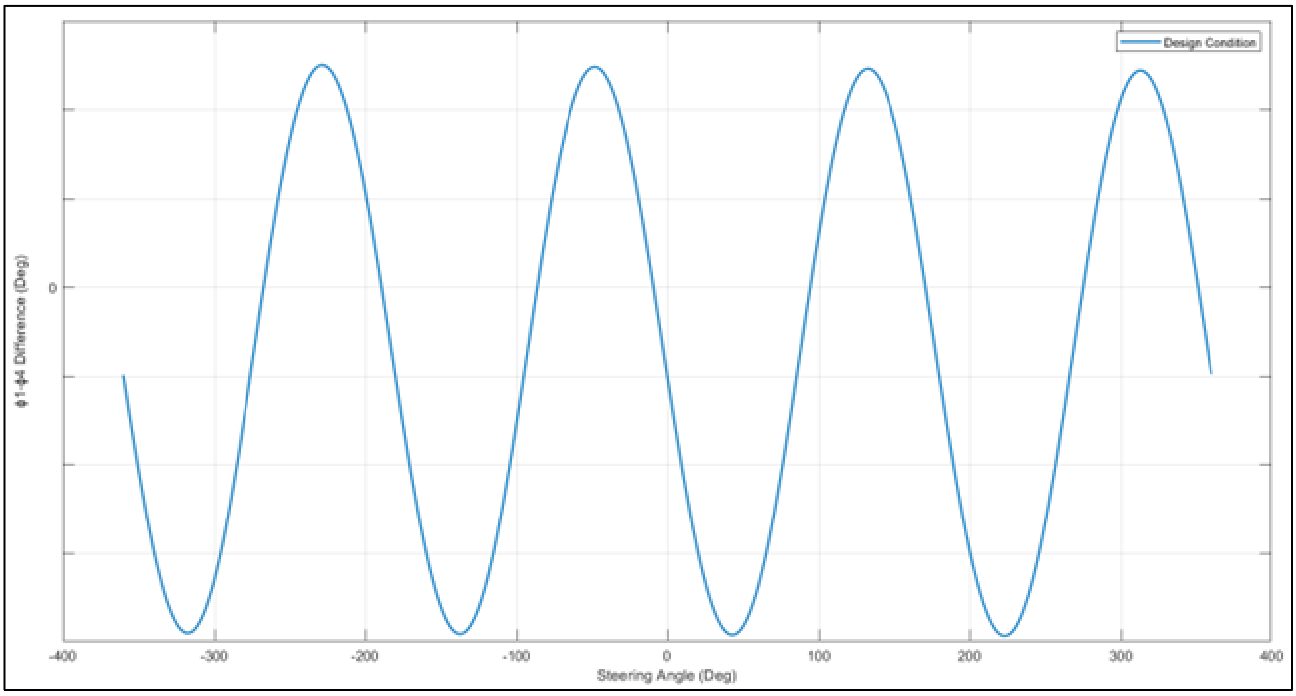

Figure 4.42: Difference of ϕ_1 and ϕ_4 in a steering test performed on the design condition

4.6 Conclusions regarding the steering test

A static test that involves steering as the one performed in this chapter is important in evaluating how the suspension will react to different steering inputs, the first part of the chapter was intended as an explanation of different methods to model a steering system. Some parameters are close to values obtained by models of higher precision, while others will need an accurate model to be properly expressed, the evaluation performed can underline which values require an accurate model to be correctly displayed.

The part on motion irregularity is relevant in evaluating how well the system is connected by the different hooke joints, the optimization performed in this test is a first approach on how to improve the system, two main things are important to be said about this test: The optimization is limited by the fact that it was done by a common laptop connected to a virtual machine. Using a more performant computer may allow to obtain an optimization across all the possible angles that each hooke joint could have and not just around the design condition, secondly it was found that the design condition is almost optimal in terms of irregularity, the optimization delivered values that are not far from the design condition in terms of result, this is a confirmation of the robustness of the method used.

Even if the design condition has constraints that will limit its performance, the fact that this system reached the production phase means that it gave good results, the confirmation that the system works in a proper way gives validity to both the method and the model used in this test.

In terms of the definition of a good procedure to evaluate how a steering system work: It is important to check the steering ratio evolution over the steering manoeuvre. This parameter will reflect the results both in terms of irregularity and steer angle that the system presents.

Looking at geometry parameters the two projection arms give a good indication of the movement of the wheel, it is important to check both scrub radius and caster moment arm. A high-enough value will improve the self-centring ability of the system.

5 Suspension Tests: parallel and opposite wheel travel

5.1 Parallel wheel travel on the front suspension

The first suspension test performed is the parallel wheel travel, this test makes both wheels to follow the same movement.

This and the following test were performed considering the most accurate model, the one with universal joints and torsion bar. The parallel wheel motion is characterized by a rebound of 80mm and a bump of 60mm, bump represents a compression of the suspension, while the rebound shows by the extension of it.

By looking at Figure 5.1 it is clear that wheel travel will change the suspension geometry leading to some variation as the wheel travel changes, the suspension will react differently.

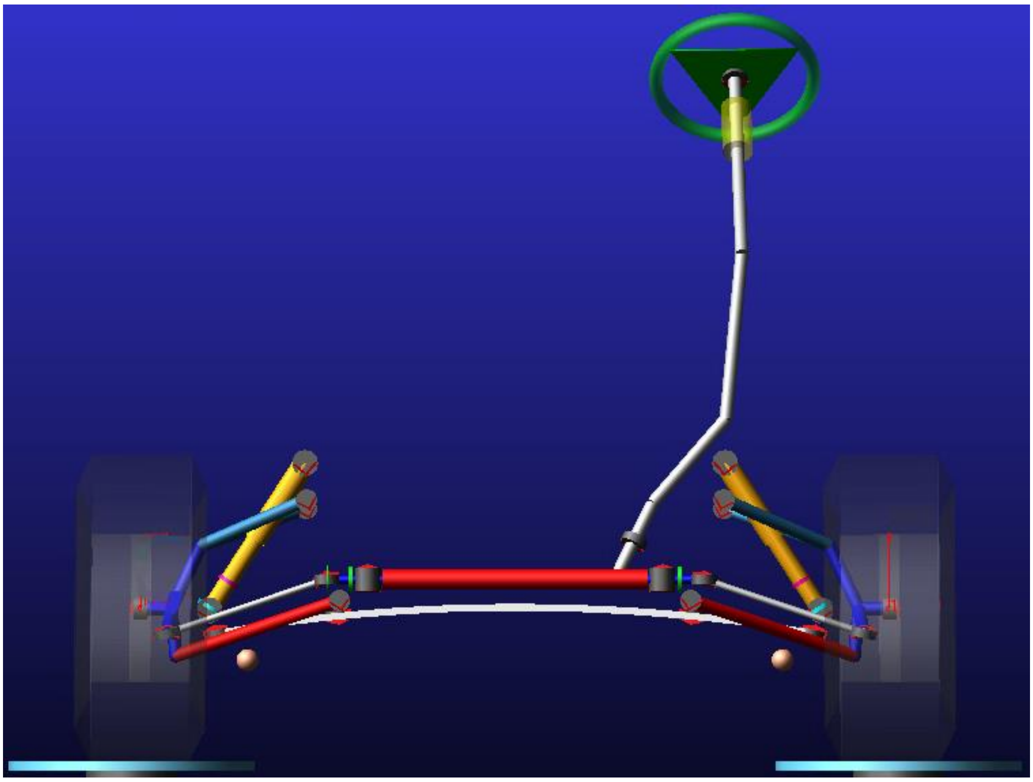

Figure 5.1: Screenshot of the parallel wheel travel simulation when the system is fully extended

The first parameter that is taken into consideration is the camber angle. The vehicle in exam does not have a null camber when the vehicle is resting in neutral position, meaning that when the vehicle is standing still the wheels are not perfectly straight when seen from the front: They have some degree of negative camber when the travel is equal to zero.

The double wishbone suspension allow for some camber variation when an upward or downward movement is imposed to it. By analyzing the graph in Figure 5.2 it is possible to see that when the suspension is compressing, towards the right of the envelope, the camber tends to go towards more negative values, the opposite happens when the suspension is extending towards the rebound condition.

In this case there is a change in behaviour near the end of the considered suspension extension, in fact at two/thirds circa of the extension the camber angle reaches a maximum, that is slightly negative, and then starts rising again up to the rebound condition met at the -80mm travel mark. This may be due to the fact that the vehicle is reaching its max extension and so wheels start to lose contact with the test rig platforms.

Left and right wheels show almost the same values, with minimum differences between them, even if they are still noticeable from the graph.

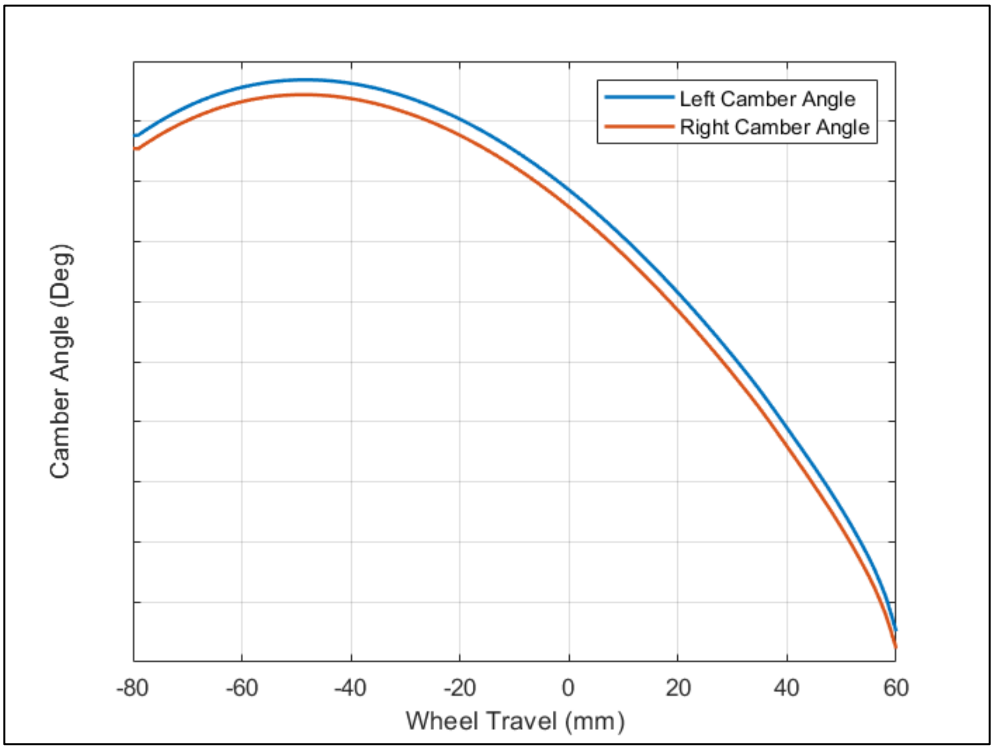

Figure 5.2: Camber angle for the left and right wheel in case of a parallel wheel travel condition

Over the vertical translation sustained over this test, the variation in camber is commonly expected from a double wishbone suspension like the one in analysis.

Caster angle variation is closer between left and right wheels compared to the variation in camber angle, so close that in Figure 5.3 it will be very difficult to notice any difference.

The two characteristics will almost overlap, this result is explained by the fact that parallel wheel travel happens on the same way between the two sides, since caster is related to the steering axis line, that is commonly defined by the two outer ball joint positions, that will be in the same position between left and right, this leads to a minimal variation in caster between the two wheels.

The last characteristic angle analysed is the toe angle, its behaviour is shown in Figure 5.4 in terms of variation and not of absolute value.

Like it is expected the two values have opposite sign envelopes between left and right wheel, in this case being that the right wheel has a positive angle and the left one has a negative angle the system is in a toe-in condition, the toe angle is almost constant along the wheel travel, except near the bump stops, where it suddenly increases for both wheels. This condition happens when the suspension is near its maximum compression, this shows that as the suspension moves from a compression to an extension the system will have settled in different positions leading to a discrepancy from the value set as static toe. Even when the steering wheel is straight a bump on the road may induce some steering motion due to the variation in toe.

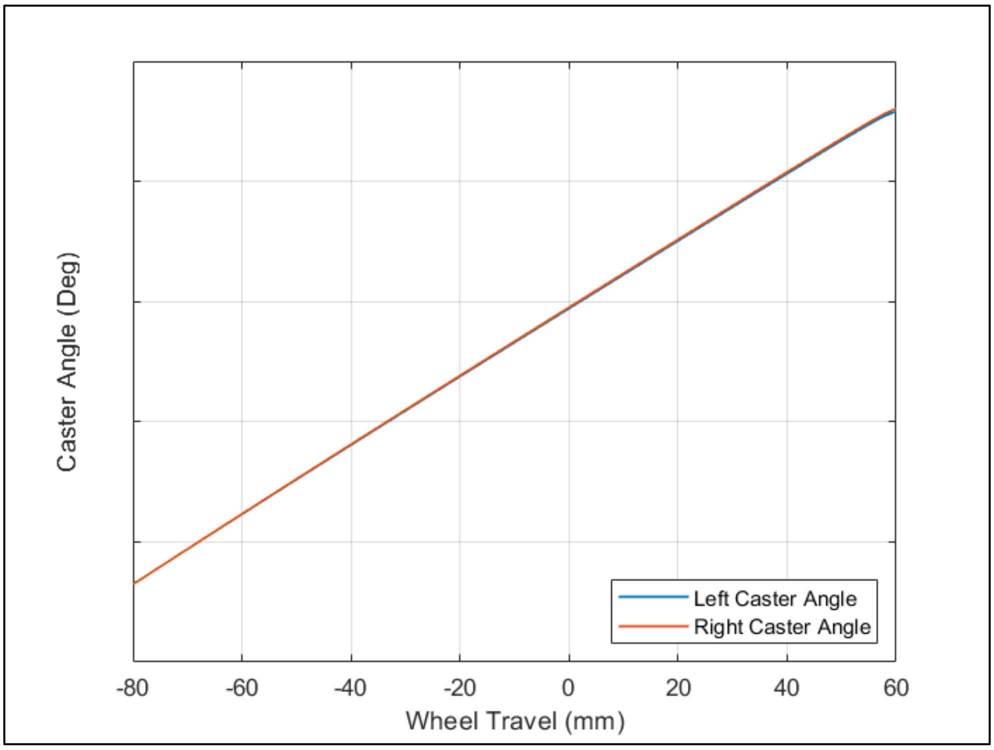

Figure 5.3: Left and right caster angles for a parallel wheel travel test

In Figure 5.5 it is possible to catch the variation in displacement regarding the centre of the wheel, along the X direction the envelope has an almost linear shape, while along Y there are big variations when the suspension is extending, while along the compression part a parabolic shape with small variation in values is present.

The last analysis carried out in the parallel travel test is on the anti-dive, this parameter is expressed in Figure 5.6 in percentage.

Anti-dive expresses how much the vehicle resist the dive motion over a braking manoeuvre. Due to the weight transfer that occurs during braking, the vehicle will load more the front axle and tilt forward. An anti-dive of 100% will mean that the suspension will not deflect during braking and so the chassis will not nose downwards. To correctly compute this value in Adams Car it is needed to set the parameters of the full vehicle in terms of sprung mass, centre of gravity height and wheelbase, as well as the brake bias.

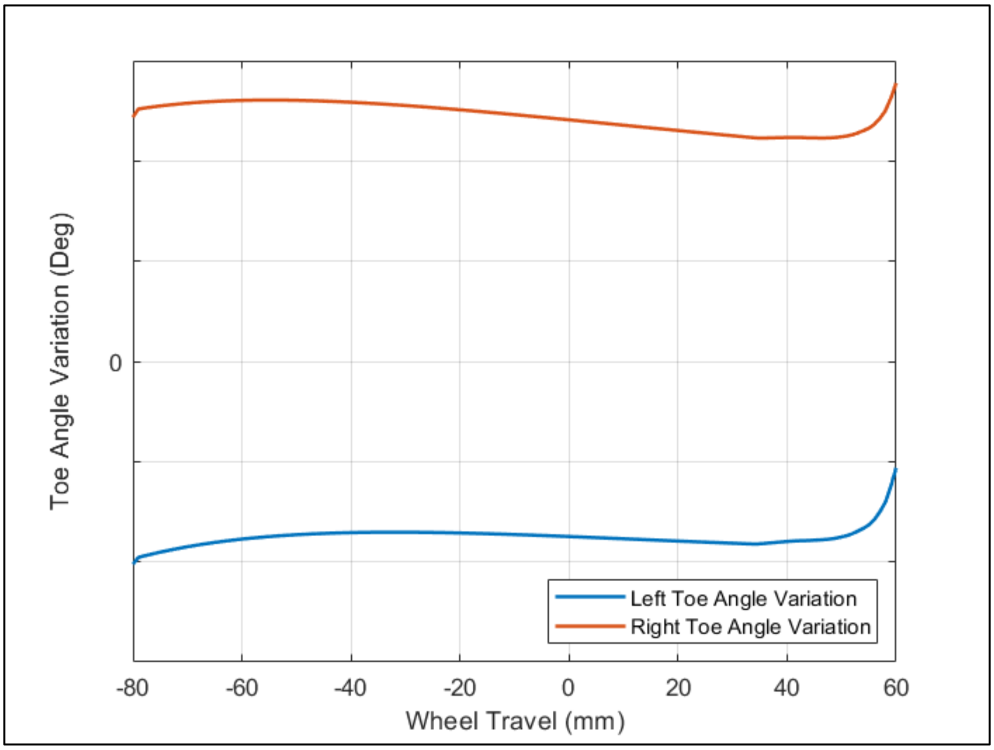

Figure 5.4: Toe angle variation in the parallel wheel travel simulation

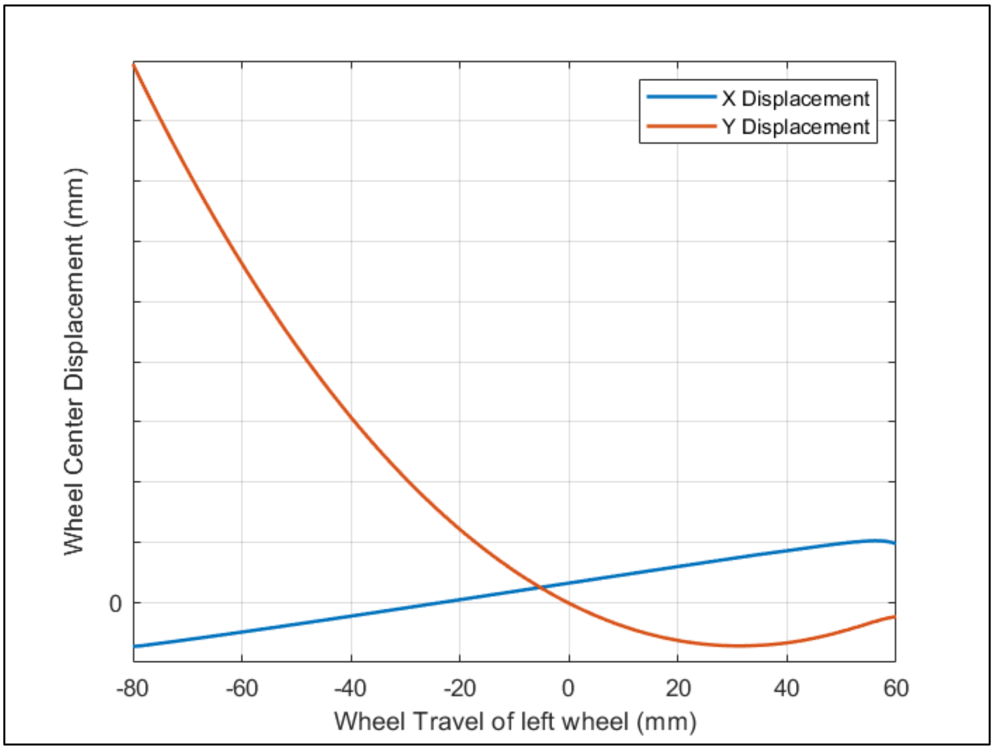

Figure 5.5: Wheel centre displacement variation in function of the parallel wheel travel

The test is done for both vehicles, with the shorter vehicle showing an higher amount of anti-dive, this is mainly due to the fact that the short vehicle is in fully loaded condition and has a lower centre of gravity compared to the 4120mm long vehicle, this will result in a better fight against the diving motion that the braking manoeuvre will try to induce, the procedure followed to evaluate anti-dive has been analysed on paragraph 3.4.

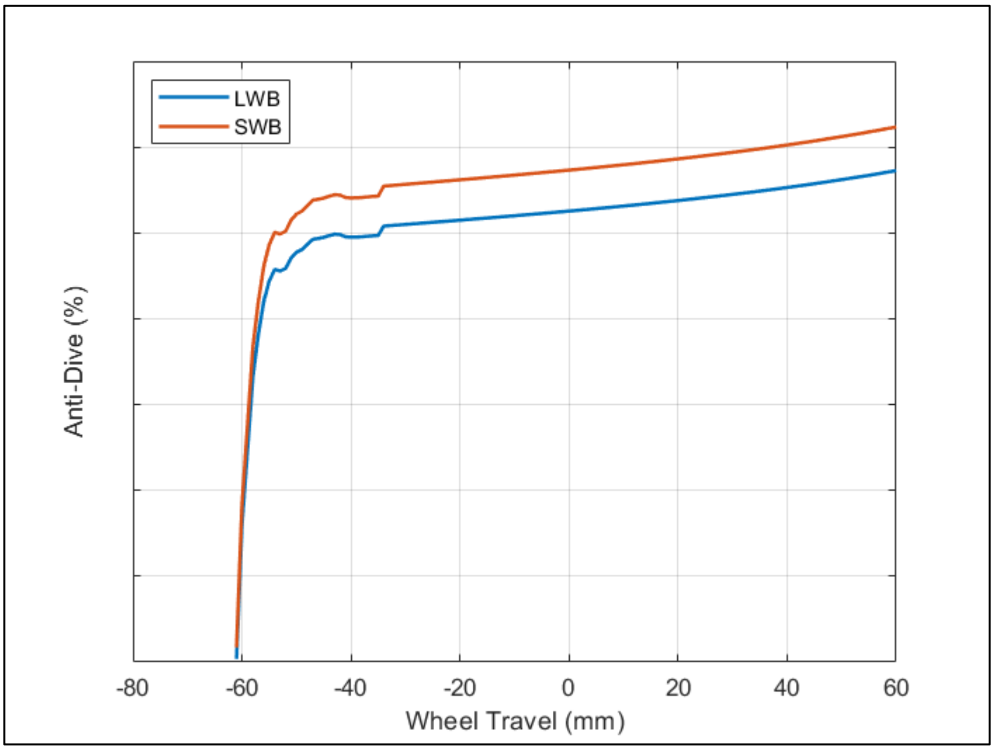

Figure 5.6: Percentage of anti-dive in a braking manoeuvre for the two vehicles taken in analysis

5.2 Opposite wheel travel on the front suspension

The second test performed consist of an opposite wheel travel motion, this test is made interesting by the typology of suspension used by the vehicle in examination, as it was stated in chapter three this vehicle has a transversally mounted leaf spring that acts as a front anti roll bar.

Utilizing a system like this creates a constraint between the two wheels that can act differently from what a classic anti-roll bar system could do, in this case the movement of a wheel is somewhat connected to the movement of the other through the spring deflection, and not simply trough a classic anti-roll bar.

In Figure 5.7 it is possible to see how the leaf spring deflects in this test, the connection is different compared to a classic anti-roll bar and will reflect this in the results.

This test, compared to the previous one, greatly highlights how the two wheels are connected, a test like this could, in some way, be representative of what happens to the vehicle when it is parked in an uneven surface, with some degree of approximation it is possible to see what the suspension geometry is when the vehicle leans into a corner.

The wheel that highly compresses represents the outer wheel and vice versa, mind that this is a static simulation, so it is possible that results in a dynamic manoeuvre may differ.

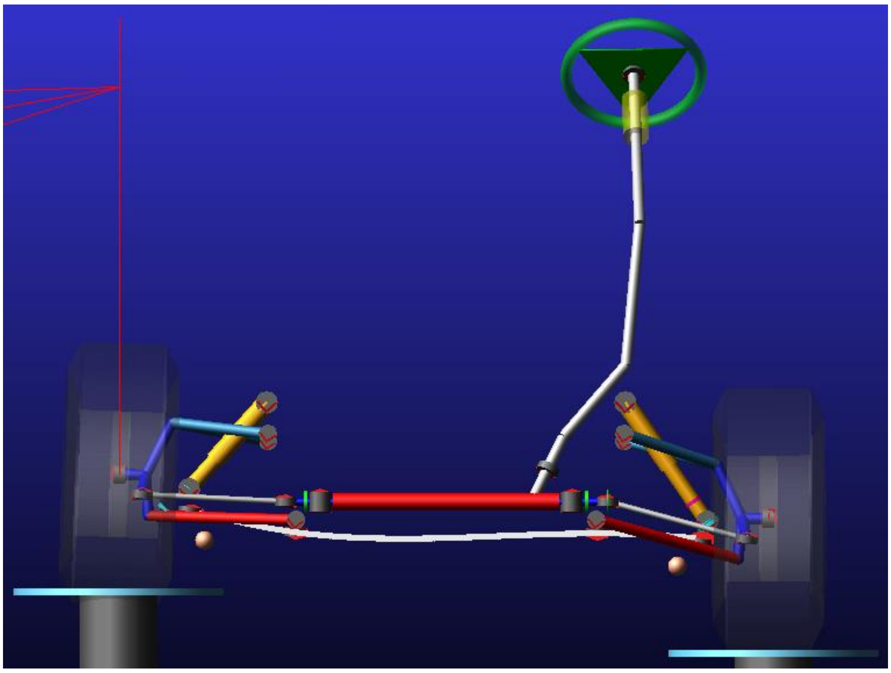

Figure 5.7: Opposite wheel travel representation, in this case shown at the initial point of the test

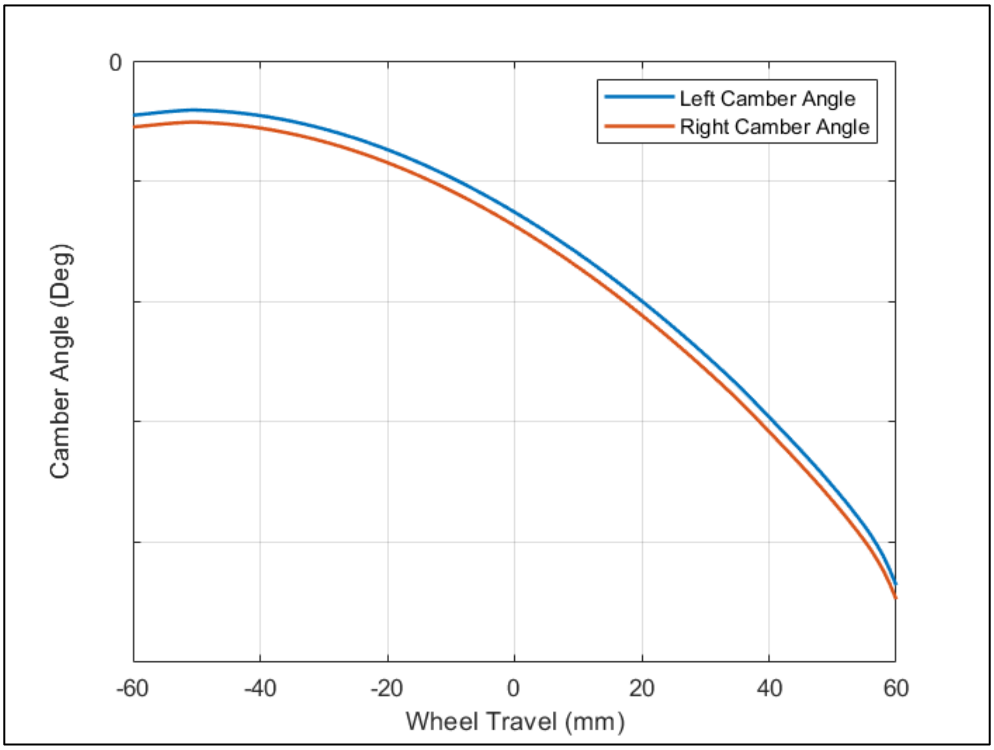

Figure 5.8: Left and right camber angle in function of opposite wheel travel

In Figure 5.8 it is possible to see how the camber angle changes for both the front wheels, the situation is similar to the one shown for the parallel wheel travel case, the values between the two tests are very similar, the difference mainly comes from the fact that the inversion of trend towards the end of the extension considered in the test is less pronounced, this is actually due to the fact that the wheel travel range is not the same between the two test and not because there are some differences between the two behaviours.
Caster angle has a linear characteristic for both wheels, the difference between the two is minimal, this means that the geometry of the suspension in side view is not affected by the fact that one wheel is in compression while another is in extension, results are shown in Figure 5.9.
The first value that shows some difference compared to what happened in the parallel wheel travel test is the toe angle variation shown in the graph in Figure 5.10, the range of variation of the toe is higher compared to the first test and the shape of the line is less constant and more linear.

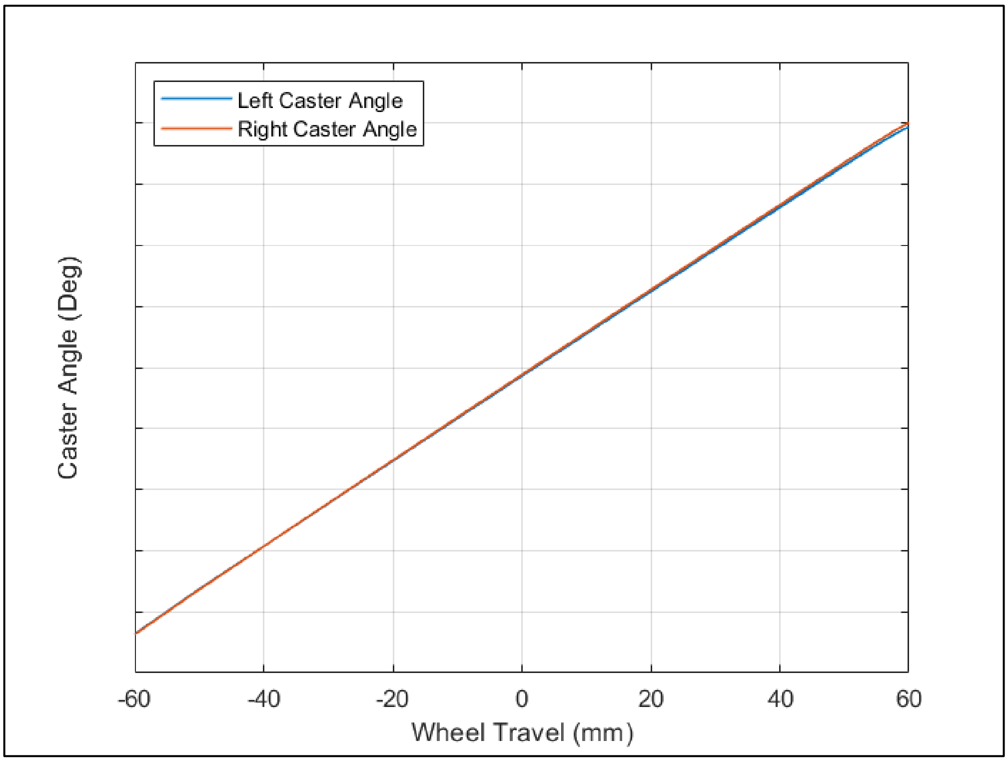

Figure 5.9: Caster angle variation for the opposite wheel travel test

Differences are also found for the wheel centre displacement, shown in Figure 5.11, the range of variation is smaller for both cases, if the difference along the Y-displacement is mainly due to the different range of the wheel travel between the two tests, the displacement along the X-axis has an envelope that is clearly less steep than the one seen in the parallel travel simulation.
The displacement along the X-axis tells that the movement of the wheel when it is seen in side-view is minimal, while the fact that the suspension geometry changes by a good margin when suspension

compresses or extends is represented by the result in displacement along the Y-axis, as the wheel moves up or down the suspension will adapt to the movement by changing its track, this will lead to a change in the coordinates of the wheel centre in this condition.

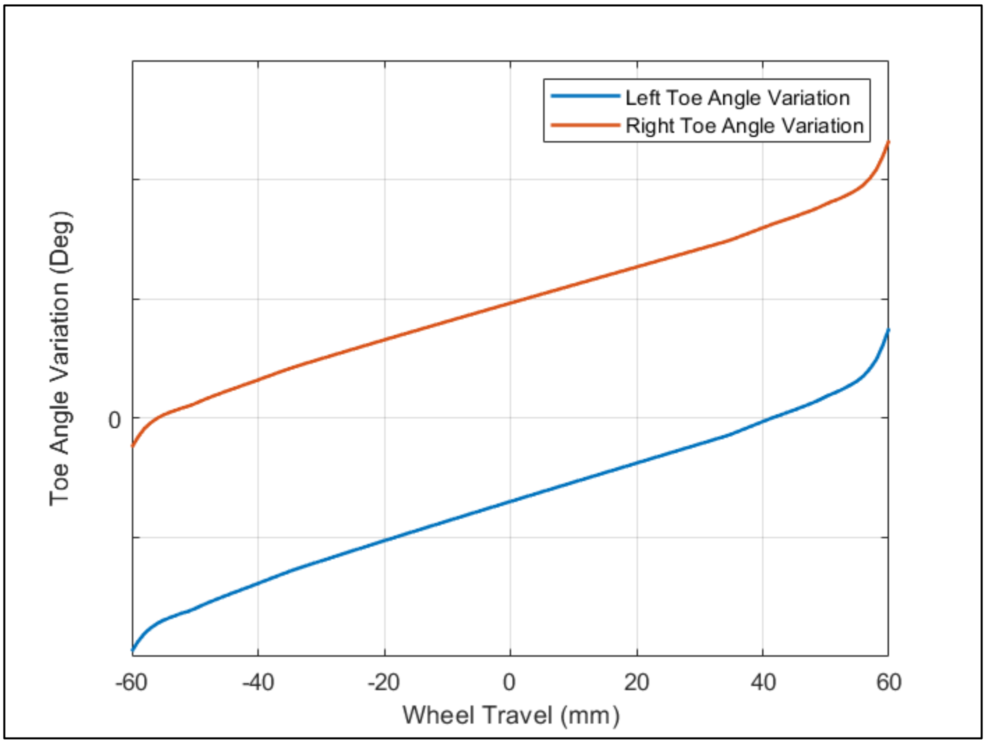

Figure 5.10: Toe angle variation in function of the opposite wheel travel, for both front wheels

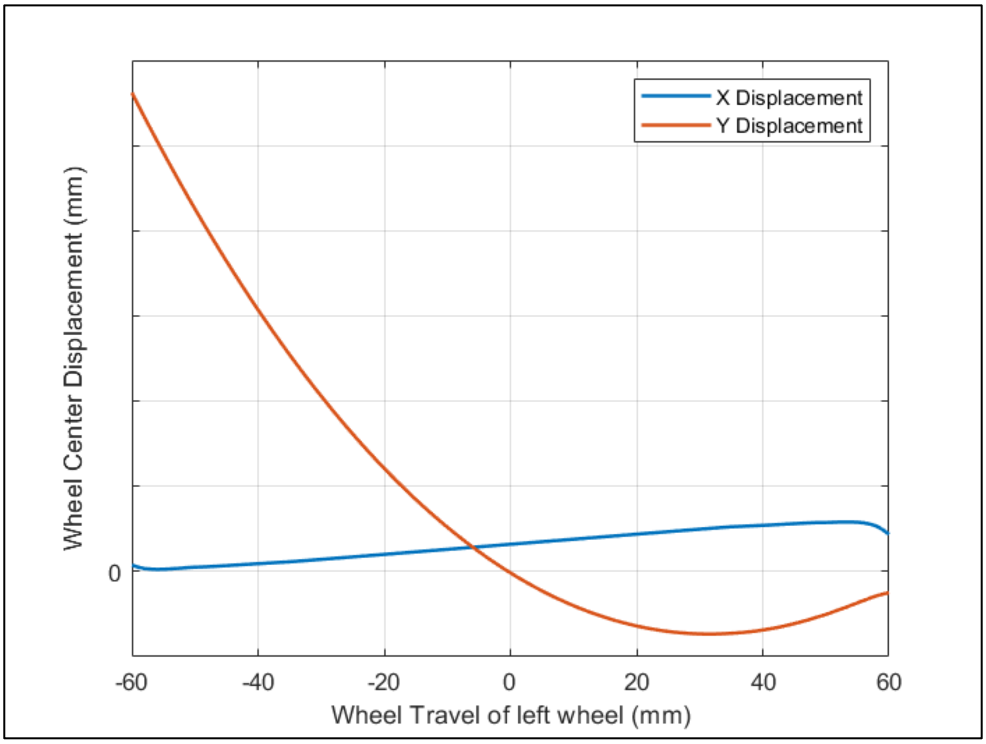

Figure 5.11: Variation in the wheel centre displacement in both X & Y direction, in function of the opposite wheel travel

5.3 Comparison between the two tests performed on the front axle

A good measure of evaluation for the two tests is the force that each wheel is submitted to along the test, to correctly compare the different simulations it was chosen to evaluate the force acting on the wheel centre, or more precisely on the point corresponding to the centre of the wheel hub, computed on average between the two wheels. Forces are Calculated along the Z-direction that corresponds to the normal direction.

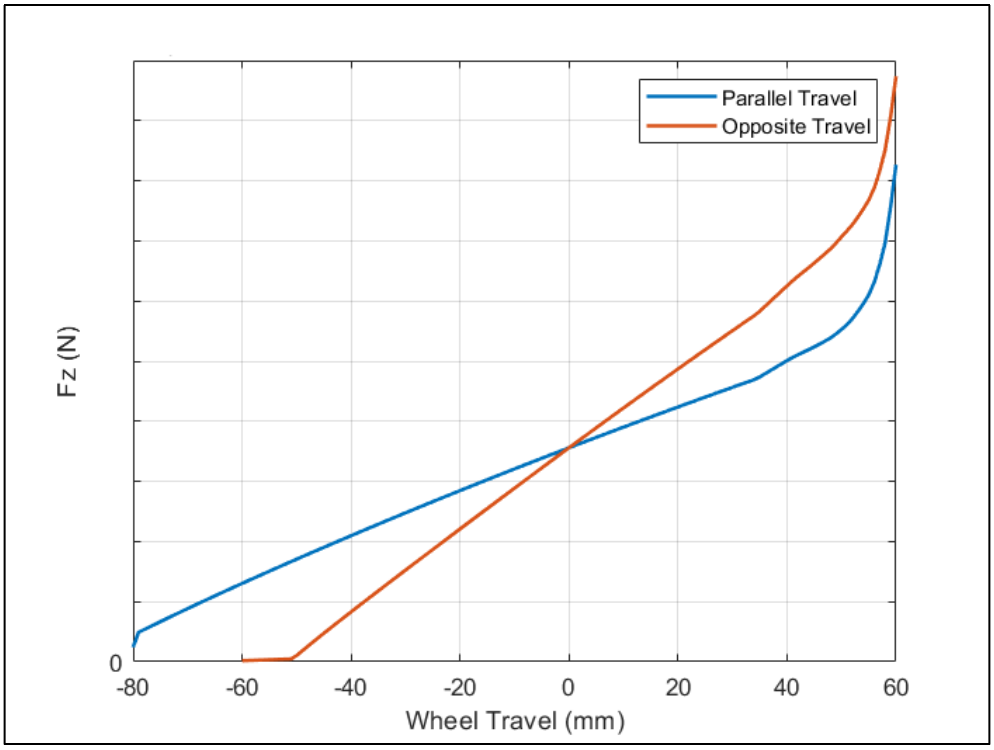

Figure 5.12: Force applied on the wheel centre between the two simulations

When comparing the two simulations, like in Figure 5.12, it is possible to see that there is a different slope between the two conditions, for the parallel wheel travel case the values of force grow slower as wheel travel increases and at the end reach lower values than the other case. Towards the end point of positive travel both tests show a sudden increase of the force characteristic, the increase is comparable in shape between the two analyses.

The opposite wheel travel case reaches an higher force at the end of its expansion, even if at the beginning of the test the vertical force is almost equal to zero for a bit, instead of the instantaneous increase in force that is present for the parallel travel case. The difference between the two test comes mainly from the reaction of the stiffness developed by the transversal leaf spring.

The other parameter that shows noticeable differences between the two tests is the contact point position in the X direction: This indicates the point of contact between the tire and the road.

The opposite travel has a smaller scatter compared to the one of the first test performed, as it is expressed in Figure 5.13. The same cannot be said for the same parameter in Y direction, in this case the difference is negligible, as it is shown in Figure 5.14, the two curves almost overlap themselves, the only difference seems to be the difference wheel travel range considered.

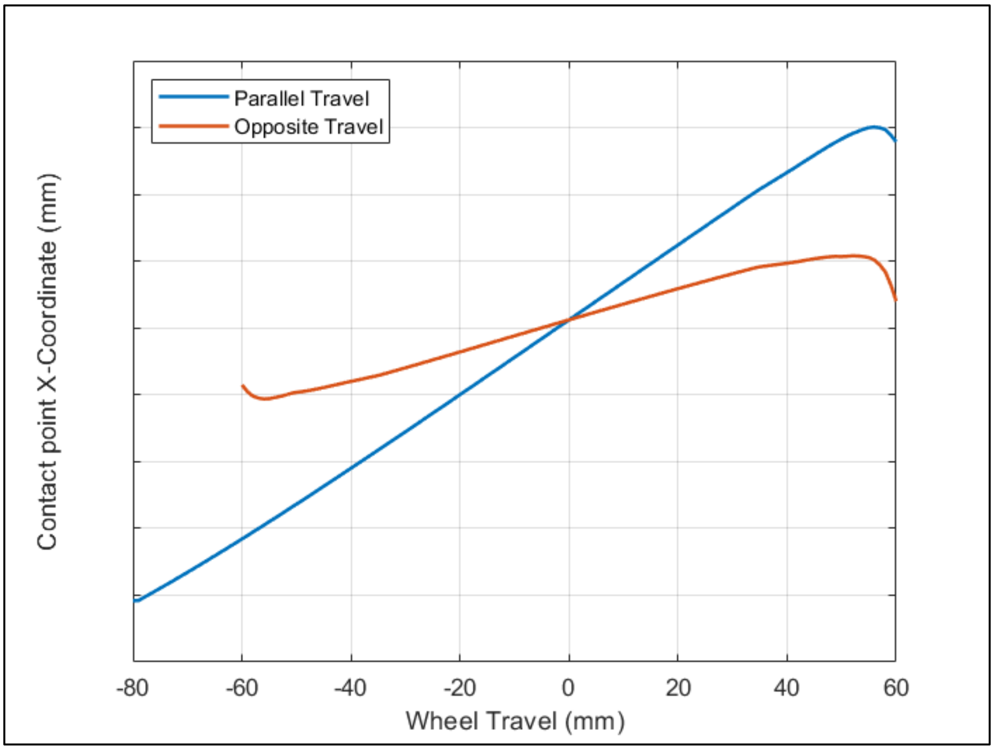

Figure 5.13: Tire contact point in the X Direction, comparison between the two different tests

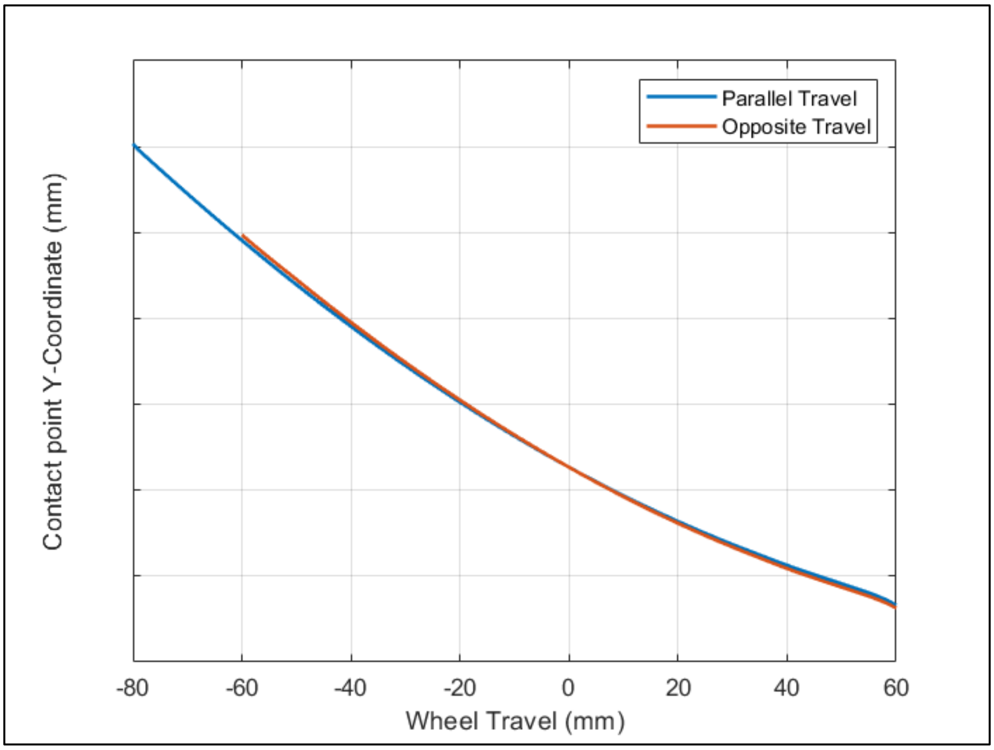

Figure 5.14: Comparison between the contact point of the tire, measured in Y direction, between the two simulations

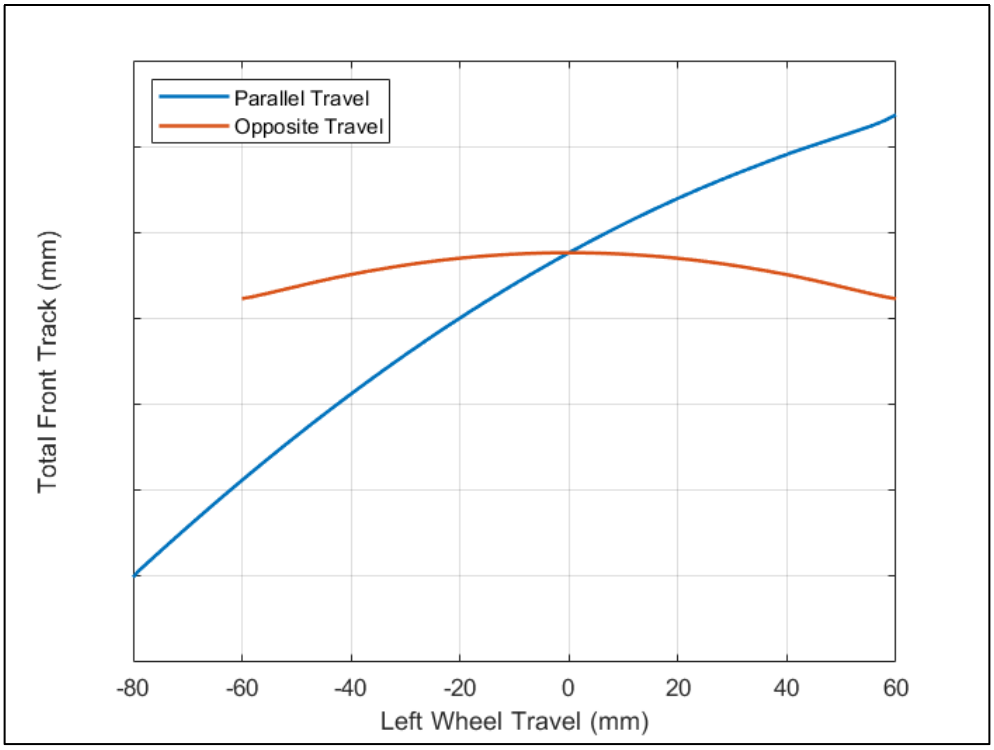

Figure 5.15: Front track variation in the two simulation cases

Interesting results are obtained from the evaluation of the total frontal wheel track in Figure 5.15, the parallel wheel travel condition has a wider extension of the track, this is mainly due to the fact that each wheel will contribute to the track variation basically in the same way, when the suspension is being compressed the track will increase, while the opposite will happen when the suspension is extending.

By watching at the opposite wheel travel case, the change in wheel track is small compared to the former case, this result is due to the fact that when one wheel is in extension, the other one will be in compression and vice versa, this balances the variation in track because one wheel will be balanced by the other, when compressed it will gain more offset towards the outer part of the vehicle and vice versa when extended.

Another useful parameter to be evaluated is the kingpin angle: This parameter evaluates the angle of the steer axis of the suspension compared to wheel vertical line in front view. The steer axis in a double wishbone suspension is set by the line that connects the upper control arm and the lower control arm ball joints. The graph in Figure 5.16 is shown for the left wheel, the graph of the right one will be exactly the same: In the parallel wheel travel test the kingpin angle will increase from the value at zero travel over the bump phase, while during the rebound phase the angle will decrease up to a minimum and then increase. A higher kingpin angle will increase the effect of wheel self-centring when the steering wheel is turned, the main noticeable effect is an increase in front ride height as the wheel are steered for positive kingpin angles.

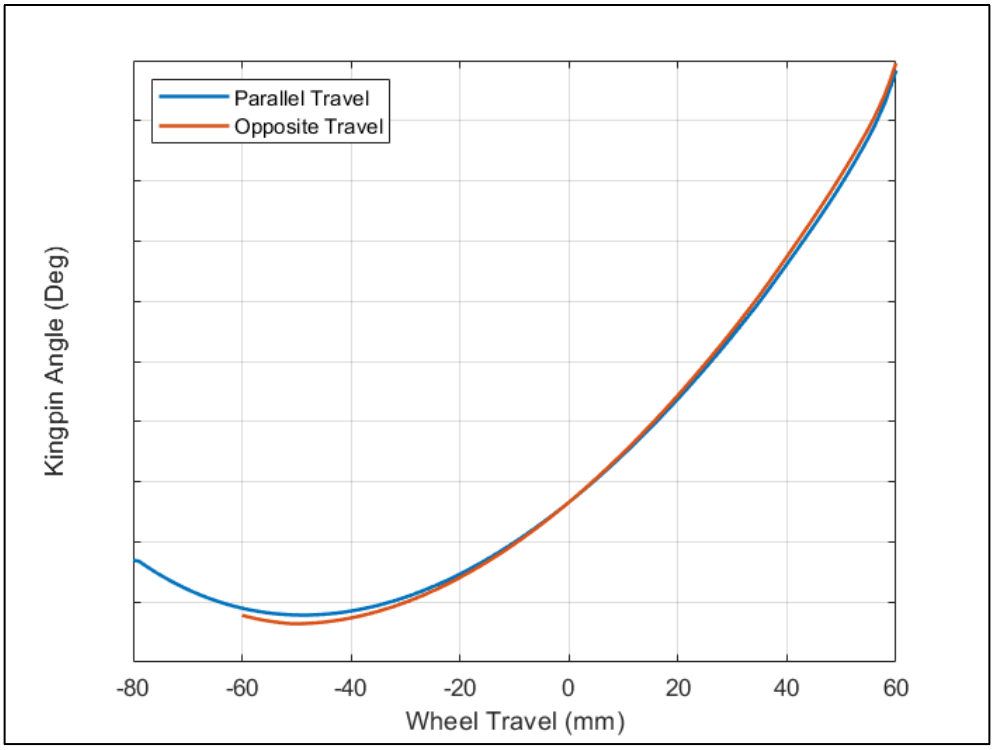

Figure 5.16: Kingpin angle evolution comparison between the two tests

Kingpin angle will increase straight-line stability, especially during braking, and also decrease the scrub radius, the kingpin angle will also affect the camber when turning the wheel leading to a positive camber angle for the outer wheel that may be not exactly beneficial in achieving the maximum grip possible.

Commonly, in cars and commercial vehicles the suspension is set to give the highest stability and safety level, so kingpin angle is somewhat useful for achieving this objective.

Another side effect of kingpin angle is the fact that some positive camber will be induced to the wheels as they are steered.

What was found for the parallel wheel travel, is again valid for the opposite wheel travel test for what concerns the kingpin angle effect, the behaviour will be very close to the one seen in the parallel wheel travel test.

The effect is not perfectly comparable to what happened for the parallel wheel travel test due to the different rebound values, but the behaviour is clearly almost identical.

At last, it was deemed useful to analyse some other parameters regarding the front alignment of the vehicle.

The first parameter taken into consideration is the scrub radius, this distance represents the distance between the kingpin axis and the centre of the wheel's contact patch when seen in frontal view. This value is somewhat related to the kingpin angle, due to the fact that a change in kingpin angle will also change the position of the steering axis, likely changing the distance between the two points that define the scrub radius, the analysis shown in Figure 5.17 is performed on the left wheel for both tests.

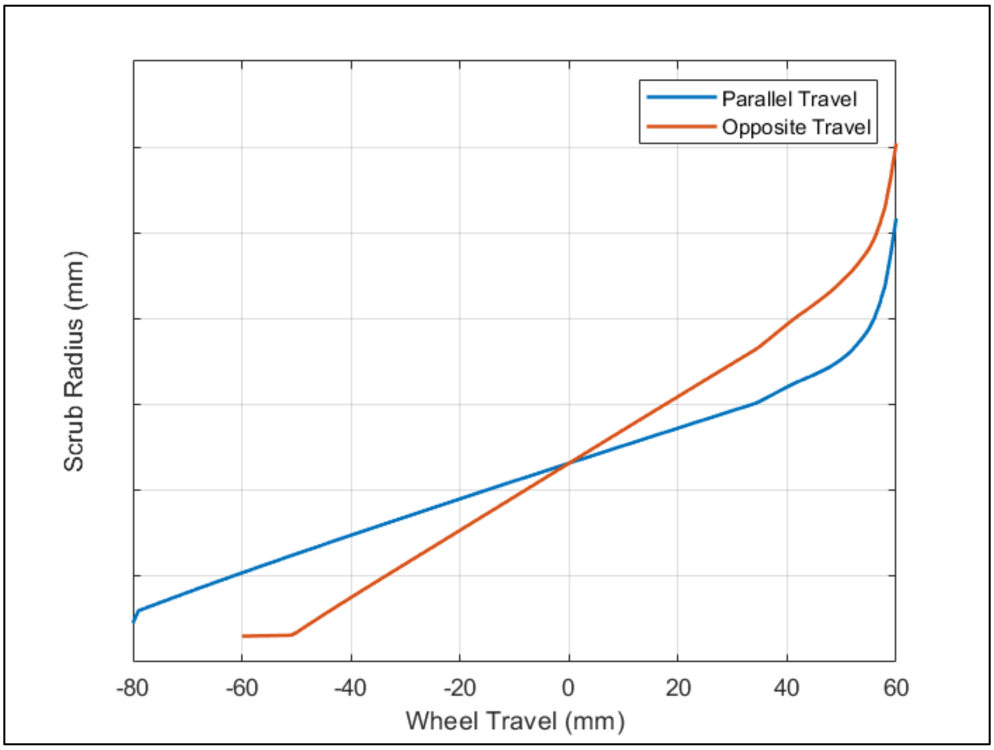

Figure 5.17: Comparison of scrub radii between the two simulations

The opposite travel test will show an higher value at the maximum positive travel position, and a steeper curve compared to the parallel travel test, over the majority of the test the scrub radius behaviour is almost perfectly linear with a sudden increase in both cases towards the end of the compression motion, this can be related to the fact that camber angle is moved towards negative values as the suspension compresses, increasing the distance that is referred by the scrub radius, in Y-direction the contact point of the tire has a similar behaviour between the two tests, and follows an homogeneous line with no particular drops or variations, this can lead to think that the sudden increase in scrub radius is mainly due to alignment parameters that change the distance that is intrinsically related to the scrub radius.

The caster moment arm follows the same idea of the scrub radius in its definition, the scrub radius is seen in front view, while the caster moment arm is obtained from the side view of the wheel. To simply put it: If the caster angle is null the arm will be also null.

As the caster increases in absolute value the distance between the steering axis and the line that defines the mid plane of the wheel, passing through the wheel centre, will increase. This distance is the caster moment arm, that is defined as the projection on the ground of the caster angle, even if it is expected that the highest variation is experienced when looking at the suspension from the front, the wheel travel will largely affect the caster moment.

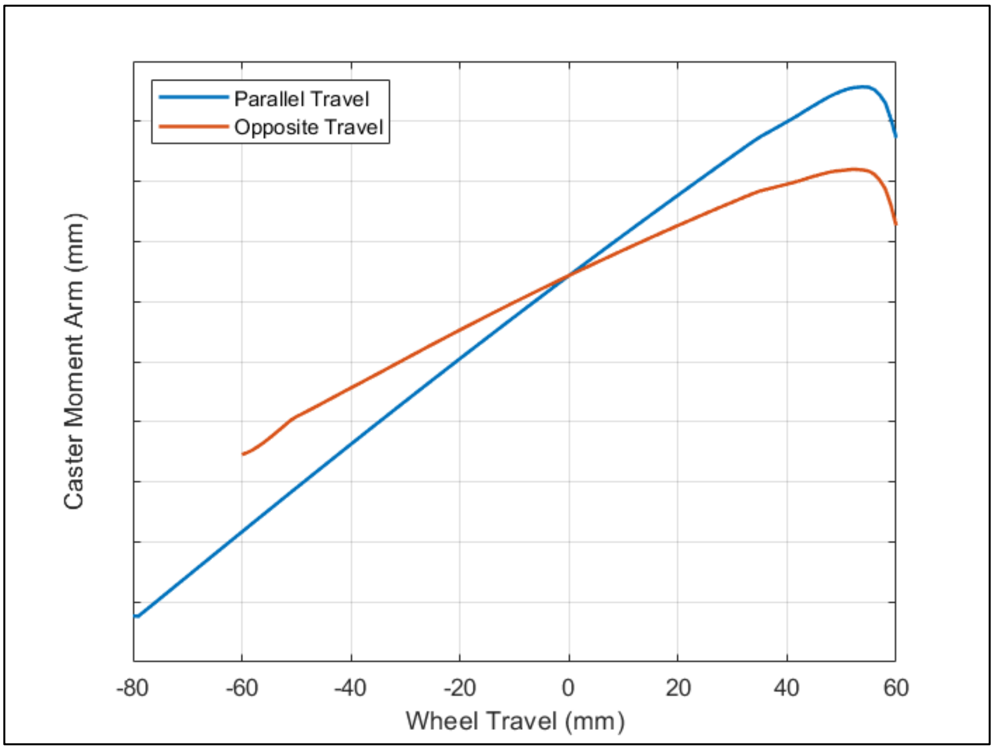

Figure 5.18: Caster moment arm length between the two simulations

In Figure 5.18 the parallel travel test showed a steeper curve compared to the other test, as it is shown, the behaviour is very similar between the two test, as it happened in the scrub radius analysis, the drop in value present towards the end of the graph is explained by the drop in the position of the contact point in X-direction, as it is possible to see in Figure 68 and 74, caster angle has a linear behaviour in both tests, this meant that the drop is mainly due to the change in contact point position.
In Figure 5.19 it is possible to follow the variation in the roll centre vertical position as the two different tests proceed, as the suspension compresses and expands the two arms of the suspension will change their position and will be angled differently, changing the instantaneous centre and so the position of the lines that define the roll centre angle by their intersection.
As it was said for the wheel track, when the two wheels follow the same wheel travel direction the characteristic will have a clear behaviour. In this case as the suspension goes towards negative travel the roll centre height increases and vice versa. In the opposite wheel travel the effect of a wheel will somewhat balance the effect of the other and so the variation is less significant: Highest variations come near the end of each side of the simulation, in one way this is due to the fact that the suspension reaches its maximum compression or extension, on the other way the results will be less reliable near

the end region of the test. Due to the fact that the bump stops will come into play some variability in the calculations will be induced, this is seen from the oscillations that are present in the final parts.

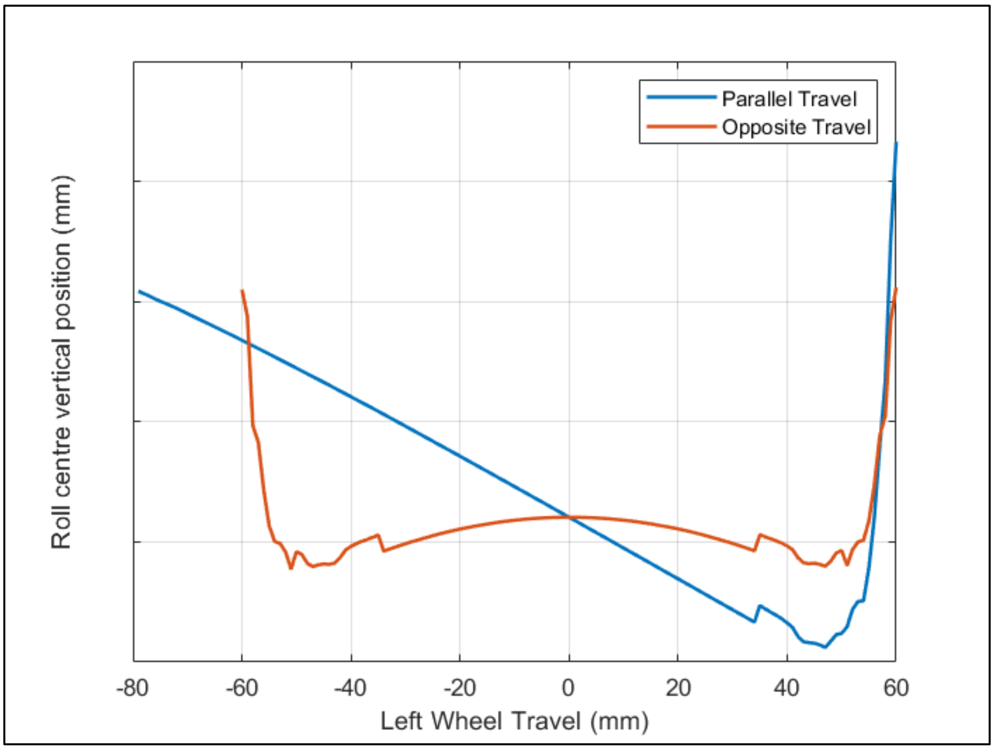

Figure 5.19: Roll centre vertical position as wheel travel changes over the two tests

5.4 Wheel travel tests performed on the rear suspension

After the definition of the front suspension, an analysis on the rear suspension is made to understand how each suspension will behave when placed on the full vehicle.

The simulations were done using the same settings of the analysis performed on the front suspension, except the fact that bump and rebound are symmetric from -60 to +60 mm of wheel travel.

The first parameter to be considered is the vertical force that is applied to the wheels, shown in Figure 5.20: The opposite travel case resulted into a perfectly linear characteristic, the analysis on the parallel travel is also linear but it has a higher slope and will change its slope when the simulation is near the full extension condition. The force expressed in this graph is the total force on the axle, for the parallel travel each wheel will exert the same force at the same time, while in the opposite wheel travel case each wheel will have a different contribution.

The evaluation on track presented in Figure 5.21 follows what was found for the front axle, opposite travel will balance more the variation in track, while the parallel test will show a steeper curve. On the front this was mainly due to the ability of the suspension to adapt to an opposite travel, on the rear is mainly due to the stiffness characteristic of a solid axle.

For the rear suspension the stiffness in the opposite travel is higher than what is found in the front, this is due to the fact that the solid axle suspension at the rear will be more rigid than the double wishbone employed at the front axle.

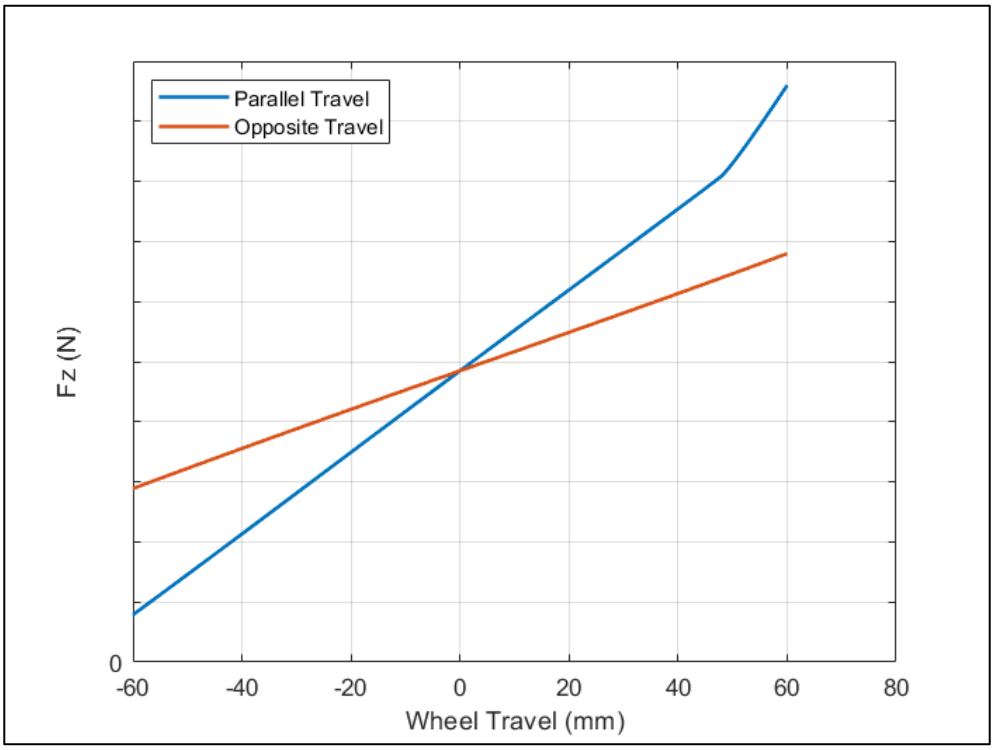

Figure 5.20: Vertical force experienced by the rear suspension in function of wheel travel

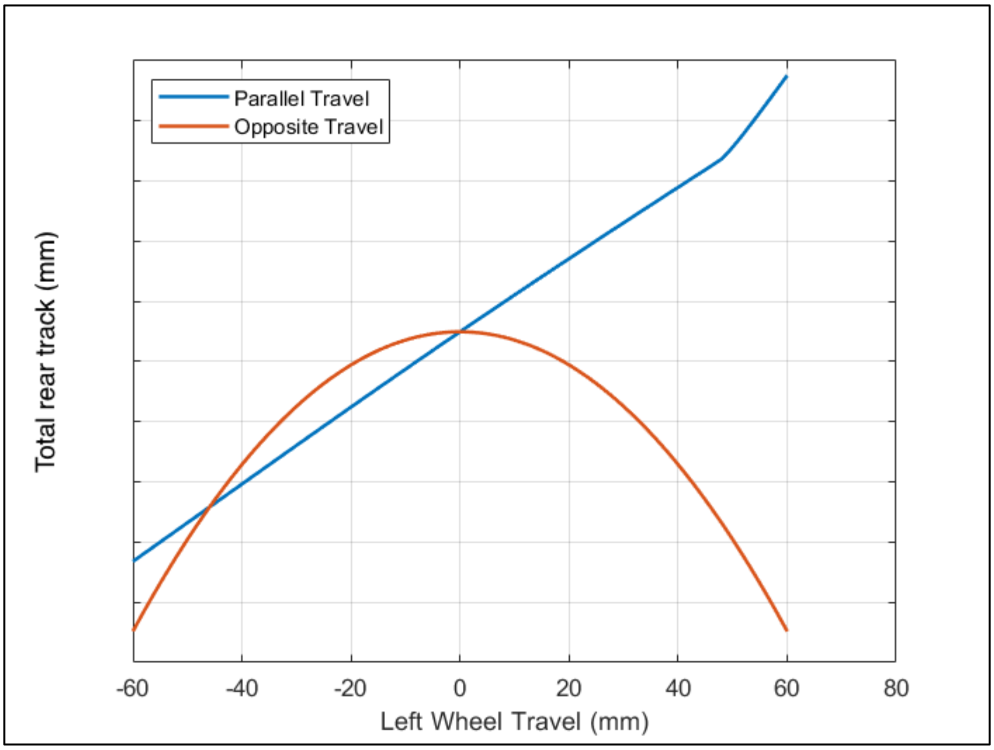

Figure 5.21: Total Rear Track Variation in function of wheel travel

Contact points positions in Figure 5.22 and 5.23 define how much the wheel moves when the suspension changes its travel, calculations are done on the left wheel.

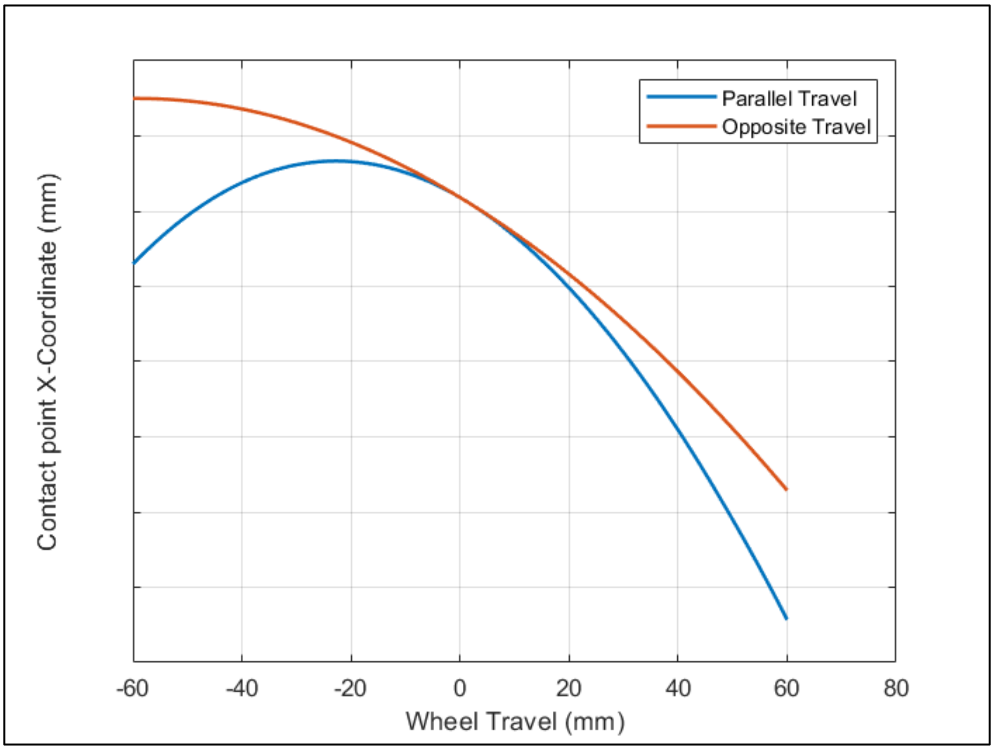

Figure 5.22: Contact point along X-axis in function of wheel travel

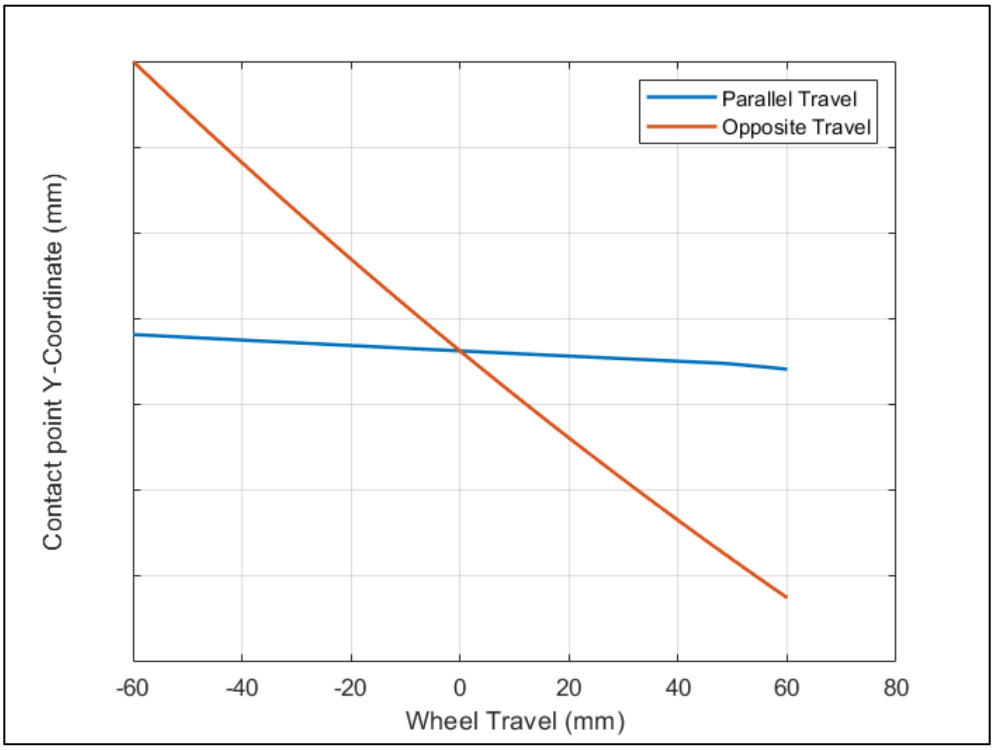

Figure 5.23: Contact point along Y-axis in function of wheel travel

Parallel travel will have a small variation in position along the Y-axis but a large envelope in the variation of position along the vehicle's side. Opposite travel will show a large variation in the Y-axis displacement, variation in X-axis is relevant but less pronounced than the parallel wheel travel case, from these tests it is possible to understand that wheel travel will move the wheel in side-view, changing the wheelbase as an effect.

The roll centre variation will be linear for the parallel wheel travel and almost constant with a parabolic trend for the opposite travel case, this is clearly shown in Figure 5.24.

This parameter follows what was found for the wheel track, the opposite wheel travel condition will make the roll centre position balance itself as the two wheels show a travel that has opposite trends between them.

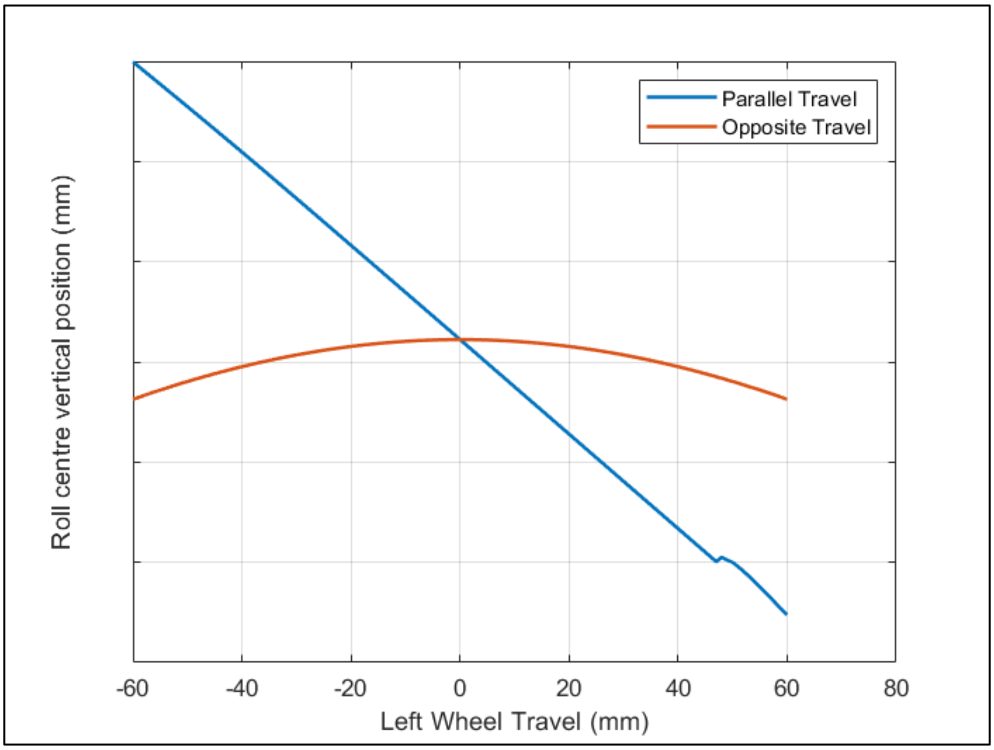

Figure 5.24: Roll centre variation for the rear axle

To conclude the analysis on rear steering an analysis on the Anti-lift during braking was performed in Figure 5.25 comparing the two vehicle configurations.

Anti-lift is a characteristic that evaluates how much a vehicle resist to the motion of the vehicle that during braking will make the nose pitch down and the rear of the vehicle to lift, an anti-lift of 100% at the rear will mean that the vehicle is flat during braking.

The two configurations react similarly between them, the highest difference come from positive wheel travel conditions, near neutral travel, especially for negative values the two characteristic almost overlap.

To conclude, it is important to know that the rear suspension also reacts to static excitations like the ones present in this study, by comparing the graph between the front and the rear axles it is possible to see how much difference there is between the two suspension systems.

Alignment parameters such as toe are not evaluated for the rear axle, due to the fact that a solid axle will have a negligible variation in toe and the variation in camber will be better explained in paragraph

6.1, the main difference comes from the contact point distribution and the fact that anti-lift is almost the same between the two vehicles.

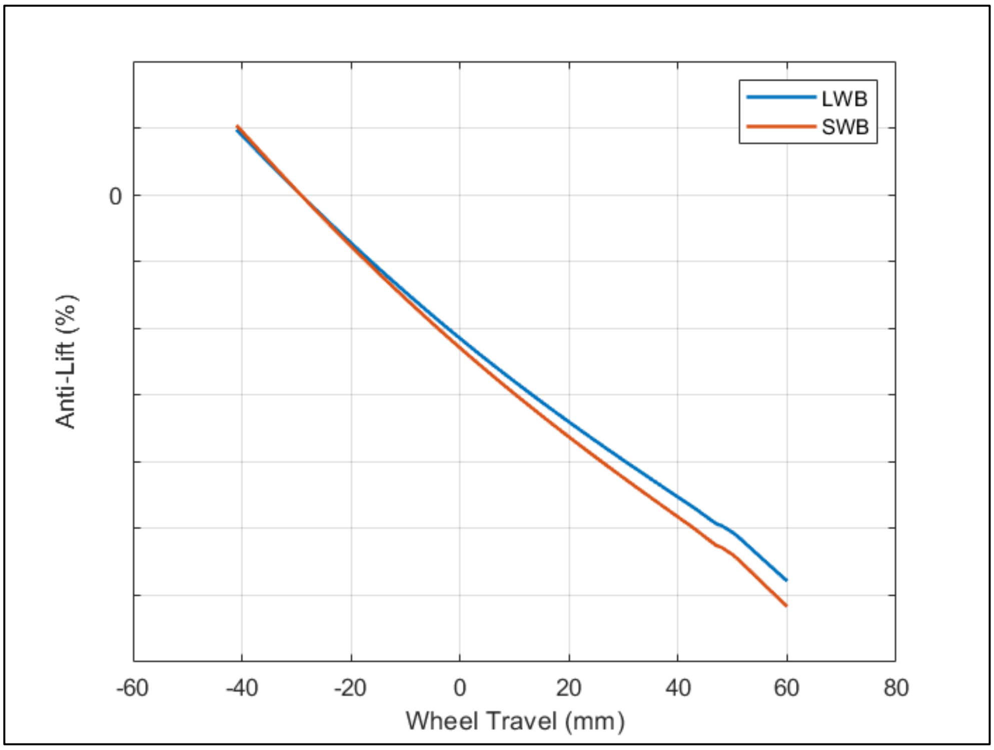

Figure 5.25: Anti-Lift characteristic during braking in function of wheel travel

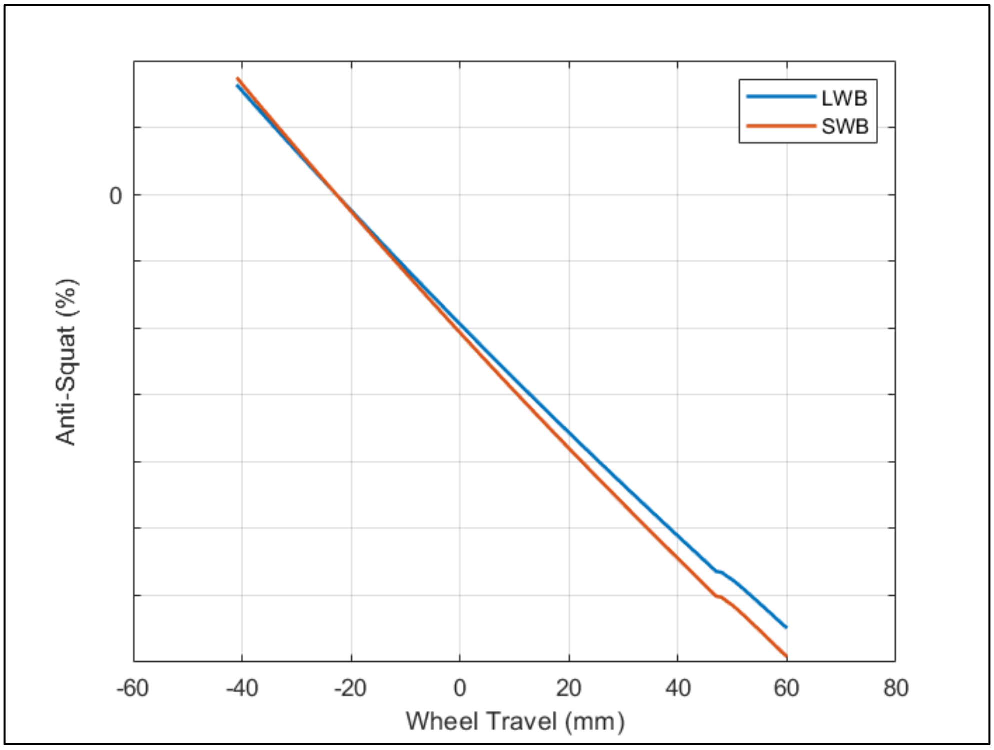

Figure 5.26: Anti-Squat Characteristic for the rear suspension during acceleration

The graph passes from positive values to negative values, this changes the characteristic to a pro-lift, it means that the suspension geometry will induce lifting in the suspension, and not counteract it, during braking, the compression of the suspension largely affects the instantaneous centre location and this leads to a change in sign for the characteristic.

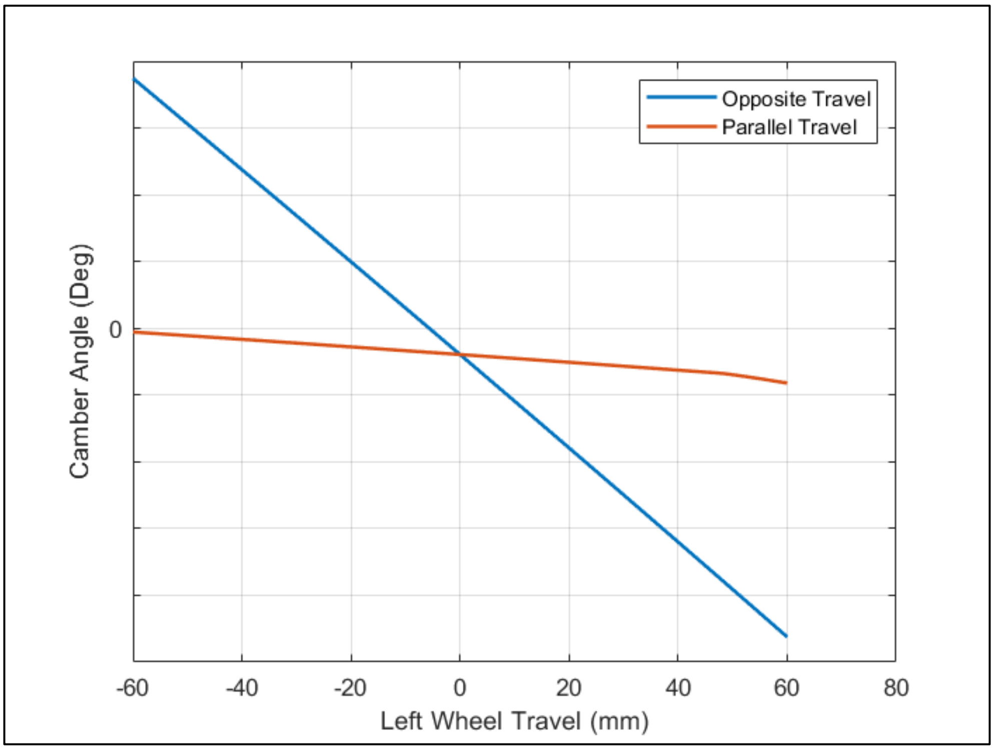

Figure 5.27: Camber angle variation on the rear suspension in function of wheel travel on the left wheel, the right wheel characteristic will be the same

Since the vehicle is rear wheel driven, it is also interesting to check the anti-squat characteristic of the suspension, this resulted in the graph in Figure 5.26.

This characteristic expresses how much the vehicle will counteract the squat that will happen when the vehicle accelerates: In acceleration the torque applied on the rear wheels will induce the rear suspension to compress and lower themselves resulting in a nose-up of the vehicle. An higher anti-squat percentage will mean that the suspension will counteract this motion more, a negative anti-squat will favour the squatting motion of the suspension. This characteristic will be positive only towards negative wheel travel points, the difference between the two configurations is clearer for positive wheel travels, the shorter vehicle will have a higher slope compared to the long wheelbase vehicle.

To end the discussion on the rear suspension an analysis on camber angle is performed, mind that camber angle is expressed in relation to the body vertical line, as explained in Chapter 2.

Parallel travel will show almost no variation in camber, while opposite travel will show high variations, this is mainly due to the fact that a suspension like this will not have camber recovery. A twist of the suspension system showed by an opposite wheel travel motion will induce a camber variation, that will be almost symmetric between positive and negative wheel travels, the variation will also be affected by the fact that the vertical line from which camber is evaluated will also change in tests like this, that basically induce some roll angle to the vehicle, this will amplify the difference in the case of the opposite wheel travel test. Results are shown in Figure 5.27.

5.5 Conclusions on static wheel travel tests

Both parallel and opposite wheel travel test help in understanding how the suspension changes its geometry as wheel travel changes.

The objective of these tests is to find which are the important parameters to evaluate: In simulations like these the main point of interest is the evaluation on geometry. Considering this fact, it is mostly important to check how kingpin angle, scrub radius, caster angle and caster moment arm vary. These elements define the steering axis of the suspension on the front: From the results obtained is it possible to know, for each displacement of the wheel which is the steering axis.

Steering axis is useful for what concerns the front axle, at the rear the evaluation of the same values has no useful meaning. What is useful for both front and rear suspension is the evaluation of anti-dive and anti-lift over braking, as well as anti-squat over acceleration for the rear suspension.

These values will define how much the vehicle is prone to movements during straight-line events.

6 Tests on the complete vehicle: Ramp, step & sweep steer

6.1 Ramp Steer

6.1.1 Introduction to the tests performed

The ramp steer manoeuvre is a simple test that increases gradually the steering angle with a set ramp increase measured in deg/s, this means that the vehicle will be steered at an incremental degree with a rate equal to the one set by the ramp input.
This test is usually characterized by a slow rate of steering and is aimed at simulating how the vehicle reacts to gradual steering manoeuvres, like it is shown in Figure 6.1.

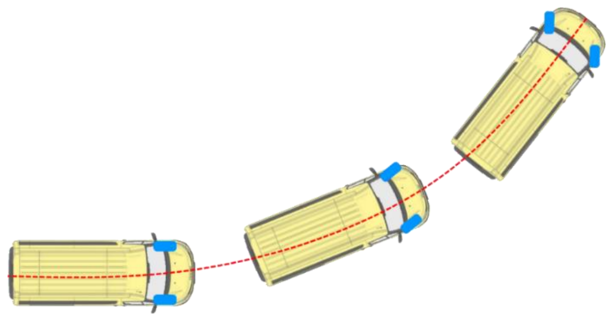

Figure 6.1: Drawing that demonstrates how, as the manoeuvre proceeds, the steer angle increases gradually

For this particular study the test was performed on two different vehicles, the first in short wheelbase configuration (3520 mm), and the second with a longer wheelbase (4120 mm), the suspension setup and the powertrain adopted are equal between the two vans. The differences between the two vehicles comes from the fact that the short vehicle is in its fully loaded configuration, while the long one is in a condition with no cargo, this is due to the availability of reliable data from the manufacturer.
The parameters that could be changed in the simulations were four:

- The speed at which the vehicle is travelling
- The gear selected for the manoeuvre
- The rate of the ramp steer in deg/s
- The delay from the starting point at which the actual ramp steer started

In Table 6.1 it is possible to catch the simulation parameters between the two vehicle configurations, the tests were carried out on the same conditions except for the vehicle model used.

Test	Speed (km/h)	Gear	Ramp (Deg/s)	Weight	Body Type
#1	80	4	10	2.5 Tons	Long Wheelbase (4120mm)
#2	80	4	10	3.4 Tons	Short Wheelbase (3520mm)

Table 6.1: Different ramp steer tests performed

Even by watching Figures 6.2 and 6.3, without any analysis, it is possible to see how the vehicle reacts, the body roll is significant in both tests and the front and rear axles reacts differently, the front axle will show a more compliant behaviour thanks to the double-wishbone geometry, the rear suspension will be less prone to change its position.

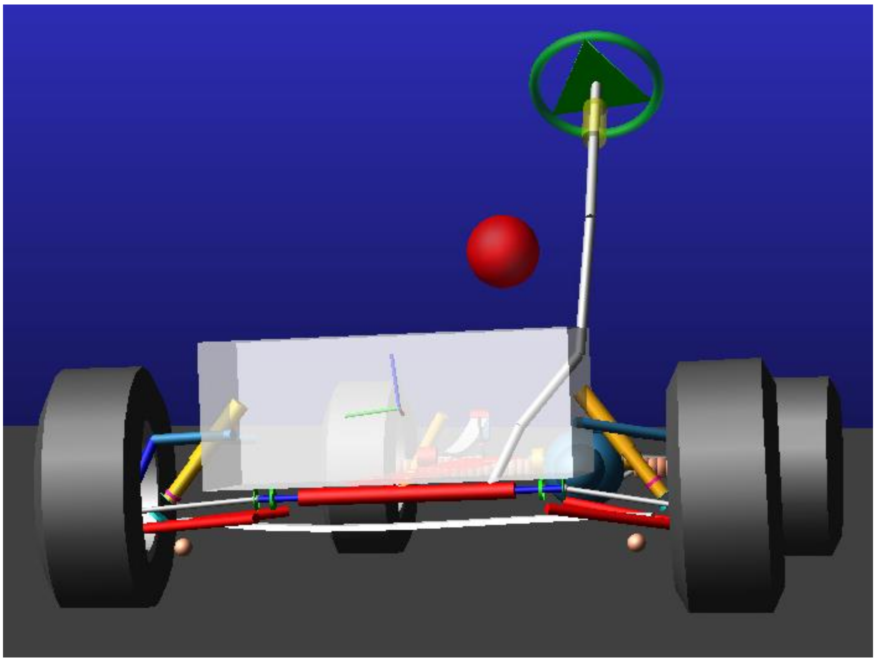

Figure 6.2: Representation of the vehicle during the manoeuvre seen from the front

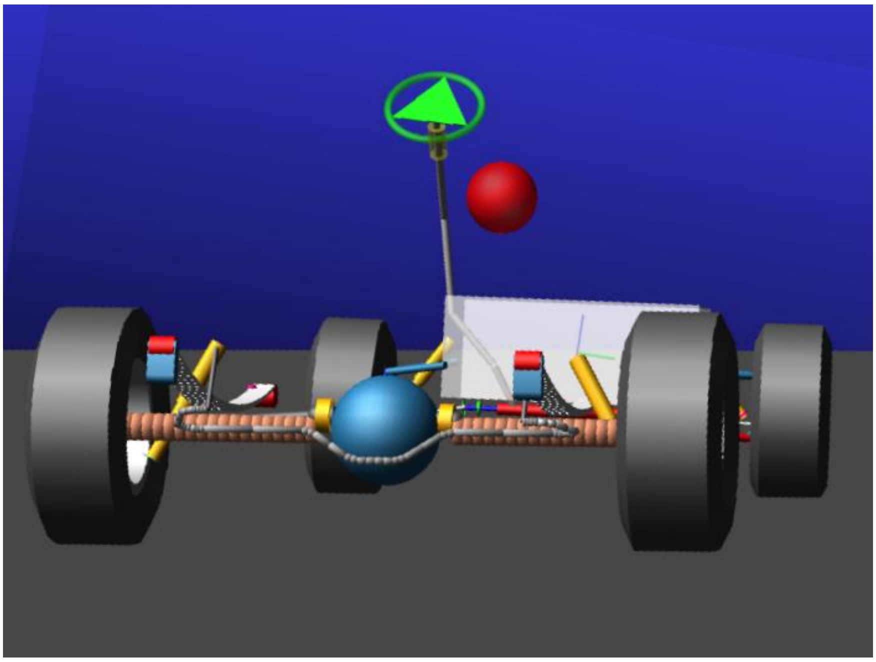

Figure 6.3: Representation of the vehicle during the manoeuvre seen from the rear

The speed selected is of 80 km/h, this speed was selected because it is a good representative of the average speeds at which vehicles of this type usually travel on secondary roads with a good amount of corners, higher speeds that are more representative of highway driving are not analysed because on roads like that corners are rarer and of smaller radius.

The gear selection was performed in a simple way, for each vehicle speed, Adams Car suggests a gear to be used given the powertrain parameters, the software suggested the use of the fourth gear when travelling at 80 km/h. This can be realistic for roads with a certain slope, most likely higher gears would be selected in the real world to save fuel if the road is flat, the gear selected is not a parameter that will affect the results by much, so the gear suggested by the software is selected. The ramp is kept constant at 10 Deg/s through all the tests performed.

For what concerns the delay, it was chosen to start the steering manoeuvre two seconds after the actual start of the test, this allowed the system to settle in the straight driving part at constant speed before the steering motion, the simulation starts with a slightly negative steering angle, this is due to the settling that the software does before starting the manoeuvre.

This first part of the study was performed to evaluate how the two vehicles behaved with respect to a ramp input, after this first evaluation it was decided to evaluate how alignment factors such as the static camber and toe values changed the behaviour of the vehicle. This test was performed considering just the long wheelbase vehicle, keeping as the variable between tests only the static camber and toe settings.

6.1.2 Comparison between different vehicle configurations

As stated in the introduction, two different vehicles were considered in the first evaluation, the short wheelbase model was provided by Iveco, while the long wheelbase one was adapted from the 3520mm vehicle using data from the manufacturer, the former vehicle is at its maximum payload while the latter is in unladen conditions.

The interesting thing about the comparison between these two different vehicles, is the fact that mechanically these two vans are exactly the same: Same suspensions, same wheels, same engine and powertrain, the difference relies only on the body length and on the weight.

This can give useful results in how different configurations may affect the driving dynamics of the vehicle, this is especially important in the world of commercial vehicles, due to the variability in layouts that these vehicles usually have.

The first impressions on the differences between the tests can be seen in Figure 6.4, this picture shows the radius of the curvature created during the steering manoeuvre. The first peak corresponds to the moment when the steering wheel is first moved, then it gradually decreases due to the higher steering angle the test proceeds: In this case the differences mainly depend on the type of ramp input that is selected. It is possible to see that the difference between the same test but with different vehicles is minimal, this is important for our results because it means that the vehicles will follow very similar trajectories, the longer vehicle will show a slightly higher radius due to the reduced agility compared to the short wheelbase vehicle, given its increase in length.

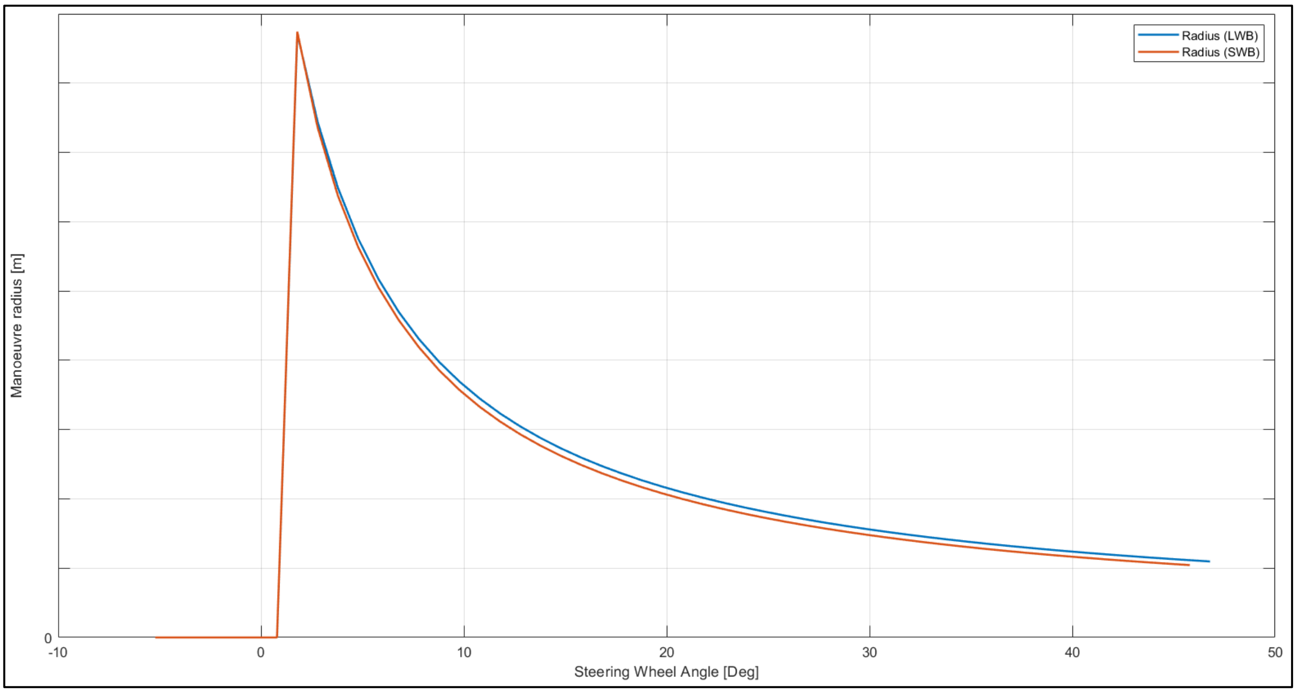

Figure 6.4: Radius of the manoeuvre in function of the steering wheel angle

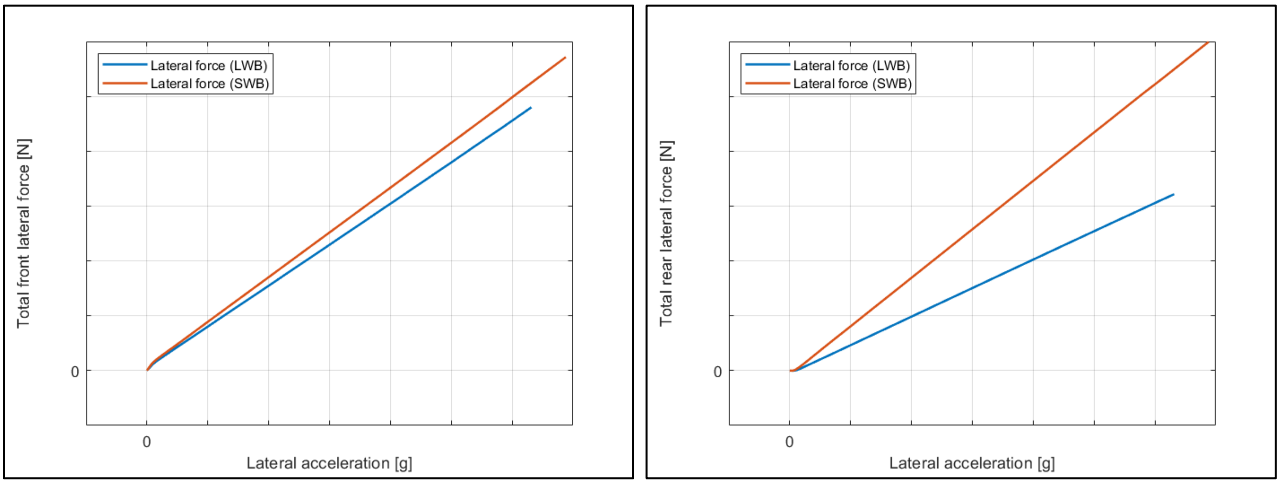

Figure 6.5: Total lateral force on the front and rear axle in function of lateral acceleration

The first parameter to be analysed is the force acting on the wheel, since the system evaluates the force on each wheel, the comparison is done using the total force on each axle, this value is computed using Equation 6.1, the value is shown in the graph in Figure 6.5 in absolute value, the force is computed at the centre of the wheel, a position corresponding to the wheel hub mounting point.

In terms of values, similar quantities of forces are measured on the front and on the rear axle, the short wheelbase van reaches higher forces and accelerations, the acceleration level that the vehicle reaches gives the maximum level of cornering performance. This explains why these graphs and the majority of the graphs of this chapter are plotted against the lateral acceleration, by plotting the graphs against lateral acceleration it is possible to evaluate the parameters up to the vehicle maximum grip level, but also after it.

$$(6.1)\ F_{tot} = F_{left\,wheel} + F_{right\,wheel}$$

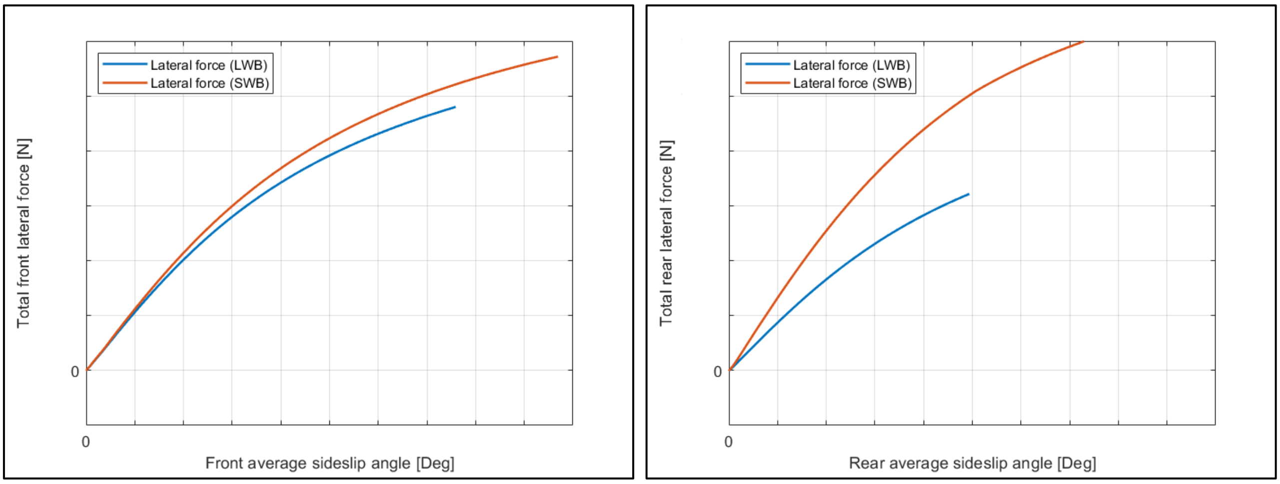

Figure 6.6: Front and rear lateral force plotted in function of the average side-slip angle

For both the short and the long wheelbase vehicles the pattern is similar, as acceleration increases, force also increases, this is valid up to the point of maximum acceleration, after this point force will continue to grow but acceleration will reach an asymptote because the vehicle will start to oversteer decreasing its performance.

What was found as valid for the front axle is also true in the rear of the vehicle, this time the difference in force is higher between the two vehicles, this is mainly related to the fact that the weight distribution is largely different between the two vehicles, the shorter vehicle is fully loaded, this higher weight will translate into higher forces on the rear axle.

Lateral force is also useful to be plotted against the average side-slip angle, as it is done in Figure 6.6, the slope of this graph will represent the cornering stiffness of the vehicle.

These graphs relate the amount of slip that a wheel, or in this case the average of the two wheels on a given axle, to the lateral force that is acting on the wheel centre, the front axle evaluation results in little differences between the two vehicles, the main difference being that the 3520mm vehicle reaches higher side-slip angle values and forces, the rear axle shows big differences instead, lateral force reaches values twice as big for the shorter vehicle compared to those experienced by the long wheelbase van, side-slip angle reaches also higher values in this case.

In both of these graphs it is possible to see that the force grows with side-slip angle, the main difference between the two vehicles comes from the behaviour on the rear axle, this is something that is somewhat expected, the front of the vehicle is unchanged between the two vehicles, this means that the front suspension will have almost the same position in space between the two vehicles, the rear axle is instead in a different position between the two configurations, by a good margin.

There is a 600mm difference in length between the two wheelbases, this will obviously affect how forces act on the vehicle, moreover the different weight distribution will further increase the difference.

The force measured at the wheels mainly reflects the load that each axle has to sustain during these manoeuvres, to further analyse the dynamics of the vehicle in study is useful to evaluate parameters that give an idea about the grip levels of the vehicle.

The side-slip angle measured at tire level shows the attitude of the vehicle in relation to the circular path during a steady-state cornering [5]. The higher the angle the more the wheel has to be steered to maintain a certain trajectory, this is due to the fact that when a side-slip angle different from zero is present the direction at which the wheel is pointing, and the direction of travel are not the same and have an angle between them: This angle is exactly the side-slip angle. The measurement of the side-slip angle is important in the definition of the dynamic behaviour of the vehicle in these manoeuvres, especially in understanding if the vehicle is in oversteering or understeering condition.

In these calculations the average side-slip angle α between the two wheels was considered, as expressed in Equation 6.2.

$$(6.2)\ \alpha_{average} = \frac{\alpha_{left\ wheel} + \alpha_{right\ wheel}}{2}$$

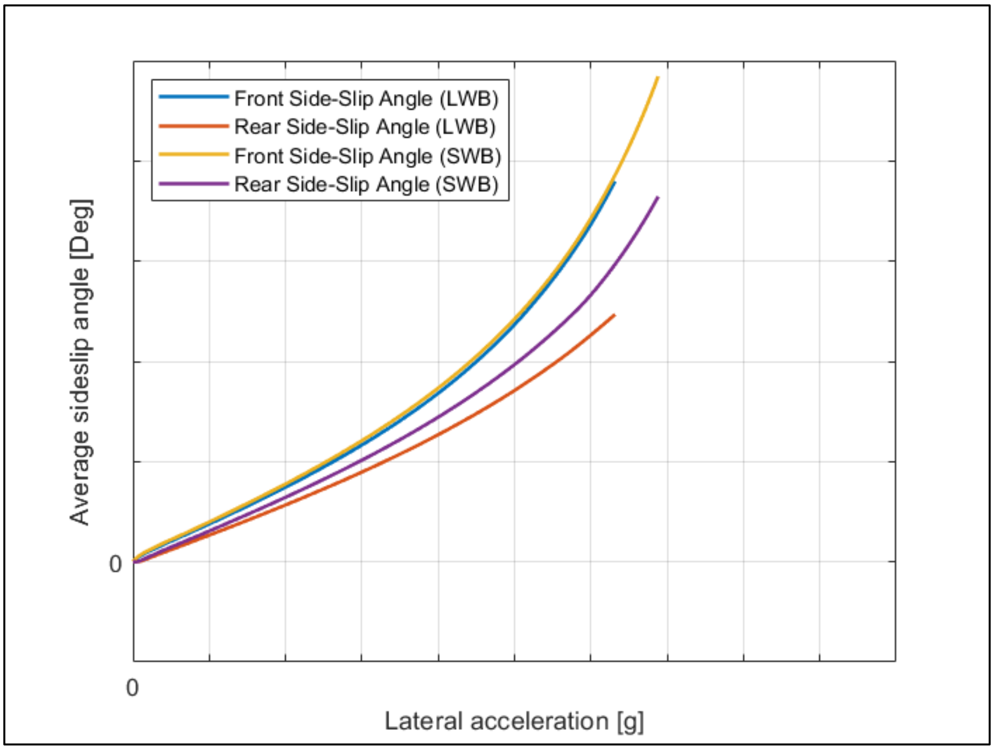

Figure 6.7: Average between the side-slip angles of the two front and rear wheels in function of lateral acceleration

By looking at Figure 6.7 it is possible to estimate how the side-slip angle is related to the vehicle lateral acceleration, for both axles.

In all the cases the vehicle will be in understeering conditions, due to the fact that absolute values of the front side-slip angles are higher than those at the rear, minding that these tests returned negative side-slip angles, leading to a front to rear ratio greater than one.

This condition is commonly found in road vehicles due to the higher predictability when driving, an understeering vehicle behaviour could be corrected by lifting off the gas usually, while an oversteering behaviour will break the driving balance of the vehicle more easily leading to more dangerous conditions, that are usually corrected by maintaining the throttle and correct the steering input or by managing the throttle mid-corner: Both techniques require high driver capability and it is easy to over react the loss of grip and make the vehicle spin, this is even more important in a rear wheel drive vehicle that will be naturally more prone to oversteer.

To evaluate if the vehicle is in understeering or oversteering conditions the graph in Figure 6.8 is used, this figure shows the difference between the front and the rear average side-slip angles. If the front side-slip angle is higher than the rear one, the vehicle will be understeering, if the opposite happens the vehicle will sustain oversteer. The evaluation was done with absolute values of the two angles, being both of them negative.

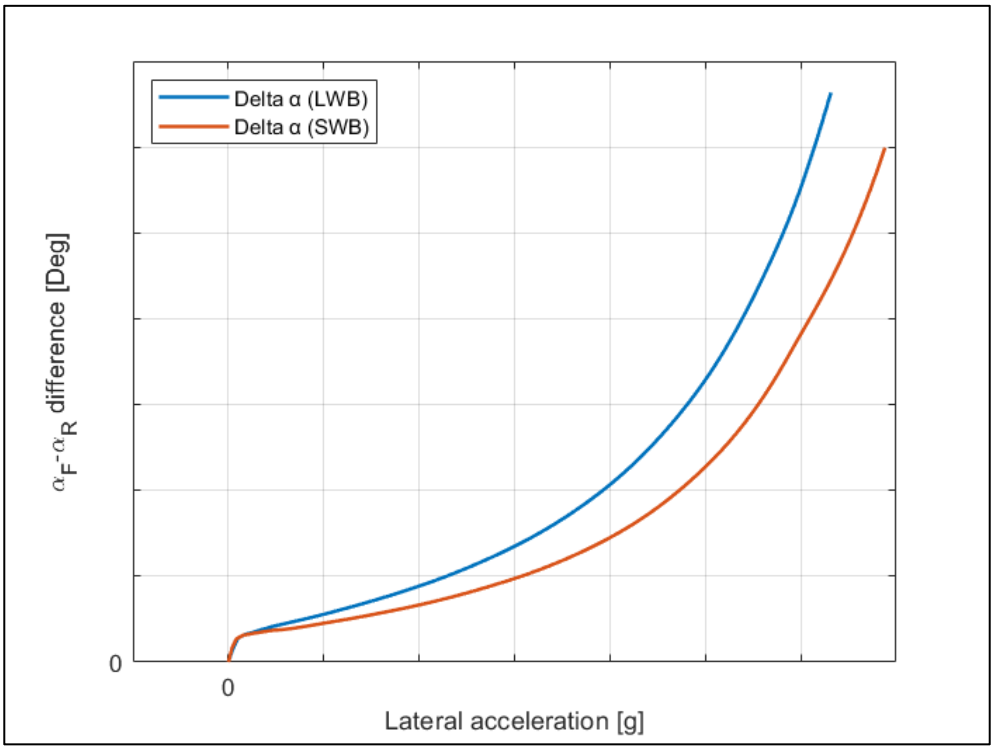

Figure 6.8: Difference between front and rear side-slip angle between the two configurations

If the values stay positive it means that the front side-slip angle is higher than the rear one, this is true through the whole test: It means that the vehicle will be understeering.
The shorter vehicle will have a less pronounced difference, meaning that it will have less understeer or more oversteer depending on the point of view. Maximum acceleration has a relatively small difference between the two angles, the tendency of increased oversteer from the shorter vehicle is expected: A reduction in wheelbase will usually make the rear of the vehicle pivot faster round a corner, increasing the oversteering effect.
As the vehicle will perform the manoeuvre, the camber angle will change, the front wheels show similar behaviour and values, the inner wheel will show higher camber values compared to the outer one, results are shown in Figure 6.9. The behaviour of the rear axle is largely different from what is seen in the front, this is largely due to the fact that a rigid axle is employed, leading to a behaviour where the two wheels will lean in the same way due to the force acting on them.
The sign of the angle is opposite between the two sides, even if the values are very similar between the two wheels, albeit with higher absolute values for the inner wheel. The inner wheel will have a positive camber condition, while the outer wheel will have negative values, results for the rear axle are found in Figure 6.10. The other relevant alignment parameter analysed is toe angle, the behaviour will follow the steering angle closely.

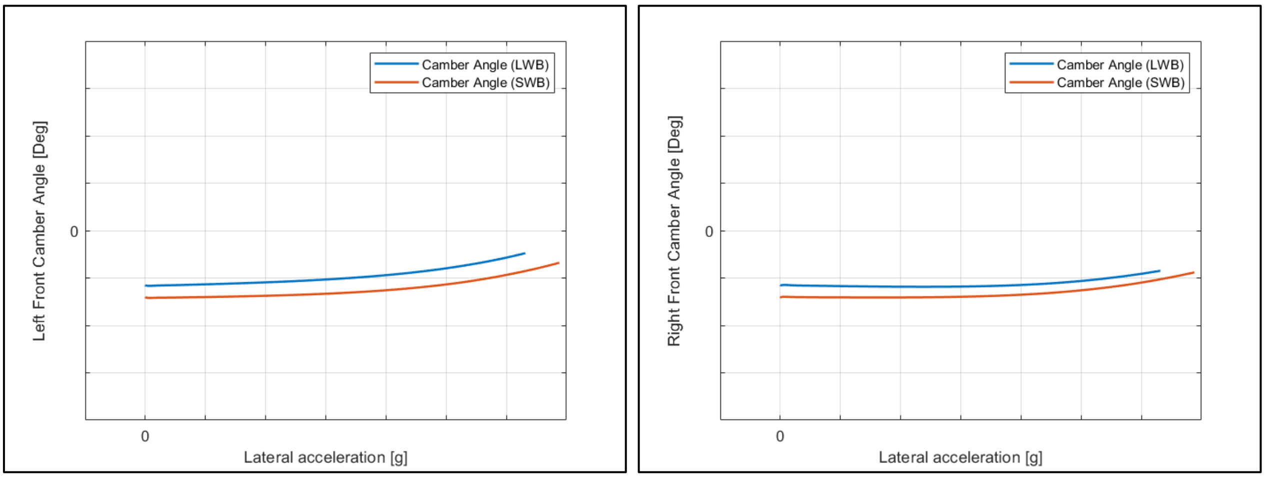

Figure 6.9: Left & Right front Camber angle variation in function of the lateral acceleration

By looking at the graph in Figure 6.11 it is possible to see some similarities to the graph in Figure 6.15 that plots the steering wheel angle in function of the lateral acceleration, by comparing these graphs it is possible to understand that toe angle and steering angle have a close relationship, this is clear when seeing the wheel from the top. As the wheel will be steered the rotation will change the amount of toe of the vehicle, the analysis on toe was performed just on the front axle, the rear axle will show small values due to the fact that a solid axle will have almost no toe variation.

It is useful to evaluate how the inclination angle changes during the manoeuvre. This angle is strictly related to the camber angle: It is defined on the same way as the camber angle, but it is referred to the ground and not to the vehicle body.

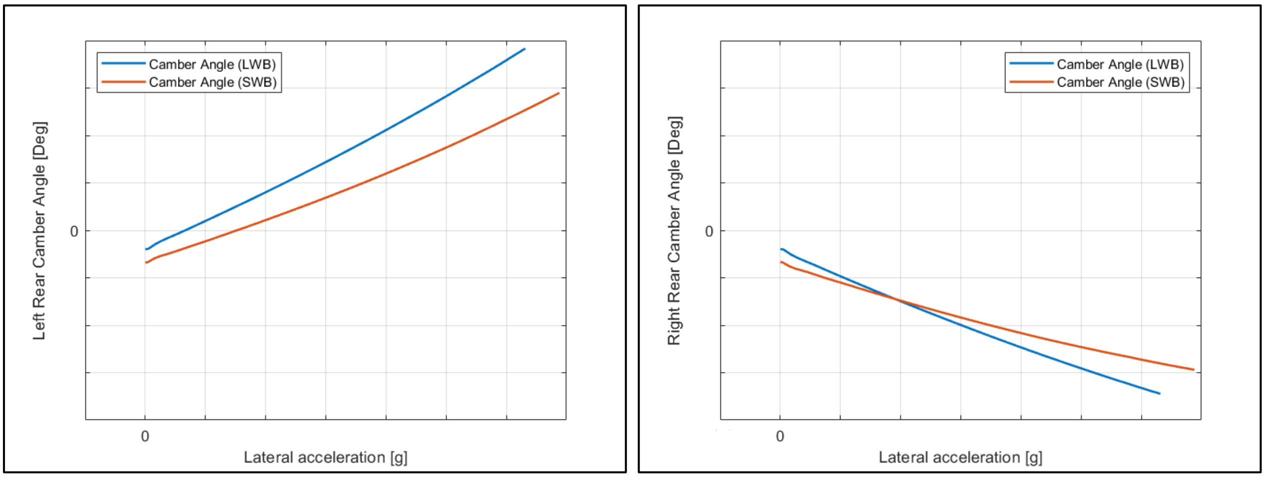

Figure 6.10: Left & Right rear Camber angle variation in function of the lateral acceleration

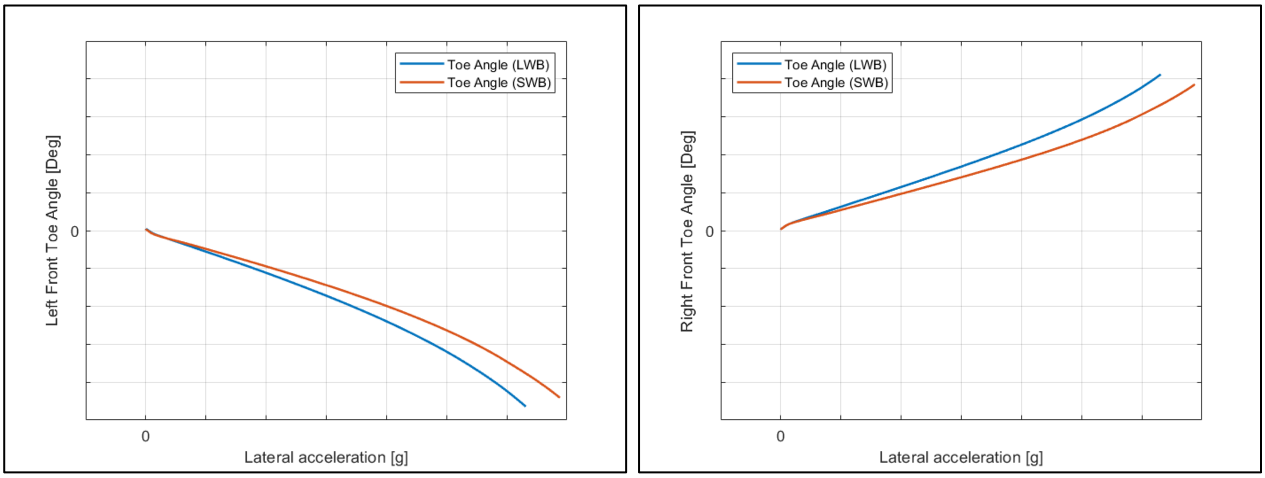

Figure 6.11: Left & Right front toe angle variation with lateral acceleration

In manoeuvres like this the vehicle will experience some degree of roll and so this calculation is more representative of the true angle that the wheel makes with respect to the ground.

In Figure 6.12 it is possible to see the results for the front axle: The vehicle has a higher angle on the inner side, while the outer side shows lower values.

When looking at the variation the situation changes: Given that the vehicle starts from a negative static camber condition, the variation in angle that the outer wheel sustains is higher than that found on the inner wheel by a small margin.

On the rear axle, as shown in Figure 6.13, the situation is similar. The only notable difference is an inversion of trend for the right rear wheel: At a certain point the shorter vehicle will experience higher angles than the long wheelbase one.

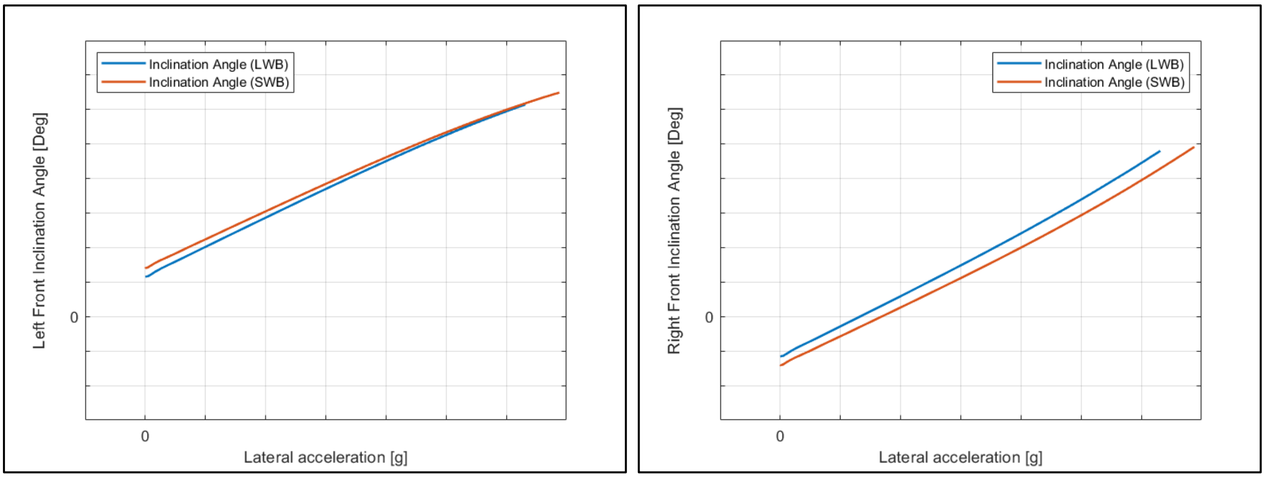

Figure 6.12: Inclination angle variation on the front axle, for the two vehicles in study

The last important angle of the vehicle is the roll angle, this value is especially relevant for vehicles such as the one in study, these vehicles are usually tall: The roll angle is one of the most noticeable effects on the driving experience, results are shown in Figure 6.12.

The long wheelbase vehicle will have a slightly higher maximum value of roll angle and for the same will show a higher lateral acceleration for the same angle compared to the longer vehicle, this is mainly due to the fact that the centre of gravity is placed higher up in the higher vehicle, this will induce more roll.

The difference between the two is, by the way, small, the loaded shorter wheelbase vehicle will be favoured in terms of roll due to the lower weight and centre of gravity position.

The best way to sum up how the vehicle, ultimately, behaves is to plot the understeer characteristic.

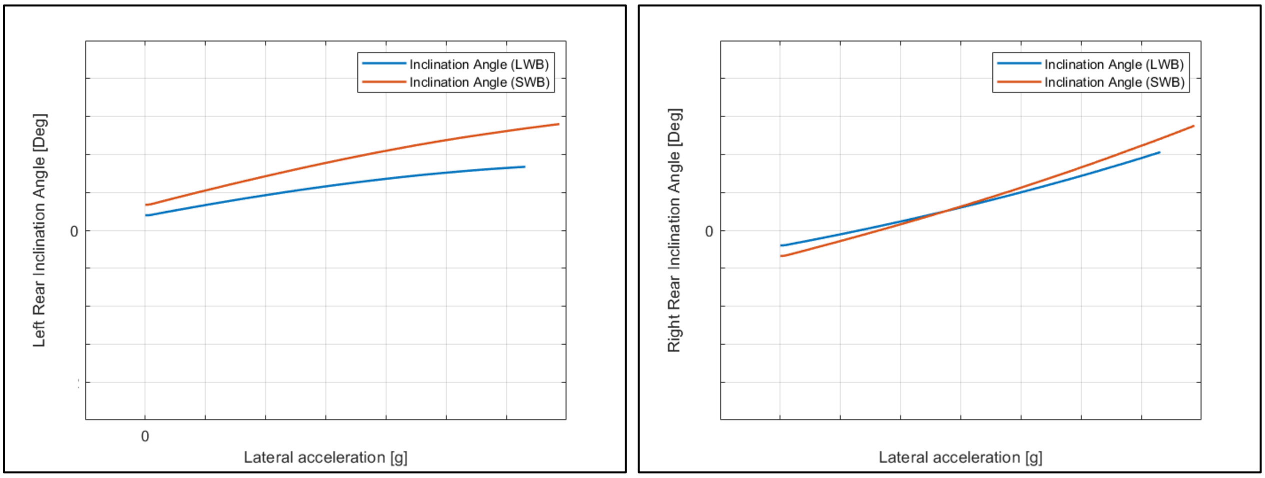

Figure 6.13: Inclination angle variation on the rear axle, for the two vehicles in study

Understeer characteristic is shown in Figure 6.15 and the variation of the side-slip angle computed at the centre of gravity of the vehicle with lateral acceleration, as it is done in Figure 6.16.

In these graphs the neutral steer line would be a straight diagonal line, in both configurations the lines move towards the upper side of the graph, meaning that the vehicle is in the understeer case, the long wheelbase vehicle shows higher understeer than the shorter one.

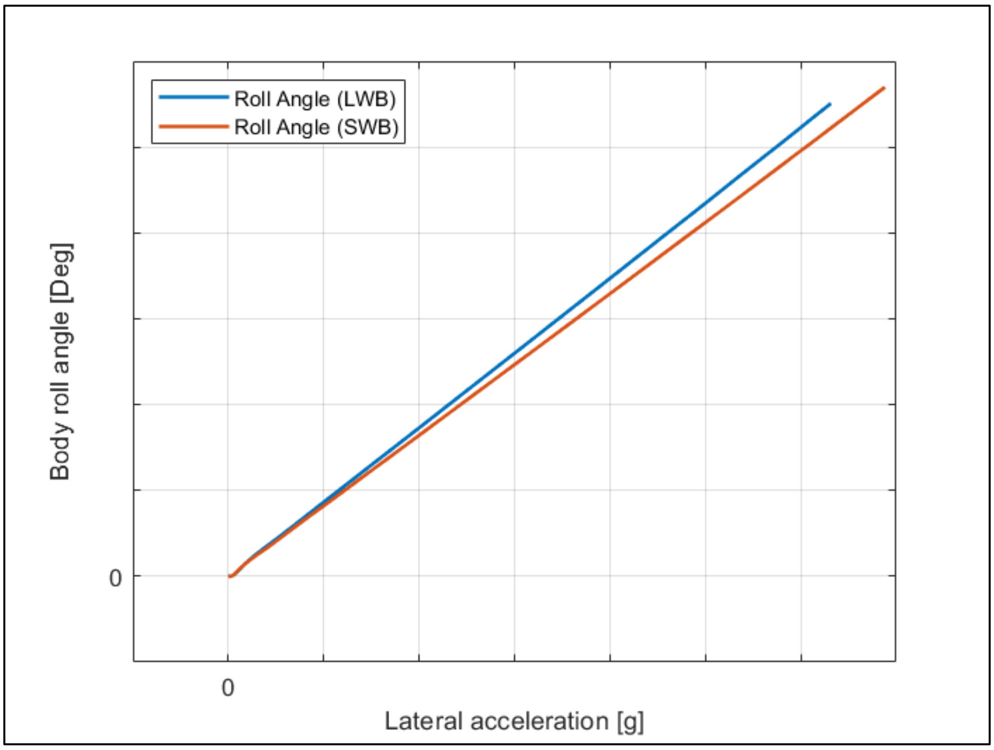

Figure 6.14: Body roll angle in function of lateral acceleration for the two vehicles

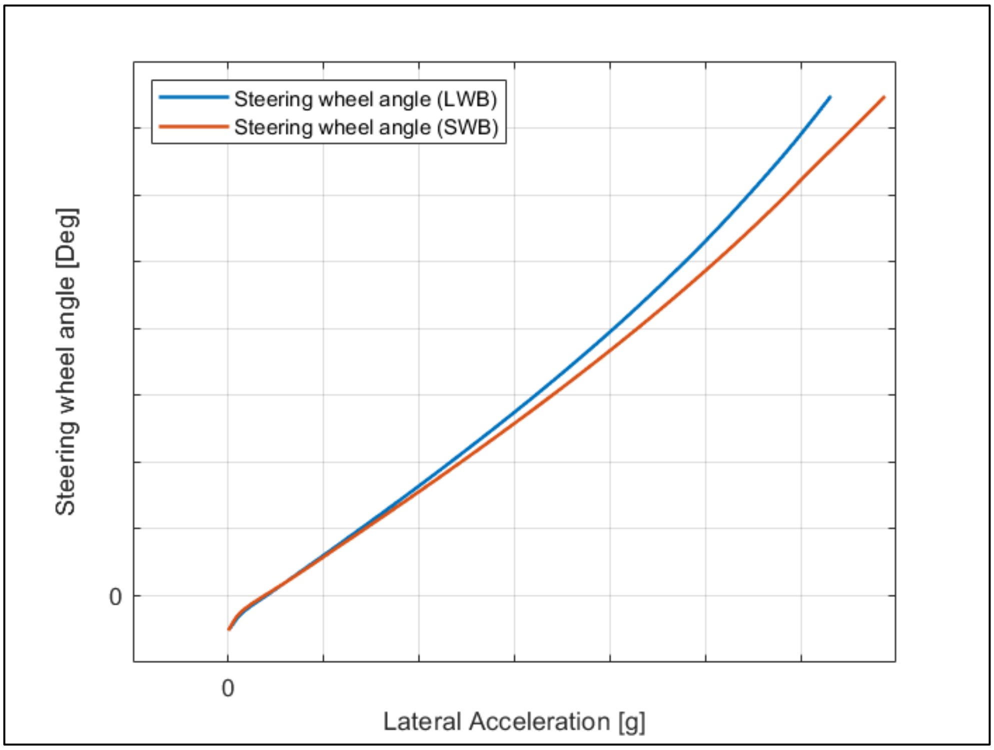

Figure 6.15: Understeer characteristic for the four tests performed

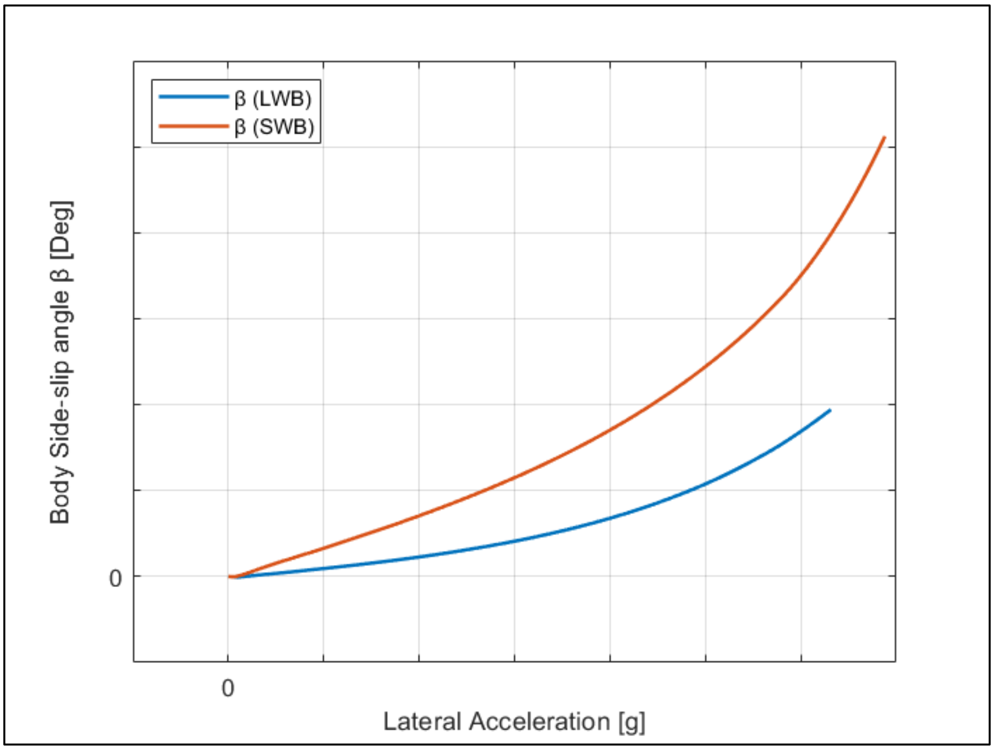

Figure 6.16: Side-slip angle computed at vehicle centre of gravity in function of the lateral acceleration of the vehicle

Body side-slip angle plot is another graph useful in setting how the vehicle behaves, in this case the shorter wheelbase vehicle will show higher side-slip angles compared to the longer one. The short wheelbase vehicle will steeply increase the side-slip angle towards the point of maximum acceleration, the longer vehicle will show a more gradual curve.

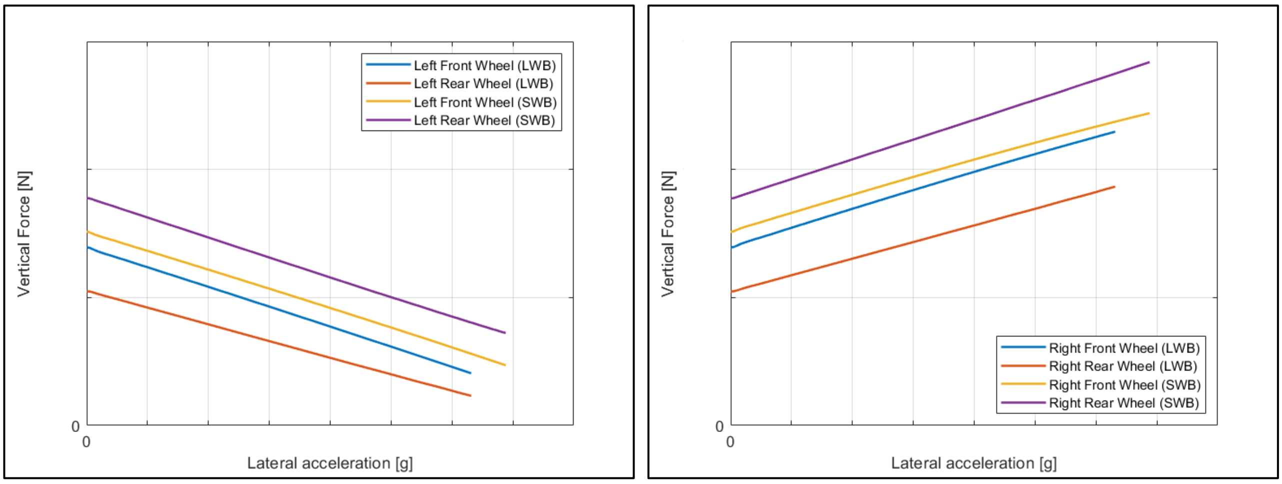

Figure 6.17: Vertical force acting on each wheel for the two configurations

To conclude the comparison between the two vehicle configurations, the vertical force acting on each wheel was computed in Figure 6.17.

On the left the graph of the left front and rear wheels of the vehicle is presented, on the right the other side is shown: On the left the vertical force will decrease as acceleration increases, while the opposite happens on the right, the starting point is common between the two sides in term of values, this condition is easy to understand, at the beginning the vehicle is moving on a straight line, the weight is distributed equally left to right and no acceleration is imposed laterally to it. As the vehicle will begin its turn towards the left the right wheels will be more loaded as the manoeuvre continues, while the inner wheel will see a reduction of the load applied to them in favour of the outer wheels. The weight of the vehicle is constant, what happens during a corner is the phenomenon of weight transfer, this will lead to a higher disparity between the two sides of the vehicle as the values of lateral acceleration rise.

6.1.3 Suspension behaviour related to a static camber variation

After having evaluated how the two vehicles behaves it was decided to check how some changes in suspension parameters may affect the behaviour of the vehicle, the 4120mm long vehicle configuration was used for these tests.
The first parameter to be changed is the static camber angle, this value defines the value of camber that is present when the vehicle is standing still and the steering wheel angle is placed at zero degrees. The variation was evaluated by changing the camber value on the front axle starting from the neutral position of zero degrees, the design condition is set to have a slightly negative camber angle. For this test it was decided to start from a neutral condition, just to evaluate how the system reacts to the manoeuvre starting from the wheels with no static camber applied to them.
A first test applied one degree of negative camber while the second test applied one degree of positive camber, as shown in Table 6.2.
The variation in camber angle is done while keeping the toe in the neutral condition of zero degrees, this is done to avoid mixing the effects of the two alignment modifications.

Condition	Camber Angle	Toe Angle
Neutral	0	0
Test 1	-1	0
Test 2	1	0

Table 6.2: Tests performed on the camber angle variation

Camber angle variation has little effect on the force measured at the wheel centre, the rear axle shows overlapping curves between the conditions used: On the front the negative camber condition will reduce the force while the positive camber will increase it, both compared to the neutral condition, as shown in Figure 6.18. Camber variation has a small effect on the side-slip angle: The overall behaviour is of the understeering type in all tests, as it is possible to see in the graph in Figure 6.19, obtained from the delta between the absolute values of the average side-slip angles.

By looking the graph up to the max grip point it is possible to see that a negative camber at the front will reduce the understeering characteristic of the vehicle.

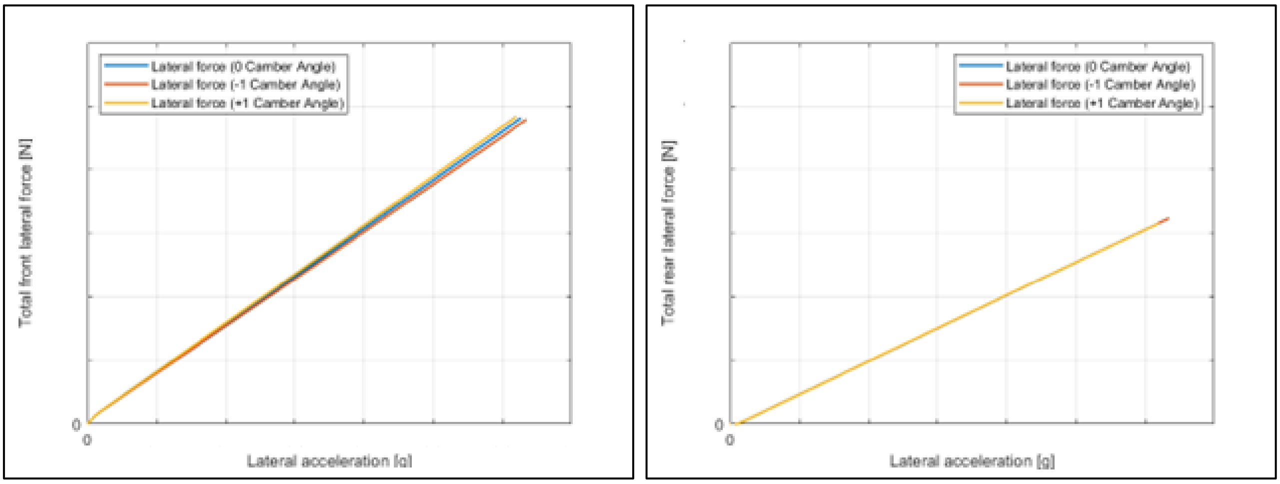

Figure 6.18: Front and rear lateral force in function of lateral acceleration for different static camber settings

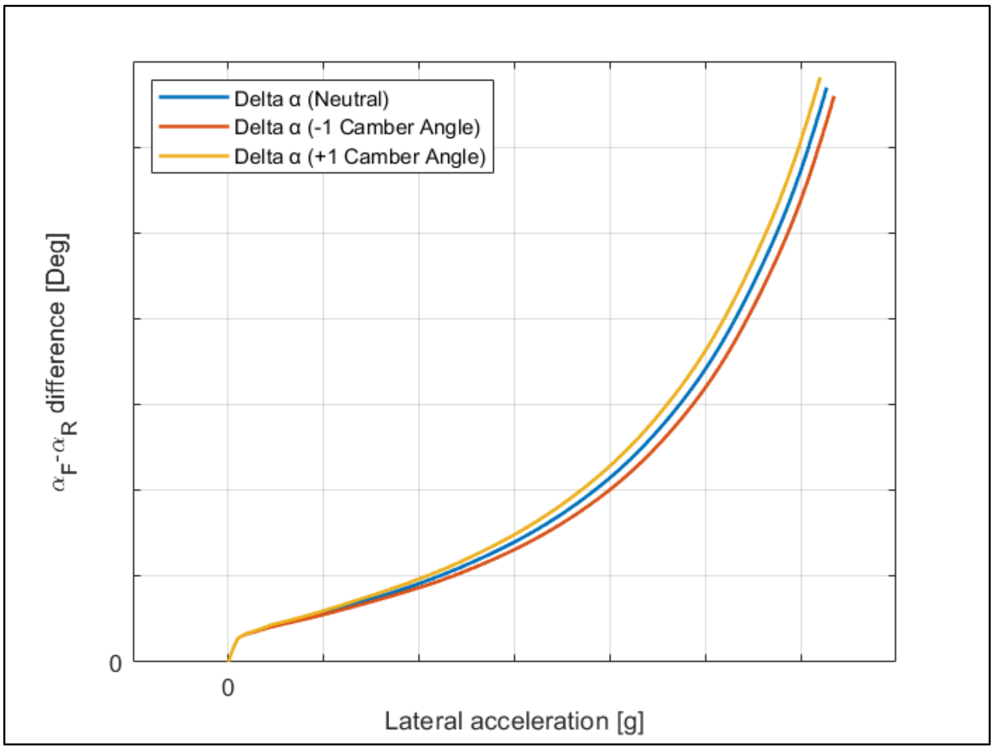

Figure 6.19: Difference between front and rear average side-slip angle as static camber changes

The same small differences are seen in terms of lateral acceleration, in this case a negative static camber angle will lead to a higher absolute peak value of acceleration at the vehicle limit, the difference between test is not high but a common trend is defined.

It is important to understand that the static value of camber imposed at the beginning of the test is not immune to changes.

As it is shown in Figure 6.20, in the front axle the value will slowly move towards more positive values as the test proceeds, after the max grip level the vehicle will understeer. Translating in an increase in camber, this phenomenon is less relevant than what happens below the max acceleration. The variation in camber is more pronounced for the inner wheel compared to the outer wheels, this is mainly related to the fact that the body will roll towards the outer side and load more the outer wheel, leaving the inner wheel to be freer to move.

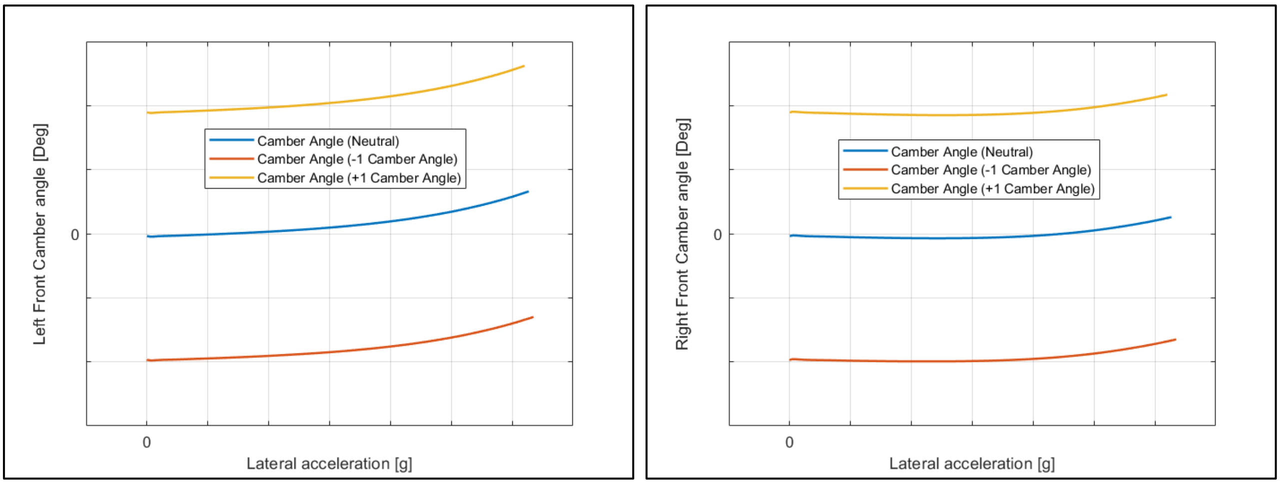

Figure 6.20: Actual left and right front camber angle variation for different values of the static camber angle

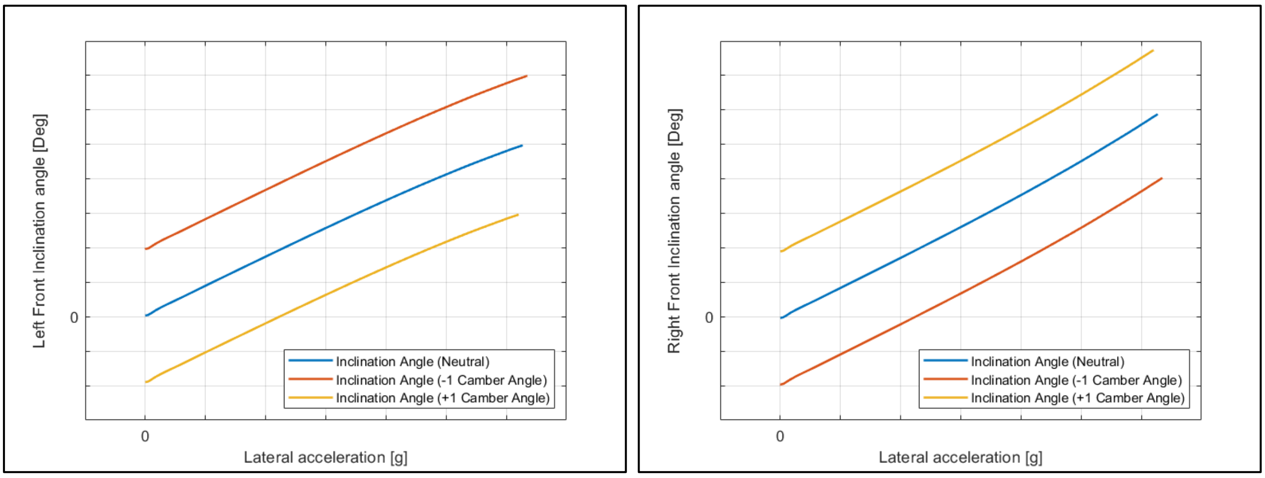

Figure 6.21: Inclination angle variation on the front axle as camber angle is changed

The same analysis has been carried out on inclination angle, similar results to those found for camber angle are found in Figure 6.21. Similar variations are found between left and right wheels on the front axle.

The neutral camber line shows that the outer wheel will have a higher variation compared to the inner one, the same follows for the camber variations performed. The three lines in the graph are almost parallel between them, for both left and right.

Camber angle variations will also affect slightly toe and roll angles, the variation with camber is minimal and can be considered negligible.

To evaluate how camber affects the vehicle, the best way is to evaluate the understeering behaviour of the system, graphs in Figure 6.22 and 6.23 sum-up the behaviour for the three angle variations.

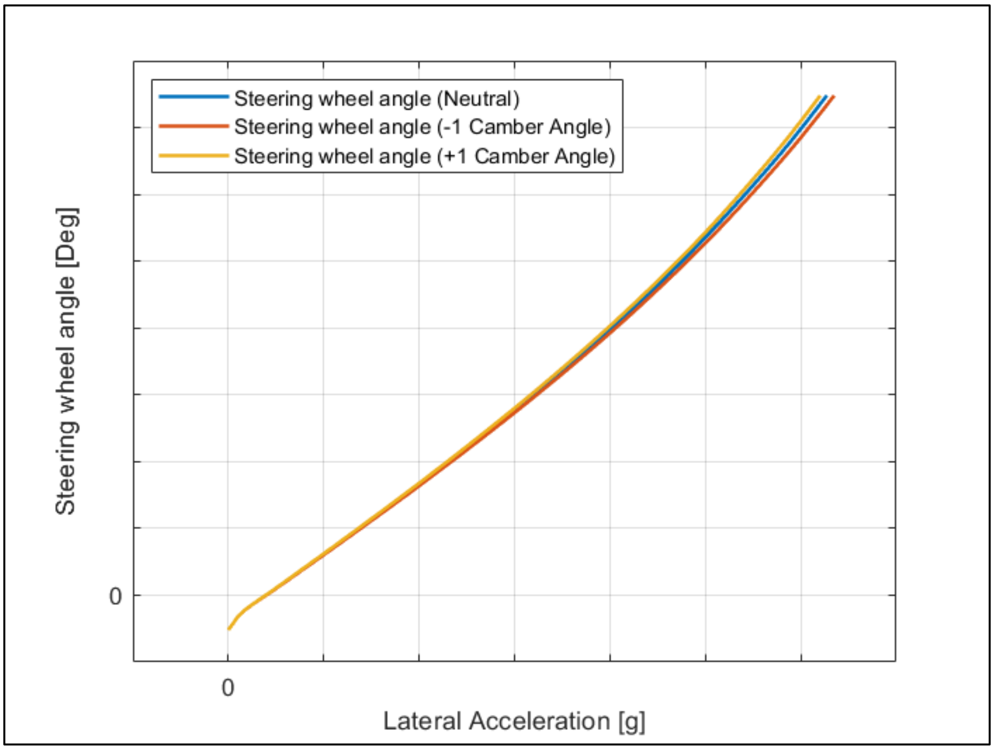

Figure 6.22: Understeer characteristic as the camber angle is changed

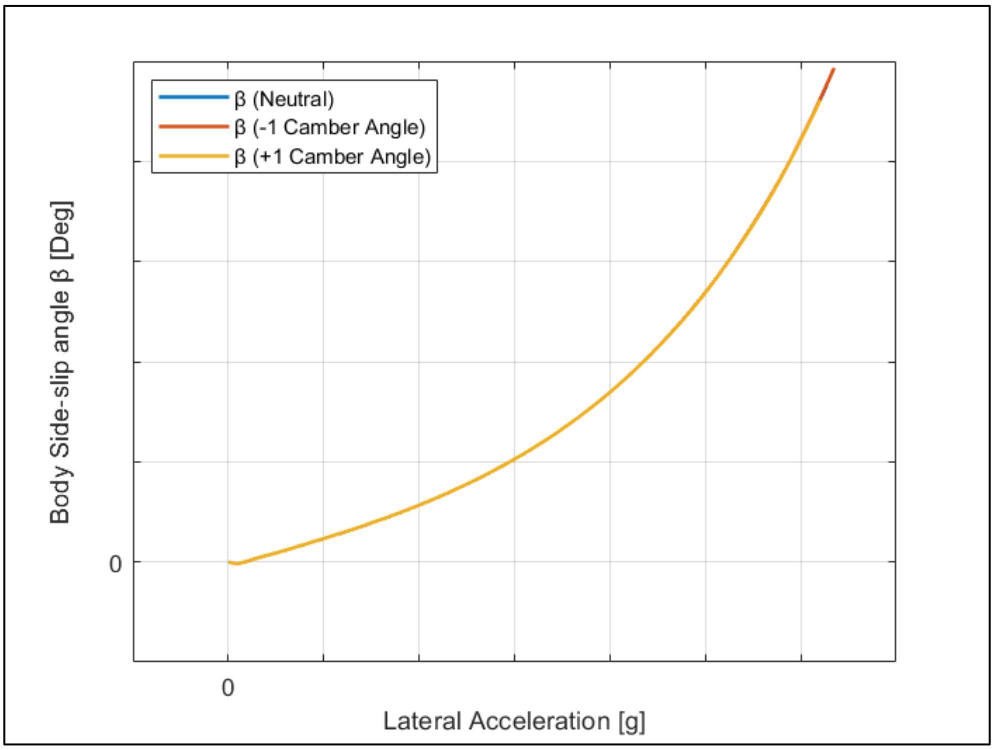

Figure 6.23: Body side-slip angle in function of the lateral acceleration as camber angle is varied

From this evaluation it is possible to have an idea on the routes to follow when setting up the vehicle, a negative camber angle will move the lateral acceleration limit to higher values, while a positive angle will move the limit towards lower values.
The negative camber condition will reach the same side-slip angle at higher accelerations, increasing the limit of grip of the vehicle. The main differences between the configurations become clear only as the vehicle reaches the grip limits, for small side-slip angles the difference is, basically, unnoticeable. By watching these graphs, it is possible to understand that negative camber angles will be, most likely, better than positive values concerning the cornering behaviour, due to the fact that a reduction in understeer is obtained, this is a good confirmation of the slightly negative value of static camber used by the design condition.

6.1.4 Suspension behaviour related to a static toe variation

The same variation done for the camber is also applied to the static toe angle, again on the front axle, in this case a negative toe angle will equal to a toe-out condition, while a positive condition will be called toe-in.
The effects are more noticeable compared to what was seen for the static camber variation, in terms of lateral acceleration the maximum acceleration is reached for a toe-in condition.
In Figure 6.24 it is possible to see a clear variation in the lateral force as the manoeuvre reaches the end, a positive toe angle will lead to increased lateral force while a negative value will bring the force down, this is valid for both axles.

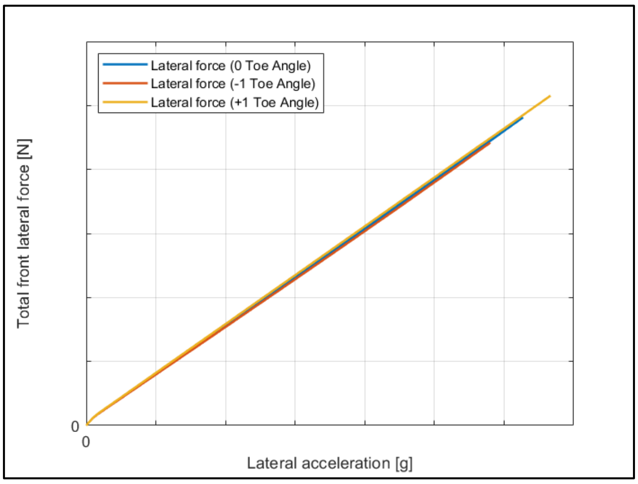

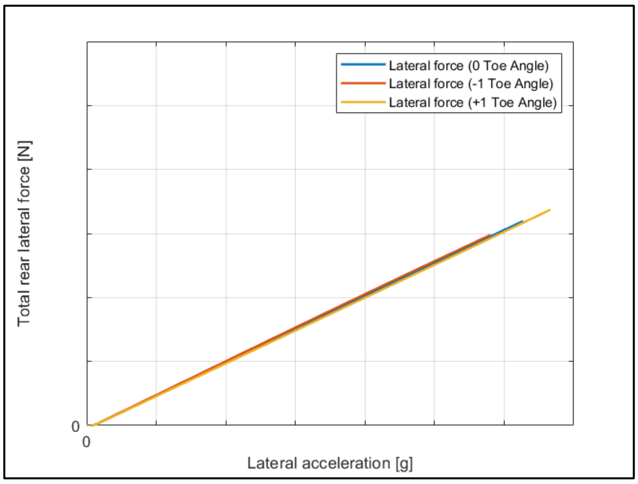

Figure 6.24: Front and rear lateral force in function of lateral acceleration for different static toe settings

Differently from what was valid for the static camber variation test, even a variation of one degree of toe will lead to larger differences in value, the characteristic is similar between the three tests and the neutral angle case lies almost exactly in the middle between the other two. The way that the curve approaches the limit is similar between the three conditions, all the cases it seems to be gradual in their variation.

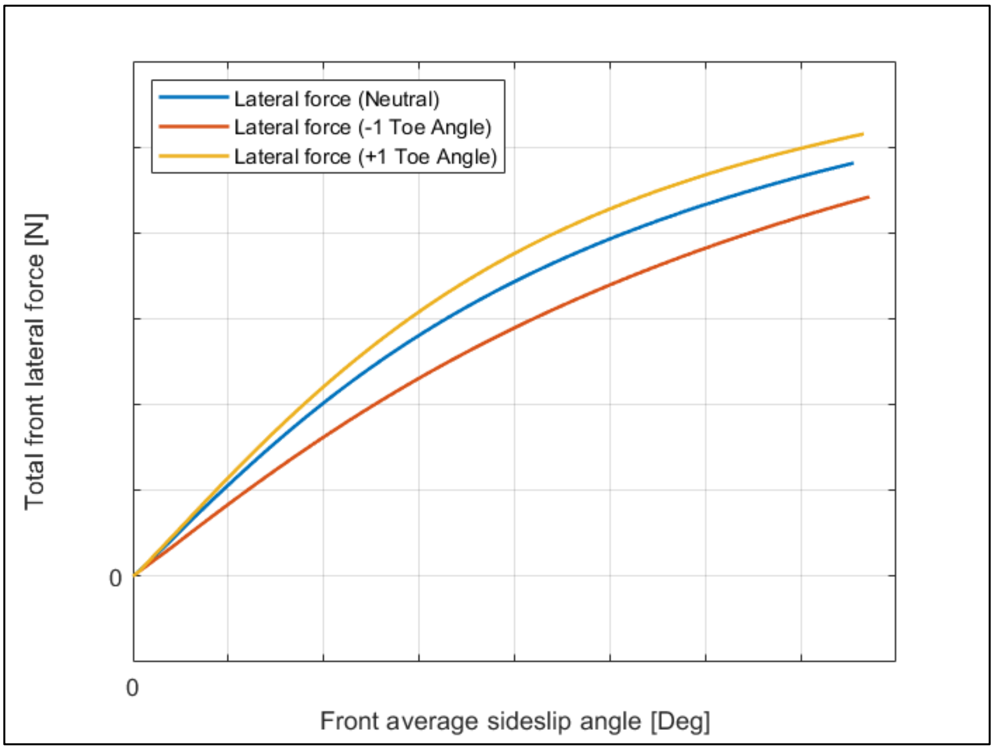

Figure 6.25: Lateral force in function of the average side-slip angle on the front axle

Lateral force is evaluated also in function of the average side-slip angle, on the front axle the value of force will be lower for a negative toe angle when keeping the average side-slip angle constant in the comparison, the rear axle will not be affected by variations in toe at the front.

The graph in Figure 6.25 is useful to understand the cornering stiffness of the vehicle, this parameter reflects the ability of the tire to resist deformation in shape during a cornering event: It can be obtained by computing the slope of the curve that plots lateral force in function of the side-slip angle: This relation is valid for slow slip angles, hence why the first part of the graph is characterized by a linear behaviour: Thanks to the fact that the lateral force is related to the side-slip angle only by the cornering stiffness in this phase.

Case	Difference in slope from neutral angle
Toe Angle -1	-20,15%
Toe Angle +1	+8,60%

Table 6.3: Differences in slope in reference to the neutral case

A comparison between the cases where the alignment was modified from the neutral condition is shown in Table 6.3, the variation in percentage confirms what was seen in the graph. A negative toe angle will reduce the cornering stiffness and vice versa, a negative toe angle value will have a clearly less pronounced slope leading to a decrease in cornering stiffness. The effect of the positive toe angle is to increase the cornering stiffness, when moving towards positive values the percentage variation in absolute value will be less pronounced than what happens towards negative values.

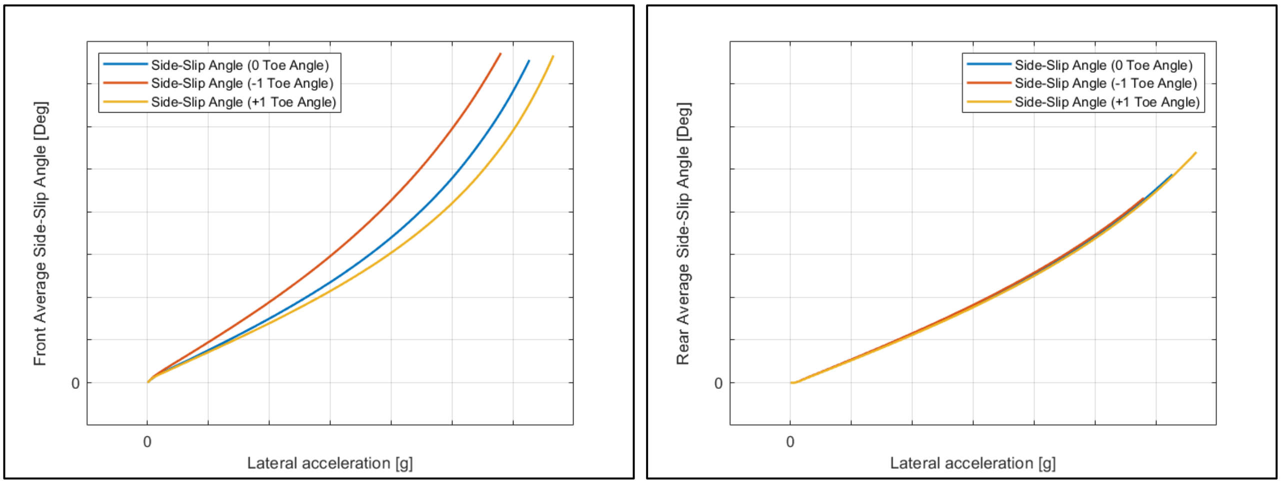

Figure 6.26: Average Side-Slip angle evolution for different toe angle values

By plotting the average side-slip angle in function of the lateral acceleration in Figure 6.26 it is possible to see that toe largely affects the side-slip value that the wheels will experience, a negative toe value will show higher side-slip angles and a lower peak lateral acceleration. The effect is very pronounced, the difference when applying a positive toe angle is less relevant but will deliver lower angles and higher peak accelerations, the rear axle will be more uniform in shape between cases.

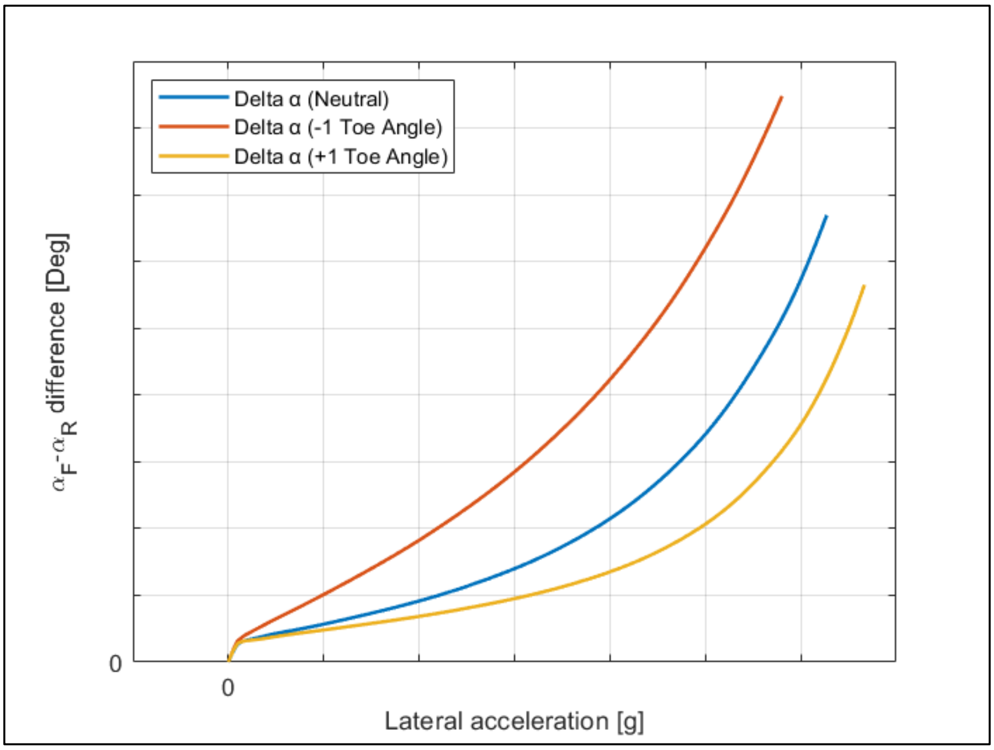

Figure 6.27; Difference between the two side-slip angles as the toe angle varies

In this case the most relevant graph is the one in Figure 6.27, this graph tells that a negative toe angle will likely increase understeer, due to the fact that the difference between the two side-slip angle absolute values is higher. A positive static toe will instead reduce the understeering phenomenon.
Camber angle is also largely affected by the value of toe angle, as it is seen in Figure 6.28 on the front, it is so affected that the variation is higher than the one experienced by directly acting on the static camber, camber angle variation follows the sign of the toe variation.

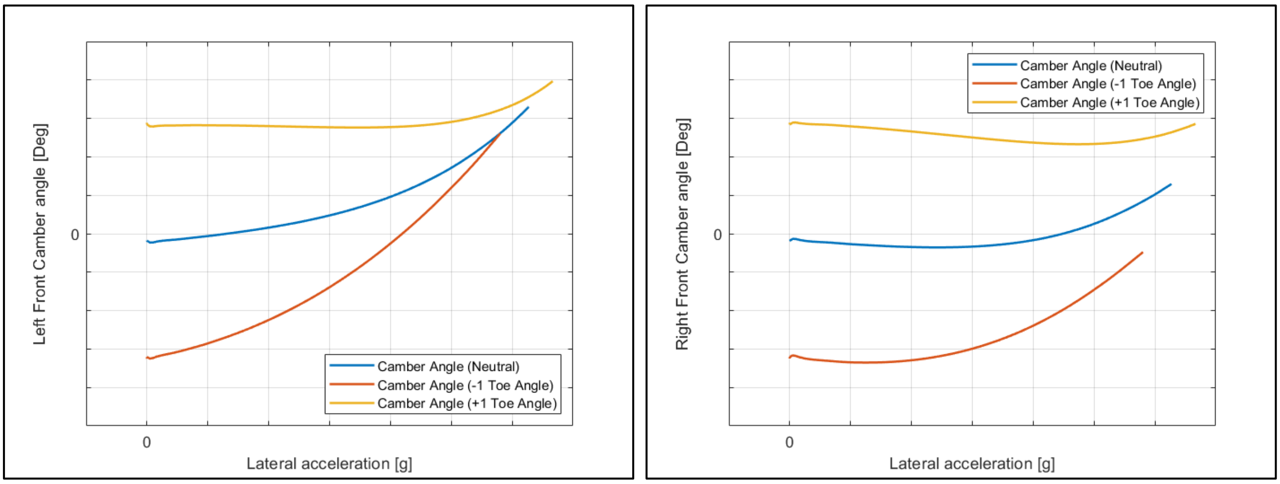

Figure 6.28: Real front camber angle variation with respect to lateral acceleration, for different toe values

Like what happened with camber, the toe angle will change as the steering motion continues, as it can be seen in Figure 6.28: On the front axle differences between tests will become smaller as the test goes on. The values of toe and camber found on the rear axle are very small, so small that it is possible to say that the variation in toe is negligible on the rear axle as the toe angle is changed.
Inclination angle also gives a good inside on how the suspension reacts to static toe variations, results are presented in Figure 6.29.

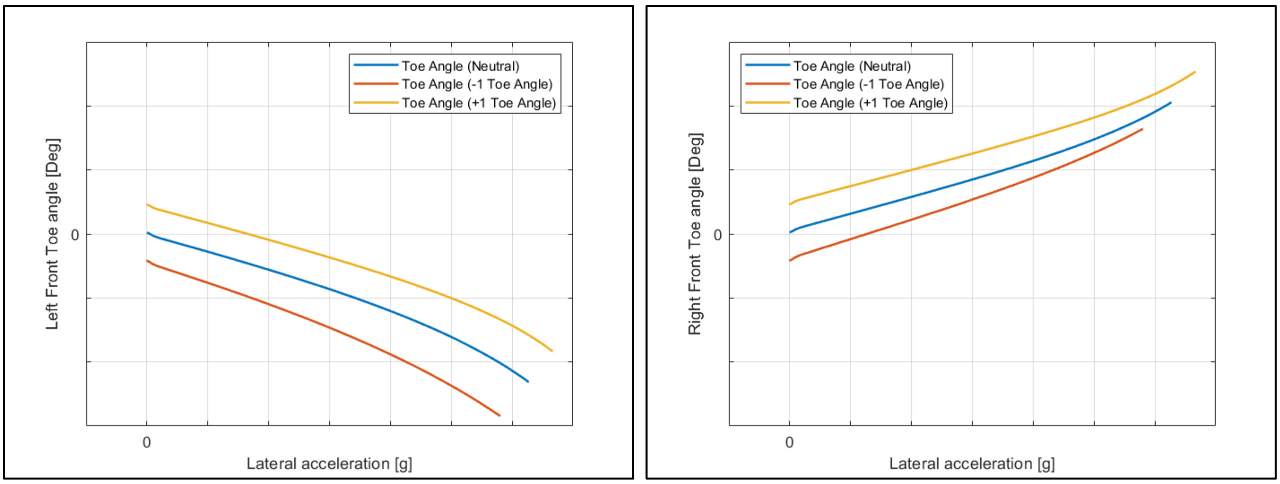

Figure 6.29: On the left the actual toe angle value variation is shown for the left front wheel, on the right the same is done for the right front wheel

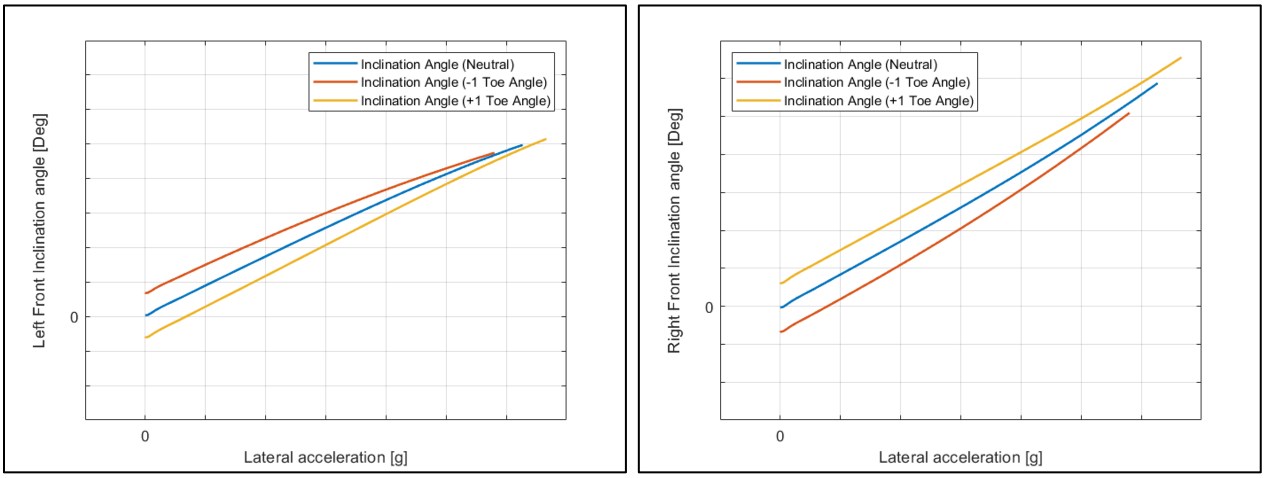

Figure 6.30: Inclination angle variation on the front axle as toe angle is changed

Inclination angle results clearly show that the toe angle will also affect the value of static camber, sign of toe and camber will be the same on the outer wheel and vice versa.

As the static value is defined differences will be high, the differences among configuration will become smaller as the manoeuvre proceeds.

At higher steering angles the effect of static toe on the inclination will be reduced, being that the suspension has largely changed its geometry compared to the case in the beginning. Results are shown in Figure 6.30

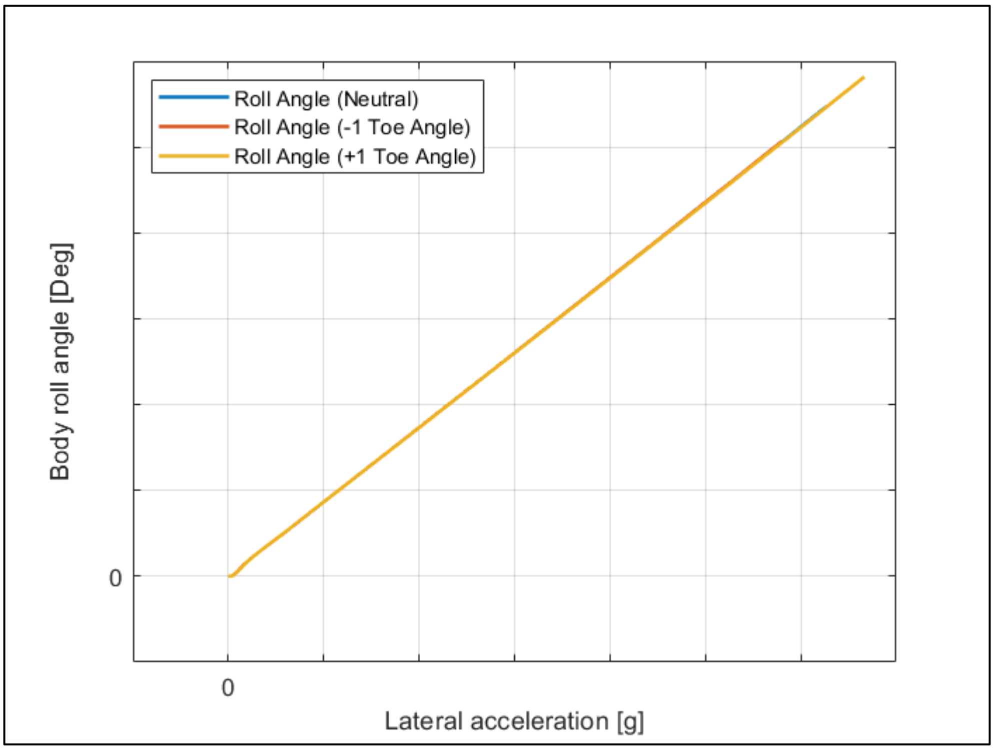

Figure 6.31: Roll angle variation with lateral acceleration, again shown for the three variations in static toe

Roll angle shows a straightforward evolution with lateral acceleration, it will be reduced by negative toe and increased by positive toe, the variation is minimal between the three tests, results are seen in Figure 6.31.

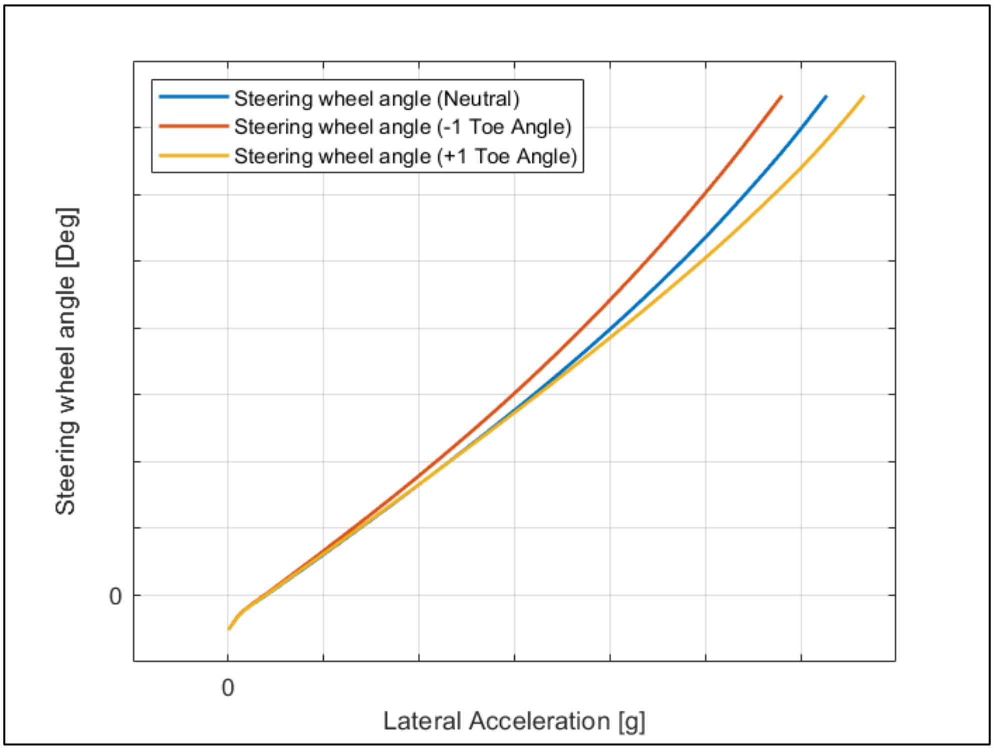

Figure 6.32: Understeer behaviour as the toe angle is changed

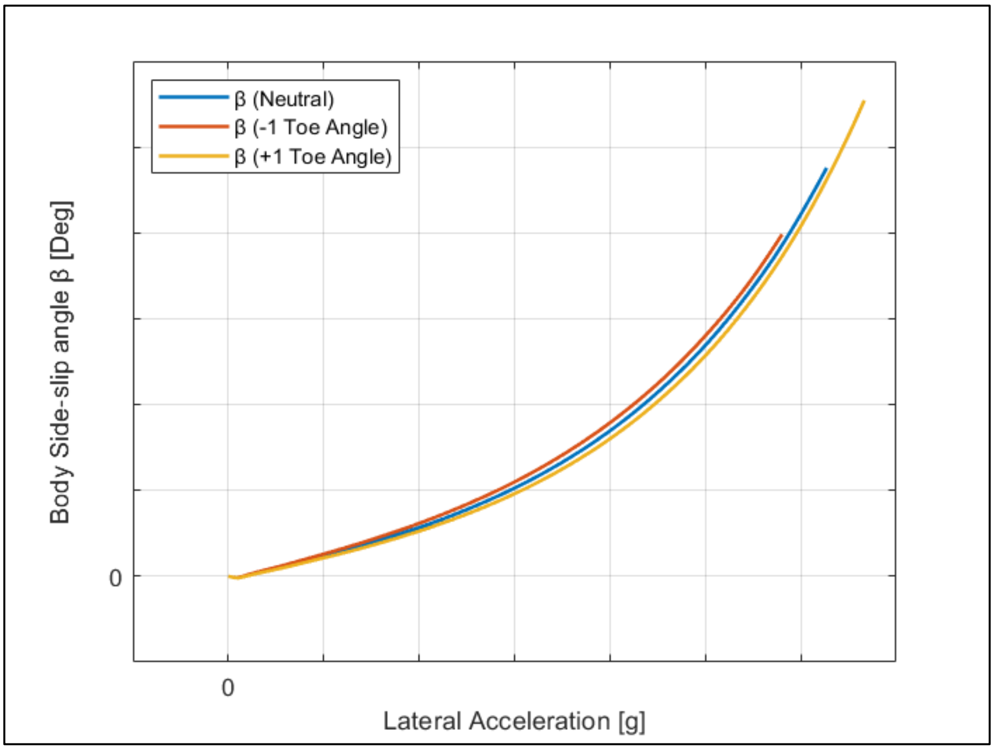

Figure 6.33: Side-slip angle computed at the centre of the vehicle model, as the toe angle is changed

By looking at the graph in Figure 6.32, it is possible to see that the situation is clearer compared to the tests about camber angle variation. The differences between the tests are larger, toe-out will decrease the lateral acceleration values that are reached at a given steering angle but will make the behaviour more gradual compared to the other two tests.

In this case the best compromise seems to be the neutral condition. The graph showing the body side-slip angle in function of lateral acceleration is showed in Figure 6.33. Toe-in condition will reach a given value of side-slip angle at higher values of lateral acceleration compared to the other two tests. From this evaluation it resulted that toe leads to large changes in how the vehicle reacts to different manoeuvres, especially at low steering angles. By looking at the graphs the condition of neutral toe seems to be the best compromise, being always in the middle between the two, obviously the tune depends on the vehicle mission, some changes in toe can bring changes in behaviour that in some conditions are beneficial, while in others they are not.

6.1.5 Conclusions on the ramp steer test

The test performed on the ramp steer is one of the most important in determining how the vehicle reacts to cornering events, the main take from this test is the definition of the limits that the vehicle has during a corner. Defining the maximum acceleration that a vehicle can sustain during a cornering event is crucial in the process of understanding what the vehicle in analysis is capable of: This is true for commercial vehicles, for passenger cars and for race cars, higher limits for the vehicle mean higher safety and higher performances.

The test compares two different vehicles, a fully loaded short wheelbase van and an empty long wheelbase vehicle, the longer vehicle resulted to be more prone to understeer and reached lower lateral acceleration values. The fact that one vehicle is a lot heavier than the other did not affect much the shorter vehicle, the increased agility given from the shorter wheelbase compensated the fact that there was a large difference in weight between the two.

The study on the alignment was also crucial in defining how to carry a process that leads to the choice of the optimal alignment values, in this study the focus was on performance, so no consideration on tire wear was performed, obviously variation in alignment may bring an uneven wear on tires that on vehicle used in fleets like vans can have economic implications. By just focusing on performance the trend of different parameters was found as these angles were changed, this study objective was not to find the optimal alignment of the vehicle, but just to understand how each parameter reacted to a change in alignment. This creates a guide on what to expect when changing alignment, some parameters will be more affected, some less, optimization of the alignment parameters mainly depends on what is the aim of the optimization, some mission profiles may work better with a given set of parameters, some with others.

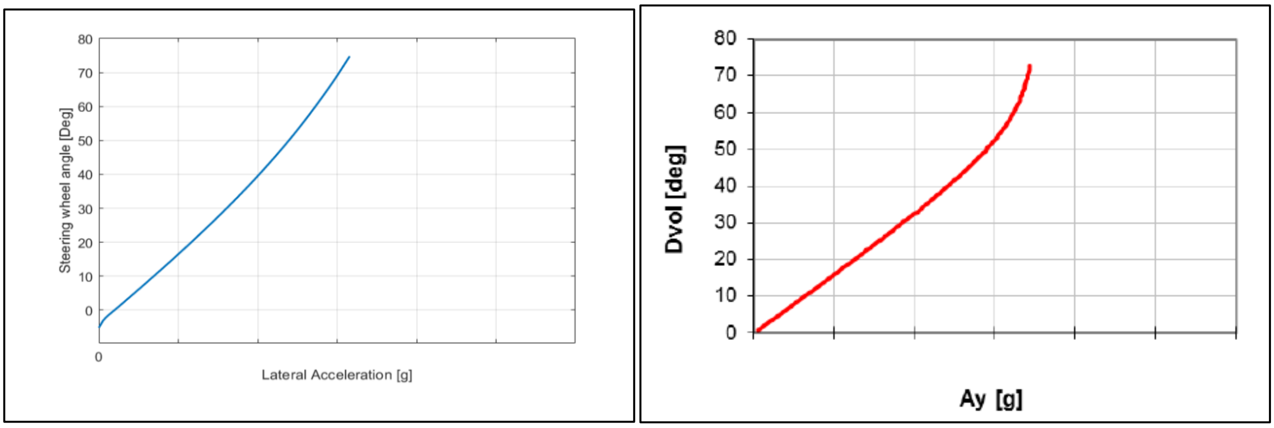

Figure 6.34: Comparison between experimental data and data found in the analysis

In Figure 6.34 it is possible to see a comparison between experimental data and data evaluated in this analysis, the two graphs are similar but show some differences, mainly the fact that the asymptote is clearer in experimental data and occurs at a slightly higher value of acceleration, this means that the limit appears sooner on the experimental data.

The comparison between these two graphs is not done in the same conditions: As it is expressed in this chapter, there is an error at the beginning of the test that makes the vehicle start from a steered condition, second the value of ramp employed on the experimental test is not known. It may employ a different value that leads to some differences in values.

Considering the fact that the steering is simulated with no compliance and elements such as power steering are not implemented, this can be considered a good starting point. The elements of the steering system are mostly rigid, and some data may benefit from more accurate parameters as setting. By obtaining more accurate experimental data it will be possible to model the steering system with higher accuracy and perform a better comparison. As it stands, with the actual data available and with the known approximations performed, this model represents the real system with a good approximation value, or at least a good starting point for future evaluations.

Furthermore, it was needed useful to check the validity of results of the ramp steer test.

To understand if the ramp steer test is coherent with what was found in the static test it is possible to compare the value found in the test with the contributions from each static test.

Equation 6.1 expresses how the contribution is evaluated for both Camber & Toe, in the equations only camber is shown: Equations for Toe will be equivalent.

The contribution of lateral force is evaluated from a static load test with the range of forces that the vehicle sustains in the ramp steer test; The contribution in wheel travel is evaluated on a opposite wheel travel test for the travel that each wheel has in the ramp test; The contribution in steering angle is obtained from a static steering test for the value of steering angle that the vehicle has in the ramp steer simulation.

These three parameters when summed together give the total contribution from static test to camber.

$$(6.1)\ Camber\ Contribution = Static\ Camber + \Delta_{F_y} \cdot F_y + \Delta_{Travel} \cdot Travel + \Delta_{\theta} \cdot \vartheta$$

$$(6.2)\Delta_{F_y} = \frac{Camber(END) - Camber(START)}{Lateral\ Force(END) - Lateral\ Force(START)}$$

$$(6.3)\Delta_{Travel} = \frac{Camber(END) - Camber(START)}{Wheel\ Travel(END) - Wheel\ Travel(START)}$$

$$(6.4)\Delta_{\theta} = \frac{Camber(END) - Camber(START)}{Steering\ Angle(END) - Steering\ Angle(START)}$$

0,2 g	Δ(Fy)	Δ(Travel)	Δ(θ)
Left Camber	39%	44%	17%
Left Toe	25%	9%	66%
Right Camber	59%	24%	17%
Right Toe	19%	5%	76%
0,5 g	**Δ(Fy)**	**Δ(Travel)**	**Δ(θ)**
Left Camber	32%	46%	22%
Left Toe	17%	8%	75%
Right Camber	56%	25%	18%
Right Toe	17%	5%	78%

Table 6.4: Weight of each contribution to the alignment parameters

In Table 6.4 it is possible to check how each parameter affects each of the alignment parameters, the effect of lateral force is the most relevant in camber evaluation for the outer wheel; The inner wheel is instead mostly affected by the wheel travel.

As expected, steering angle has the highest effect on toe angle, given the fact that the two parameters are strictly related. Wheel travel has almost no effect on toe angle. Regardless of the acceleration level

In Table 6.5 it is possible to evaluate how much the contribution from static tests moves away from the ramp steer results, except for the inner wheel camber at a value of lateral acceleration of 0,5 g all the results are similar. This result is more of an outlier, since all the other parameters seem to behave similarly to what is expected from the static tests. In the static tests only the suspension was modelled, this made the camber and toe values dependent only on the suspension geometry and characteristics,. When moving to the complete vehicle there is higher variability that will lead to different results. At low acceleration it is possible to reliably do this comparison since differences in values are not high, except for the value of right camber the comparison is close also at higher accelerations.

PARAMETER	LEFT WHEEL		RIGHT WHEEL	
	Ramp	Static	Ramp	Static
Camber @ 0,2 g	Reference	-2,6%	Reference	3,0%
Toe @ 0,2 g	Reference	-1,2%	Reference	12%
Camber @ 0,5 g	Reference	-37%	Reference	0,2%
Toe @ 0,5 g	Reference	-2,0%	Reference	7,6%

Table 6.5: Variation in camber from the ramp steer simulation

6.2 Step Steer

6.2.1 Introduction to the step steer analysis

The second test performed to evaluate the behaviour of the vehicle is step steer, this test consists of a sudden steering manoeuvre performed in just a few seconds. This test mainly evaluates how the vehicle reacts to emergency manoeuvres and how much time it takes to stabilize its behaviour.
In Figure 6.35 the steering pattern is shown, as it is clearly seen at the one second mark the steering motion begins and in three tenths of a second it reaches the 45-degree mark that is set for this test.

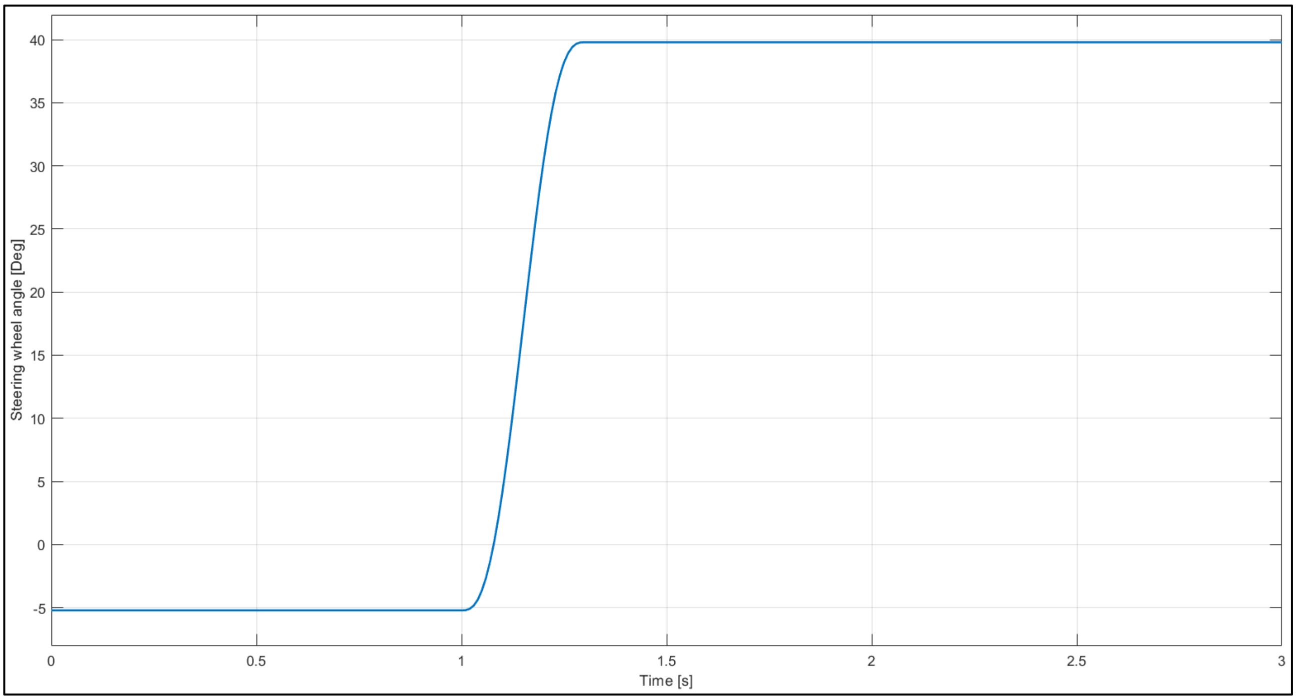

Figure 6.35: Steering pattern through the test

The manoeuvre lasts five seconds, this was decided to be sure that the system had time to stabilize its parameters, the graphs will be plotted up to three seconds, this is done because it was found that the simulation will be already stabilized at that point and reducing the max value of time will zoom the effect of stabilization that each parameter will take.
A test like this will likely introduce an instability to the system, due to the fact that both tires and

suspensions will adapt to the sudden variation in forces and accelerations that is related to an analysis of the step steer type.

First of all, a comparison between the two different vehicles was evaluated, followed by an analysis on how the vehicle reacts to variations in static toe and camber values. In Figure 6.35 it is possible to see that the test does not start from zero degrees of steering angle even if simulation parameters are set at the straight steering wheel condition: This is mainly due to some stabilization that the software does before starting the test that may lead to some error in the steering angle in this phase. Results are still valid even in this condition because the manoeuvre itself and the stabilization phase that occurs are not affected, the fact that the steering starts from a position rather than another is less relevant than the steering motion itself.

6.2.2 Comparison between two different vehicles

The first step steer test performed has the role to understand how the results change between the two different vehicles, which are the same two configurations used by the test on ramp steering, all the other parameters are kept equal between the two trials, as seen in Table 6.6.

The first representative value of how the vehicle performs is shown in Figure 6.36: As it is possible to see the side-slip angle will eventually reach a final value that will be constant. Towards the end of the test the vehicle will basically drive in circles with the same steering wheel angle and so the side-slip angle will stabilize at the value of that given steering wheel angle. Being the speed constant, what's relevant to check in this test is how the vehicle reacts to the steering motion.

Body	Speed	Gear	Final Steering Value	Steer start	Duration
SWB	80 km/h	4	45°	1 s	0,3 s
LWB	80 km/h	4	45°	1 s	0,3 s

Table 6.6: Sum-up of the two tests performed in this paragraph

The settlement of the vehicle is shown with a sinusoid where the peak is higher in absolute value, than the final value for both tests. It is clear to see that the two vehicles react very differently to the steering manoeuvre. The short wheelbase vehicle experiences higher values of side-slip angle at the centre of gravity of the vehicle, the longer vehicle experiences a higher angle just at the beginning but then the condition dampens quickly. The short vehicle experiences higher absolute values in the end, this is also somewhat reflected in the stabilization phase, this result can give a first idea on the stability of a vehicle during a motion like this, in this case the 4120mm long vehicle behaves better.

By looking at the graph in Figure 6.37, it is possible to see the evolution in lateral acceleration experienced by the vehicle, the acceleration increases suddenly as the steering motion starts, then it reaches its peak, and then it gradually decreases as the manoeuvre goes on. In this case the differences in values between the two tests are not so high, again this time the system takes more time to stabilize itself for the shorter vehicle, lower absolute accelerations are experienced by the longer vehicle.

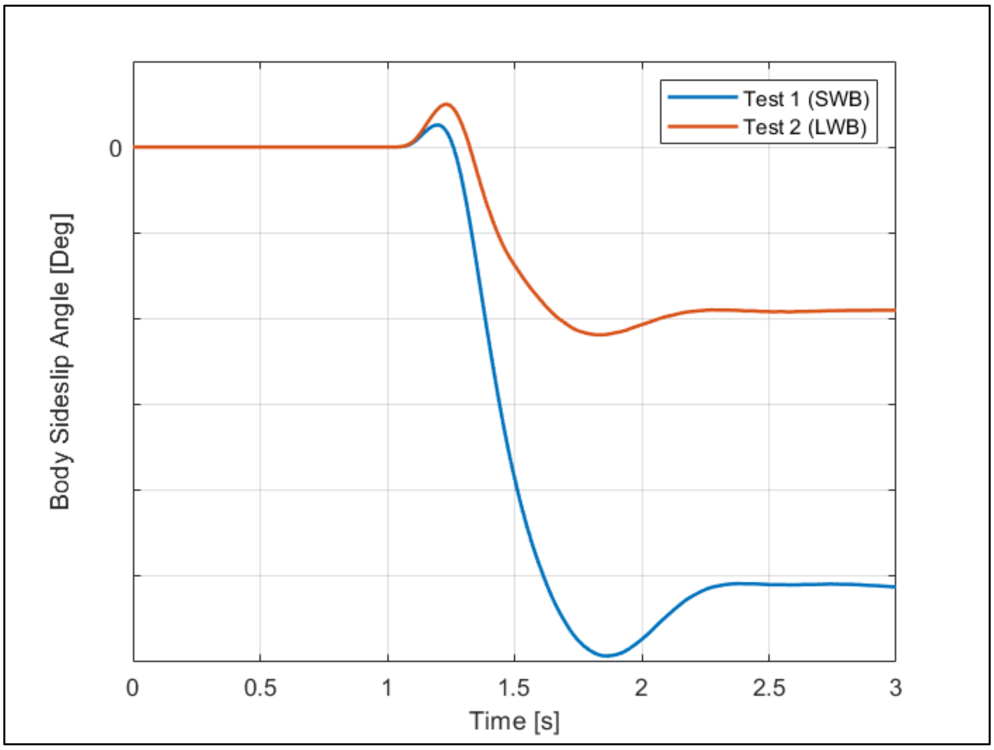

Figure 6.36: Body side-slip angle between the two tests performed

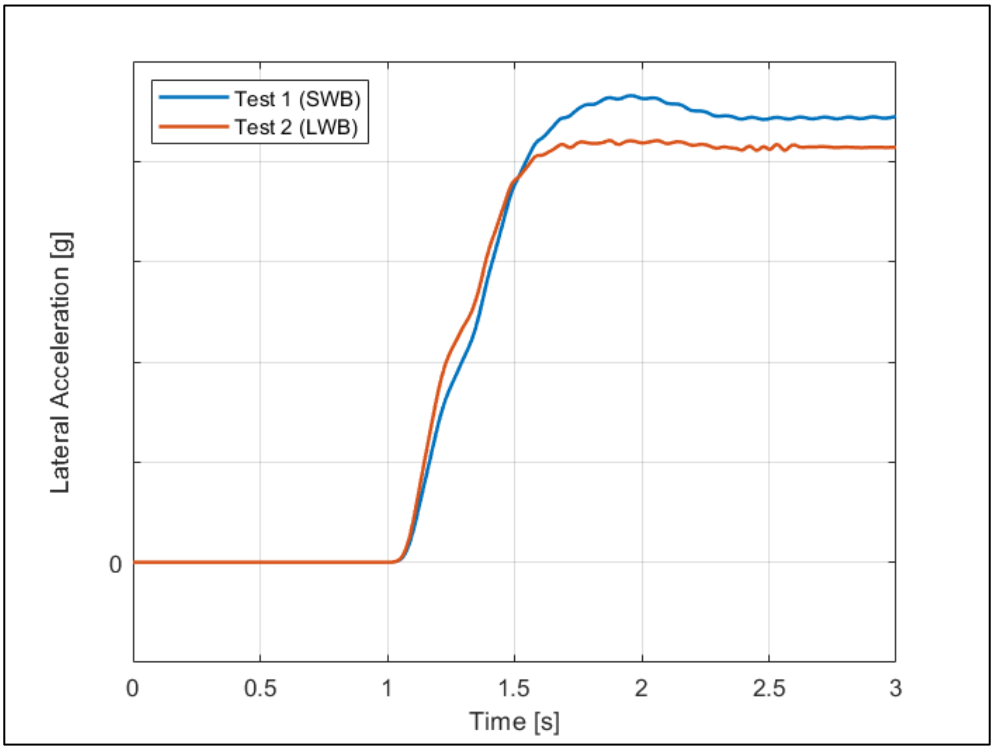

Figure 6.37: Lateral acceleration experienced by the vehicle in the two tests

In order to understand the phase where the suspension tries to stabilize its motion is important to check how the alignment parameters change during the test motion, concerning camber it is possible to see that there is a sudden variation as the steering wheel is changed, from there the values will follow the same pattern where the system oscillates up to the final constant value. The sudden steer manoeuvre will generate an unbalance in the suspension that will create the large peak that is possible to see in the first part of the graph in Figure 6.38 and 6.39.

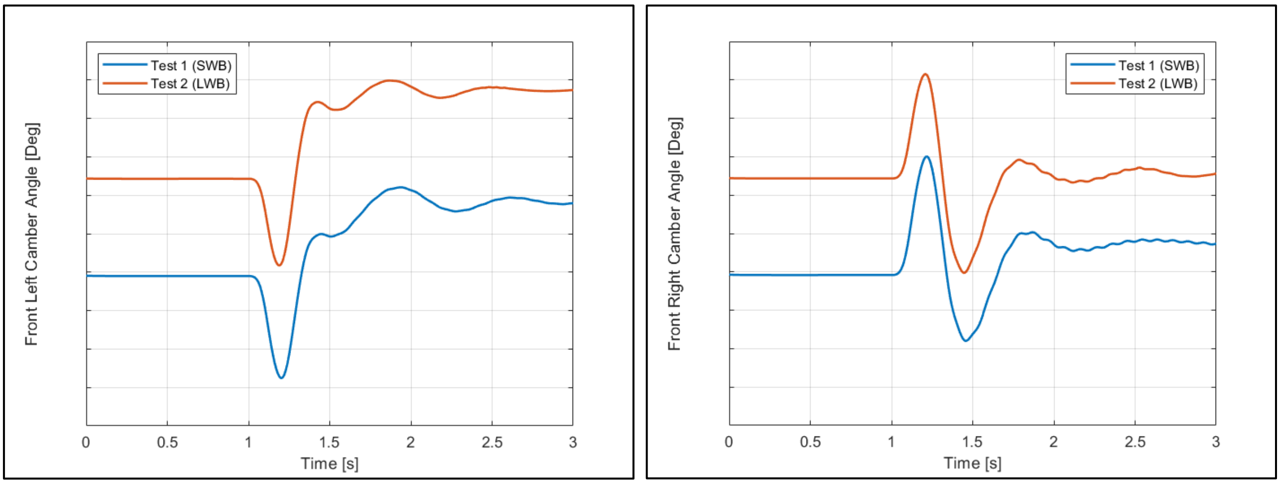

Figure 6.38: Camber angle variation in the two front wheels, for the two different tests

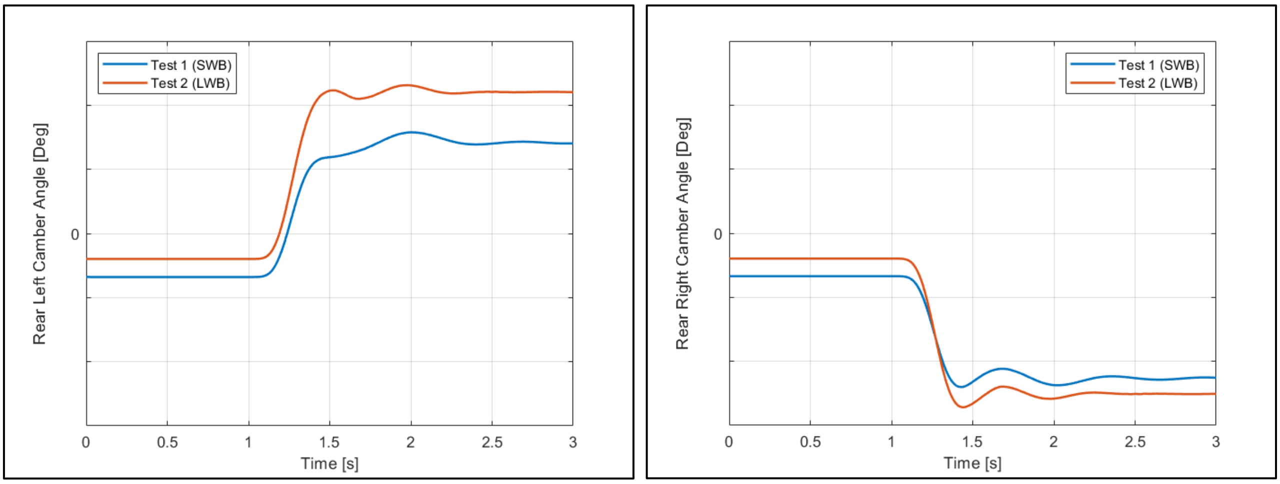

Figure 6.39: Camber angle variation in the two rear wheels, for the two different tests

For the front wheels there will be negative values for both tires, considering that the design condition static camber is slightly negative. In this manoeuvre the most loaded wheel is the right one, being the outer of the two, the left wheel has higher difference between the two vehicles, the outer wheel will converge to a higher negative camber value on the front wheel. The stabilization phase where the function oscillates is similar between the two wheels. A similar behaviour is experienced by the rear wheels, albeit with lower intensity. The rear left wheel experiences positive camber angles while the rear right wheel experience negative ones, this is mainly because a rigid axle is employed at the rear, changing the behaviour compared to the double wishbone used up front.

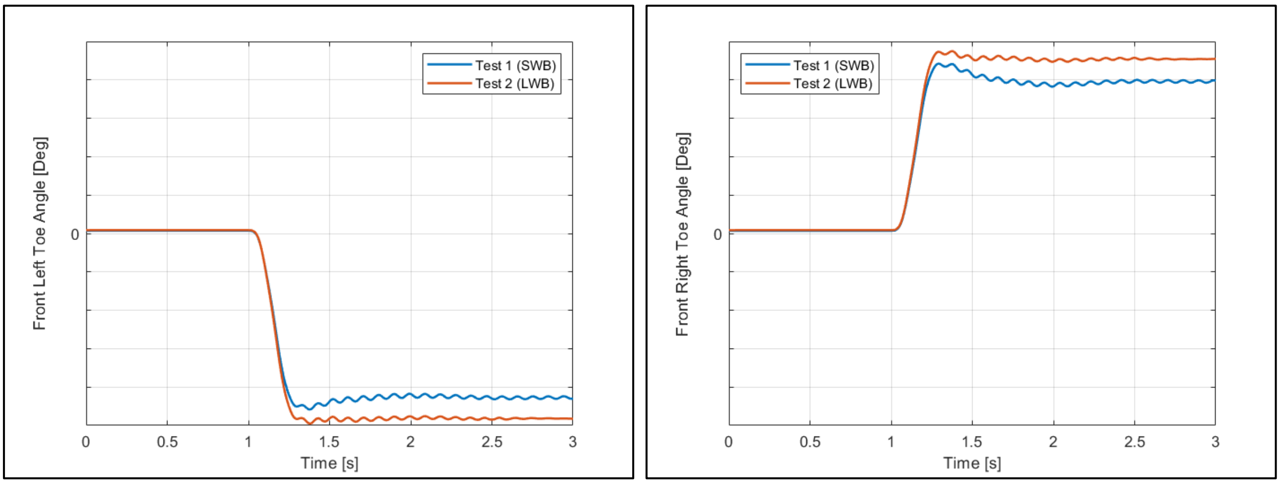

Figure 6.40: Toe angle variation in the two front wheels, for the two different tests

The second fundamental alignment value is toe angle, as shown in Figure 6.40, the variation is less pronounced compared to the camber values. Values are almost perfectly symmetric in peak between the two front wheels, with the left wheel showing negative values compared to the positive ones experienced by the right wheel. The settlement is more gradual compared to the previous tests, showing smaller peaks that will slowly fade into the final value at which the system converges, additionally, in both cases the system will be very close to the final value as the steering motion is completed, in this case the shorter vehicle will experience lower values compared to the long wheelbase one.

Inclination angle analysis performed in Figure 6.41 and 6.42 gives an idea on how the wheels will react to lateral motions in term of angle.

The analysis on camber angle was affected by the fact that the angle was evaluated with respect to the vehicle body, inclination angle is, instead, not affected by the movement of the vehicle body.

On the front axle the two analyses give similar variation starting from the initial static value, there will be a difference in sign between the two since the reference system is placed in the middle of the vehicle.

On the rear an higher difference is present, weight will have an effect in this, it is expected that the two cases have the same static value since there is a solid axle. There is a slight difference in angle given the fact that the two vehicles are differently loaded and so the weight will act differently on the suspension. Weight distribution is also different given the fact that there is also a difference in wheelbase.

Differences are more noticeable on the inner side, most likely due to the fact that it will be the least loaded side when the steering motion starts.

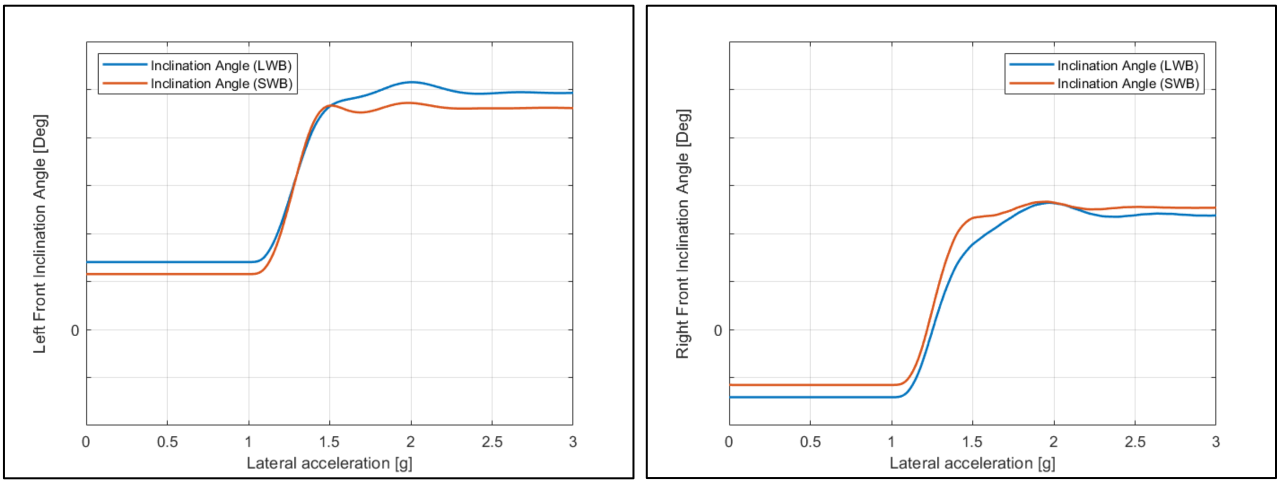

Figure 6.41: Front axle inclination angles, between the two configurations in analysis

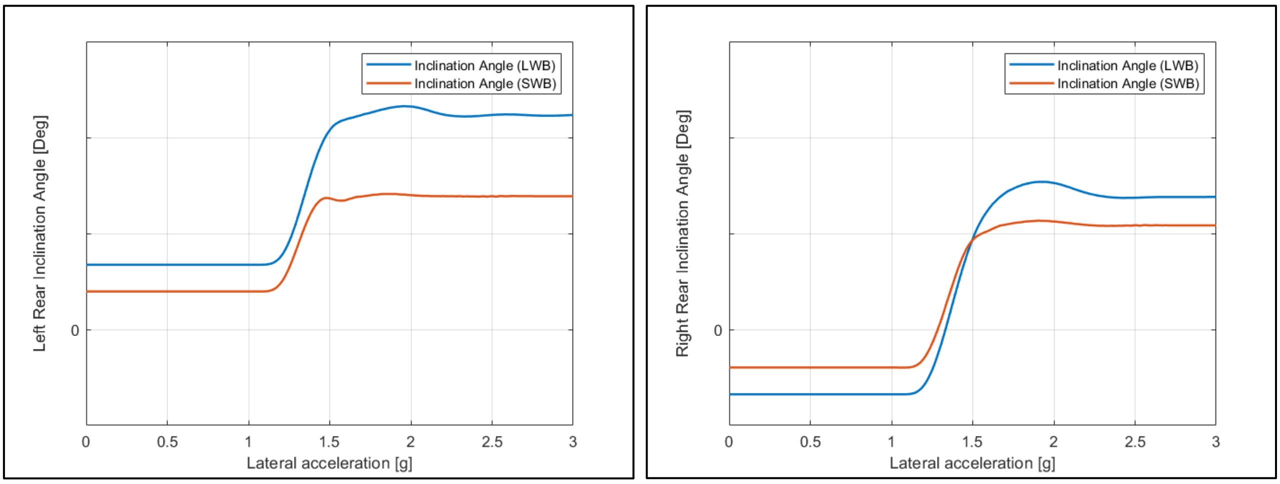

Figure 6.42: Rear axle inclination angles, between the two configurations in analysis

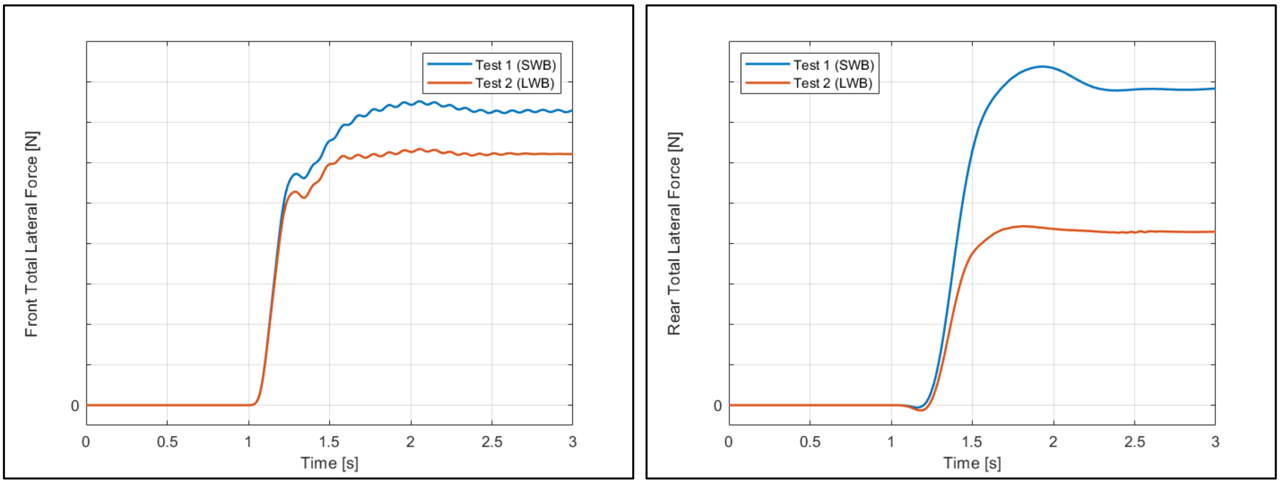

Figure 6.43: Lateral force evaluation, front axle on the left, rear axle on the right

The evaluation of the total force in Figure 6.43 confirms what was already found in this paragraph: There is a large increase in force as steering starts, then it fluctuates and finally it stabilizes to a final value for both tests. The front axle has higher frequency peaks in its stabilization phase compared to the rear one, what's interesting between the two is how the forces are distributed between the two axles, the short vehicle will have the two axles with comparable values, a clearer difference between the two will be present for the long wheelbase vehicle. The front axle will be more loaded than the rear one by a good margin, this reflects the different weight distribution between the two vehicles.

6.2.3 Evaluation of system's behaviour as static camber angle is changed

This paragraph has the objective of evaluating how the system behaves when the value of static camber is changed. Three different tests were conducted, the first one has the role of setting the reference for the other two and is performed with the wheels in a neutral camber condition. The other two represent positive and negative camber variations, all the different configurations used in this analysis are shown in Table 6.7, all the tests were conducted on the long wheelbase vehicle.

Test	Static Camber	Static Toe
Neutral Camber	0°	0°
Negative Camber	-1°	0°
Positive Camber	+1°	0°

Table 6.7: Tests conducted on static camber variation

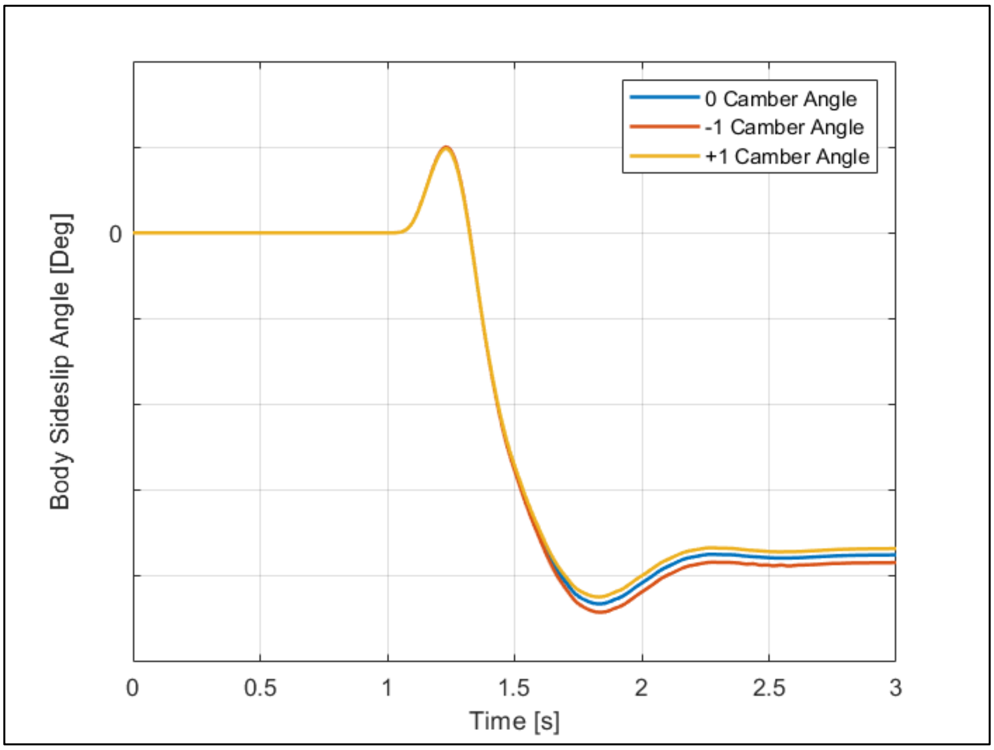

Figure 6.44: Body side-slip variation as the camber angle is changed

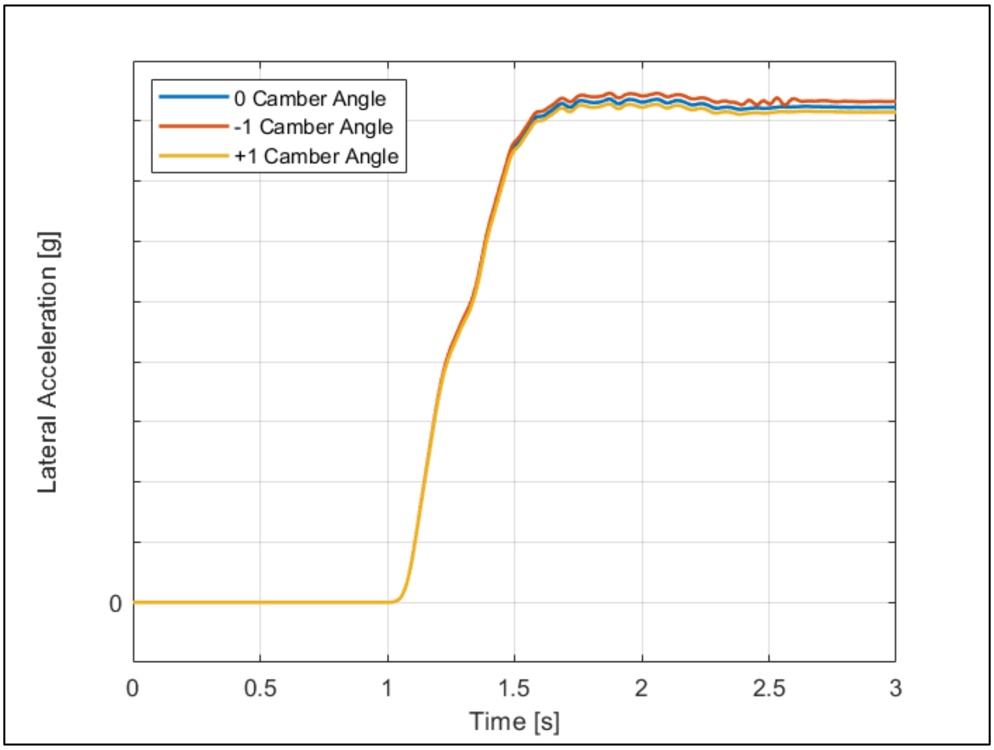

Figure 6.45: Lateral acceleration variation as the camber angle is changed, magnified in the second graph

Like in previous cases, analysis on side-slip angle and lateral acceleration gives a good idea on how the vehicle behaves overall during the manoeuvre, these graphs are important because they give an idea on how the system changes with camber, the differences in values between the different configurations are small but the trend that each parameter follows is clear, both side-slip angle and lateral acceleration will increase as the camber value moves towards more negative values.

The opposite happens towards positive values, the shape of the curve is basically the same between all the configurations, results are found in Figure 6.44 and 6.45.

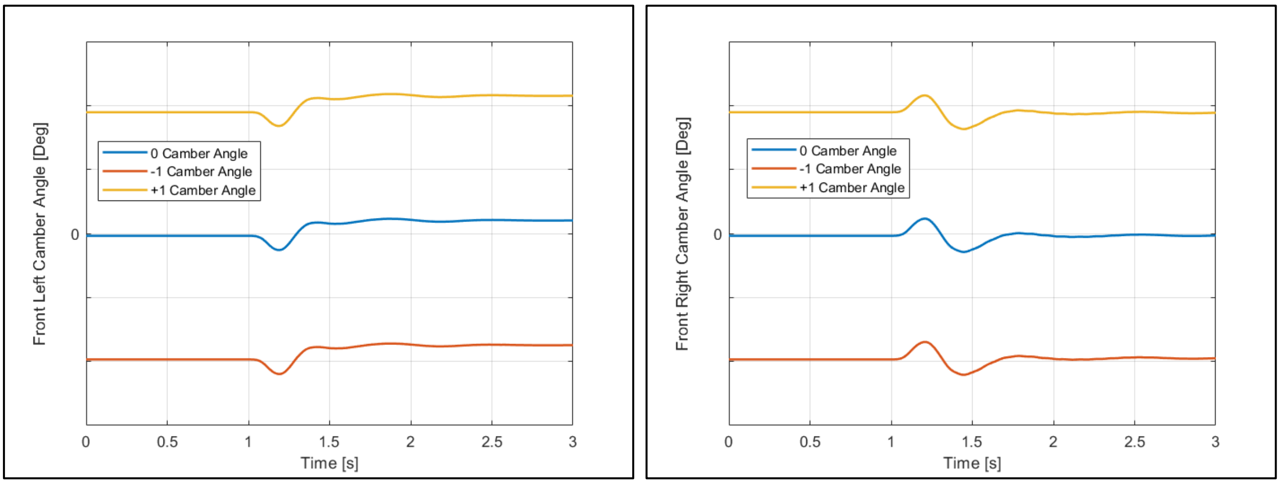

Figure 6.46: Camber angle variation as static camber is changed, experienced in the front wheels

Camber angle will slightly change from the static value as the manoeuvre occurs, by watching the graph in Figure 6.46 it is possible to split the camber analysis in three different phases:

1. A first phase before the start of the step steering motion where camber is equal to the static camber value set.
2. A second phase representing the step steer itself, in this phase the system will try to react to the steering motion, this results in an oscillation of the camber values shown by a sinusoid.
3. A final phase where the camber reaches the value that will keep during the corner, when the steering wheel is set at the defined angle.

For the front wheels, there are some differences between the left and the right wheel, the most loaded wheel is the outer one, in this case the right wheel, on this side the camber value will basically go back to the static camber value after the oscillation. The inner wheel will instead move towards more positive angles, this is mainly related to the roll angle experienced by the vehicle. The rear axle experiences what was found in all the other cases, the rigid axle will make the inner wheel move towards positive values and the outer towards negative values, comparing Figure 6.46 and 6.47 it is possible to understand how a suspension with camber recovery reacts compared to a suspension typology where camber recovery is not possible. When evaluating the inclination angle, it is possible to have a better representation of how the wheels actually vary in angle. When comparing Figure 6.48 with Figure 6.46 it is possible to see that after the steering motion the inclination angle will change.

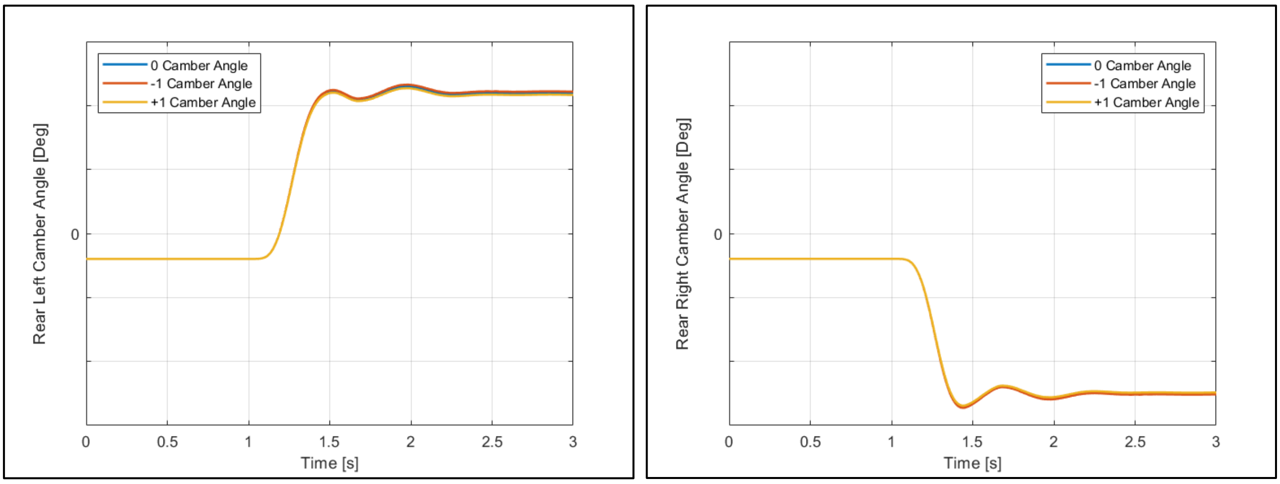

Figure 6.47: Camber angle variation as static camber is changed, experienced in the rear wheels

Camber angle variation could not catch this phenomenon, mostly due to the fact that reference systems changed before and after the steering phase. By keeping the reference system fixed to the one that defines the ground it is possible to evaluate how much the angle changes.

Left to right variations are comparable and the difference from the neutral condition is almost symmetrical for positive and negative variation. The stabilization phase is almost identical between the three cases.

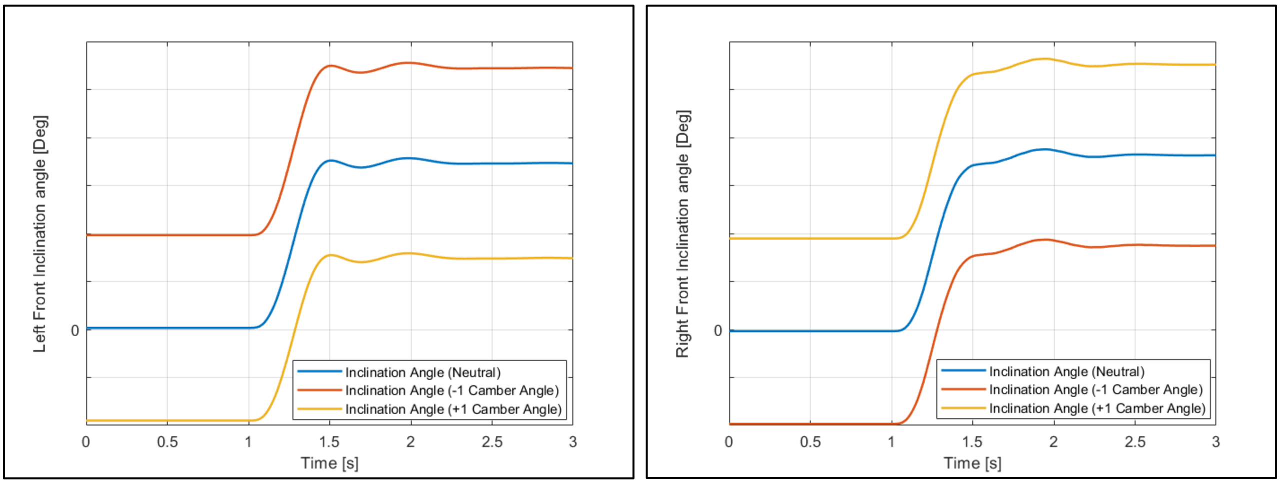

Figure 6.48: Inclination angle variation with static camber variation, for the front axle

On the rear axle, shown in Figure 6.49 it is possible to see that differences between the conditions studied are negligible, the main change is on the static value at the beginning. Distance between left and right curve is halved after the stabilization phase, compared to the initial difference. At the beginning only weight may affect this angle: As the vehicle will be steered, the roll angle will load more one side changing the relationship between left and right angle.

Toe angle results to be not affected by the value of static camber, the variation between the different tests is very minimal, both in values and shape.

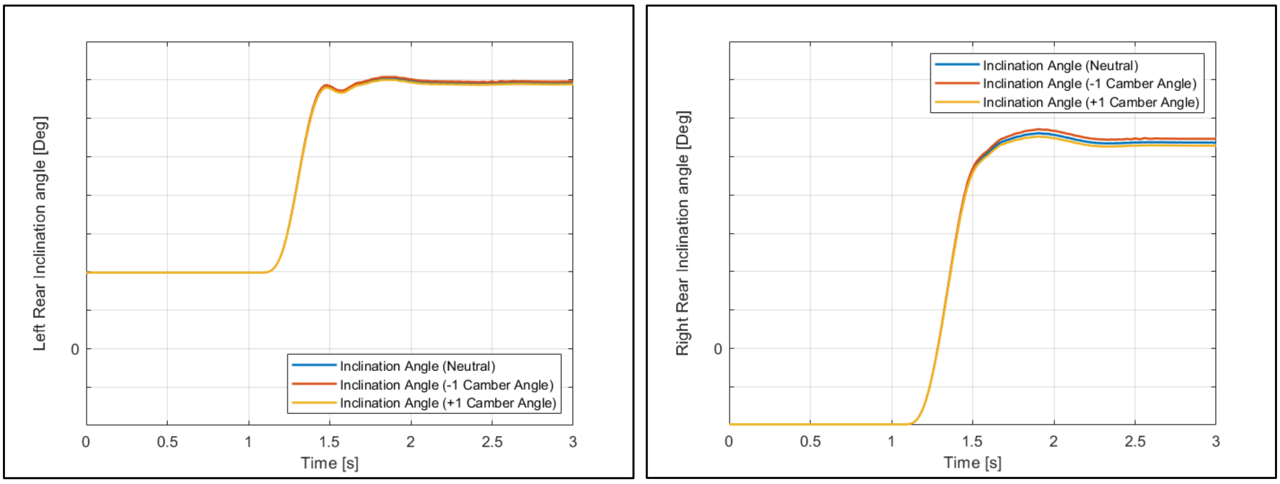

Figure 6.49: Inclination angle variation with static camber variation, for the rear axle

Computation of forces along the duration of the test gave interesting results, as it is shown in Figure 6.50: In term of values there is a small difference between the three tests, what is important to catch is the inversion of trends between front and rear axle. On the front, the total force in the axle will increase as the static camber moves towards positive values; The opposite happens on the rear axle, when camber moves to positive values lateral force will decrease on the rear axle. Negative camber will move the lateral load from the front to the rear and vice versa, this will likely affect the understeering or oversteering behaviour of the vehicle.

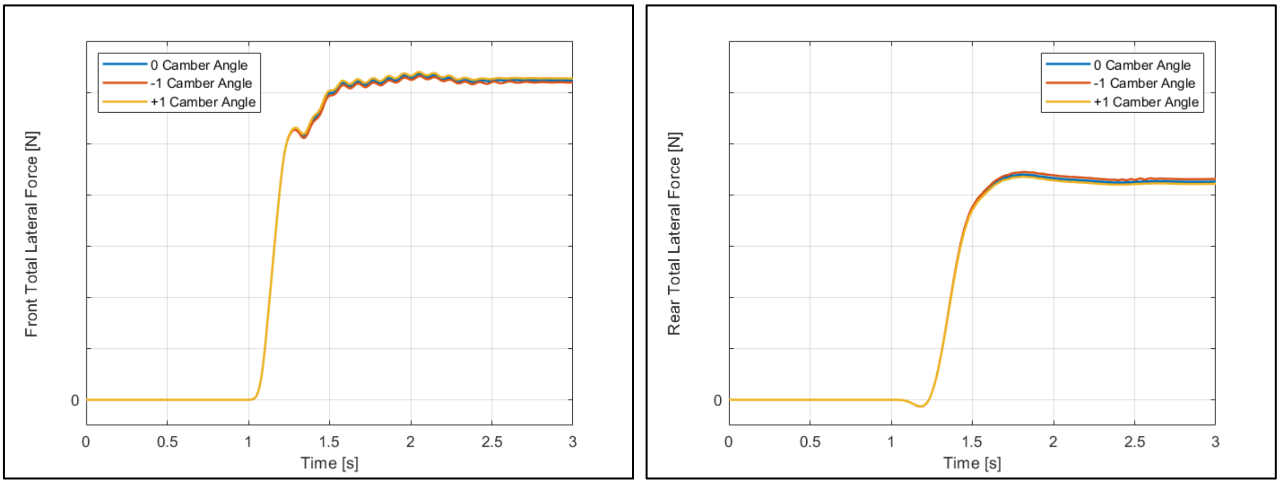

Figure 6.50: Lateral force variation experienced by the front and rear axle as camber angle is changed

6.2.4 Evaluation of system's behaviour as static toe angle is changed

An analysis very similar to the one done for camber angle was performed varying the value of the static toe angle, starting from the neutral configuration a negative and a positive angle were tried, as shown in Table 6.8.

The first parameter that was considered is the side-slip angle in Figure 6.51 seen from the centre of gravity of the vehicle, when toe is moved toward positive angles there is little difference compared to the neutral condition, larger differences are found when the toe angle is set as negative, in this case the side-slip angle decreases compared to the neutral condition.

Test	Static Camber	Static Toe
Neutral Toe	0°	0°
Negative Toe	0°	-1°
Positive Toe	0°	+1°

Table 6.8: Tests performed on static toe variation

The shape of the curve is very similar between the three study cases, it is characterized by an increase of the side-slip angle towards positive values if the steering is moved. When the steering wheel reaches its final position the side-slip angle will decrease suddenly, and then stabilize to the final value, which is negative in all cases.

Lateral acceleration shown in Figure 6.52 gets results that are very similar to the ones found for the side-slip angle, negative toe reduces the lateral acceleration while positive values will increase it.

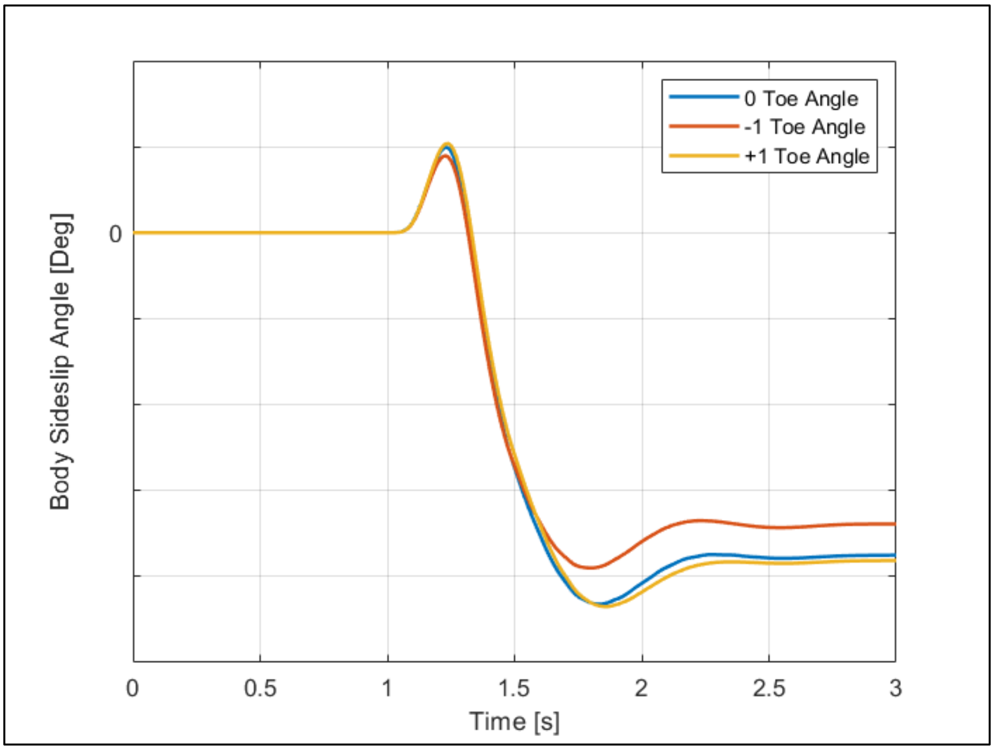

Figure 6.51: Body side-slip angle evolution as toe angle is changed

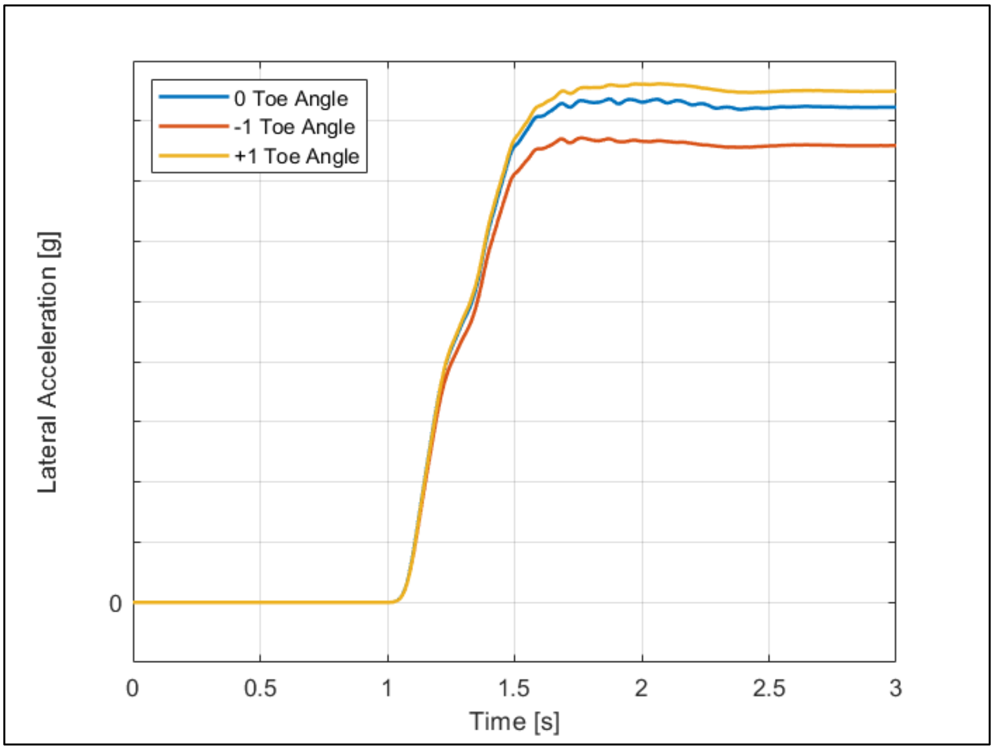

Figure 6.52: Lateral acceleration comparison between the different tests

Concerning camber, toe variation has some effects on its variation: A static toe variation will force the static camber to change of some degree as a result, the phases are the same as before. The outer wheel has little difference between the final value and the static one. The inner wheel has a high variation in the final value compared to the static one when the toe goes towards negative values, while the difference is minimal when the toe angle is positive.

The rear axle reacts almost symmetrically, the main difference being that the inner wheel will experience positive camber values, while the outer has negative values, this again shows the differences in behaviours between the two suspension typologies, results are shown in Figure 6.53 and 6.54.

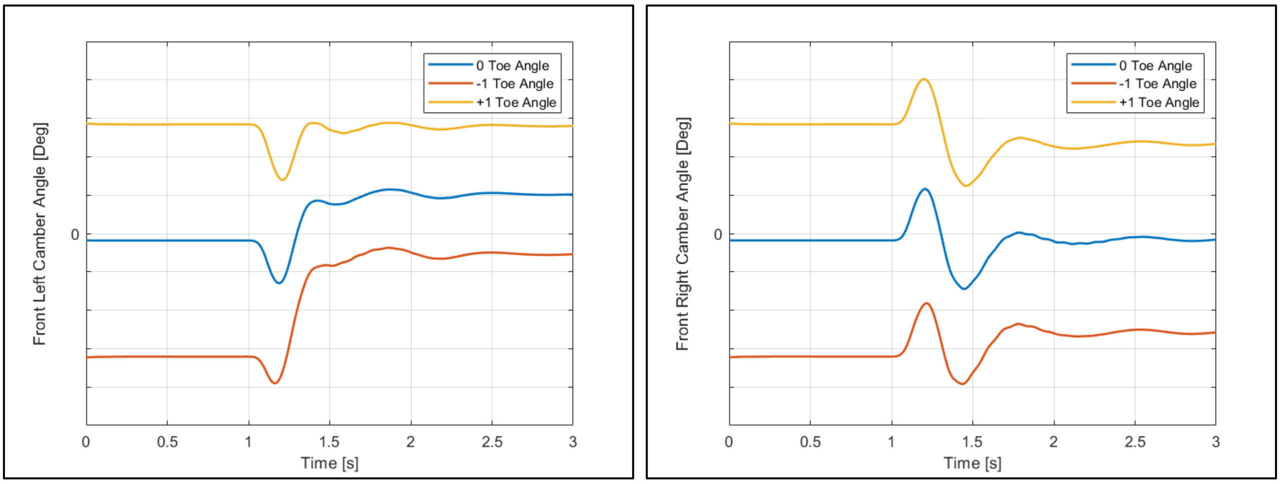

Figure 6.53: Left and right front camber angle variation as toe angle is changed

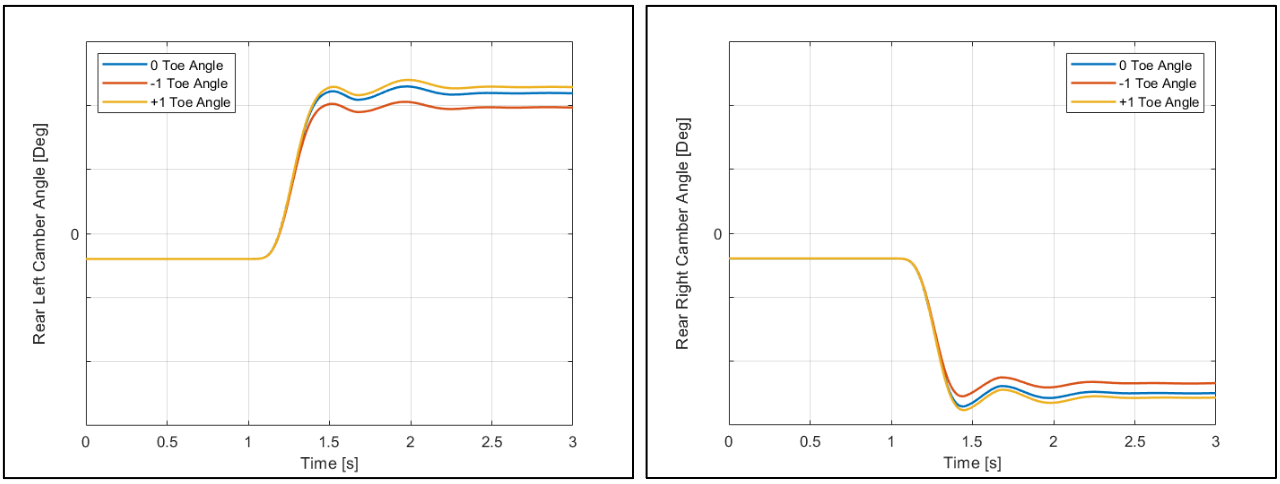

Figure 6.54: Left and right rear camber angle variation as toe angle is changed

Variation in toe is easier to read compared to camber, as it is shown in Figure 6.55, as the vehicle steers the inner wheel drops in value and the outer increases its value after a stabilization phase characterized by a sinusoid with small peaks it stabilizes to the final value. The behaviour of toe is mostly defined by the setting of the initial static value and its variation from the static value is constant between all these cases.

The same analysis has been performed on inclination angle for static toe angle variations.

The front axle in Figure 6.56 shows different characteristics between the two wheels: On the left the curves will be closer together compared to the right. This phenomenon is mainly related to the fact that steering is not symmetric, one wheel will steer more than the other, affecting the effect of toe on the wheel.

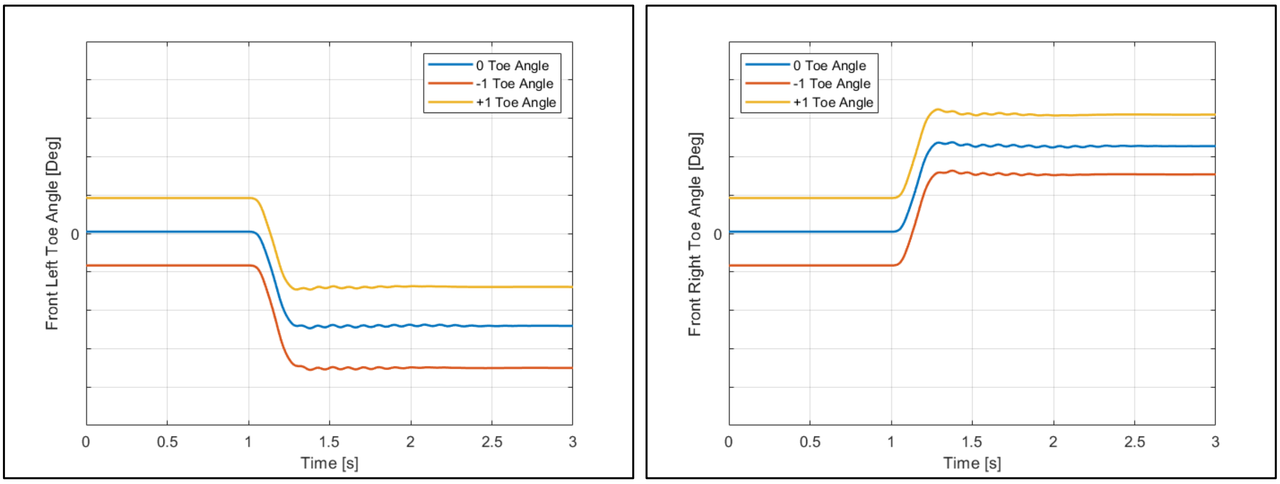

Figure 6.55: Left and right front toe angle variation as toe angle is changed

Different loads on each side will also make a difference, stabilization phases are similar between the different conditions.

Figure 6.57 shows the results on the rear wheel: In this case the results obtained are similar to those from the static camber variation. Differences are more noticeable on the outer wheel. It is also possible to see that the negative toe condition will move from the neutral case further than what the positive variation can do.

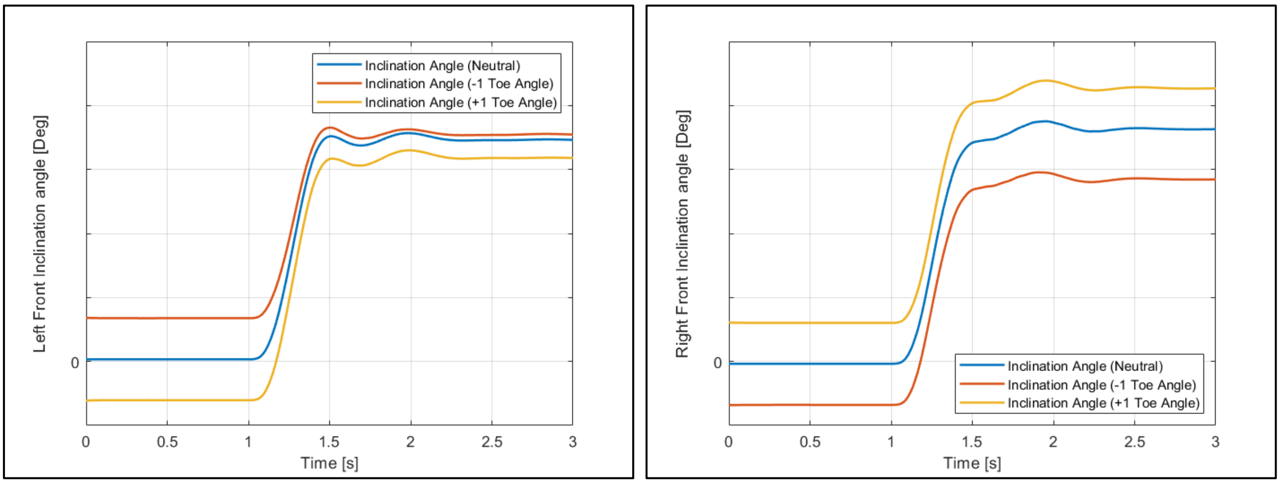

Figure 6.56: Inclination angle variation with static toe variation, for the front axle

Lateral forces increase as toe angle moves towards positive values: This is true for both axles. The rear axle has a seamless characteristic, with just one major sinusoid with a small peak. The front axle takes a different approach in its stabilization, with more small peaks one after the other, in terms of values the variation in toe angle affects the lateral force more than static camber variation, these results are shown in Figure 6.58.

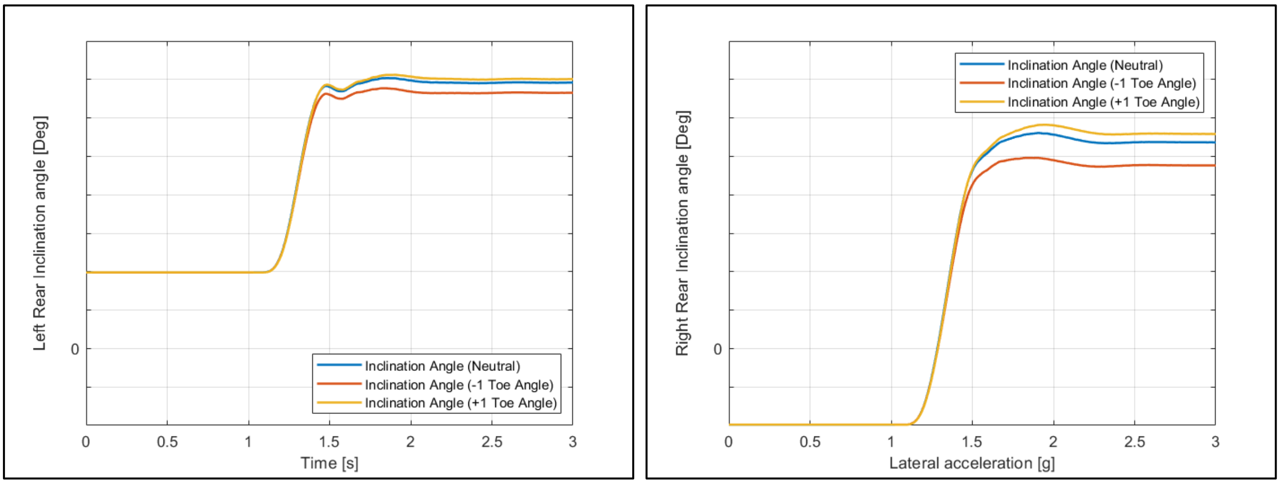

Figure 6.57: Inclination angle variation with static toe variation, for the rear axle

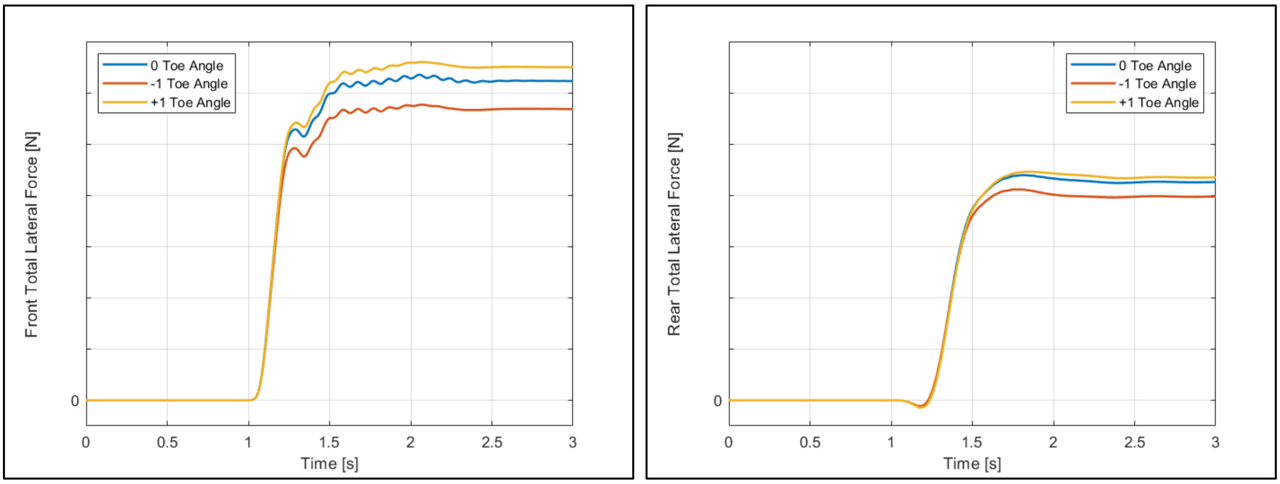

Figure 6.58: Front total lateral force comparison between the three configurations

6.2.5 Conclusions on the step steer manoeuvre

At last, a study on roll angle between the different conditions was performed, the difference between the two body types is minimal in this case as it is clear to see in Figure 6.59, this is explained by the fact that the two vehicles have limited variations of the centre of gravity in terms of height: the factor that affects the most the roll angle. Interestingly, higher variations were found when changing toe angle instead of changing the vehicle itself.

Camber has little effect on roll angle, as it is seen from the fact that curves almost overlap in Figure 6.60.

Toe variation can lead to interesting results, a negative toe angle reduces the roll angle by a relatively high margin, this result can be very useful considering that roll angle in this type of manoeuvre and vehicle can be critical, these types of vehicles usually need to be high in order to increase the loading capability, this condition will decrease largely the cornering performances in terms of roll.

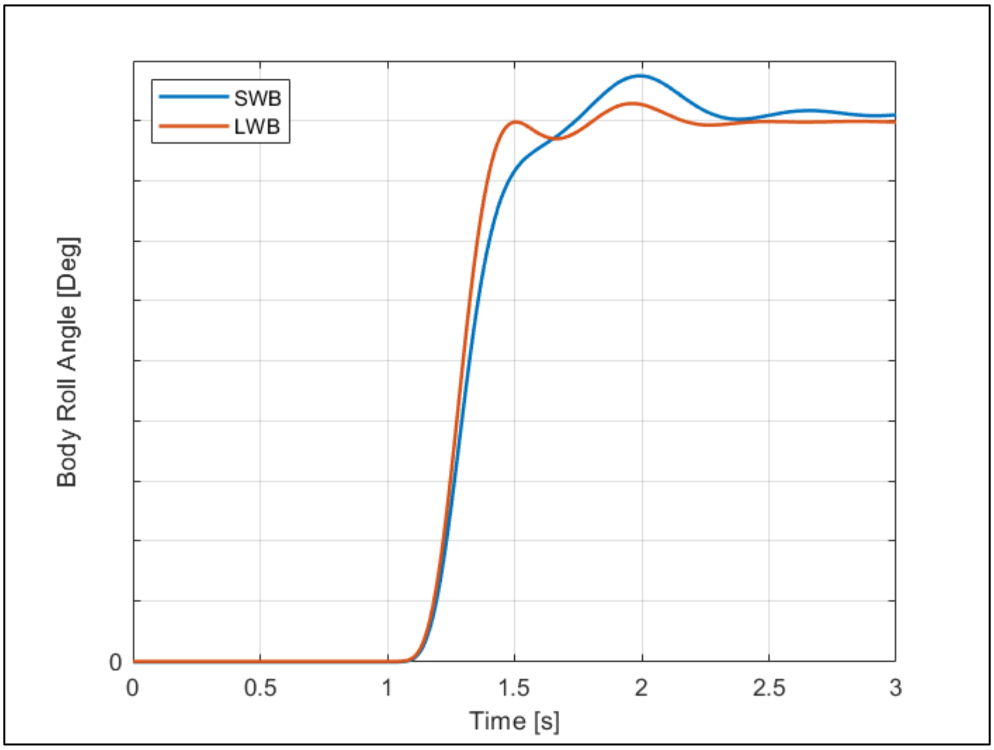

Figure 6.59: Roll angle evolution between the two different vehicles

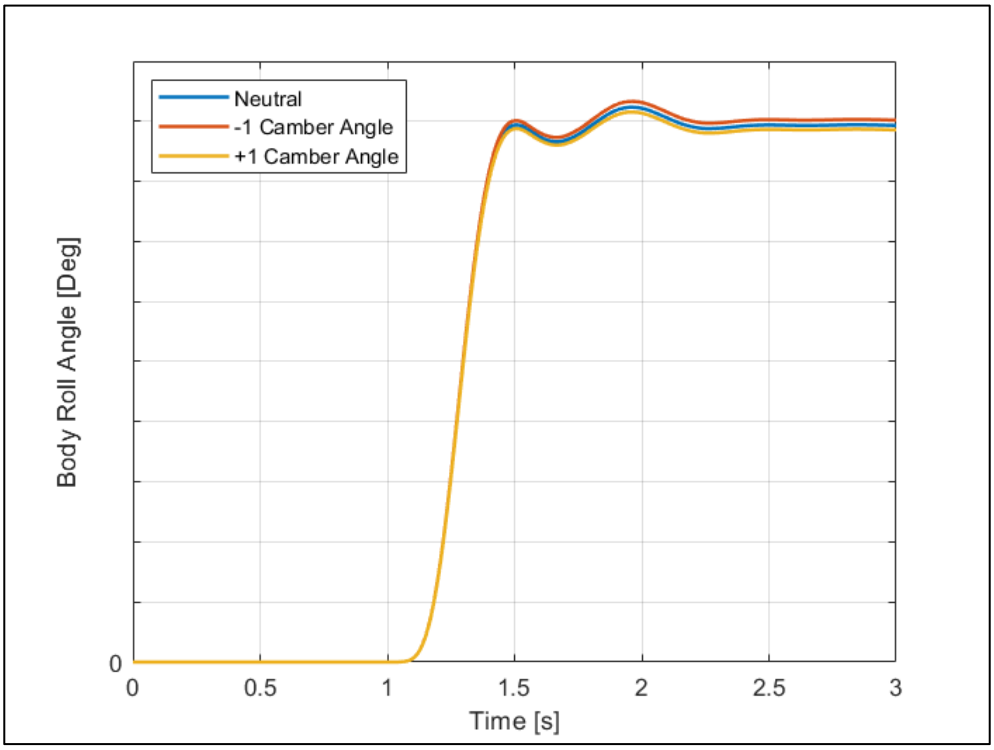

Figure 6.60: Roll angle evolution for different static camber settings

From the results in Figure 6.61, a simple alignment condition such as toe angle can have high effects on the roll angle of the vehicle, a fine-tuning of this parameter can improve the performances of the vehicle without having to redesign any component in the suspension or the vehicle.

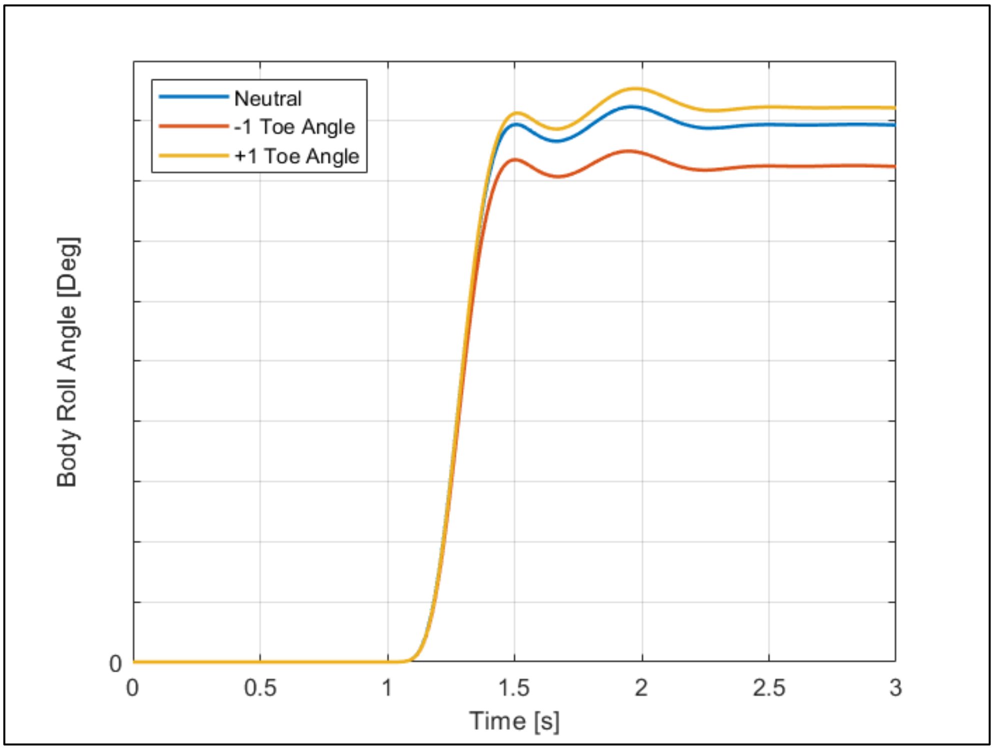

Figure 6.61: Roll angle evolution for different static toe settings

To close the chapter on step steer it is important to say that the focus of the analysis is to see the time that the system takes in reaching the final value, this will translate in the time that the vehicle needs in its stabilization after a sudden manoeuvre such as step steer.

The response time is usually largely related to the unsprung masses of the suspension, commercial vehicles commonly have heavy duty components that increase this weight in order to have greater durability over time.

With this analysis it is possible to see that acting on some simple parameters such as camber and toe it is possible to change the behaviour in these kind of manoeuvres without having to redesign any component. This is very important in the phase where the suspension is defined in terms of design and only the final tuning of the system has to be defined.

6.3 Sweep Steer

6.3.1 Introduction to the sweep steer test

The last test performed on the full vehicle model is the sweep steer test, this test consists of a sinusoidal steering input as it is showed in Figure 6.62: The aim of this test is to find the frequency response of the system: In this case the test was performed comparing the different vehicles that were introduced in the previous paragraphs of this chapter.

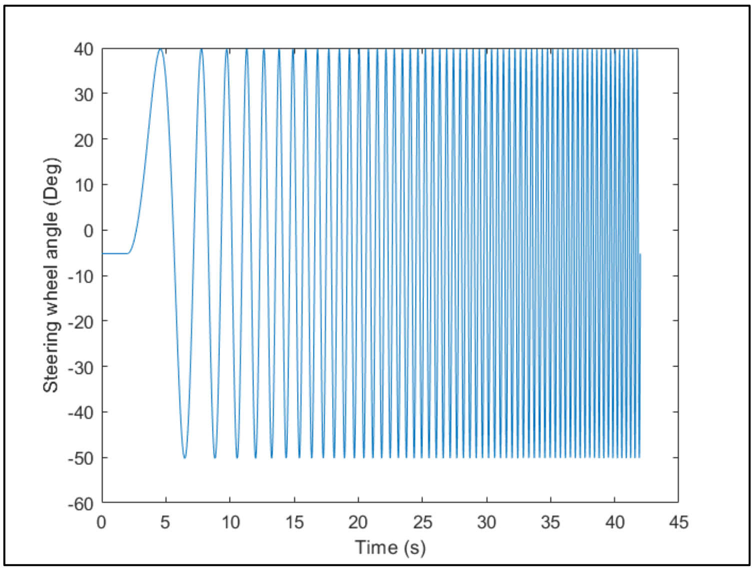

Figure 6.62: Steering input as the manoeuvre proceeds

The analysis has been set using the parameters shown in Table 6.9: Like the step steer analysis the test starts from a slightly negative steering angle. As the manoeuvre goes on, this initial condition becomes irrelevant, except for the fact that when steering left and right there is a small difference in steer angle peak values, compared to the expected maximum steer value.
To have good results a high frequency was selected to define the step size, in this case 100 Hz, this leads to 4200 steps to complete the simulation that lasts for 42 seconds. The frequency rate is defined as the ratio between the delta between maximum and initial frequencies and the delta between start and end time.

Start Time	2 s
End Time	42 s
Step Size Frequency	100 Hz
Vehicle Speed	80 km/h
Maximum steer	45°
Initial Frequency	0.1 Hz
Maximum Frequency	3.1 Hz
Frequency Rate	0,075

Table 6.9: Parameters used in sweep steer analysis

Bode plots were created in linear scale and all the figures are made of three different graphs, the first shows the amplitude of the system, the second shows the phase, the third shows the result of the magnitude squared coherence estimate, this graph gives an idea on the reliability of the results obtained, all the parameters were evaluated with respect to steering wheel angle.

6.3.2 Comparison between the two different vehicles in exam

The first study performed on bode plots consisted of a comparison between the two vehicles in exam, the testing parameters were set as shown in Table 6.9 for both configurations.

The first parameter to be analysed is the yaw rate, shown in Figure 6.63, this factor indicates the lateral rotation that a vehicle experiences around its centre of gravity, that indicates the pivot point for the vehicle.

Bode plots start to be relevant after the simulation reaches the relevant parameters of the analysis, before 0.1 Hz, there is no definition of the sweep steer motion. Considering the fact that the analysis starts after an initial settling time: The first part of the graph often shows different behaviours compared to what happens in the beginning.

By watching the coherence function it is possible to understand that up to a frequency of 0.2 Hz circa the relationship between input and output is not reliable enough. Concerning yaw rate, graphs show similar characteristics between the two configurations, in terms of amplitude the shorter vehicle reaches a higher peak compared to the long wheelbase one. At higher frequencies there is an inversion of trends that has the longer vehicle as the one with higher amplitudes, in terms of phase the two vehicles show similar behaviour, phases are negative in this plot, so the shorter wheelbase configuration will have higher values in absolute value, again.

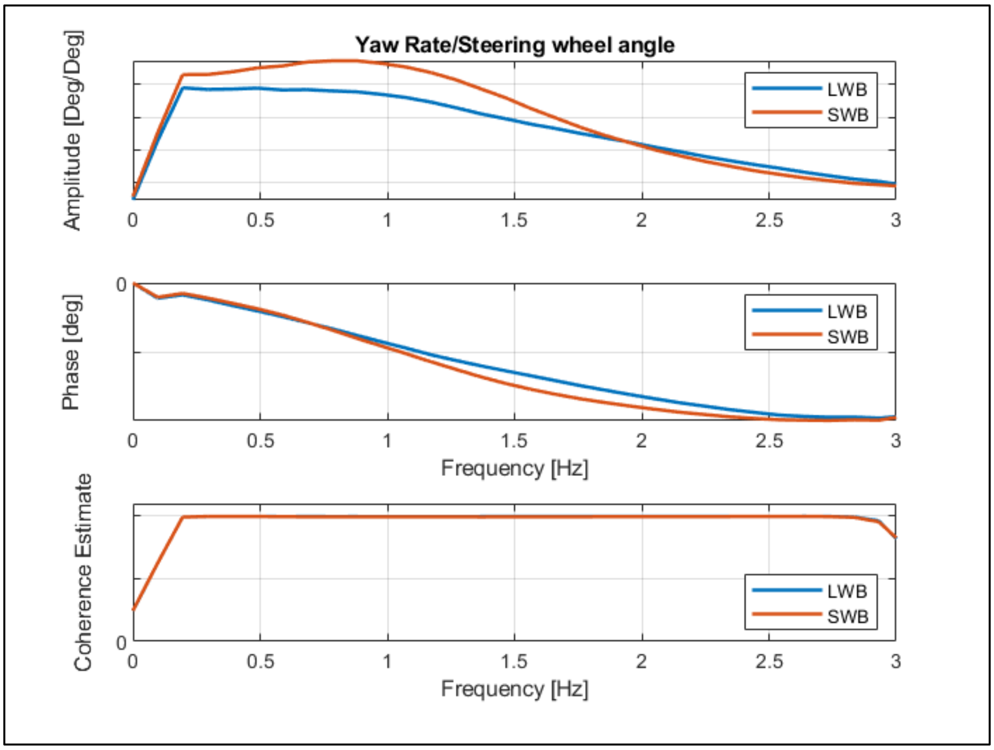

Figure 6.63: Yaw rate bode plot showing the comparison between the two vehicle configurations

Roll angle is also relevant in these types of manoeuvres, looking at Figure 6.64 it is possible to catch that the situation is more complex compared to what was found for the yaw rate: In the middle of the analysis there is a minimum point of amplitude for the short wheelbase vehicle and a maximum for the longer configuration.

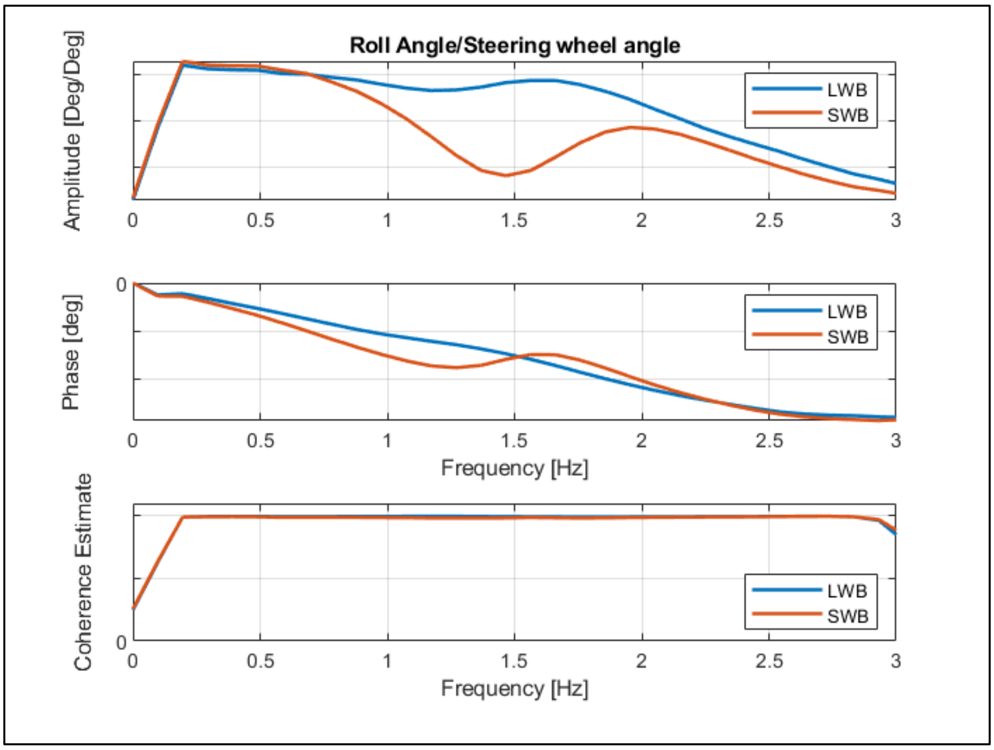

Figure 6.64: Roll angle bode plot showing the comparison between the two vehicle configurations

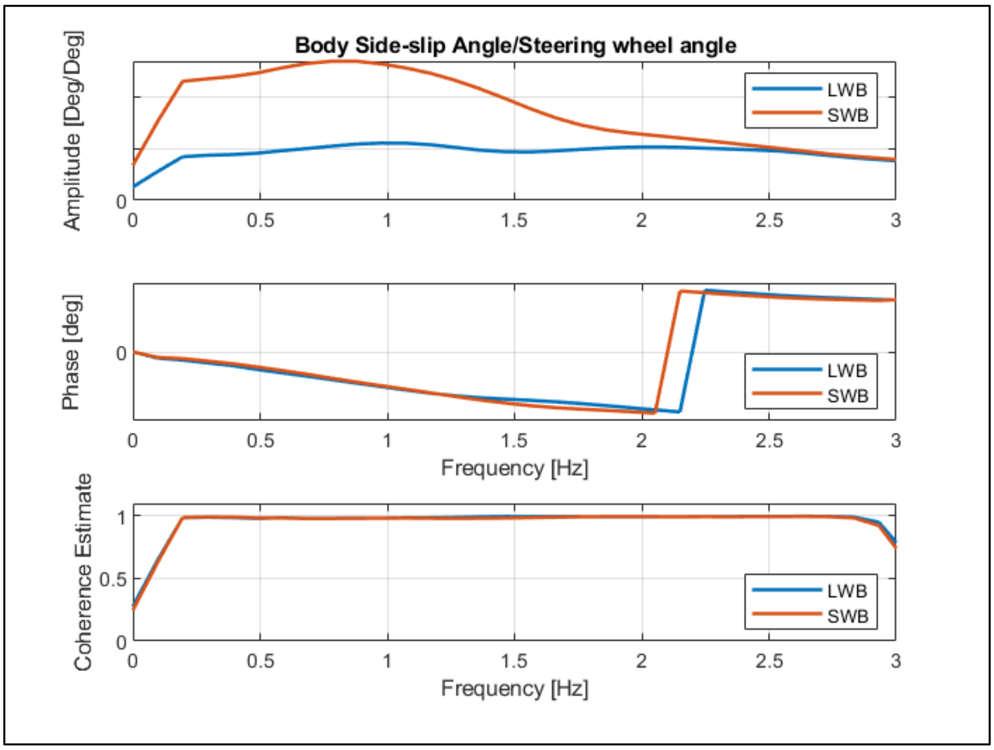

Figure 6.65: Body side-slip angle bode plot showing the comparison between the two vehicle configurations

The major difference from the almost linear behaviour that is shown before and after this region is present on the 3520mm long vehicle. The same behaviour is appreciable in the phase graph: Here, the graph is almost perfectly linear for the long wheelbase configuration, while it shows a sinusoid for the shorter vehicle. The point of intersection between the two lines is in the middle of the frequency range considered. This result gives that the two configurations are different between them in this middle range, especially in amplitude, while they have similar characteristics for low frequencies and up to the 3 Hz limit of the range considered in this study.

The body side-slip angle β has a characteristic similar to the yaw rate, in terms of amplitude the shorter vehicle experiences higher values and a less regular behaviour, while the long wheelbase one is almost constant in terms of amplitude, differences in phase are minimal.

Phase has an interesting behaviour for this parameter, it experiences a steep phase shift above 2 Hz, from this region the amplitude between the two vehicles becomes similar again. Results are seen in Figure 6.65.

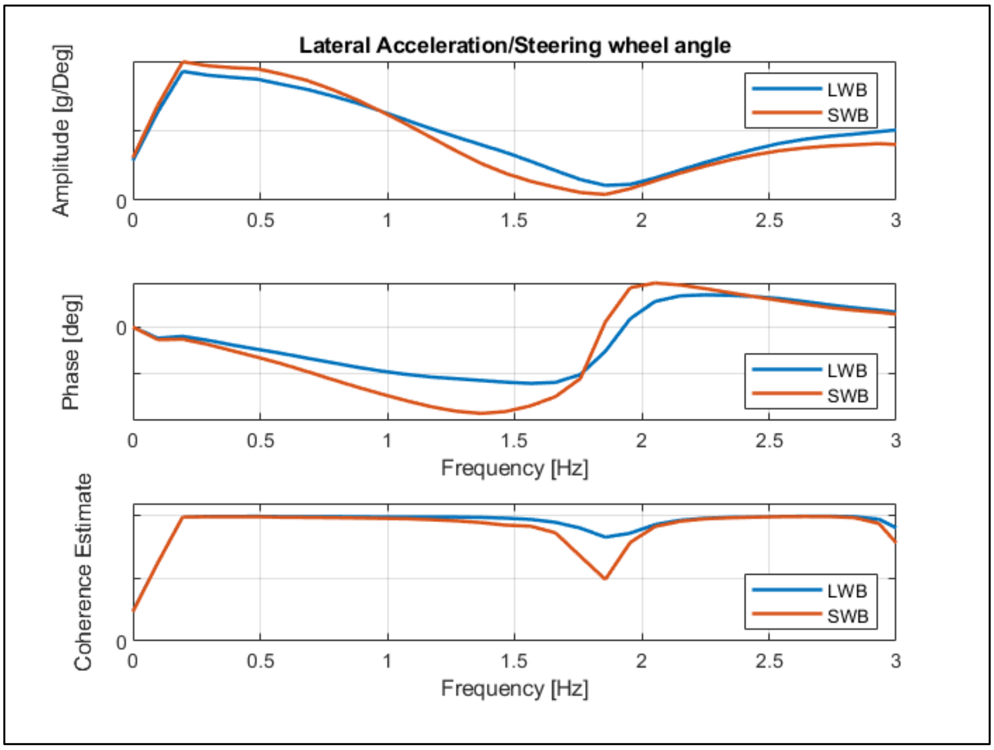

Figure 6.66: Lateral acceleration bode plot showing the comparison between the two vehicle configurations

At last, the relationship between lateral acceleration and steering wheel angle is considered, the two vehicles show characteristics that are very similar between them. Particular attention has to be taken when looking at results from this bode plot, when looking at the graphs from Figure 6.63 to 6.65, the coherence estimation is equal to one from the first settlement up to the 3 Hz limit, this estimation gives a good result in the relationship between input and output when is unitary.

When looking at the estimation in Figure 6.66 it is possible to see that the value drops between 1.5 and 2 Hz, this basically tells that the analysis can be considered reliable up to 1.5 Hz circa, interesting to note that this drop in coherence is placed when the system has an inversion of trends in phase and amplitude, the longer vehicle has a smaller drop and so a better relationship, but the drop is still noticeable.

6.3.3 Comparison between linear and non-linear field

This paragraph focuses on the comparison between two frequency fields analysis performed on the same vehicle. The test was done for the two vehicles, results are shown for each parameter for the short vehicle first and for the longer vehicle after.

The type of field of the analysis is decided by the lateral acceleration that is experienced by the vehicle, up to values of two m/s^2 the analysis is taken in the linear field. When moving to higher accelerations, above six m/s^2 circa, the analysis moves in the non-linear field. To evaluate the differences between these two fields it was necessary to have two tests at different accelerations.

When doing a sweep manoeuvre the two parameters that mainly define lateral acceleration are the speed at which the vehicle is travelling and the steering angle.

The speed was kept equal to the one used in the comparison between the two different configurations at 80 km/h. This meant that steering angle was the variable to define the two fields in analysis: A value of 15° seemed like a good value for the linear field, while a value of 90° was selected to represent the non-linear field.

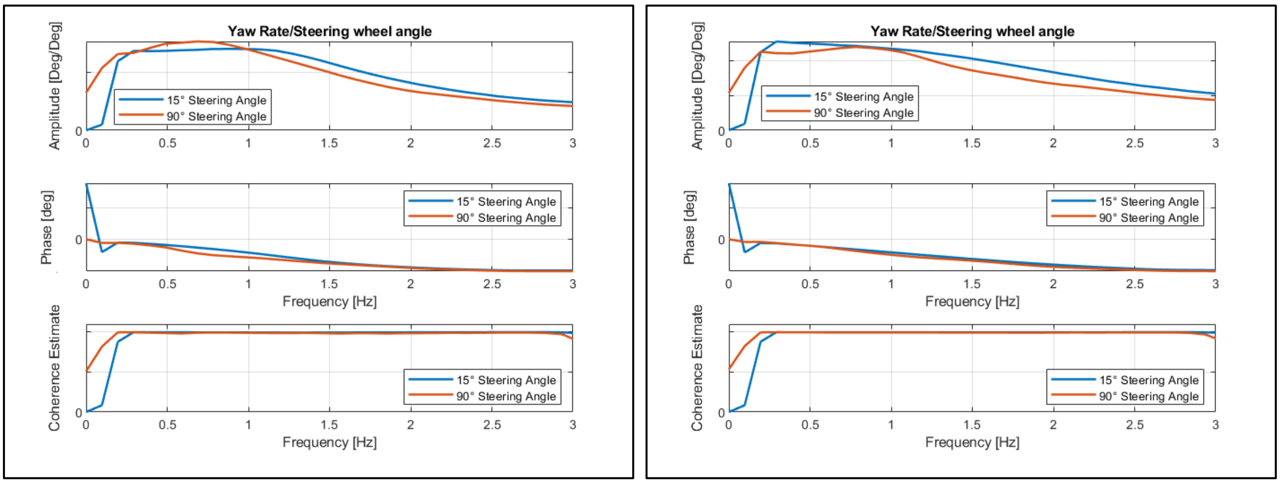

Figure 6.67: Yaw rate bode plot for two different degrees of acceleration, SWB on the left. LWB on the right

Yaw rate is the first parameter to be analysed in Figure 6.67, the difference between the linear and the non-linear field is not high for this test. The phase is very similar between the two cases, for the longer vehicle, the non-linear case shows a slightly sinusoidal behaviour that differentiates it form the test done at a smaller steering angle. Differences are less pronounced for both amplitude and phase in the longer unloaded vehicle case, the main difference between the two fields comes from the settling that happens at low frequencies: The linear field shows a linear characteristic, while the non-linear field shows a slight bump before descending in amplitude. Coherence converges to one for the length of the test, even if differences are small, a first idea on how the two trends differ between the different fields starts to be clear.

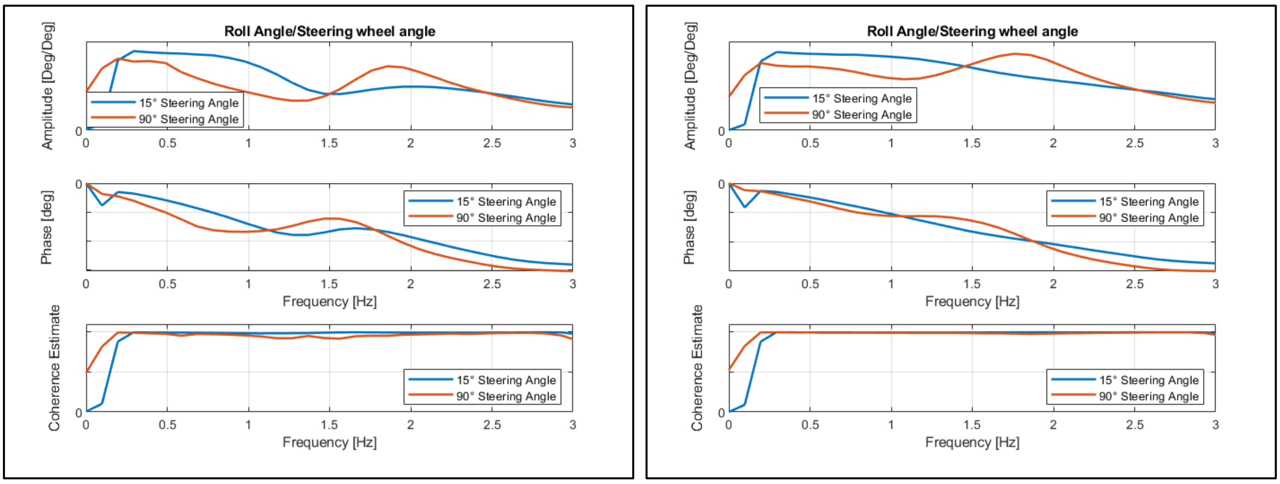

Figure 6.68: Roll angle bode plot for two different degrees of acceleration, SWB on the left. LWB on the right

Roll angle evaluation gives higher differences between the two fields as it is shown in Figure 6.68, especially when looking at the longer vehicle: In this case the non-linear field shows a clear sinusoidal behaviour for all the tests, the linear field is more regular but still has some variability. The longer vehicle has higher differences between the trends of the two tests performed, coherence is perfect for the longer vehicle, the short wheelbase vehicle shoes some variability in coherence for the test at higher accelerations that has to be considered when looking at the results.

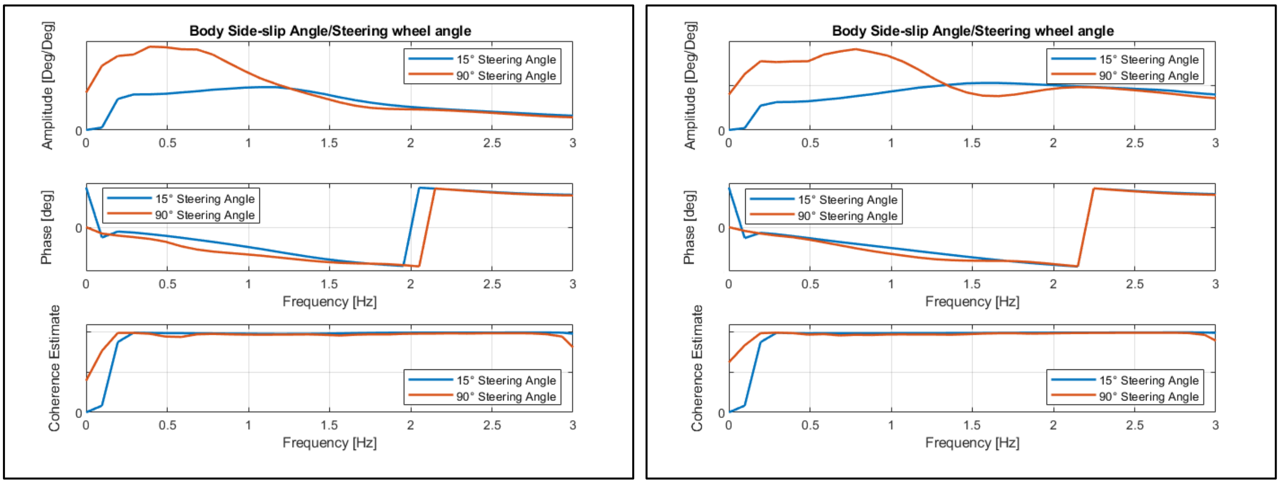

Figure 6.69: Body side-slip angle bode plot for two different degrees of acceleration, SWB on the left. LWB on the right

The evaluation of the vehicle's Beta angle gives the highest difference in terms of amplitude between the two tests as it is shown in Figure 6.69. Graphs are similar between the two configurations in characteristic: The high difference in amplitude is related to the fact that higher accelerations will deliver higher slip angles due to the fact that the vehicle will be closer to the grip limit of the vehicle and will have a higher degree of slip, coherence is good again for both configurations.

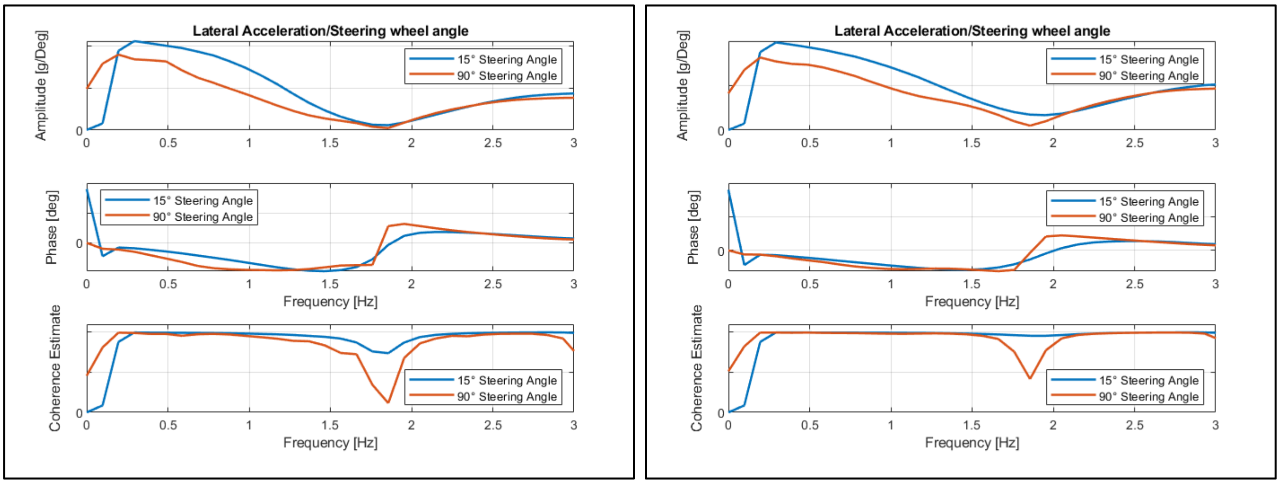

Figure 6.70: Lateral acceleration bode plot for two different degrees of acceleration, SWB on the left. LWB on the right

At last, lateral acceleration was evaluated in Figure 6.70, results from this analysis have to be considered knowing that the coherence function is valid up to a certain point. The test at higher acceleration is the one that gives the worst result in terms of coherence and also shows a curve that is a lot less regular than the one of low speeds. On the long wheelbase configuration, for a steering angle of 15° the coherence function is almost perfectly unitary for the entirety of the test.

This gives as a result how the acceleration on steering angle relationship will behave in case of good coherence. The curve in this case is more gradual when the system surpasses its minimum point and starts to grow again in phase and amplitude.

6.3.4 Conclusions on the sweep steer test

A test like the one performed in this paragraph has the aim of evaluating the frequency response of the system, by itself an analysis like this gives results on how some parameters reacts at different frequencies but it is not easy to catch how these parameters will change the vehicle dynamics.

Each of the input/output analysis performed have a relationship to vehicle performance, as it was said, considering the fact that the analysis were reliable up to 1.5 Hz it is possible to select a common frequency from where results are taken among the different parameters, commonly 0.5 Hz could be taken as a reliable enough value to compare the different tests.

The main parameters that are able to compare the different vehicles are Gain and Delay of the frequency response that is evaluated. These parameters are related to Amplitude and Phase of the system.

From the relationship between the acceleration and steering wheel angle as well as the one between yaw rate and steering angle it is possible to evaluate how well the vehicle will enter a corner and so its predictability when changing directions.

From the relationship on roll angle, it is possible to evaluate how much the vehicle will lean into corners and how stable it will be.

Looking at the side-slip angle it is possible to understand the directionality of the vehicle.

From the results presented in this paragraph it is possible to define some performance indexes basing on amplitude gain and phase delay, computed as the first derivative of the phase response of the input/output systems. The common frequency that is set to take the values is decided on the element that has the lowest coherence: In this analysis the acceleration showed the least coherence with a reliability up to 1.5 Hz. Even if the other systems had good coherence the limiting factor still has to be set as 1.5 Hz. Taking 0.5 Hz or similar guarantees that results are reliable enough.

7 Conclusions

After six paragraphs and many studies and simulations this study has come to an end, it is now possible to reflect on the work performed and draw some conclusions.

The first part to learn from has to be the part on modelling, the focus is on the steering system. The model started from a system with two shafts, the model contained in this work follows the hardpoints of the real world system and is more representative of the real system employed on vehicles like this. Like every model, also this one can be further improved, for simplicity this system has no power steering and the definition has been made through generic Adams Car parameters, a more in depth study on the real system could improve the reliability of the system by introducing more accurate parameters, as it sits, the model used in this work is accurate enough.

The study on parallel and opposite wheel travel delivered results on how the suspension parameters change in value as the suspension displacement varies. This is not only relevant for static analysis but also gives an idea on how each parameter is affected by a change in wheel travel that can also happen during a cornering manoeuvre due to the roll motion.

By comparing the results obtained by a full vehicle manoeuvre to the results obtained in the wheel travel tests it is possible to understand how much each parameter is affected by the dynamic forces and accelerations that will act on the wheel and suspension and how much by the suspension travel that will change its geometry.

The core of the simulation comes from the analysis on the complete vehicle, two comparisons were made on these tests, on one side two different vehicles were compared, on the other side it was evaluated how the system reacted to different alignment parameters.

The most valuable comparison comes from the analysis between the two vehicles, this study is limited by the fact that reliable data could be found just for two vehicles, that are in different conditions. Important results were obtained from this simple study, the short wheelbase vehicle resulted in an higher grip limit with comparable results in other tests to the long wheelbase vehicle, even if that vehicle was in unloaded configuration: This gives the idea that the wheelbase of a vehicle is more important than the actual weight the vehicle has in these tests, especially considering that vehicle like these are commonly designed to work in fully loaded condition, and so can react to changes in weight.

The largest differences between the two vehicles came from the rear axle behaviour, the fact that one vehicle was loaded, and one was not largely affecting how these systems behave.

When the study moved to the evaluation of the effects of alignment parameters important results were also obtained, camber variations did not affect much the system, toe gave more important variations, especially towards negative values. The main results from the studies on alignment are the main trends that were set when passing from a positive to a neutral, up to a negative value of toe and

camber, this study wants to be a guide on how a change in parameter affects the behaviour in term of trend, not in values.
By following the graphs obtained on this work it is possible to understand how a change in parameter will affect the results that will define how well the vehicle performs. By following the patterns created in this work it is possible to tune these parameters knowing towards which value each parameter will move when a modification is applied.
At the end, as it was valid for the previous work on which this thesis started from, a starting point for something more in depth. By improving the model and having more data available from different vehicles it would be possible to have a comparison among many vehicle configurations and evaluate how each of them can be tuned to improve performances, while having the highest standardization possible. This work can serve as a basis for a comparison among the full line-up of vehicles offered by Iveco in this category, this can help on one side the manufacturer in evaluating how each vehicle compares to the other but can also be useful to clients that want to know which configuration best suits their needs.
As it is stated along this work this thesis has the aim to serve as a basis for future works, important elements such as compliance between steering elements and power steering are not included in this analysis. The addition of these elements and a higher accuracy in the evaluation of the parameters used by the model with respect to the real system will surely bring results closer to the real world condition. To do so, a higher amount of data is needed, with the initial data obtained from the manufacturer it was possible to find interesting results already, but a higher accuracy is needed to develop a model that can fully simulate the behaviour of the real vehicle.

Appendix 1: Procedure used to define, in a parametric way, phase angles of hooke joints in Adams Car

This appendix will show how to set parametric phase angles in Adams Car, this will be valid for any system that uses hooke joints. In this case the application concerns a steering system of a light commercial vehicle, the same rules apply regardless of the system studied.

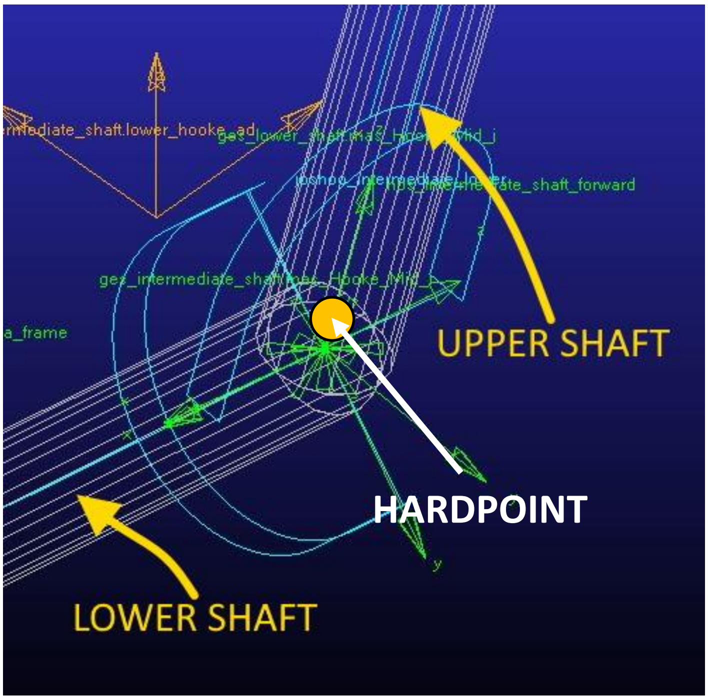

Figure A.1:System analysed in the case of study

In Figure A.1 it is possible to see the system studied in this analysis, the shaft placed before the cardan joint will be called 'Upper Shaft', and the shaft next to it will be called 'Lower Shaft'.

A1.1 Creation of required markers

As a first step it is necessary to create two markers, the first will be called Marker **'i'** and the second will be called **'j'**. The first marker will locate the joint relative to the upper shaft, while the second will locate the joint to the lower shaft.

To create a new marker click the *'Build'* button on the top menu in the Adams Car template interface, then *'Marker/New' button*. A menu like the one in Figure A.2 will open.

- In the first text box (**Marker**) enter the name of the marker wanted, the marker will be called **'Hooke_Marker_i'** as an example.
- In the second text box (**Part**) enter which part the marker refers to, in this case the part of the Adams Car environment that defines the Upper Shaft: This part will have a name of the type **'ges_upper_shaft'** or similar, for simplicity it is better to right-click on the text box and select

the *'Pick'* option, at that point it is possible to click with the left mouse button on the part, in case the system is very complex making it difficult to understand which is the correct part to click, use the right button in the area adjacent to the part and then select it from a drop-down menu. The system should automatically select the correct *'Type'* option.

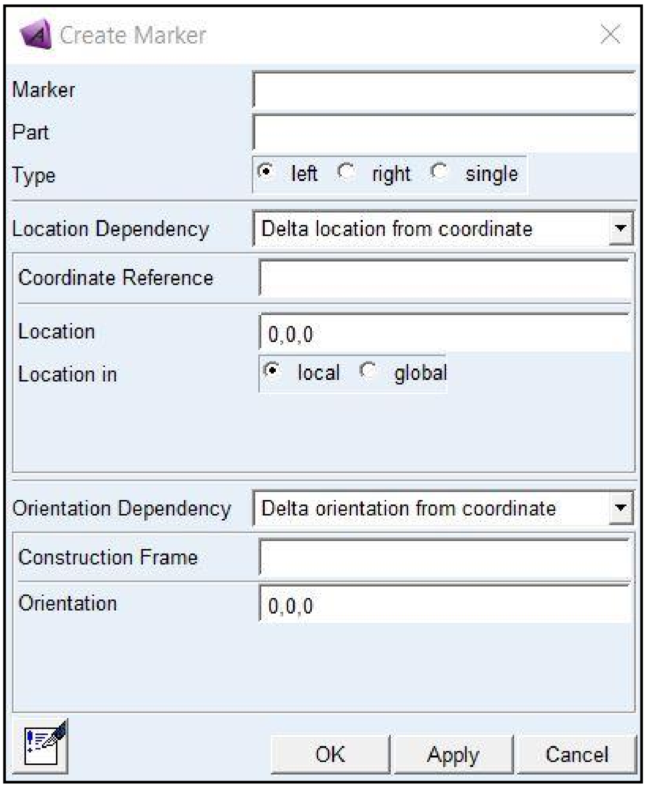

Figure A.2:Marker creation menu

- At this point select the *option 'Delta location from coordinate'* in the drop-down menu *'Location Dependency'*.

  In the third text box (**Coordinate Reference**) select the hardpoint defined between the two shafts, this point will usually be the same that is used to define the joint, the *'Pick'* method shown above can also be used to select this point, leave the coordinates in the 'Location' box as 0,0,0 to perfectly center the marker with respect to the hardpoint.
- In the *'Orientation Dependency'* menu, select *'Delta orientation from coordinate'* in the fourth text box (**Construction Frame**) select a reference system that defines the orientation of the shaft in space. In this case it is possible to choose as a reference system the *'Inertia Frame'* related to the chosen part or create a special *'Construction Frame'* using the *'Orient axis along line*' function as orientation, and choosing as two reference points the hardpoint at the beginning of the shaft and the one at the end. Currently, it is possible to leave the *'Orientation'* box at the standard values.

Select which axis will define the rotation of the cardan joint, necessary to define the actual phase angle, in this case the axis around which the joint rotates is the z-axis, depending on the reference system used the situation may change

In the event that it is impossible to define reference systems, use the *'User entered values'* function and enter the orientation values that can be found by right-clicking on the part and selecting *'Info'*, but doing so the values will have to be changed each time in case the shaft is moved and/or rotated.

The same procedure can be repeated for the creation of the second marker that we will call **'Hooke_Marker_j',** in this case select as part the one equivalent to the Lower Shaft with its relative reference system to define the orientation, the hardpoint taken as reference remains the same.

A1.2 Parameter variable function definition

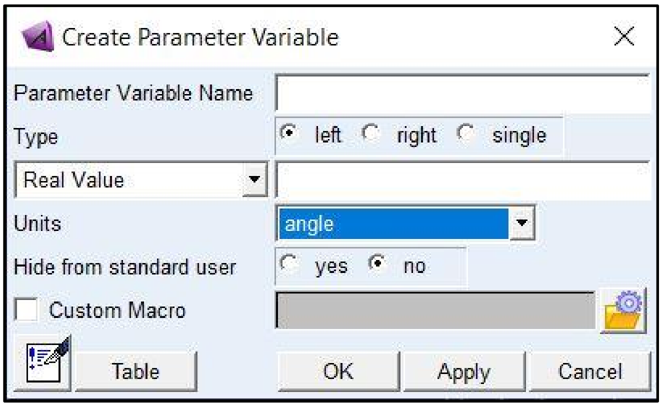

Figure A.3: Parameter Variable Menu

After creating the two markers it is possible to define the '*Parameter Variable*', which will be necessary to have a parametric variable in the definition of the timing angles. To create the function, select '*Build*' in the top menu, then '*Parameter Variable / New*', at this point a menu equivalent to that of figure A.3 will open.

In the first text box (**Parameter Variable Name**) enter the desired name for the variable, in the case analyzed it will be called '**Hooke_Angle**', make sure that the *'Type'* option is on *'single'*. At this point select *'Rear Value'* in the drop-down menu located under *'Type'*, and *'angle'* in the drop-down menu corresponding to *'Units'*. In the second text box put a value like 0.0 or 10.0 initially, it is not relevant because this will be the value that will be parametrically changed.

A1.3 Markers modifications to include the parametric function

After creating the functions to have parametric angles it is now possible to insert the parametric values in the markers.

Firstly, click on the '*Tools*' box in the top menu, then on *'Command Navigator'*, at this point double click the mouse on *'marker'* and then on *'modify'*, a window like the one found in figure A.4 will open:

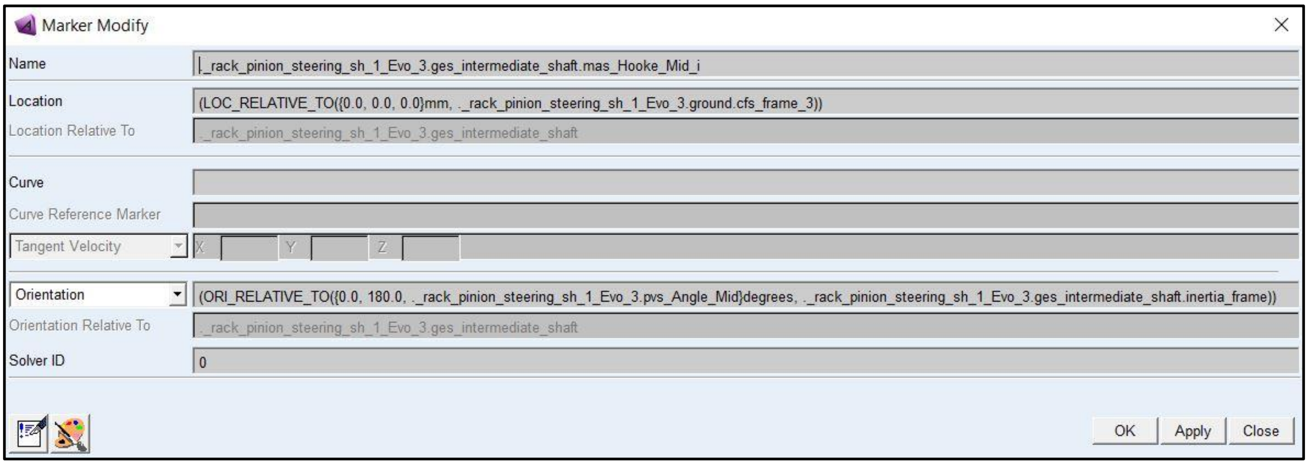

Figure A.4: Marker modify window

- First select the marker that is wanted to be changed, right-click on the first text box (**Name**), and select '*Marker/Browse*', the markers created previously are under the relevant parts, for example the marker **Hooke_Marker_i** will be under the Upper Shaft and the **Hooke_Marker_j** under the Lower Shaft, it is important that each marker is relative to the correct part.
- At this point it is possible to change the function present under the '*Orientation*' box, this function will be, in case the marker was created with the reference system method, of the type:
  ORI_RELATIVE_TO({x, y, z}degrees,Template_Name.Reference_System_Name)
  The only value to change will be the value of the axis around which the joint will rotate, in this case the z-axis.
  Template_Name.pvs_Angle_Function_Name is the formula that will define the parametric phase angle function, **Template_Name** will be the name of the template used, **pvs_Angle_Function_Name** will instead be the name given to the Parameter Variable, in this case **'Hooke_Angle',** in case our template is called **'Steering'** we should insert a function like: **'Steering.pvs_Hooke_Angle'**.

A1.4 Cardan joint references definition

In this case the procedure will be explained starting from the assumption that the cardan joints have already been created on Adams Car. To change the joint, click on Tools/ Command Navigator/ constraint/ modify/ joint/ hooke, a window equivalent to the one in Figure A.5 will open:

- Select the cardan joint in the first text box (**Joint Name**) using the *'Pick'* or *'Browse'* tools.

- Choose in the fourth text box (**I Marker Name**) the marker related to position i, '*Hooke_Marker_i*' in this case, also in this case it is possible to use tools such as '*Browse*' to find the marker more easily.
- Choose in the fifth text box (**J Marker Name**) the marker related to position j, '*Hooke_Marker_j*' in this case, also in this case it is possible to use tools such as '*Browse*' to find the marker more easily.

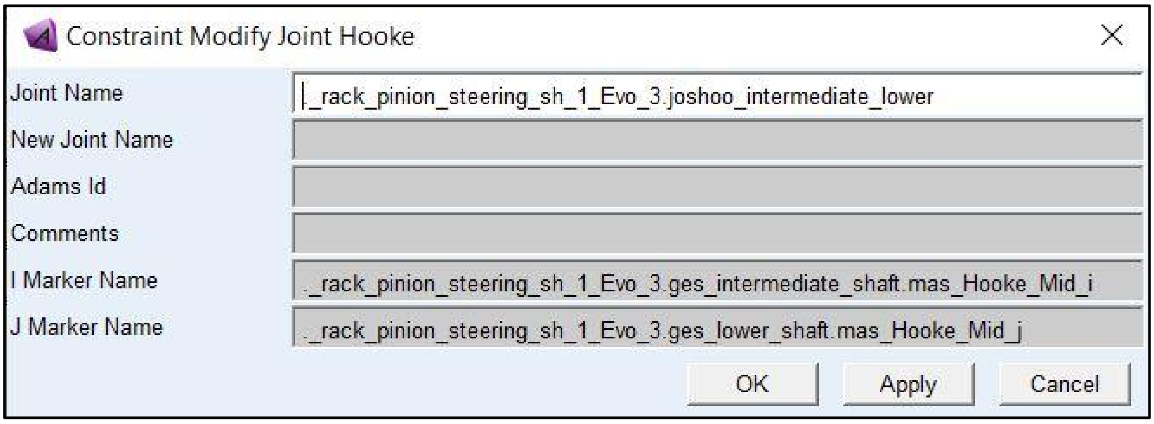

Figure A.5: Hooke joint modification window

If it is necessary to create from scratch the joints, the procedure is the same, just enter the correct markers during creation without having to make further changes.

A1.5 Conclusions and suggestions on the procedure

After these steps it is possible, by entering a value in the function Hooke_Angle created, to configure the phase angle of the cardan joint, if the system has more joints it is recommended to perform these steps for each joint creating as many functions as there are joints, in this way it is possible to insert a different phase angle for each joint.

It is recommended to try varying the angle of the function to see that the rotation of the joint is consistent. Care should be taken to ensure that the function that defines the phase angle is inserted in the correct coordinate, that is, that of the axis around which the shaft rotates.

Appendix 2: Procedure used to perform an Adams Insight experiment starting from a simulation in Adams Car

The procedure explained in this appendix has the objective of defining a standard path to follow when an optimization is wanted to start from an Adams Car experiment, for this thesis this procedure was followed in the phase angle optimization case, explained thoroughly in paragraph 4.5.

The same procedure can be followed for any optimization experiment, not only on one parameter, but also on multiple parameters.

A2.1 Creation of a .cmd file to create necessary markers and requests

To perform the optimization successfully it is necessary to define a .cmd file that will create the markers and requests that are required by the software for a correct set up of the parameters that need an optimization. This is required because the requests are created in the test rig and not on the suspension itself, each time the simulation will be reopened each request will be erased, this file makes the creation of these parameters easier and faster, given that this program must be used each time the software is started, an example of the content of the file used in this thesis is shown below:

```
marker create  &
marker_name = .FS.testrig.whr_wheel.destro  &
location = (LOC_RELATIVE_TO({0, 0, .FS.testrig.pvs_wheel_cm_offset},
.FS.testrig.whr_wheel))  &
orientation = 0.0, 0.0, 0.0
!
marker create  &
marker_name = .FS.testrig.whl_wheel.sinistro  &
location = (LOC_RELATIVE_TO({0, 0, .FS.testrig.pvs_wheel_cm_offset},
.FS.testrig.whl_wheel))  &
orientation = 0.0, 0.0, 0.0
!
output_control create request  &
request_name = .FS.msc_steer_model.steer_irregularity  &
component_units =
'no_units','angle','angle','angle','no_units','no_units','no_units','no_
units'  &
component_names = '','angolo_destro','angolo_sinistro','angolo
medio','','steering_ratio','',''  &
f2 = '-AZ(.FS.testrig.whr_wheel.destro,.FS.ground.origo)'  &
f3 = '-AZ(.FS.testrig.whl_wheel.sinistro,.FS.ground.origo)'     &
f4 = '(-AZ(.FS.testrig.whl_wheel.sinistro,.FS.ground.origo)-
AZ(.FS.testrig.whr_wheel.destro,.FS.ground.origo))/2' &
```

```
f6 =
'(AZ(.FS.msc_steer_model.ges_steering_wheel.jxs_joint_i_5,.FS.ground.jxs
_joint_j_5))/((-AZ(.FS.testrig.whl_wheel.sinistro,.FS.ground.origo)-
AZ(.FS.testrig.whr_wheel.destro,.FS.ground.origo))/2)'
```

The first two commands of the type ***'marker create'*** create two markers that define the steering angle to the wheels. These markers for many simulations are redundant since the angles are already present in the standard requests of the test rig but are necessary for the other two requests of the system. **'f2'** and **'f3'** represent the steering angles of the vehicle, **'f4'** represents the average angle and **'f6'** represents the steering ratio, note well that **'f1'** and **'f5'** were not used to define the various functions within the request, in fact these two functions are usually left empty as they are used as system variables by Adams: This leads to have a maximum of six variables for each request, given the presence of eight function boxes, it is essential to know that the first set of characters between the colon defines the assembly that is used, in this case **'FS'**, it is important to be sure that this value refers to the right assembly, change the .cmd file as needed to reflect the correct assembly.

As soon as the .cmd file has been created, it is possible to launch Adams Car in the standard interface environment and open the necessary assembly.

At this point, press the F2 key from the keyboard, a window like the one in Figure A.6 will open, where it is possible to select the cmd file just created, just click on the correct file icon (a window with two gears) with the right button and the system will process the commands contained in the file.

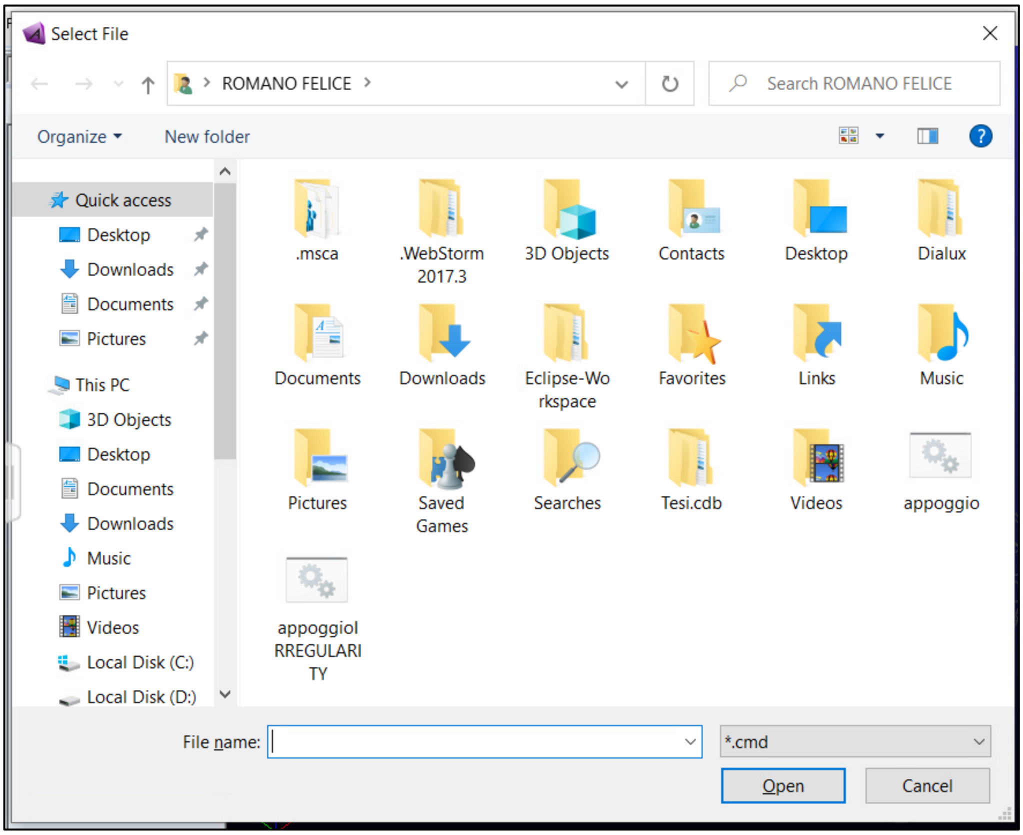

Figure A.6: Selection window of the .cmd file

A2.2 Simulation launch and definition of the Insight experiment in Adams Car

At this point, it is possible to launch an analysis, in this case it was chosen to use a dynamic analysis to evaluate the system with an input angular velocity set as Joint Motion from Adams View interface. In order to launch a simulation like this, check the Dynamic box under suspension analysis and define the desired simulation parameters, as soon as you have defined the simulation you can launch it by clicking on the OK button, a window like the one in Figure A.7 will open:

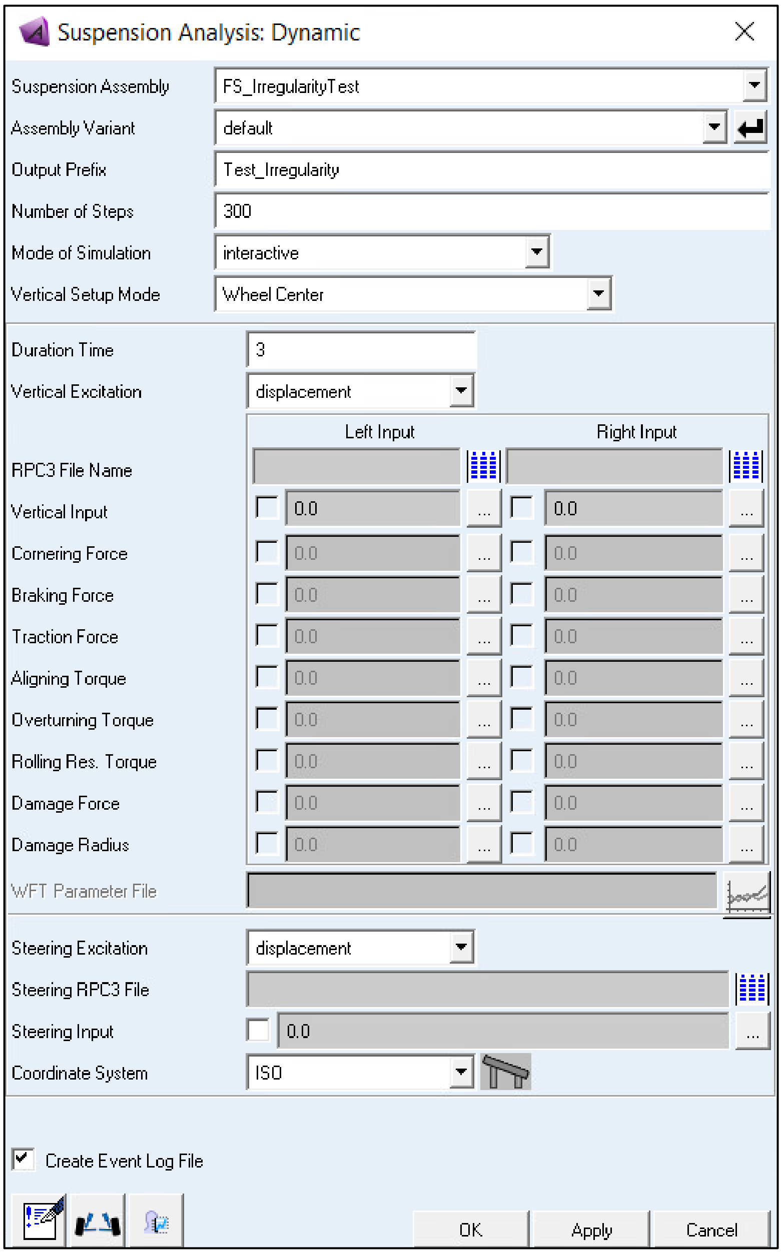

Figure A.7: Dynamic simulation set up window

After completing the simulation, it is now necessary to define the goal or objectives of the experiment, in this case a minimization of the amplitude of the angular velocity of the pinion that connects the steering to the rack.

Click on ***Simulate/DOE Interface/Design Objective/New***, at which it is possible to select a name for the design objective, which components define it, and which value must be controlled, the window that will open is shown in Figure A.8.

Select a name that is easy to understand, on **'Definition by'** select **'Existing Result Set Component (Request)'** to have the various requests used by the system, in this case the measure that calculates the angular velocity at the pinion was selected. The box **'Design Objective's value is the'** has various options as shown in Figure A.8, in this case select **'RMS during simulation'** and click **'OK'**, mind that this option has been selected for this specific simulation because the amplitude of the system is what is relevant, in the case that the objective of the simulation is different select the correct objective.

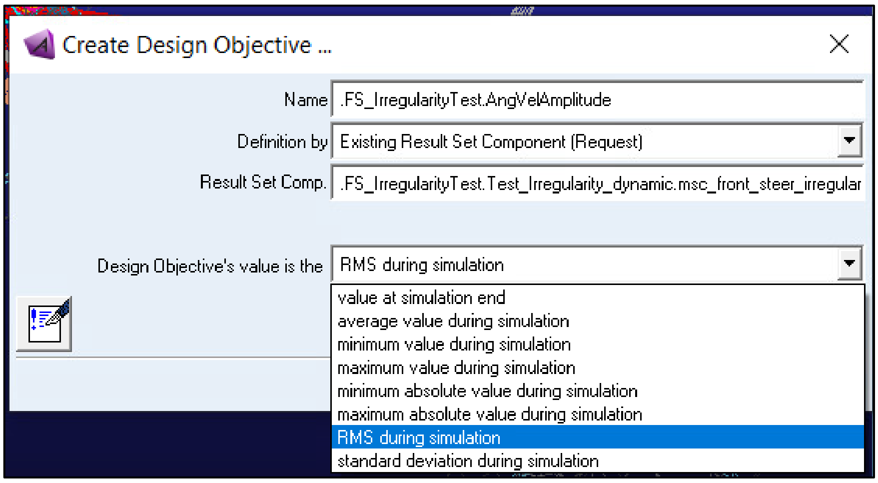

Figure A.8: Design objective creation window

After defining the objective of the experiment, it is possible to move to the Adams Insight environment, this can be done directly from the standard interface, following the commands ***Simulate\DOE Interface\Adams Insight (Legacy)\Export***, as shown in Figure A.9:

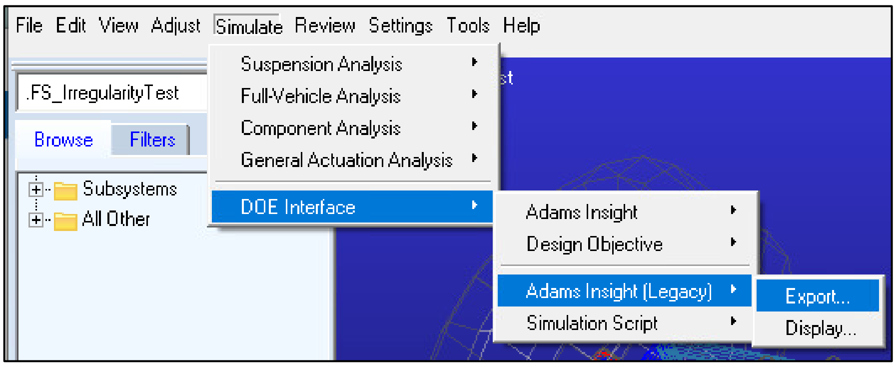

Figure A.9: Commands necessary to open the experiment from Adams Car

As soon as the **'Export'** button is clicked a window like that in Figure A.10 will open, select the assembly used by the simulation, as **'Simulation Script'** select the simulation to be optimized, if it not found among the values in Browse, select **'Last_Sim'** if the desired simulation is the last simulation launched. **'Experiment Name'** is at the user's choice, it is recommended to be clear enough in the name to avoid confusion when comparing to other experiments, check that the selected script is the right one, it cannot be changed after this point.

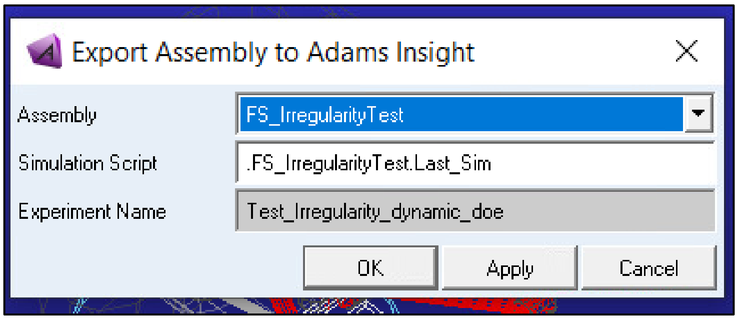

Figure A.10: Window that is used to export the assembly into Adams Insight

A2.3 Defining the experiment in Adams Insight

After exporting the assembly, Adams Insight will automatically open, showing the window in Figure A.11, first click on **'Responses'** and find the item defined as a goal under the **'Candidates'** box

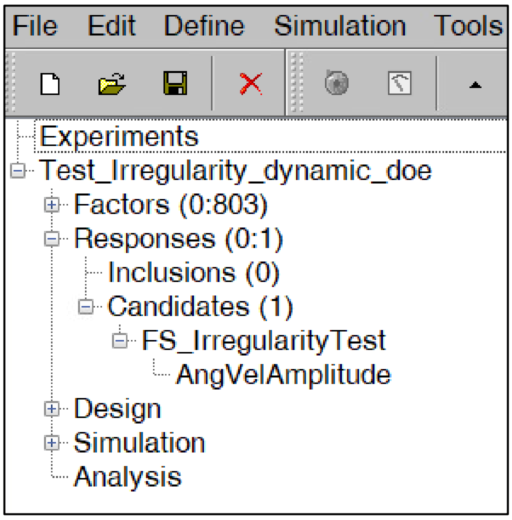

Figure A.11: Drop-down menu that is found in Adams Insight

Click on the design objective, a window like the one in Figure A.12 will open, change the **'Abbreviation'** box with a clear name to understand, it is possible to leave the description box empty with the standard values, then click on **'Optimization'** and select the desired action, in this case **'Minimize'** with the values left as standard, at this point click on **'Apply'**, as shown in Figure A.13. After deciding the parameters of the objective, click on the arrow that points upward in the top bar, this command is called **'Promote to inclusion'**, it will include the objective in the experiment, if everything went well the element that was previously in **'Candidates'** will be in **'Inclusions'**, check that every parameter that has to be optimized is among the ones included by the software, if not redo the steps above before continuing.

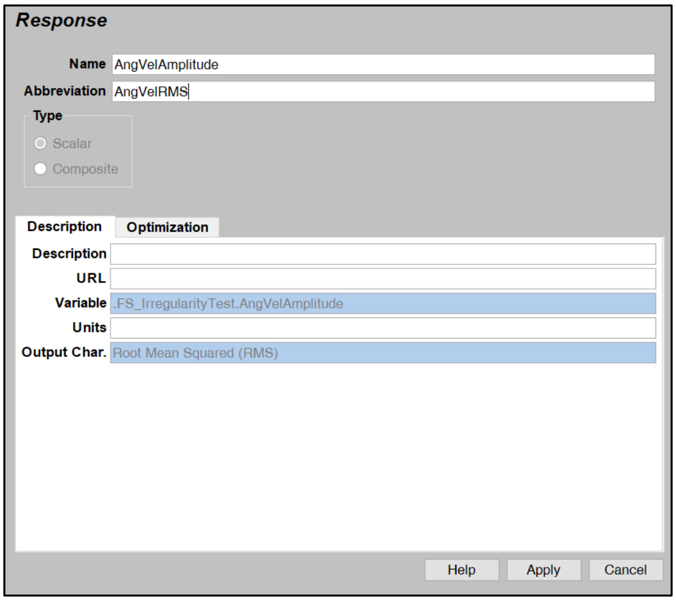

Figure A.12: Window that opens when selecting the desired response to optimize

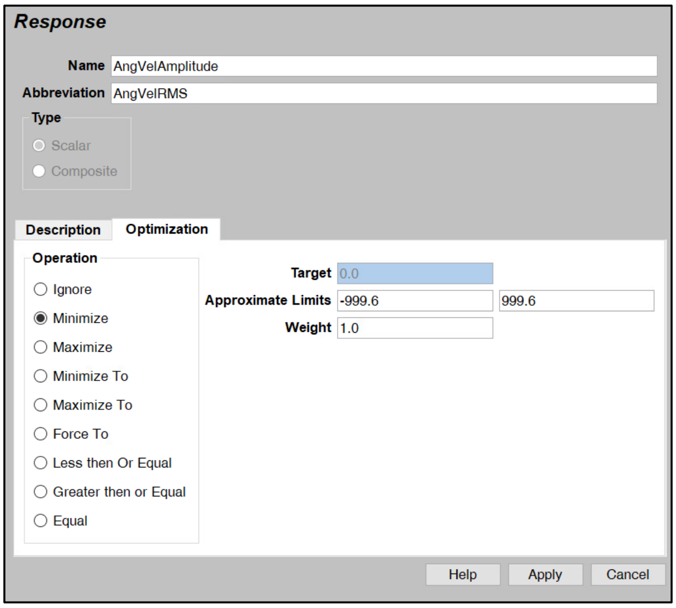

Figure A.13: Optimization sub-window, opened from the one showed in Figure 152

At this point it is possible to move to the **'Factors'** box, find the requests or measures that the experiment has to change to optimize the system, in this case the three parameter variables that define the phase angles, defined in appendix 1, as done in Figure A.14, give **'Abbreviation'** a clear name to understand.

On **'Settings'** it is possible to define various settings for the variable, in this case it was decided to leave the standard values.

On **'Variation'** it is possible to define the type of distribution that the parameter under study will have, in this case a normal distribution with a standard deviation of 5% has been chosen.

Click on **'Apply'** and click on the **'Promote to inclusion'** button like it was done for the responses, do the same thing for all the factors to be evaluated.

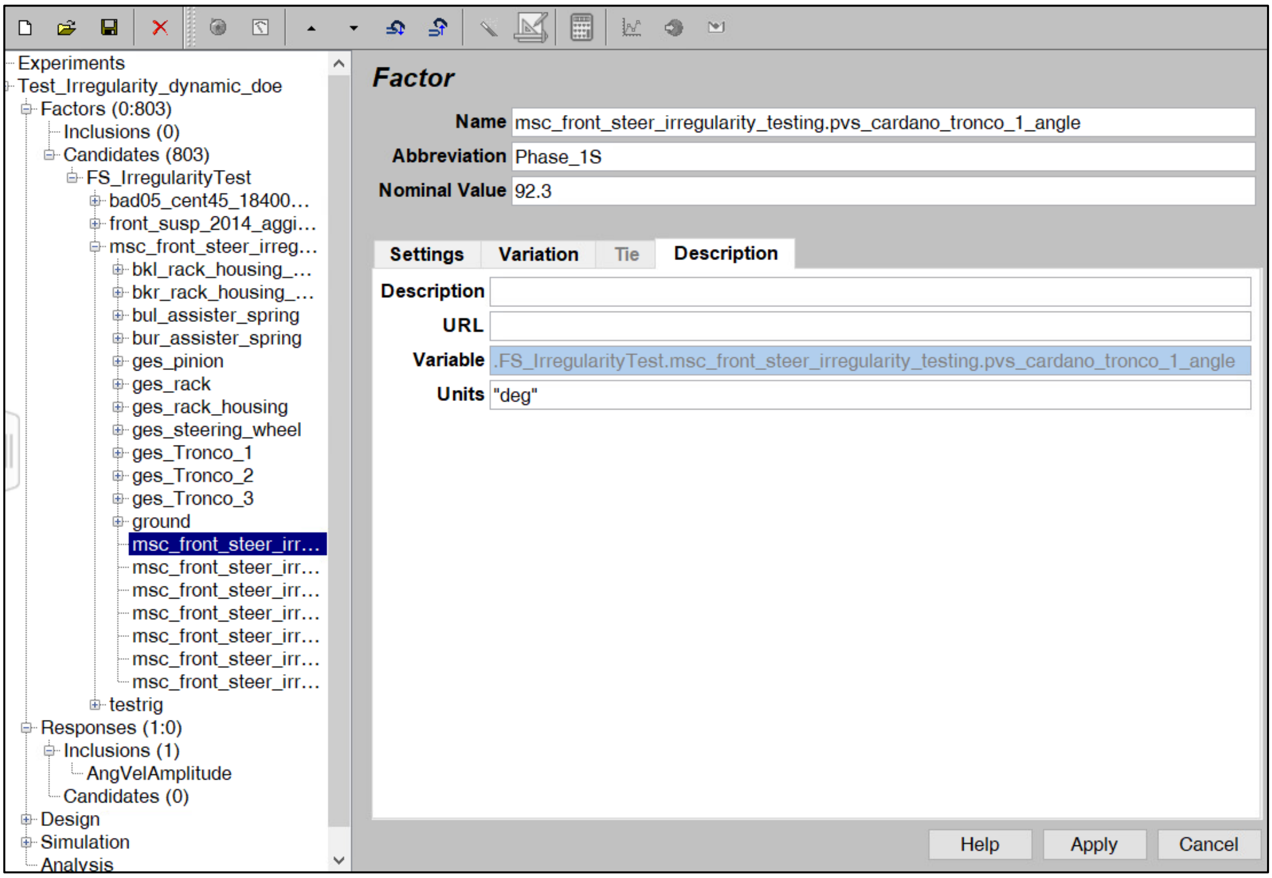

Figure A.14: Window that opens to define the factors to be optimized

After defining all the factors click on **'Set design specification'** button as seen in Figure A.15, this box will be recognizable by an icon in the shape of a magic wand

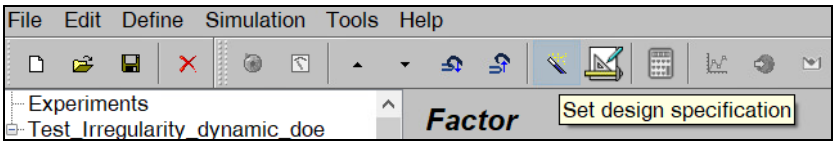

Figure A.15: Path to follow to select the 'Set design specification' button

The window shown in Figure A.16 will open, select the type of investigation strategy desired and the number of attempts to try, after choosing the desired values click on **'Apply'**, in the thesis work an analysis of the Monte Carlo and Latin Hypercube type was made, here a DOE screening will be shown, in all cases the procedure is identical for any selected strategy.

After clicking on **'Apply'**, click on the **'Generate Work Space'** icon that is found in the top bar as an icon that shows a blank sheet and a ruler, the different attempts will be created and a table will be shown with the values of the various selected factors, as shown in Figure A.17.

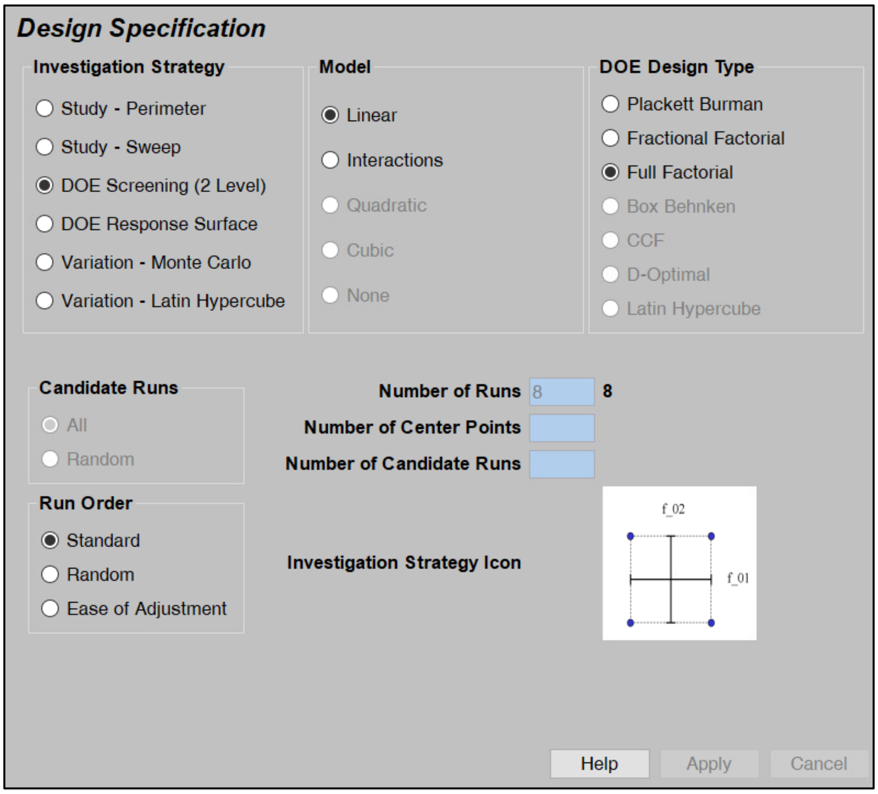

Figure A.16: Window that allows to select the experiment design specification

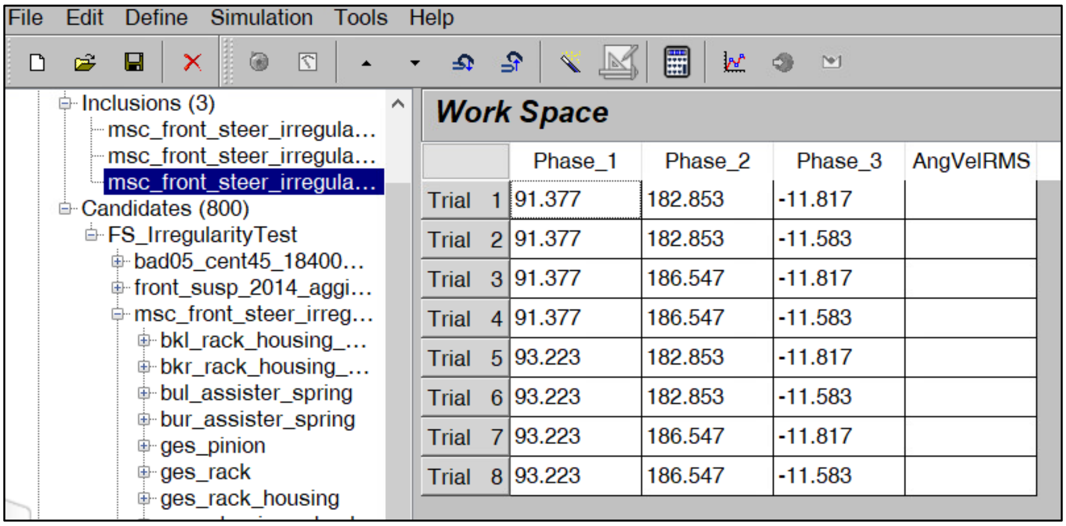

Figure A.17: Window that shows all the different experiments that will be simulated

A2.4 Launch of the experiment and optimization of required parameters

At this point, launch the simulations through the calculator icon on the top bar, this icon is called **'Run all simulations'**, this will launch the simulations on Adams Car, wait until all the simulations have been completed before proceeding. At the end of the simulations a warning like the one in Figure A.18 will appear if all the simulations have been successful.

Following the commands in Figure A.19, it will be possible to switch back to the Adams Insight interface by clicking on the **'Display'** button and selecting the experiment created earlier.

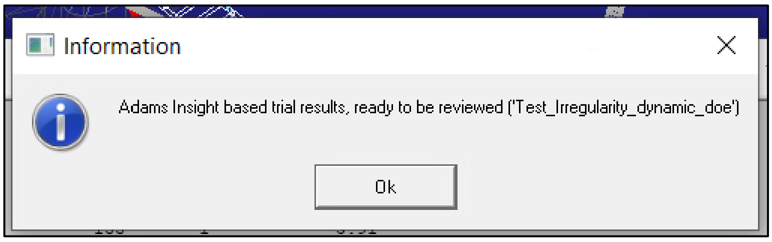

Figure A.18: Warning that appears after the simulations are completed

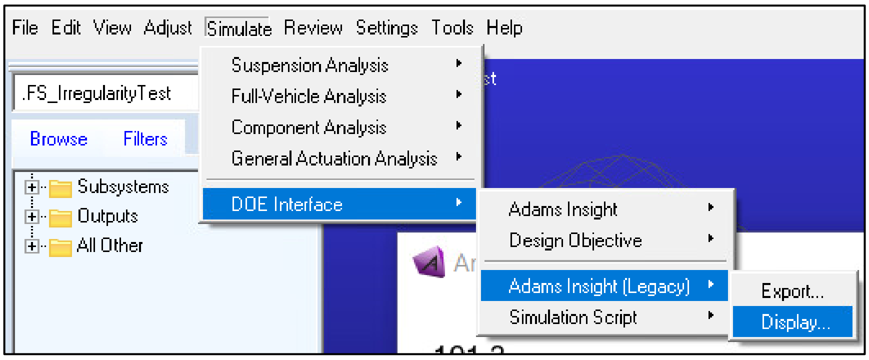

Figure A.19: Set of commands to follow to go back to Adams Insight interface

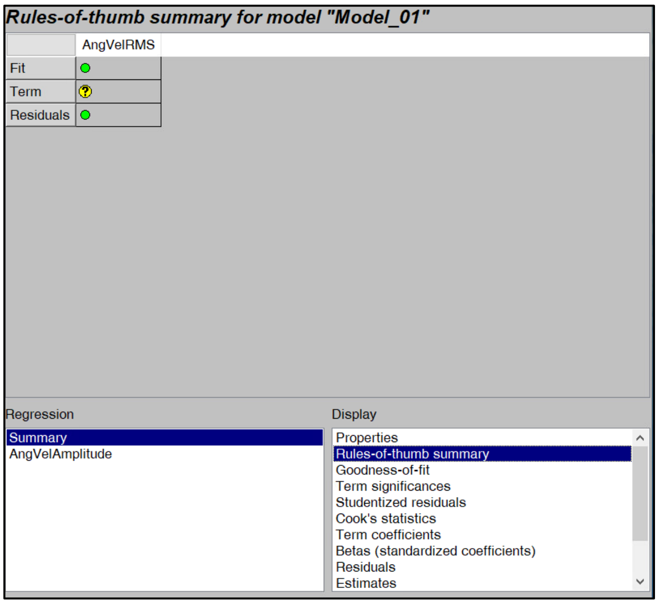

Figure A.20: Window that is opened after pressing the 'Display' button

As soon as Insight has opened click on the chart icon called **'Fit results'** shown as an icon with a dotted graph connected by red lines. A window like the one in Figure A.20 will open, in this window the program will inform us if the simulation has statistical validity in terms of the values obtained, in the **'Rules-of-thumb summary'** box a summary of the fundamental parameters for the evaluation of the experiment is found, the **'Display'** menu is full of detailed information about the experiment, the most important are **'Goodness-of-fit'**, **'Term significances'** and the two about the residuals, by opening these menus all the different trials will be shown with their relative parameter, it is possible to see for each simulation how good the results were and also have some graphs that will summarize the results between all the different trials.

By clicking on **'Optimize'**, which is the last box of the top bar on the right, it will be possible to have the actual optimization window shown in Figure A.21.

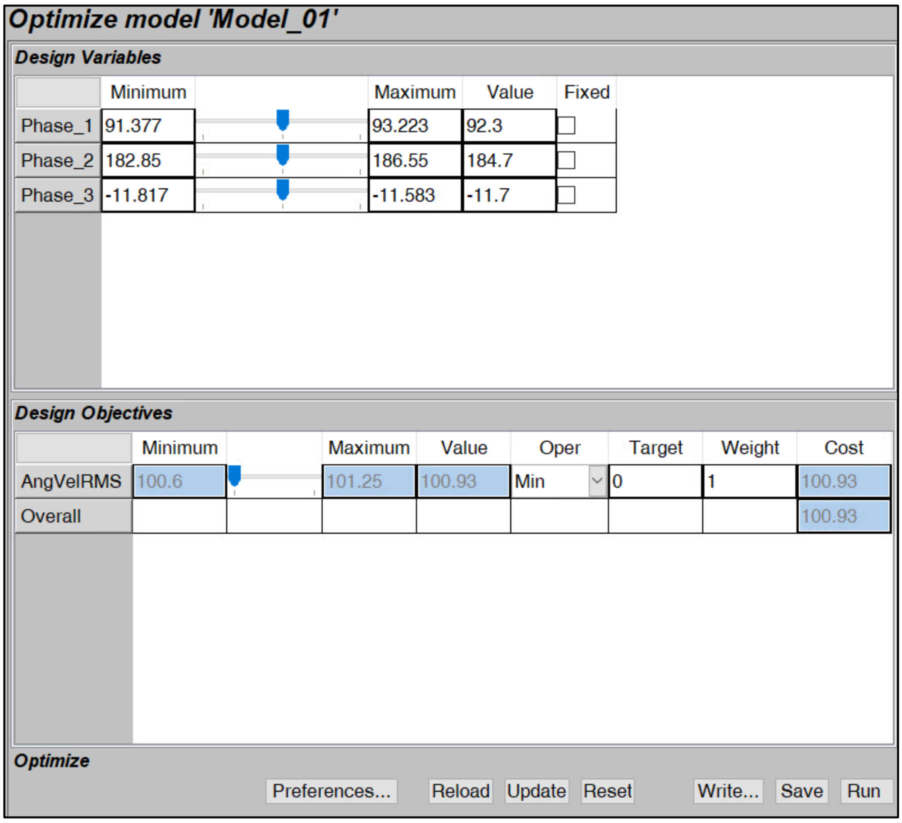

Figure A.21: Optimization window

In this window it is possible to define the maximum and minimum values that the variable can take and decide whether to fix one of the parameters by ticking the **'Fixed'** box, it is recommended to leave everything unchanged on the design parameters and click on **'Run'**, doing so, the initial values that were under the **'Value'** column will be replaced by new values that represent the optimized values.

A2.5 Conclusions and final comments on the optimization

All that remains is to try with a new simulation with those values and see if the parameter of interest has improved, it is not said that Insight finds a condition that improves the system, it must always be tried on Adams Car for confirmation, never give the values of Insight for good.

This guide refers to a specific case but is valid for any evaluation of experiments between Adams Car and Adams Insight, just follow the same steps and change what is needed to achieve the optimization result desired.

References

1.Milliken, W., Milliken, F.: Race Car Vehicle Dynamics, First Edition, SAE International, Warrendale, 1995

2. Genta, G., Morello, L.: The Automotive Chassis Volume 1: Components Design, Second Edition, Springer, Heidelberg, 2009

3.Harrer, M., Pfeffer, P.: Steering Handbook; First Edition, Springer, London, 2017

4. Adams Car Built-In Help Documentation, Hexagon AB, 2021

5. Pasquale M. Sforza, Chapter 8 - Spacecraft Flight Mechanics, Pasquale M. Sforza, Manned Spacecraft Design Principles, Butterworth-Heinemann, 2016

Ringraziamenti

Questo lavoro segna la fine della mia carriera universitaria al Politecnico di Torino. Un cammino non sempre lineare ma che, nel bene e nel male, mi ha dato tanto e mi ha fatto crescere come uomo.

Desidero ringraziare chi mi ha aiutato in questo lavoro di tesi: Il professor Galvagno, Lorenzo e Luca in primis per il supporto fornitomi nella stesura di ogni parte di questa tesi. L'Ing. Bianco, Garofalo e tutta l'Iveco Group per il materiale fornitomi. L'Ing. Casolo, Catelani e tutta l'MSC Software per il supporto nell'apprendimento del software.

Il più grande ringraziamento va alla mia famiglia. Non solo ho sempre ricevuto supporto e affetto incondizionato durante questi anni, ma ho ricevuto valori e insegnamenti che sono a dir poco inestimabili: A mamma per avermi dimostrato cosa vuol dire amare una persona, sacrificando talvolta i propri desideri per fare in modo che il prossimo sia felice. Mai una volta si è tirata indietro per aiutare tutti noi, anche in situazioni dove quella ad avere più bisogno d'aiuto fosse lei, grazie per essere la nostra colonna portante; A papà per avermi insegnato cosa significa essere dedito al lavoro, e per avermi dimostrato che aldilà della sfida che la vita ci mette dinanzi, basta farsi forza e affidarsi a chi ci è più caro; A Peppo per aver dato nuovi significati al termine Fratello, non ringrazierò mai i miei abbastanza per avermi donato un fratello come lui, la persona migliore che potessi avere accanto.
A nonna Lucia, a nonno Felice e nonno Pippo. Per avermi guidato da lassù in tutti questi anni.
A mia nonna Lella, per aver fatto il ruolo di quattro nonni in contemporanea. Per avermi fatto capire che il cammino che ho percorso ha qualcosa di straordinario, ogni chiamata riguardo l'università ha avuto quel carico di ammirazione e affetto che mi ha dato la forza di andare avanti nei tempi più bui.

Grazie alla mia famiglia Torinese: Fabio, Fra, Giulia e Nicolò. Lo studente fuorisede è, in un modo o nell'altro, costretto a cambiare famiglia, mai avrei pensato di ritrovarmi quattro persone che mi potessero fare sentire a mio agio così lontano da casa, auguro a tutti voi il meglio. Ho sempre desiderato altri fratelli, questa esperienza universitaria mi ha donato tre fratelli e una sorella, direi che non mi posso lamentare.

Desidero infine fare una dedica particolare: In certi momenti della mia carriera universitaria mai avrei pensato di arrivare a questo momento. Troppe persone questo momento non possono, purtroppo, viverlo. Dedico questa tesi a chiunque non possa permettersi di scegliere la sua carriera universitaria preferita; A chi, per colpa della malattia o della situazione economica, è costretto ad abbandonare gli studi e soprattutto a chi, per l'università, si è tolto la vita. Queste persone ci fanno ricordare ogni giorno quanto straordinario sia un obiettivo come una Laurea.